ISSN 0216-762X (Print)
ISSN 2528-388X (Online)

INERSIA

JURNAL TEKNIK SIPIL DAN ARSITEKTUR

INERSIA	VoL 22	No. 1	Hlm. 1-127	May 2026

JURNAL TEKNIK SIPIL DAN ARSITEKTUR
INERSIA

Vol.22 No.1 (2026):May

ISSN 0216-762X (Print)
ISSN 2528-388X (Online)

JURNAL TEKNIK SIPIL DAN ARSITEKTUR
INERSIA

Vol.22 No.1 (2026):May
ISSN 0216-762X (Print)
ISSN 2528-388X (Online)

E-ISSN: 2528-388X
P-ISSN: 0213-762X

INERSIA
Vol. 22, No. 1, May 2026

Study on the Potential of Environmentally Friendly Fire Bricks Based on Local Waste Materials Using Ceramic Powder, Glass Powder, and Rubber Ash

Muhammad Thariq Resmaindra*, Cintri Anjani Rahmada Putri, and Sofian Arissaputra

Building Construction Technology Program, Department of Civil Engineering and Infrastructure, Astra Polytechnic, Bekasi 17530, Indonesia

Keywords:
Fire Bricks
Materials
Refractory
Sustainable
Waste

ABSTRACT

Fire bricks are widely used as refractory liners in high-temperature applications such as furnaces and boilers. However, conventional fire brick production is energy intensive and contributes to carbon emissions. This study investigates the development of sustainable fire bricks using industrial waste materials (rubber ash, glass powder, and ceramic waste) combined with mineral additives (kaolin, alumina, and bentonite) as binding and strengthening agents. Five mixture compositions (S1–S5) were prepared and experimentally evaluated after firing at 1250 °C. The physical and mechanical properties were assessed through density, compressive strength, and thermal resistance tests. The results indicate that the proportion of alternative materials significantly influences the performance of the fire bricks. The highest density was obtained in sample S2 at 2604.48 kg/m³ with a maximum compressive strength of 15.26 MPa. Increasing the proportion of waste materials resulted in reduced density and compressive strength, likely due to increased porosity within the matrix. In contrast, sample S1 exhibited the highest thermal resistance, reaching SK30 according to ASTM C24, while the remaining compositions (S2–S5) showed lower refractoriness at approximately SK10. These findings highlight the importance of optimizing waste material proportions to achieve a balance between mechanical performance and thermal resistance in sustainable refractory brick production.

1. Introduction

Fire bricks, also known as refractory bricks, are construction materials that function as heat-resistant linings in furnaces, boilers, and industrial building components exposed to high temperatures. Conventional fire bricks are typically produced using base materials such as alumina and silica in high concentrations. The extraction and processing of these materials involve energy-intensive operations, including mining, refining, and high-temperature treatment, which contribute significantly to carbon emissions [1]. With the growing emphasis on sustainability, innovation in alternative materials is essential to replace the primary constituents of fire bricks with locally available resources. A study by Samad, A. [2] previously demonstrated the utilization of local red clay in refractory brick production. The use of locally sourced materials can be further optimized by incorporating nearby industrial waste, which not only supports environmental conservation but also promotes community empowerment. Several industrial waste materials such as rubber ash, glass powder, and crushed ceramic powder possess high potential as partial substitutes for conventional fire brick raw materials due to their relatively high silica and alumina content.

Rubber ash, or waste derived from the combustion of rubber tires, is an industrial byproduct. The addition of small amounts of this material has the potential to enhance the mechanical properties of concrete matrices [3] and increase the compressive strength of cement-based concrete [4]. This indicates its potential application in improving the strength characteristics of fire bricks. Glass powder, which is widely available in the surrounding environment, also exhibits potential as an alternative constituent material for fire brick production. It has been

*Corresponding author.
E-mail: m.thariq.Resmaindra@polytechnic.astra.ac.id

https://doi.org/10.21831/inersia.v21i2.90789
Received 24 October 2025; Revised 9 March 2026; Accepted 22 April 2026
Available online 1 May 2026

reported that the incorporation of glass powder can improve the compressive strength of clay bricks [5], suggesting its role in reinforcing the brick matrix. The pozzolanic effect of glass powder can further enhance the mechanical properties of mortar [6] and may serve as a partial replacement for cement [7]. This also highlights its potential contribution to strengthening the matrix of alternative fire bricks. A similar potential is observed in ceramic waste, a commonly encountered material in daily life with various functional uses. However, manufacturing defects, human errors, and the end of service life can lead to significant accumulation of ceramic waste, which requires proper waste management [8]. Crushed ceramic waste, when ground into fine powder, has shown potential as a cement substitute [9][10][11]. Moreover, ceramic waste can be reused as an alternative material for refractory ceramics [12].

Although various waste-derived materials have been explored for sustainable construction products, the use of rubber ash in refractory applications remains limited. In particular, studies investigating the combined utilization of waste-based materials in fire brick formulations are still scarce. This study proposes a fire brick composition incorporating rubber ash, glass powder and ceramic waste and evaluates its thermal and physical performance. In this research, additional materials such as kaolin, alumina, and bentonite were also incorporated, as they contribute to the mechanical and thermal resistance matrix of alternative fire bricks. Kaolin, a type of clay containing kaolinite, can transform into mullite ($3Al_2O_3{\cdot}2SiO_2$) upon firing, which enhances mechanical strength, creep resistance, flexural strength, and thermal stability [13]. Bentonite, a pozzolanic material derived from volcanic ash, can serve as a cement substitute due to its high SiO_2 content and lower carbon emissions [14]. Moreover, bentonite has been reported to improve fire resistance [15]. Alumina was also utilized, as it is commonly applied as a refractory material with excellent fire resistance properties [16]. The results provide new insight into the feasibility of utilizing waste–based composite materials as a sustainable alternative for refractory applications.

2. Methods

This research is an experimental study carried out under controlled laboratory conditions, designed to evaluate the influence of varying compositions of alternative materials on the physical and mechanical properties of environmentally friendly fire bricks. The study was conducted with the objective of formulating a sustainable refractory material by partially substituting conventional components with locally available and waste-derived materials. The experimental work focused on assessing how changes in the proportion of these materials affect key performance indicators such as density, compressive strength, and thermal resistance, which are critical parameters in the characterization of refractory materials.

2.1 Materials

The primary materials used in this study consisted of refractory cement, kaolin, alumina, bentonite, rubber ash, glass powder, and crushed ceramic powder. Each material was selected based on its specific role in the composite formulation. Refractory cement served as the primary binding matrix and provided heat resistance required for high-temperature applications. Kaolin, alumina, and bentonite function as supplementary refractory binders that contribute to the mechanical strength, thermal stability, and microstructural integrity of the bricks. On the other hand, rubber ash, glass powder, and ceramic fragments serve as alternative waste-derived materials intended to substitute a portion of the conventional raw materials.

The refractory cement utilized in this study was *castable LR 68*, a commercial-grade product manufactured by PT Indoporlen, selected due to its high-temperature endurance and compatibility with various mineral additives. Kaolin, bentonite, and aluminate were purchased from commercial suppliers. The crushed ceramic powder used in the study were sourced from accumulated ceramic waste deposits located in the Cikarang Pusat area, where discarded tiles and sanitary ceramics from industrial production and household renovation waste are abundant, as shown in Figure 1.

Figure 1. Ceramic Waste Pile in the Cikarang Pusat Area

Table 1. Chemical Composition of Glass Powder, Crushed Ceramic Powder and Rubber Ash

Parameter	Unit	Glass Powder	Crushed Ceramic Powder	Rubber Ash
Iron Trioxide (Fe_2O_3)	%	0.12	4.77	8.9
Aluminum Trioxide (Al_2O_3)	%	1.02	17.47	29
Calcium Oxide (CaO)	%	8.78	7.25	4.2
Magnesium Oxide (MgO)	%	4.03	1.25	2
Manganese Oxide (MnO)	%	Less than 0.01	0.27	0.2
Chromium Trioxide (Cr_2O_3)	%	Less than 0.01	0.01	Less than 0.01
Sodium Oxide (Na_2O)	%	14.11	1.39	Less than 0.01
Potassium Oxide (K_2O)	%	0.31	2.32	0.6
Silicon Dioxide (SiO_2)	%	70.72	63.65	49.6
Titanium Dioxide (TiO_2)	%	0.02	0.74	1.3
Zinc Oxide (ZnO)	%	Less than 0.01	0.07	Less than 0.01
Phosphorus Pentaoxide (P_2O_5)	%	0.02	0.22	1.1
Sulfur Trioxide (SO_3)	%	0.65	0.53	2.5

Table 2. Mass Proportion of Alternative Materials

Sample Name	Mass Proportion						
	Castable Refractory Cement	Kaolin	Aluminate	Bentonite	Rubber Ash	Glass Powder	Crushed Ceramic Powder
S1	1	0.1	0.1	0.01	0.1	0.1	0.1
S2	1	0.1	0.1	0.01	0.2	0.2	0.2
S3	1	0.2	0.2	0.02	0.2	0.2	0.2
S4	1	0.2	0.2	0.02	0.3	0.3	0.3
S5	1	0.2	0.2	0.02	0.4	0.4	0.4

The ceramic waste obtained was first crushed using a hammer and then ground using a Los Angeles abrasion machine to achieve fine particle size. The resulting material was subsequently sieved using a 4.75 mm sieve to obtain ceramic waste in powdered form. The chemical composition of the ceramic material is presented in Table 1. The rubber ash was sourced from the combustion process of tire production by PT Hirundo Tyre Utama and packaged by PT Komala Agung Langgeng Perkasa, with its chemical composition shown in Table 1. The glass powder was obtained from Toko Sandblasting Niaga Elektronik, and its chemical composition is also presented in Table 1.

2.2 Sample Preparation

Five mixture compositions (S1–S5) were formulated to evaluate the effect of varying proportions of alternative materials on the mechanical and thermal properties of the bricks, as shown in Table 2. The mixture variations were designed to evaluate the influence of material proportions on the density, compressive strength, and thermal performance of the fire bricks. In this experimental design, the refractory cement was kept constant as the primary base component with a fixed mass ratio of one unit. The components kaolin, alumina, and bentonite functioned as mineral matrices that contributed to the mechanical strength of the fire bricks, while rubber ash, ceramic powder, and glass powder represented waste matrices derived from industrial by-products with potential for reuse in the production of fire bricks. The variations used in this study are presented in Table 2. The composition pattern was systematically arranged to establish a structured relationship between the mineral content and waste content. The initial stages (S1–S2) focused on increasing the proportion of the waste matrix from 0.1 to 0.2, while maintaining the mineral content constant at 0.1. This stage aimed to evaluate the extent to which the addition of waste materials influences the fundamental properties of the fire brick without the reinforcement effect of increased mineral content.

Subsequently, in S3, the mineral content was increased from 0.1 to 0.2, while the waste content remained constant at 0.2, in order to assess the strengthening or stabilizing effect of the mineral phase within a system already containing waste materials. The following stages (S4 and S5) were focused on gradually increasing the waste content to 0.3 and 0.4, respectively, while maintaining the mineral content at a higher constant value of 0.2.

All mixtures were placed into paving block molds with dimensions of 20 cm × 10 cm × 6 cm and compacted using a tamping rod. The specimens were then demoulded and left to cure for 7 days as in Figure 2. After the curing period, the samples underwent a firing phase using a Nabertherm chamber furnace, as shown in Figure 4, with the temperature gradually increased to 400°C for 2 hours, followed by 800°C for 2 hours, and finally 1250°C for 1 hour, as shown in Figure 3.

Figure 2. Production Process of Alternative Fire Brick Samples

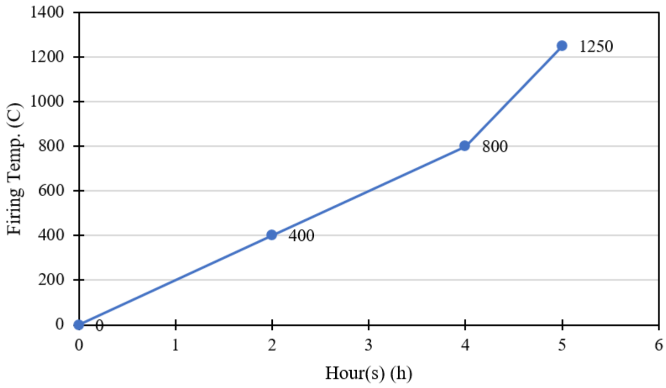

Figure 3. Firing Program of Alternative Fire Bricks

Figure 4. Firing Process of Samples

Figure 5. After Firing Process of Samples Using a Chamber Furnace

After firing process, fired brick samples, as shown in Figure 5, were first allowed to cool naturally for a period of 24 hours to ensure that any residual thermal stresses induced during the firing process were relieved. This natural cooling process is critical for minimizing microcrack formation and structural damage, thereby maintaining the integrity of the fired bricks. After cooling, compressive strength tests were conducted on all specimens in accordance with ASTM C133. Prior to testing, the specimens were carefully cut into cubic shapes measuring 5 cm × 5 cm × 5 cm to ensure uniformity and comparability of the results. The tests were performed using a compression testing machine at a loading rate of 0.52 kN/s (or 31.2 kN/min) [17], and the maximum load at failure was recorded to determine the compressive strength of each sample.

In addition to mechanical testing, thermal resistance evaluation was carried out to assess the ability of the fire bricks to withstand high-temperature exposure. This test employed the Pyrometric Cone Equivalent (PCE) or Seger Cone method in accordance with ASTM C24, which is widely used in refractory material assessment to determine the effective service temperature of ceramics. The test determines the refractoriness of a material by comparing its softening behavior with standard pyrometric cones during controlled heating. In this method, the sample is ground, mixed with a small amount of binder or water, and molded into a cone-shaped specimen, which is then dried prior to testing. The test cone is placed in a furnace alongside standard cones with known deformation temperatures and heated at a controlled rate. The PCE value is determined by identifying the reference cone that deforms to the same extent as the test specimen and the refractoriness of the material is expressed as the equivalent cone number [18]. The tests were conducted at the Center for Ceramics Research and Testing (Balai Besar Keramik), Bandung. The results from the thermal resistance tests are expected to provide insight into the high-temperature performance of the environmentally friendly fire bricks.

4. Results and Discussion

From the production process, visual observations were obtained for each sample. Before the firing process, the surface of the samples appeared gray in color, similar to the color of cement, as shown in Figure 6. After the firing process, the samples exhibited a color change to yellowish tones, as illustrated in Figure 7 to Figure 11.

Figure 6. The visual appearance of the surface of the unburned sample appears gray, similar to the color of cement

Figure 7. The visual appearance of the surface of sample variation S1.

Figure 8. The visual appearance of the surface of sample variation S2.

Figure 9. The visual appearance of the surface of sample variation S3.

Figure 10. The visual appearance of the surface of sample variation S4.

Figure 11. The visual appearance of the surface of sample variation S5.

From the visual observation, noticeable differences were identified in both the color and surface texture of the produced fire bricks across all variations. Before firing, the samples exhibited a gray coloration similar to that of ordinary cement. After undergoing the firing process, the samples experienced a distinct transformation in appearance, changing from gray to reddish-yellow hues. This color change indicates that mineral and chemical transformations occurred during the high-temperature sintering process. Furthermore, a gradual color gradation was observed among the variations, with darker tones appearing as the proportion of alternative materials increased. This phenomenon suggests that the inclusion of waste-derived components such as rubber ash, glass powder, and crushed ceramic powder influenced the surface oxidation and hardening process, thereby altering the overall visual characteristics of the fire bricks. From the test results, the average density, PCE test and compressive strength data were obtained, as shown in Table 3.

Table 3. Density, compressive strength, and PCE test result

Sample Name	Density (kg/m^3)	Compression Strength (MPa)	PCE Result
S1	2442.29	8.71	SK-30 (~1636°C)
S2	2604.48	15.26	SK-10 (~1282°C)
S3	2466.51	9.26	SK-10 (~1282°C)
S4	1735.61	9.71	SK-10 (~1282°C)
S5	1457.74	8.87	SK-10 (~1282°C)

The density results indicate that sample S2 exhibited a higher density compared with S1. This increase may be associated with improved particle packing and stronger bonding between the constituents, particularly between the refractory cement and the fine waste particles, which likely contributed to a more compact microstructure. In contrast, a reduction in density was observed in sample S3 compared with S2. This decrease may be associated with the increased proportion of mineral additives, which could affect particle packing and promote the formation of micro-voids during firing. A similar trend was observed in samples S4 and S5, where the density decreased further as the mineral content increased. The corresponding compressive strength results support this observation, indicating that increased porosity within the matrix likely contributed to reductions in both density and mechanical strength.

The compressive strength test results revealed that the highest strength was achieved by sample S2, with a mass proportion of fire cement: kaolin: alumina: bentonite: rubber ash: glass powder: crushed ceramic powder of 1 : 0.1 : 0.1 : 0.01 : 0.2 : 0.2 : 0.2. Compared with S1, the higher proportion of waste material in S2 contributed to improved mechanical performance. This enhancement may be attributed to the filler effect of the fine waste particles and possible pozzolanic interactions within the cementitious matrix. These mechanisms may have promoted improved particle packing and additional bonding within the matrix, thereby increasing the overall compressive strength of the fire brick. However, as the substitution of waste materials continued to increase in subsequent variations, a decline in compressive strength was observed. This trend suggests that excessive incorporation of replacement materials may lead to incomplete bonding and increased porosity, which weakens the brick matrix. A similar effect was observed when the proportions of kaolin, alumina, and bentonite were increased while maintaining constant cement and waste material contents. This is evident from the comparison between S2 and S3, as well as between S4 and S5, where higher mineral content corresponded to lower compressive strength. The reduction in strength is likely associated with increased porosity and reduced matrix continuity, which limit the formation of a dense and mechanically stable structure.

Based on the Pyrometric Cone Equivalent (PCE) test results, S1 exhibited the highest thermal resistance, reaching SK30 (approximately 1636 °C). In contrast, the other samples showed lower performance, reaching only SK10 (approximately 1282 °C). These results indicate that the optimal mixture composition was achieved in variation S1 for thermal resistance, while higher proportions of the added materials resulted in a reduction in the thermal resistance of the bricks. The results indicate that increasing the proportion of waste material reduces the thermal resistance of the fire bricks, suggesting that the waste component may introduce fluxing oxides which can promote liquid-phase formation during firing and reduce the softening temperature of ceramic materials[19]. Alkali elements are known to react with aluminosilicate refractory matrices, forming secondary phases that degrade structural stability at high temperatures [20].

The addition of mineral additives such as kaolin, bentonite, and aluminate did not significantly compensate for this effect. This can be observed by comparing compositions S1 and S2, as well as S3 and S4, where the inclusion of minerals such as kaolin, bentonite, and aluminate did not result in a higher refractoriness classification. In both cases, the thermal resistance remained similar compared to the corresponding mixtures without more additional minerals. These findings suggest that the reduction in thermal resistance is primarily influenced by the increased proportion of waste material, while the added minerals were insufficient to compensate for this effect in the tested formulations. Therefore, the optimal formulation for thermal resistance was achieved at lower waste content, where the balance between refractory minerals and waste-derived components was maintained.

While the inclusion of alternative waste materials such as rubber ash, glass powder, and crushed ceramic powder can improve certain physical and mechanical properties, their optimal dosage is limited. Beyond a certain threshold, these materials tend to increase porosity and reduce both density and compressive strength. Based on the study results, sample S2 showed the most favourable formulation in terms of compressive strength, reflecting a balanced combination of material substitution and density. In contrast, sample S1 exhibited the highest thermal resistance among the tested compositions, indicating that the optimal mixture depends on the targeted performance criterion.

5. Conclusions

Five mixture variations (S1–S5) were evaluated to examine the influence of mineral additives and waste-derived materials on the thermal and mechanical performance of the developed fire bricks. Based on the results of the study, it can be concluded that:

1. Sample S2 demonstrated the highest compressive strength, indicating that moderate incorporation of waste materials may improve densification and load-bearing capacity. However, the addition of minerals such as kaolin, bentonite, and aluminate did not sufficiently compensate for the reduction in thermal resistance when the waste content increased.
2. Pyrometric Cone Equivalent (PCE) test indicated that sample S1 exhibited the highest thermal resistance, reaching SK30 according to ASTM C24, while the remaining samples (S2–S5) showed significantly lower refractoriness at approximately SK10. These results suggest that higher proportions of waste-derived materials reduced the thermal resistance of the bricks, likely due to the dilution of refractory phases and the presence of fluxing components that promote early softening at elevated temperatures.
3. The density increased in S2 compared to S1, while the addition of kaolin, alumina, and bentonite composition caused a decrease, which may have occurred due to increased porosity as observed in the comparison between S2 and S3 as well as S4 and S5.
4. Overall, the results indicate that mixture composition strongly influences the balance between thermal stability and mechanical strength, with S1 providing optimal refractory performance and S2 offering improved compressive strength.

For future work, further investigation on thermal conductivity, long-term durability through prototype incinerator testing, and the effect of repeated heating cycles is recommended to refine the formulation. An optimized fire brick composition derived from this research has potential practical applications in small- to medium-scale incinerators, biomass furnaces, and other thermal processing units where lightweight, thermally stable, and sustainable refractory materials are required. The development of such materials may support more efficient heat retention, reduce material weight, and promote the utilization of waste-based resources in refractory production, thereby increasing the feasibility of industrial implementation.

Acknowledgment

The author gratefully acknowledges the financial support provided by the LLDIKTI Region III, which enabled the successful completion of this research. The funding facilitated the procurement of materials, laboratory equipment, and analytical resources required for the experimental work.

The author also expresses appreciation to Politeknik Astra, particularly the Department of Civil Engineering and Infrastructure for providing research facilities and technical support throughout the study. We also express our appreciation to colleagues, research assistants, and students who contributed to the experimental work, particularly in sample preparation, testing, and data recording.

References

[1] M. Z. Khaiyum, S. Sarker, and G. Kabir, "Evaluation of carbon emission factors in the cement industry: An emerging economy context," *Sustainability*, vol. 15, no. 21, p. 15407, 2023, doi: 10.3390/su152115407.

[2] S. Abdus Samad *et al.*, "Manufacture of refractory brick from locally available red clay blended with white Portland cement and its performance evaluation," *GEOMATE Journal*, vol. 20, no. 80, pp. 105–112, 2021.

[3] M. S. Senin *et al.*, "The optimum content of rubber ash in concrete: Flexural strength," *IOP Conf. Ser.: Mater. Sci. Eng.*, vol. 271, p. 012009, 2017, doi: 10.1088/1757-899X/271/1/012009.

[4] V. Kumar *et al.*, "Experimental study on the substitution of waste rubber tyre ash with natural sand in the cement concrete," *E3S Web Conf.*, vol. 529, p. 01016, 2024, doi: 10.1051/e3sconf/202452901016.

[5] R. D. Mohsin, H. Al-Khazraji, S. K. Zemam, T. H. Majeed, and A.-Z. H. Abbood, "Investigation of wastes plastic and glass to enhance physical–mechanical properties of fired clay brick," *Civil and Environmental Engineering*, vol. 19, no. 1, pp. 248–259, 2023, doi: 10.2478/cee-2023-0022.

[6] C. I. Teran Mejia *et al.*, "Bricks made from glass residues: A sustainable alternative for construction and architecture," *Chem. Eng. Trans.*, vol. 100, pp. 91–96, 2023, doi: 10.3303/CET23100016.

[7] B. O. Rabiu and M. A. Mosaberpanah, "Sustainable utilization of waste glass powder and brick dust as cement replacements: Effects on mortar performance and environmental benefits," *Sustainability*, vol. 17, no. 3, p. 1298, 2025, doi: 10.3390/su17031298.

[8] S. Ray *et al.*, "Use of ceramic wastes as aggregates in concrete production: A review," *J. Build. Eng.*, vol. 43, p. 102567, 2021, doi: 10.1016/j.jobe.2021.102567.

[9] O. M. Olofinnade, A. N. Ede, and C. A. Booth, "Sustainability of waste glass powder and clay brick powder as cement substitute in green concrete," in *Handbook of Environmental Materials Management*, C. M. Hussain, Ed. Cham, Switzerland: Springer, 2019, pp. 2927–2948, doi: 10.1007/978-3-319-73645-7_112.

[10] M. J. Taher, E. H. Abed, and M. S. Hashim, "Using ceramic waste tile powder as a sustainable and eco-friendly partial cement replacement in concrete production," *Mater. Today Proc.*, 2023, doi: 10.1016/j.matpr.2023.04.060.

[11] T. A. Tawfik *et al.*, "Sustainable reuse of waste ceramic tiles powder and waste brick powder as a replacement for cement on green high strength concrete properties," *Innov. Infrastruct. Solut.*, vol. 9, no. 5, p. 166, 2024, doi: 10.1007/s41062-024-01498-2.

[12] G. A. Khater *et al.*, "Utilizing ceramic factory waste to produce low-cost refractory ceramics," *Recycling*, vol. 9, no. 5, p. 98, 2024, doi: 10.3390/recycling9050098.

[13] M. Sobhani and A. Balooch, "Fabrication of lightweight clay-based refractory bricks using recycled EPS polymer," *Case Stud. Constr. Mater.*, vol. 22, p. e04683, 2025, doi: 10.1016/j.cscm.2025.e04683.

[14] K. Hasan, R. P. Jaya, and F. M. Yahaya, "Application of bentonite in cement-based composites: A review of current status, challenges and future prospects," *J. Build. Eng.*, vol. 98, p. 111171, 2024, doi: 10.1016/j.jobe.2024.111171.

[15] S. Farhan Mushtaq *et al.*, "Effect of bentonite as partial replacement of cement on residual properties of concrete exposed to elevated temperatures," *Sustainability*, vol. 14, no. 18, p. 11580, 2022, doi: 10.3390/su141811580.

[16] S. Li, J. Xin, and R. Chen, "Achieving high strength and low thermal conductivity: Additive manufacturing of mullite lightweight refractory," *Ceram. Int.*, vol. 50, no. 16, pp. 27880–27888, 2024, doi: 10.1016/j.ceramint.2024.05.084.

[17] ASTM International, *Standard Test Methods for Cold Crushing Strength and Modulus of Rupture of Refractories*, ASTM C133–97(2018), West Conshohocken, PA, USA, 2018, doi: 10.1520/C0133-97R18.

[18] ASTM International, *Standard Terminology of Refractories*, ASTM C24/C24M–22, West

Conshohocken, PA, USA, 2022, doi: 10.1520/C0024_C0024M-22.

[19] M. U. Rehman, M. Ahmad, and K. Rashid, "Influence of fluxing oxides from waste on the production and physico-mechanical properties of fired clay brick: A review," *J. Build. Eng.*, vol. 27, p. 100965, 2020, doi: 10.1016/j.jobe.2019.100965.

[20] J. Stjernberg, B. Lindblom, J. Wikström, M.-L. Antti, and M. Odén, "Microstructural characterization of alkali metal mediated high temperature reactions in mullite based refractories," *Ceram. Int.*, vol. 36, no. 2, pp. 733–740, 2010, doi: 10.1016/j.ceramint.2009.10.018.

E-ISSN: 2528-388X
P-ISSN: 0213-762X

INERSIA
Vol. 22, No. 1, May 2026

Influence of Constitutive Models on Cyclic Pore Pressure and Liquefaction Assessment in Srandakan, Bantul, Indonesia

Anisa Nur Amalina*, Lalu Makrup and Elvis Saputra

Department of Civil Engineering, Universitas Islam Indonesia, Yogyakarta, 555834, Indonesia

Keywords:
Hardening Soil
Mohr-Coloumb
PLAXIS 2D
PSHA
PM4SAND

ABSTRACT

Liquefaction potential in earthquake-hazard areas is correlated with earthquake-induced cyclic loading. This condition leads to an important selection in the constitutive soil model in numerical site response analysis. This study aims to evaluate the effect of different constitutive soil models on cycling pore pressure by using a numerical model. The case was taken in Srandakan, Bantul, Indonesia, which consists of sand and clay soil. A representative ground motion was derived from a probabilistic seismic hazard analysis, with PGA ≈ 0.31, in a one-dimensional dynamic analysis using PLAXIS 2D. Three constitutive models, Mohr–Coulomb (MC), Hardening Soil with small-strain stiffness (*HSsmall*), and PM4Sand, were compared in terms of excess pore pressure development and pore pressure ratio (R_u) evolution. The results showed that MC neglected a pore-pressure accumulation, while HSsmall captured only a limited nonlinear response. Meanwhile, PM4Sand predicted more significant cyclic pore pressure changes in sandy layers due to its state-dependent plasticity formulation. Nevertheless, Ru values remained well within acceptable limits at all depths, indicating that the applied seismic excitation did not trigger liquefaction. The findings demonstrated that model selection substantially affected pore pressure response in seismic liquefaction analysis.

1. Introduction

Liquefaction is a phenomenon in which saturated, cohesionless soils (typically sandy soils) lose strength and stiffness due to an increase in pore-water pressure, often triggered by seismic activity. This increase in pore water pressure reduces the effective stress in the soil, causing it to behave like a liquid [1], [2], [3], [4], [5]. This process poses serious risks to structures, potentially leading to foundation failure and collapse. Therefore, assessing liquefaction potential is essential, particularly in areas planned for development. Earthquakes, through the propagation of seismic waves, are the primary triggers of liquefaction. Developing reliable models to evaluate liquefaction potential is thus critical for seismic risk mitigation.

Earthquake ground motions can be characterized using either deterministic or probabilistic approaches. Probabilistic Seismic Hazard Analysis (PSHA) has become the standard tool for estimating site-specific ground motions. In Indonesia and Southeast Asia, PSHA has been extensively applied to produce seismic hazard and spectral maps and support microzonation studies and revisions of the national seismic building code [6], [7], [8], [9], [10], [11].

Ground motion modification techniques are essential in geotechnical analyses to evaluate the impact of seismic loading on soil and foundation systems, particularly for assessing liquefaction potential. These techniques involve altering recorded ground motions to match a target response spectrum, which helps in reducing the number of ground motions required for analysis and ensures consistency in seismic evaluations [12], [13], [14].

Liquefaction potential has likewise been widely studied in Indonesia and abroad. Previous works have evaluated liquefaction hazards using SPT data, state parameter analysis, and ground motions derived from probabilistic approaches. These studies consistently highlight the importance of integrating seismic hazard analysis with

*Corresponding author.
E-mail: anisa.amalina@uii.ac.id

https://doi.org/10.21831/inersia.v21i2.95996
Received 20 February 2026; Revised 13 April 2026; Accepted 13 April 2026
Available online 01 May 2026

geotechnical site response to better capture liquefaction risk [15], [16], [17].

Site response analysis (SRA) is a critical tool in seismic design, particularly for understanding how local site conditions affect ground response during earthquakes [18]. This method is robust to manual comparisons of Cyclic Resistance Ratio (CRR) and Cyclic Stress Ratio (CSR), as it enables a more detailed, dynamic analysis of soil behavior, including the development of pore pressure under cyclic loading.

Site response analysis using finite element platforms such as PLAXIS can help model the effect of cyclic loading on soil. Moreover, it offers several constitutive models that offer insights into soil behaviour under various conditions [19] and [20]. Soil behavior in dynamic analysis can be represented by various constitutive models of varying complexity. The Mohr–Coulomb (MC) model is simple but does not explicitly capture cyclic pore pressure generation [21]. The Hardening Soil model with small-strain stiffness (HSsmall) improves the modeling of stiffness degradation under cyclic loading [22], whereas advanced critical-state-based models, such as PM4Sand, are specifically formulated to simulate pore pressure accumulation and cyclic mobility in sands [23]. Differences in model formulation may significantly influence predicted liquefaction indicators, particularly the pore pressure ratio (R_u).

This study compared MC, HSsmall, and PM4Sand within a one-dimensional soil column subjected to PSHA-based input motion in a liquefaction-prone area using PLAXIS 2D in Figure 1. The analysis focuses on differences in Ru evolution and the distribution of excess pore pressure to evaluate the sensitivity of liquefaction assessment to constitutive model selection. By acknowledging model limitations, liquefaction-induced damage can be mitigated through remediation methods that depend upon a thorough evaluation of liquefaction. Also, this study offers insights to improve the development of constitutive models for liquefaction analysis.

2. Methods

This study evaluates the influence of constitutive soil models on liquefaction prediction through dynamic site response analysis. Seismic input motions were selected based on a Probabilistic Seismic Hazard Analysis (PSHA) for Bantul, Indonesia. The PSHA results were used solely to define the input ground motion level and were not analyzed further in this study.

2.1 Probabilistic Seismic Hazard Analysis

The Probabilistic Seismic Hazard Analysis (PSHA) explicitly accounted for uncertainties in earthquake occurrence, magnitude, location, and ground motion characteristics. The magnitude distribution, describing the recurrence of earthquakes, is typically modelled with the Gutenberg–Richter relationship law [24]. To avoid unrealistic values, the magnitude range is truncated between a minimum magnitude (m_0) and an upper-bound magnitude (m_u). In most hazard analyses, m_0 ranges between 3 and 5 [25].

Figure 1. Srandakan, Bantul, Yogyakarta, Indonesia [26]

In this study, the recurrence law for earthquake magnitude followed the truncated exponential Gutenberg–Richter model [24] and its modification by Youngs and Coppersmith [27], known as the characteristic earthquake recurrence law. This combined approach accounted for small-to-moderate events using the Gutenberg–Richter relation and large events using the characteristic model, where the probability distribution becomes uniform as it approaches the maximum magnitude.

The distance distribution described the probability of a rupture occurring at different distances from the site. In PSHA, experts generally use the rupture width equal to the rupture length [28]. This is commonly estimated using the relative rupture area on the fault plane, assuming equal likelihood of rupture along the fault length.

Ground-motion prediction equations (GMPEs) were used to evaluate this conditional probability across different tectonic environments affecting the study area. Hazard de-aggregation was performed to identify the dominant earthquake scenario contributing to the target hazard level. The results indicate that the Opak Fault provides the largest contribution to the seismic hazard at the study location. The controlling scenario corresponds to a moment magnitude of Mw ≈ 6.32 and a hypocentral distance of approximately 15.5 km. This magnitude–distance pair was subsequently used to guide the selection of a representative strong ground motion record.

A representative strong ground motion record from the 1987 Whittier Narrows earthquake (Mw 5.9) was selected based on similarity in magnitude and source-to-site distance to the governing seismic scenario. The record was spectrally matched to the Uniform Hazard Spectrum (UHS) obtained from the PSHA at the bedrock level. Spectral matching was performed within the relevant engineering period range to ensure consistency with the target hazard spectrum while preserving realistic temporal characteristics.

The resulting modified acceleration time history had a peak ground acceleration (PGA) of approximately 0.31 g, a total duration of about 30 s, and a time increment (Δt) of 0.005 s. The matched acceleration record was applied directly as a prescribed base acceleration input in PLAXIS 2D under compliant base boundary conditions, without additional scaling (scaling factor = 1.0).

It should be noted that detailed PSHA derivations and spectral-matching procedures are not elaborated on in this paper, as the primary objective of this research is not hazard quantification itself but rather the comparative evaluation of different constitutive soil models in predicting site response and liquefaction behaviour under identical seismic loading conditions.

2.2 Ground Motion Input

The acceleration record was imported into PLAXIS 2D in tabulated format and applied directly as a prescribed base acceleration under compliant base boundary conditions. No additional scaling was applied in the numerical model (scaling factor = 1.0). The compliant base formulation allows wave transmission from the underlying bedrock while minimizing artificial reflection at the model boundary. The ground motion input is shown in Figure 2.

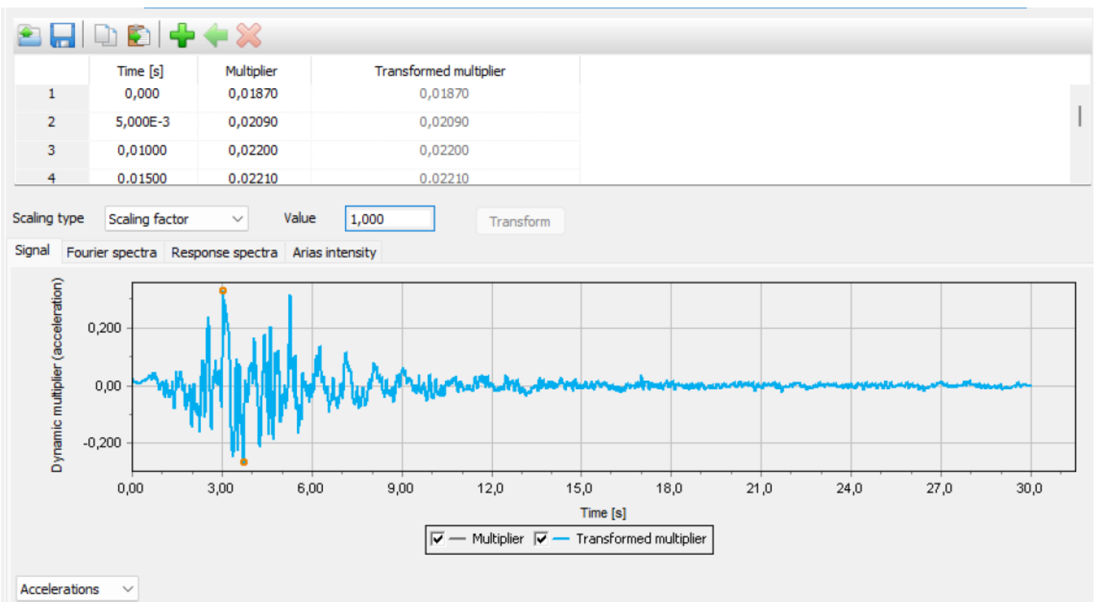

Figure 2. Ground motion input

2.3 Numerical Model Configuration

This study employed a one-dimensional soil column approach to evaluate seismic site response and liquefaction potential. The theoretical basis follows the classical one-dimensional shear wave propagation concept introduced by Bardet and Tobita [29], in which vertically propagating shear waves travel from bedrock to the ground surface within a horizontally layered soil system. The governing equation for one-dimensional wave propagation in a viscoelastic medium can be expressed as Equation (1).

$$\rho \frac{\partial^2 d}{\partial t^2} + \eta \frac{\partial d}{\partial t} = \frac{\partial \tau}{\partial z} \quad (1)$$

where ρ is the soil mass density, d is the horizontal displacement, z is the depth coordinate, t is time, τ is shear stress, and η represents the damping coefficient.

Although the physical problem corresponds to one-dimensional wave propagation, the numerical implementation was carried out in PLAXIS 2D under plane strain. A narrow soil column was modeled with tied lateral degrees of freedom to suppress horizontal deformation incompatibility, thereby enforcing a condition equivalent to one-dimensional shear wave propagation.

2.4 Geometry and Soil Profile

The analysis was conducted based on soil investigations. The average N-SPT and soil classification are shown in Figure 3. Based on SPT data, the soil classifications consisted of sand, silt, and clay. N-SPT value ranged between 25 to 20 at 0 – 12 m and below 10 at the depths of 14 m and 18 m. The dense sand was found below 20 m with N-SPT > 60. The groundwater table was assumed at 0.6m. This soil profile was input to PLAXIS 2D, and the lateral boundaries were modelled using tied degrees of freedom to enforce one-dimensional wave propagation in Figure 4.

2.5 Constitutive Models

Three constitutive models available in PLAXIS 2D were adopted to evaluate their influence on liquefaction-related response. The first is the Mohr–Coulomb (*MC*) model, a linear-elastic, perfectly plastic model with constant stiffness. The Hardening Soil model with small-strain stiffness (*HSsmall*) is a nonlinear model accounting for stress-dependent stiffness and small-strain shear modulus degradation, and PM4Sand is a stress-ratio-controlled, critical-state-based plasticity model specifically developed to simulate cyclic mobility and pore pressure accumulation in sandy soils. Each constitutive model has their own input parameters.

All soil parameters were estimated based on available SPT data and empirical correlations. For sandy layers, relative density and friction angle (φ') were correlated with NSPT values using the empirical relationships proposed by [30] and [31]. Meanwhile, for the clay soil, the correlations were based on [32] and [33]. The basic input parameters for the MC model can be seen in Table 1. These parameters consist of unsaturated and saturated unit weight (γ_{unsat} and γ_{sat}), cohesion (c), dilatancy angle (ψ), modulus of elasticity (E), and Poisson's ratio (v). Several parameters in MC were also used as input parameters for others.

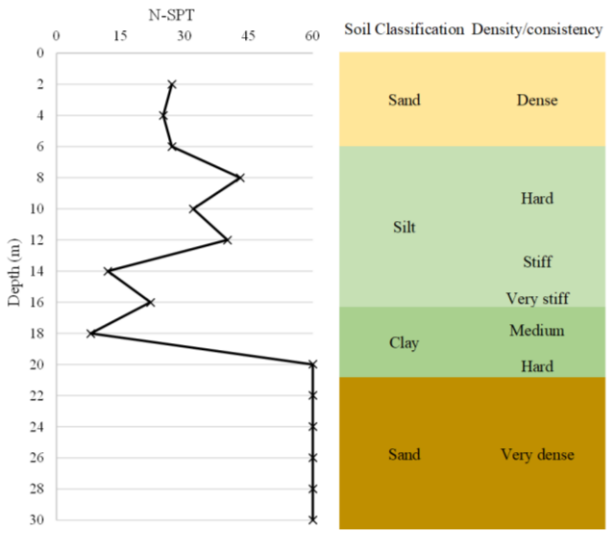

Figure 3. Soil stratigraphy in the study area

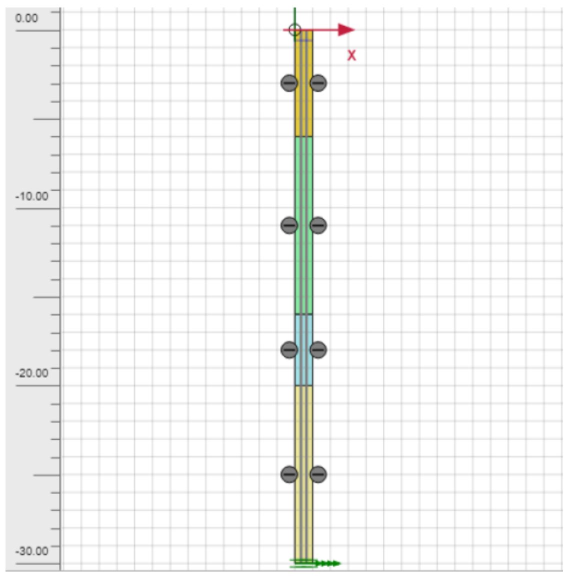

Figure 4. Soil stratigraphy in the study area

For *HSsmall*, the reference stiffness parameters ($E_{50\text{-}ref}$, $E_{oed\text{-}ref}$, $E_{ur\text{-}ref}$) were estimated using correlations with NSPT and overburden stress as suggested in [34]. The small-strain shear modulus $G_{o\text{-}ref}$ was defined based on estimated V_s.

For silt and clay layers, the *HSsmall* model was adopted under undrained conditions. Undrained shear strength was estimated from empirical SPT correlations [35], and stiffness parameters were adjusted to reflect stress-dependent behaviour. The basic input parameters for the HSsmall model are shown in Table 2. The input parameters include secant stiffness at 50% strength ($E_{50\text{-}ref}$), unloading/reloading stiffness ($E_{ur\text{-}ref}$), eodometer stiffness ($E_{oed\text{-}ref}$), small-strain shear modulus (G_{0ref}), reference shear strain ($\gamma_{0.7}$), and stress-dependency exponent (m).

For PM4Sand, this soil model is only used for the sandy soil, the cohesive layers were input as the HSsmall model. The input parameters were calibrated using relative density and the typical ranges recommended by Boulanger and Ziotopoulou [36]. The contraction rate parameter and fabric parameters were selected within recommended bounds for medium-dense to dense sand conditions, consistent with the measured NSPT values. The basic input parameters for the PM4Sand model can be seen in Table 3. The input parameters include relative density (Dr), shear modulus coefficient (G_0), contraction rate parameter (hp_0), minimum and maximum void ratios (e_{min} and e_{max}), critical state friction angle (φ_{cv}), dilatancy parameter (Q), and dilatancy surface parameter (R).

2.6 Liquefaction Assessment Parameters

Liquefaction potential was evaluated using time-dependent excess pore water pressure and pore pressure ratio (Ru). The pore pressure ratio was defined as (2).

$$R_u(t) = \frac{\Delta u(t)}{\sigma'_{v0}} \quad (2)$$

where $\Delta u(t)$ is the excess pore pressure at time t, and $\sigma'v0$ is the initial vertical effective stress obtained from the geostatic initial phase. This equation follows the effective stress principle and liquefaction framework, which states that liquefaction occurs when excess pore pressure approaches the initial effective vertical stress ($Ru \approx 1$). When Ru remains below 1, the soil does not reach liquefaction conditions. In cases where excess pore pressure becomes negative, the soil exhibits dilative behavior, reflected by a reduction in pore pressure during cyclic loading [37].

Table 1. Input parameters for Mohr-Coulomb

Layer	Sand (0–6m)	Silt (6–16m)	Clay (16–20m)	Sand (20–28m)
Model	Undrained (A)	Undrained (A)	Undrained (A)	Drained
γ_{unsat} (kN/m^3)	18	18	17.5	19
γ_{sat} (kN/m^3)	20	19.5	19	21
c' (kPa)	0	5	170	0
φ' (°)	35	33	0	43
ψ (°)	5	2	0	10
E (kPa)	79,000	90,000	43,000	180,000
ν	0.3	0.3	0.45	0.28

Table 2. Input parameters for Hardening Soil with small-strain stiffness

Layer	Sand (0–6m)	Silt (6–16m)	Clay (16–20m)	Sand (20–28m)
$E_{50\text{-ref}}$ (kPa)	79,000	90,000	43,000	180,000
$E_{ur\text{-ref}}$ (kPa)	237,000	270,000	129,000	540,000
$E_{oed\text{-ref}}$ (kPa)	79,000	90,000	43,000	180,000
G_{0ref} (kPa)	350,000	300,000	120,000	600,000
$\gamma_{0.7}$	0.0003	0.0004	0.0008	0.0002
m	0.5	0.6	1	0.5

Table 3. Input parameters for PM4Sand

Parameter	Sand (0–6m)	Sand (20–28m)
Dr	0.65	0.9
G_0	300	450
hp_0	0.55	0.4
e_{max}	0.8	0.7
e_{min}	0.5	0.45
φ_{cv} (°)	33	35
ν	0.3	0.3
Q	10	10
R	1.5	1.5

Additional response parameters evaluated include excess pore pressure evolution (Δu vs dynamic time). Representative evaluation depths were selected at 3 m, 11 m, 18 m, and 25 m to enable consistent comparison of model behaviour across layers.

3. Results and Discussion

3.1 Time-Dependent Excess Pore Pressure Response

The evolution of excess pore pressure (Δu) mostly showed a negative response in both the shallow and deep sand layers, particularly at 3 m and 25 m. This behaviour indicated a dilative behaviour. The relatively small magnitude of Δu across all depths suggests that full liquefaction conditions were not reached under the applied ground motion intensity. The results are shown in Figure 5 to Figure 8.

The excess pore pressure response (Δu) showed predominantly negative values in the sand layers, which are considered dense and very dense sand. This behaviour indicates dilative behaviour under cyclic loading. Dense sands subjected to moderate seismic excitation can develop negative pore pressures due to dilation effects, and the shear modulus decreases slowly. This behaviour enhances the undrained shear strength and reduces the likelihood of liquefaction.

Across all layers, this behaviour is commonly captured by PM4Sand, which showed a gradual development of a negative excess pore pressure of nearly -5,5 kPa at the end of dynamic loading. Even the excess pore pressure reached -18 kPa, indicating strong dilative behaviour due to the soil's stiffness. On the other hand, the other models present limited behaviour of the development of excess pore pressure.

For the cohesive layers (Figure 6 and Figure 7), the soil in the PM4Sand scenarios was still set to HSsmall. For the clay layer, especially, the response to excess pore pressure differs from that of the observed sandy layers. The MC model predicted a rapid drop of Δu at the beginning of dynamic time, in contrast, the HSsmall model, for both scenarios, produces a minor change in excess pore pressure. The MC model assumes purely elastic behavior before failure, which can lead to an overestimation of pore pressure fluctuations in cohesive soils. This is because the model does not account for pre-failure plastic deformations that can generate excess pore pressure under undrained conditions [38].

Furthermore, there is an inconsistency in the MC for modelling excess pore pressure in cohesive soil. This condition relates to the concept that MC cannot predict pore pressure generation. For the HSsmall, the behaviour difference occurred due to the main parameter, $\gamma 0.7$ and m. The silt layer has a smaller $\gamma 0.7$ value than the clay layer, thus its stiffness decreased faster and developed greater cyclic strain. This led to a larger Δu response than in the clay layer [39] to [40].

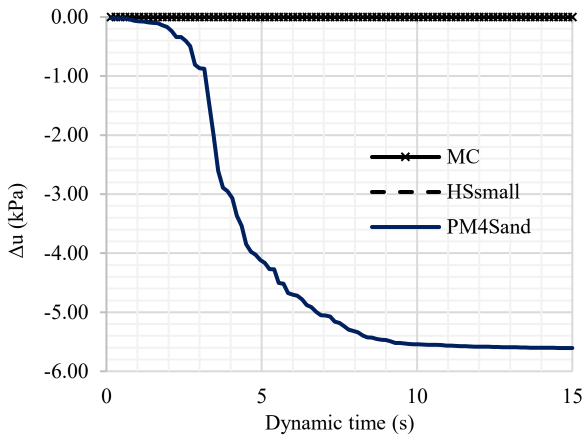

Figure 5. Δu vs Dynamic time for layer 1-Sand (3m-depth)

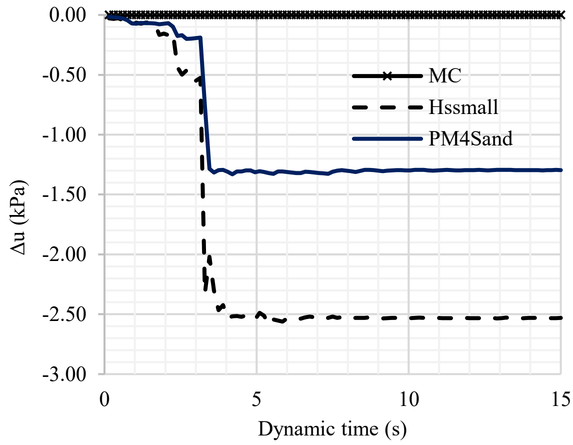

Figure 6. Δu vs Dynamic time for layer 2-Silt (11m-depth)

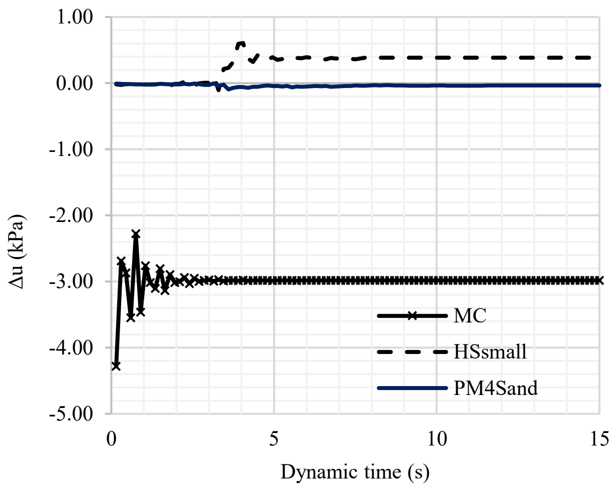

Figure 7. Δu vs Dynamic time for layer 3-Clay (18m-depth)

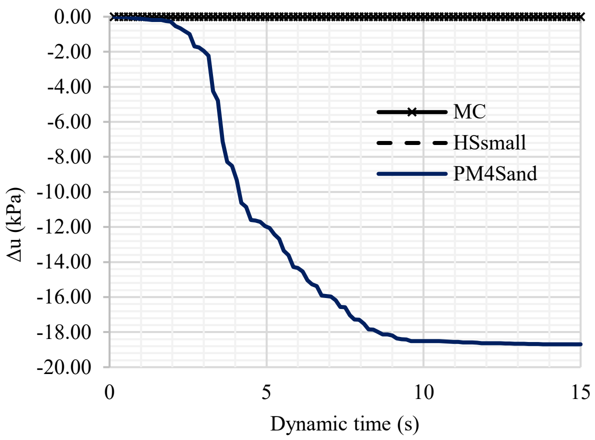

Figure 8. Δu vs Dynamic time for layer 4-Sand (25m-depth)

3.2 Generation of Pore Pressure Ratio (Ru)

Time-dependent evolution of *Ru* was used to demonstrate the liquefaction potential along the profile model under the applied ground motion of 0.31 g. In general, Ru values below 0.2 indicate that full liquefaction is not triggered under dynamic motion. In addition, *Δu* is negative in several layers, *Ru* appears positive in the PLAXIS output due to the compression-negative stress convention adopted in the software. Because both *Δu* and *σ'v0* are negative under compressive conditions, their ratio becomes positive. The results are shown in Figures 9 to Figure 12.

In the shallow sand layer (3 m), the PM4Sand model predicted an increase in *Ru* up to approximately 0.16, indicating moderate pore pressure accumulation under cyclic loading. A similar but lower trend is observed in the deeper sand layer (25 m), where *Ru* reached about 0.075. In contrast, using the HSsmall model, the silt layer (11 m) had limited *Ru* development, while the clay layer (18 m) showed minor fluctuations with relatively small *Ru* values throughout the shaking duration.

In the deep sand layer (25 m), *Ru* reached only around 0.07 under the PM4Sand model. Even though the excess pore pressure in Figure 7 is relatively large in absolute terms, the initial effective stress at greater depth will also reduce the pore pressure ratio. This result highlights that the liquefaction potential strongly depends on the confining stress level [41].

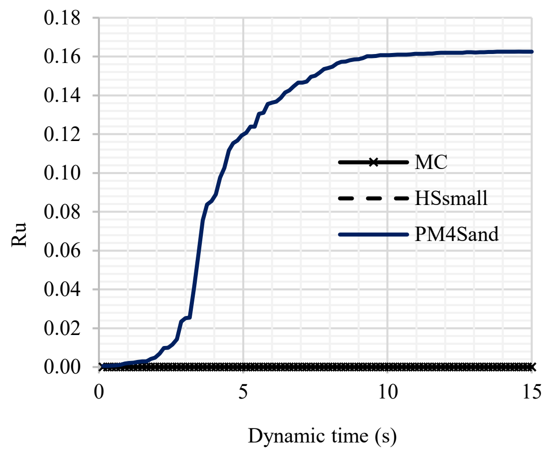

Figure 9. Ru vs Dynamic time for layer 1-Sand (3m-depth)

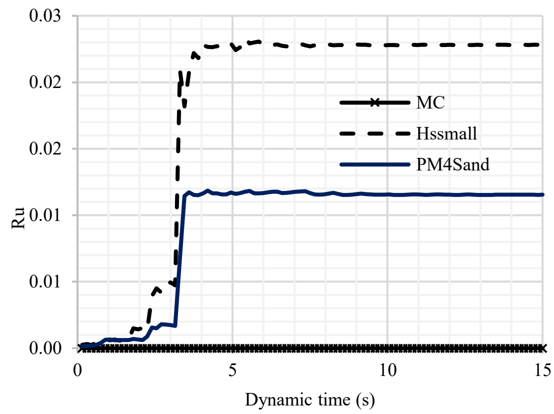

Figure 10. .Ru vs Dynamic time for Layer 2-Silt (11m-depth)

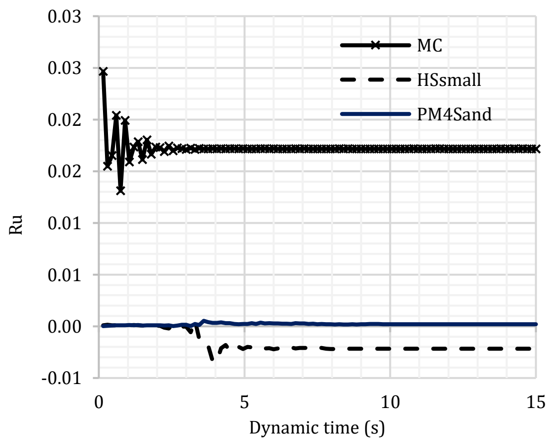

Figure 11. Ru vs Dynamic time for layer 3-Clay (18m-depth)

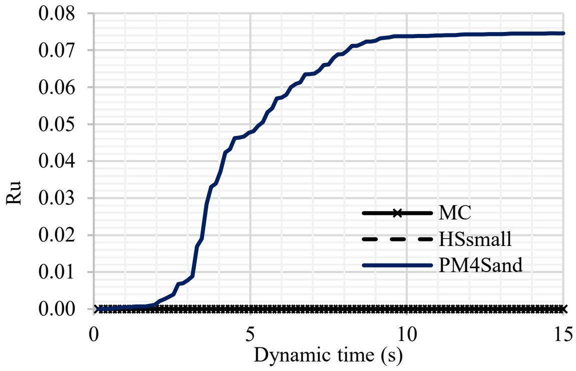

Figure 12. Ru vs Dynamic time for layer 4-Sand (25m-depth)

3.3 Depth Profile of Maximum Pore Pressure Ratio

The distribution of the maximum pore pressure ratio with depth is shown in Table 4. These results showed that MC only gave a small response or Ru at 18 m, confirming its inability to simulate cyclic pore pressure due to its elastic-perfectly plastic behaviour. HSsmall also has a limited response related to Ru and is not clearly captured. In contrast, the PM4Sand was predicted to be shallow and to exhibit a moderate response at greater depth.

Table 4. Distribution of maximum pore pressure ratio

Depth	Ru		
	MC	HSsmall	PM4Sand
3 m (Dense Sand)	0.0000	0.0000	0.1625
11 m (Silt)	0.0000	0.0228	0.0115
18 m (Clay)	0.0172	0.0000	0.0000
25 m (Very Dense sand)	0.0000	0.0000	0.0745

4. Conclusion

This study examined how different constitutive soil models influence the prediction of cyclic pore pressure response and liquefaction potential in Srandakan, Bantul, using one-dimensional dynamic analysis in PLAXIS 2D. Although the same ground motion input was applied in all simulations, the predicted pore pressure behavior varied significantly depending on the selected soil model.

The Mohr–Coulomb model produced almost no excess pore pressure accumulation, confirming that it is not suitable for liquefaction assessment under cyclic loading. The HSsmall model captured nonlinear stiffness effects but produced only limited pore pressure changes, particularly in cohesive layers, suggesting it cannot fully represent cyclic pore pressure buildup. In contrast, PM4Sand showed more pronounced pore pressure development in sandy layers, especially at shallow depth, reflecting its formulation for state-dependent cyclic plasticity.

However, the maximum pore pressure ratio (*Ru*) remained well below unity at all investigated depths, indicating that full liquefaction was not triggered under the applied seismic excitation. Overall, the results demonstrate that constitutive model selection plays a crucial role in liquefaction-oriented site response analysis, as it directly affects the predicted magnitude and distribution of cyclic pore pressure generation.

References

[1] H. Seo and D. Kim, "Analysis of behavioral characteristics of liquefaction of sand through repeated triaxial compression test and numerical analysis," *Geomech. Eng.*, vol. 38, no. 2, pp. 165–177, 2024, doi: 10.12989/gae.2024.38.2.165.

[2] A. Salahi, H. Niroumand, and K. A. Kassim, "Evaluation of stone columns versus liquefaction phenomenon," *Electron. J. Geotech. Eng.*, vol. 20, no. 2, pp. 739–759, 2015.

[3] H. B. Mason and H. Yeh, "Sediment liquefaction: A pore-water pressure gradient viewpoint," *Bull. Seismol. Soc. Am.*, vol. 106, no. 4, pp. 1908–1913, 2016, doi: 10.1785/0120150296.

[4] S. Smitha and S. M. Rangaswamy, "Effect of biopolymer treatment on pore pressure response and dynamic properties of silty sand," *J. Mater. Civ. Eng.*, vol. 32, no. 8, p. 04020217, 2020, doi: 10.1061/(ASCE)MT.1943-5533.0003285.

[5] E. National Academies of Sciences and Medicine *et al.*, *State of the Art and Practice in the Assessment of Earthquake-Induced Soil Liquefaction and Its Consequences*. Washington, DC: The National Academies Press, 2021. doi: 10.17226/23474.

[6] M. D. Petersen *et al.*, "Probabilistic seismic hazard analysis for Sumatra, Indonesia and across the Southern Malaysian Peninsula," *Tectonophysics*, 2004.

[7] M. D. Petersen *et al.*, "Probabilistic seismic hazard for Southeast Asia," in *Proc. Int. Conf. Earthquake Engineering and Disaster Mitigation*, Jakarta, Indonesia, 2008.

[8] M. Irsyam, M. Asrurifak, D. Hendriyawan, and B. Budiono, "Development of spectral hazard maps for a proposed revision of the Indonesian seismic building code," *Geomech. Geoengin.*, vol. 5, no. 1, pp. 35–47, 2010, doi: 10.1080/17486020903452725.

[9] M. Irsyam *et al.*, "The proposed seismic hazard maps of Sumatra and Java islands and microzonation study of Jakarta city, Indonesia," *J Earth Syst Sci*, vol. 117, no. S2, pp. 865–878, 2008.

[10] I. W. Sengara, M. Irsyam, I. D. Sidi, D. A. Andri Mulia, M. Asrurifak, and D. Hutabarat, "Development of earthquake risk-targeted ground motions for Indonesian earthquake resistance building code SNI 1726-2012," in *Proc. 12th Int. Conf. Applications of Statistics and Probability in Civil Engineering (ICASP12)*, Vancouver, Canada, 2015.

[11] R. L. Wood and T. C. Hutchinson, "Effects of ground motion scaling on nonlinear higher mode building response," *Earthq. Struct.*, vol. 3, no. 6, pp. 869–887, 2012.

[12] C. W. Jiang and D. B. Wang, "Effect of different modification methods on ground motions," in *Proc. Int. Conf. Advanced Materials, Structures and Mechanical Engineering*, 2016, pp. 125–130.

[13] D. Zekkos, C. Carlson, A. Nisar, and S. Ebert, "Effect of ground motion modification technique on seismic geotechnical engineering analyses," *Earthq. Spectra*, vol. 28, no. 4, pp. 1643–1661, 2012, doi: 10.1193/1.4000077.

[14] C. Carlson, D. Zekkos, A. Athanasopoulos-Zekkos, and J. Hubler, "Impact of modification on ground motion characteristics and geotechnical seismic analyses for a California site," *J. Earthq. Eng.*, vol. 18, no. 5, pp. 696–713, 2014, doi: 10.1080/13632469.2014.898602.

[15] A. Jalil, T. F. Fathani, I. Satyarno, and W. Wilopo, "A study on the liquefaction potential in Banda Aceh City after the 2004 Sumatera earthquake," *Int. J. GEOMATE*, vol. 18, no. 65, pp. 147–155, 2020, doi: 10.21660/2020.65.94557.

[16] R. A. C. Luna, R. D. Quebral, P. A. Y. Selda, F. J. T. Bernales, and S. B. R. Sayson, "Integrating local site response evaluations in seismic hazard assessments," in *Geotechnical, Geological and Earthquake Engineering*, 2022, pp. 792–800. doi: 10.1007/978-3-031-11898-2_53.

[17] D. Huang and J. P. Wang, "Integrating seismic hazard analyses with geotechnical site characterization for liquefaction potential assessment in Kaohsiung area," in *Proc. 4th Int. Symp. Geotechnical Safety and Risk (ISGSR 2013)*, 2014, pp. 201–206.

[18] T. G. Sitharam and L. Govindaraju, "Pore pressure generation in silty sands during cyclic loading," *Geomech. Geoengin.*, vol. 2, no. 4, pp. 295–306, 2007, doi: 10.1080/17486020701670460.

[19] S. Mandal, D. Mistry, and G. R. Dodagoudar, "Finite element analysis of response of earthen embankment constructed on liquefiable soil deposit," in *Lecture Notes in Civil Engineering*, 2025, pp. 107–119. doi: 10.1007/978-981-96-7285-1_8.

[20] G. Zorzi, T. Richter, F. Kirsch, A. H. Augustesen, M. U. Østergaard, and S. P. H. Sørensen, "Explicit method to account for cyclic degradation of offshore wind turbine foundations using cyclic interaction diagrams," in *Proc. Int. Offshore and Polar Engineering Conf.*, 2018, pp. 327–333.

[21] Z. Cheng and B. Damjanac, "Extension of Mohr-Coulomb model considering opening and closure of tension cracks," in *Proc. 55th U.S. Rock Mechanics / Geomechanics Symp.*, 2021, pp. 577–585.

[22] S. Chen, T. Li, F. Liang, and X. Gu, "Parameters of hardening soil model with small strain of shallow sandy silt in Shanghai Lin-Gang Special Area," *J. Tongji Univ.*, vol. 48, no. 6, pp. 841–846, 2020, doi: 10.11908/j.issn.0253-374x.19374.

[23] N. Dinesh, S. Banerjee, and K. Rajagopal, "Performance evaluation of PM4Sand model for simulation of the liquefaction remedial measures for embankment," *Soil Dyn. Earthq. Eng.*, vol. 152, 2022, doi: 10.1016/j.soildyn.2021.107042.

[24] B. Gutenberg and C. F. Richter, "Frequency of earthquakes in California," *Bull. Seismol. Soc. Am.*, vol. 34, no. 4, pp. 185–188, 1944.

[25] K. W. Campbell, "A note on the selection of minimum magnitude for use in seismic hazard analysis," *Bull. Seismol. Soc. Am.*, vol. 79, no. 1, pp. 199–204, 1989, doi: 10.1785/BSSA0790010199.

[26] Google LLC, *Google Earth, version 7.x*. (2026). [Online]. Available: https://earth.google.com/

[27] R. R. Youngs and K. J. Coppersmith, "Implications of fault slip rates and earthquake recurrence models to probabilistic seismic hazard estimates," *Bull. Seismol. Soc. Am.*, vol. 75, no. 4, pp. 939–964, 1985.

[28] R. K. McGuire, *EZ Frisk Versions 7 manual*. Risk Engineering Inc., 2005.

[29] T. Tobita and J. P. Bardet, *A Computer Program for Non-Linear Earthquake Site Response Analysis (NERA) of Layered Soil Deposit*. Los Angeles, CA, USA: Department of Civil Engineering, University of Southern California, 2001.

[30] R. B. Peck, W. E. Hanson, and T. H. Thornburn, *Foundation Engineering*, 2nd ed. New York: John Wiley & Sons, 1974.

[31] B. M. Das and K. Sobhan, *Principles of Geotechnical Engineering*, 9th ed. Boston: Cengage Learning, 2018.

[32] F. H. Kulhawy and P. W. Mayne, *Manual on Estimating Soil Properties for Foundation Design*. Ithaca, NY, USA: Electric Power Research Institute (EPRI), 1990.

[33] D. P. Stroud, "The standard penetration test in insensitive clays and soft rocks," in *Proc. European Symposium on Penetration Testing (ESOPT I)*, Stockholm, Sweden, 1974, pp. 367–375.

[34] PLAXIS BV, *PLAXIS 2D Reference Manual*. Bentley Systems, 2023.

[35] B. M. Das, *Principles of Geotechnical Engineering*, 8th ed. Boston: Cengage Learning, 2014.

[36] R. W. Boulanger and K. Ziotopoulou, *PM4Sand (Version 3): A Sand Plasticity Model for Earthquake Engineering Applications*. Davis: University of California, 2017.

[37] S. L. Kramer, *Geotechnical Earthquake Engineering*. New Jersey: Prentice Hall, 1996.

[38] W. Dong and G. Anagnostou, "The effect of constitutive modelling on estimates of the short-term response of squeezing ground to tunnel excavation," in *Computer Methods and Recent Advances in Geomechanics: Proc. 14th Int. Conf. (IACMAG 2014)*, 2015, pp. 225–230. doi: 10.1201/b17435-36.

[39] S. Likitlersuang, S. Teachavorasinskun, C. Surarak, E. Oh, and A. Balasubramaniam, "Excess pore water pressure behavior of saturated soft clay under cyclic confining pressure with different frequencies," *Soils Found.*, vol. 53, no. 4, pp. 498–509, 2013, doi: 10.1016/j.sandf.2013.06.003.

[40] J. Huang, J. Hu, H. Wang, J. Chen, and S. Liu, "Excess pore water pressure behavior of saturated soft clay under cyclic confining pressure with different frequencies," *Front. Earth Sci.*, vol. 10, 2023, doi: 10.3389/feart.2022.1035889.

[41] G. Suazo, A. Fourie, J. Doherty, and A. Hasan, "Effects of confining stress, density and initial static shear stress on the cyclic shear response of fine-grained unclassified tailings," *Geotechnique*, vol. 66, no. 5, pp. 401–412, 2016, doi: 10.1680/jgeot.15.P.032.

E-ISSN: 2528-388X
P-ISSN: 0213-762X

INERSIA
Vol.22, No.1, May 2026

Analysis of Spatial Interpolation Method for Rainfall Mapping of Hydrometeorological Disaster Mitigation Design in Denpasar, Bali

Tri Hayatining Pamungkas[1]*, Gede Sumarda[1], I Gusti Made Sudika[1], I Gusti Ngurah Eka Partama[1], I Ketut Kembarejaya[1] and Kadek Budhi Warsana[2]

[1] Civil Engineering Program, Universitas Ngurah Rai, Denpasar 80238, Indonesia
[2] Bali Penida River Basin Center, Denpasar 80235, Indonesia

Keywords:
Rainfall
Hydrometeorological hazards
Inverse Distance Weighting
Kriging
Spline

ABSTRACT

Climate change and rapid urbanization are increasing the intensity and uncertainty of rainfall in urban areas, including Denpasar City. The transition from the dry season to the rainy season is often followed by extreme rainfall that triggers floods, disrupts community activities, damages infrastructure, and significantly hinders economic activities. This condition is exacerbated by massive land conversion and the accumulation of waste that clogs drainage systems, leading to a drastic decrease in surface water holding capacity. Therefore, hydrometeorological disaster mitigation has become an urgent need, which must be supported by accurate and reliable spatial rainfall information to identify vulnerable areas and design more effective flood control strategies. This study evaluates and compares the spatial interpolation methods of Inverse Distance Weighting (IDW), Kriging, and Spline in mapping the distribution of design rainfall in Denpasar City. Data were obtained from six stations over the period 2013–2022 and analyzed based on various return periods, namely 2, 5, 10, 15, 20, 25, and 50 year. To comprehensively assess the performance of interpolation methods, statistical indicators such as Mean Absolute Error (MAE), Mean Absolute Percentage Error (MAPE), Root Mean Squared Error (RMSE), and Coefficient of Determination (R^2) were used. The results show that IDW is most accurate for short return periods, particularly 2 year, with low MAE, MAPE, and RMSE and high R^2. Kriging excels for medium to long return periods (5–50 years), producing stable predictions that closely match the observed data, while Spline tends to have higher errors and low R^2, especially for long return periods. This result confirms that IDW and Kriging are the most reliable and accurate methods for mapping the distribution of design rainfall in Denpasar City.

1. Introduction

The transition from the dry season to the rainy season in Indonesia is marked by increasingly extreme and unpredictable rainfall patterns. The Meteorology, Climatology, and Geophysics Agency (BMKG) reports that heavy to very heavy rains pose a significant threat in several regions, including Bali [1]. One of the most striking events occurred on September 9–10, 2025, when extreme rainfall triggered massive flooding in various areas. According to records from the Bali Provincial Disaster Management Agency (BPBD) [2]. More than 120 flood points were recorded in Bali, with 81 of them in Denpasar City, making it the area with the greatest impact. [3].

The floods that hit Denpasar not only disrupted community activities, but also damaged infrastructure and hampered economic activity. Extreme rainfall intensity was the primary factor causing the floods [4], [5], However, the condition is further exacerbated by massive land conversion and the accumulation of waste that clogs drainage channels, so that the surface water capacity decreases [6] – [8]. This situation emphasizes that high-density cities are highly vulnerable to hydrometeorological disasters [9]. Therefore, mitigation

*Corresponding author.
E-mail: tri.hayatining@unr.ac.id

https://doi.org/10.21831/inersia.v21i2.90147
Received 01 October 2025; Revised 1 March 2026; Accepted 13 April 2026
Available online 01 May 2026

measures are urgently needed, and one important initial step is mapping rainfall distribution [10], [11]. Spatial rainfall information is essential for identifying vulnerable areas, designing more effective flood control systems, and allocating mitigation resources appropriately [12] – [14].

Efforts to understand the spatial distribution of rainfall can be done with the help of geographic information systems (GIS) through the interpolation process, with the most commonly used methods being Inverse Distance Weighting (IDW), Kriging, and Spline [15] – [18]. Previous research has applied each method in various locations, such as mapping rainfall distribution with IDW in Kediri Regency [19], Kriging in the Kali Lamong watershed [20], and Spline in Jakarta City [21]. Several studies have compared spatial interpolation methods for rainfall mapping. In areas with a limited number of rainfall stations, such as Pontianak, the IDW method provides more accurate interpolation results. Spline produces a smooth surface through several points, and Kriging requires a strict assumption of spatial homogeneity [16]. A study on the Abab Sub-watershed, Blitar Regency showed that IDW and Spline had high agreement with field data, while Kriging produced larger errors as the return period increased, so IDW was chosen for design rainfall mapping [18]. In the Upper Brantas Sub-DAS, the IDW method showed the highest accuracy, characterized by the smallest RMSE, very good NSE, and a very strong

Correlation Coefficient [17]. Research in North Sumatra shows that the Spline method provides the best performance, with the lowest RMSE and MAE values and smooth interpolation through station points [22]. Based on these findings, a comparative analysis of interpolation methods is important because their effectiveness is highly dependent on the specific conditions of each region. However, research that comparatively assesses interpolation methods in the context of Denpasar City, a densely populated urban area prone to hydrometeorological disasters, remains limited. This study does not only compare interpolation methods, but also integrates rainfall spatial modeling into hydrometeorological disaster mitigation planning in an urban tropical environment, specifically Denpasar City, which has unique rainfall variability and rapid urbanization. In this context, the study evaluates and compares the performance of IDW, Kriging, and Spline methods to determine the most appropriate interpolation approach for the spatial characteristics of Denpasar. Furthermore, this research contributes not only methodologically but also practically by providing a scientific basis for rainfall mapping that can support decision-making in hydrometeorological disaster mitigation, particularly flood risk management in urban areas. The results are expected to serve as a reference for both researchers and policymakers in developing more adaptive and spatially informed mitigation strategies.

2. Methods

This study uses a descriptive quantitative method with a comparative approach to analyze rainfall distribution in Denpasar City, Bali. This approach involves collecting daily rainfall data from rainfall stations in the study area, followed by calculating design rainfall for various return periods. The calculation results are then processed using three spatial interpolation methods, namely Inverse Distance Weighting (IDW), Kriging, and Spline, to produce a rainfall distribution map. The final stage of the study is to conduct a comparative analysis of the three interpolation methods, using observation data from each rainfall station as a validation reference. This analysis aims to evaluate the accuracy, advantages, and limitations of each method, and determine the most appropriate approach based on the climate conditions and spatial characteristics of Denpasar City.

2.1 Research Location

This research was conducted in Denpasar City, Bali Province, as shown in Figure 1. Denpasar City, as the capital of Bali Province, is an urban area with a high population density. Geographically, Denpasar City is located between coordinates 8°35'31" to 8°44'49" South Latitude and 115°00'23" to 115°16'27" East Longitude. Denpasar City is often affected by flooding due to extreme rainfall and limited urban drainage systems [23]. This condition makes the city relevant as a research location for mapping the distribution of design rainfall, to support more effective flood mitigation planning.

2.2 Research Data

This study uses maximum daily rainfall data from six stations in Denpasar City: Buagan Station, Penatih Station, Ubung Station, Sumerta Station, Sanglah Station, and Suwung Station. The data covers the period 2013–2022 and was obtained from the Bali Penida River Basin Center and the Denpasar Region III Meteorology, Climatology, and Geophysics Office. In addition to rainfall data, this study also uses spatial data, in the form of an administrative map of Denpasar City and a map of the distribution of rainfall stations, obtained from the Tanah Air Indonesia Web portal. Figure 2 shows the distribution of rainfall stations in Denpasar City.

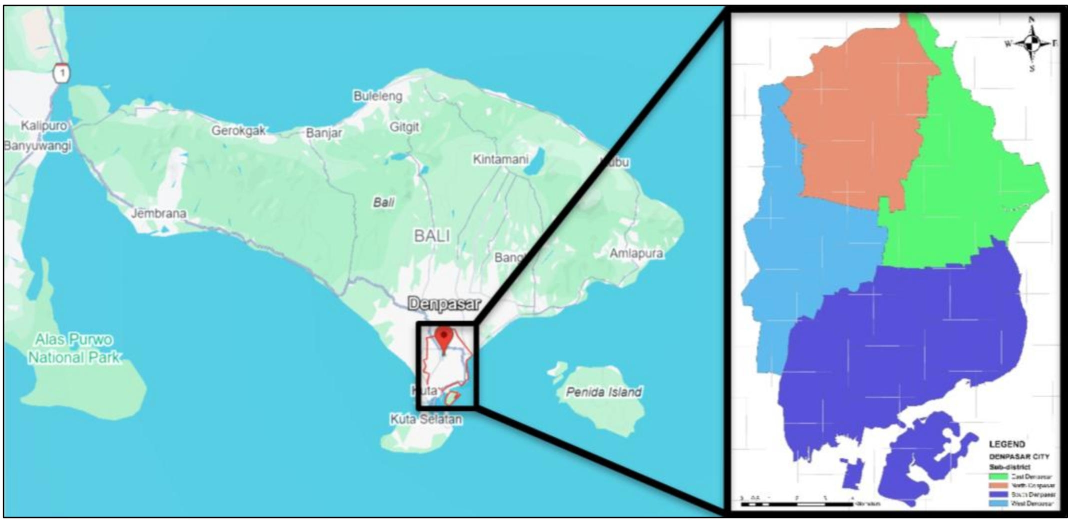

Figure 1. Research Location

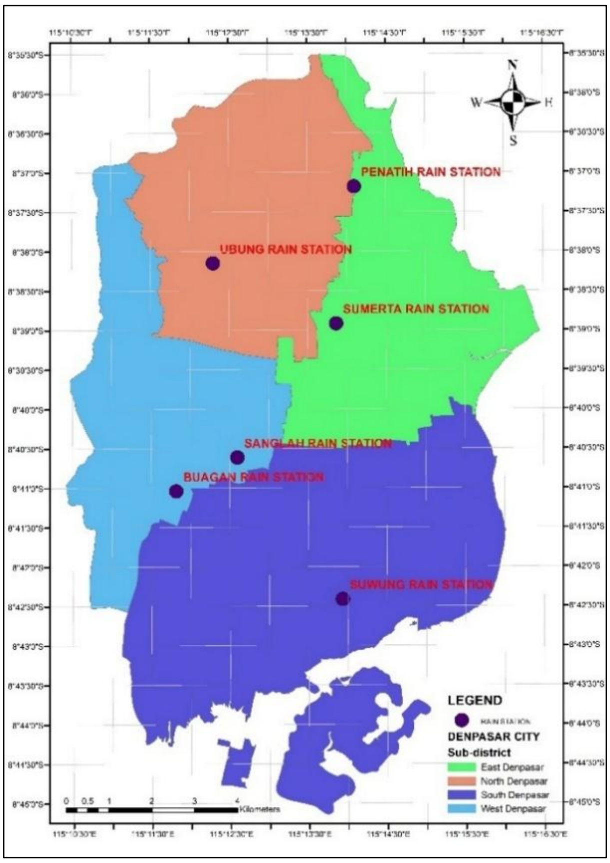

Figure 2. Distribution of rainfall stations in Denpasar City

2.3 Data Consistency Test

To obtain valid rainfall data, a data consistency test is required to ensure that the data used comes from a uniform population and is not influenced by recording errors or other non-climatic factors [24], [25]. The method used in this study is Rescaled Adjusted Partial Sums (RAPS). This method is based on testing the cumulative deviation of data against the average value, which is then normalized by the standard deviation to obtain a measure of data consistency [26], [27]. The RAPS calculation formula is presented in Equations (1) to (4).

$$So^* = 0 \tag{1}$$

$$Sk^* = \sum_{i=1}^{k}(Yi - \overline{Y}) \text{ , with } k = 1, 2, 3, n \tag{2}$$

$$Sk^{**} = \frac{Sk^*}{Dy} \tag{3}$$

$$Dy^2 = \sum_{i=1}^{n} \frac{|Sk^*|^2}{n} \tag{4}$$

Where *So** is the initial deviation value, *Sk** is the cumulative deviation, *Sk*** is the data consistency value, *Yi* is the i-th rainfall data, $\overline{Y}$ is the average rainfall data, *Dy* is the standard deviation, and n is the number of data.

For the consistency test, Equations (5) and (6) are used.

$$Q = \text{Maks } |Sk^{**}| \text{ , with } 0 \le k \le n \tag{5}$$

$$R = \text{Maks } |Sk^{**}| - \text{Min } |Sk^{**}| \tag{6}$$

With the provision that for a data set of 10 and a confidence level of 90%, the *Q/n^0.5* value must not exceed 1.05. Meanwhile, the *R/n^0.5* value must not exceed 1.21 [27].

2.4 Design Rainfall Analysis

Design rainfall is defined as the ideal rainfall intensity determined statistically based on a certain return period, so that it can represent extreme rainfall conditions that could potentially occur in the future [28], [29]. To analyze design rainfall, there are several frequency distribution methods commonly used in hydrology, namely the Normal Distribution, Log Normal Distribution, Gumbel Distribution, and Log Pearson Type III Distribution. In this study, the frequency distribution analysis used is the Log Pearson III method, which is further explained through the following steps [30]:

a. Convert the data to logarithmic form according to Equation (7).

$$X = logX \tag{7}$$

b. Calculate the logarithmic mean using Equation (8).

$$log\bar{X} = \frac{\sum_{i=1}^{n} log\, Xi}{n} \tag{8}$$

c. Determine the standard deviation according to Equation (9).

$$S = \frac{\sqrt{\sum_{i=1}^{n}(Log\, Xi - X)^{\bar{2}}}}{(n-1)} \tag{9}$$

d. Calculate the skewness coefficient using Equation (10).

$$Cs = \frac{n.\sum_{i=1}^{n}(Log\, Xi - X)^3}{(n-1)(n-2)S^3} \tag{10}$$

Where in the calculation, X_T indicates rainfall for the period *"T"* years, n is the number of years of observation, S is the standard deviation, $\bar{X}$ is the average rainfall, Xi is the maximum rainfall each year, and Cs is the skewness coefficient.

2.5 Spatial Interpolation of Rainfall Distribution

Spatial interpolation is a technique for estimating rainfall values at points where measurements have not yet been taken, by utilizing information from surrounding observation points [31]. This method allows for more comprehensive and accurate mapping of rainfall distribution, thus supporting hydrological analysis, drainage planning, and water resource management. Rainfall estimates in ungauged areas are generally performed using several interpolation methods, including Inverse Distance Weighting (IDW), Kriging, and Spline [15], [22], [32].

Inverse Distance Weighting (IDW) is a spatial interpolation method used to estimate values at a location by utilizing data from surrounding observation points [16], [33]. In this method, the influence of each observation point decreases as the distance to the target location increases. IDW is capable of producing quite detailed interpolation surfaces, especially when the observation points are evenly distributed. However, this method has limitations: the interpolation value cannot exceed the maximum value or fall below the minimum value of the observation data [20]. The IDW method is calculated based on Equations (11) and (12).

$$F(z_x) = \sum_{i=1}^{n} w_i . z_i \tag{11}$$

$$w_i(x) = \frac{\left[\frac{1}{d}\right]^p}{\sum_{i=1}^{n}\left[\frac{1}{d}\right]^p} \tag{12}$$

With n being the number of observation points, i and j being the number of observation points, w_i being the weighting factor, d being the distance between observation points and p being the power of the weight.

Kriging is a spatial interpolation method that estimates values at a location by utilizing measured values in the surrounding area through weighting [34], [35]. The determination of weights is based on the distance between the observation point and the predicted location, and takes into account the spatial structure in the form of autocorrelation between points [22]. The general Ordinary Kriging model is stated in Equation (13). Next, assuming a constant mean value and random errors that have spatial dependence, the predictor is obtained through a weighted summation of the measured data, as shown in Equation (14).

$$z(s) = m + e(s) \tag{13}$$

$$\hat{z}(s_0) = \sum_{i=1}^{n} \lambda_i * z(s_i) \tag{14}$$

Where $z(s_i)$ is the measured value at the *i-th* location, λi is the unknown weight for the measured value at the *i-th* location, s_0 is the predicted location, and n is the number of measured values.

The Spline method is an interpolation technique that aims to produce a smooth surface by minimizing the curvature of the curve, so that the estimated values pass through the sample points accurately. This method is able to predict extreme values, both minimum and maximum, by considering the effects of data distribution, and still produces a precise surface estimate even with limited available data [35]–[37]. The basic principle of interpolation using the Spline method is shown in Equation (15).

$$S(x, y) = T(x, y) + \sum_{i=1}^{n} \lambda_i . R(r)_i \tag{15}$$

Where n represents the number of observation points, λi are the coefficients obtained from the linear system, and ri is the distance between two points (x,y). The notations $T(x,y)$ and r have different interpretations depending on the selection method used.

2.6 Mapping of Design Rainfall Distribution

Mapping of the design rainfall distribution was carried out by applying the IDW, Kriging, and Spline spatial interpolation methods using a Geographic Information System through the ArcGIS application, with work procedures that include the following stages:

a. Open a new worksheet in ArcGIS.
b. Enter 10-year average daily maximum rainfall data for the entire Denpasar City area
c. Add an administrative map and basemap layer to the application.
d. Conduct spatial analysis using IDW, Kriging, and Spline methods.
e. Set data classification and map symbology display.
f. Add labels to the attribute table.
g. Create a map layout for presentation.
h. Export the analyzed map as a JPEG image.

2.7 Evaluation of Rainfall Interpolation Results

Interpolation results are evaluated to assess the accuracy and reliability of the design rainfall distribution estimates. This process involves comparing rainfall values estimated by the IDW, Kriging, and Spline methods with actual observation data at each rainfall station [22]. Some statistical indicators commonly used in model performance evaluation include Mean Absolute Error (*MAE*), Mean Absolute Percentage Error (*MAPE*), Root Mean Square Error (*RMSE*) and Coefficient of Determination (R^2) [38], [39], with calculations referring to Equations (16) to Equation (19).

$$MAE = \frac{1}{n}\sum_{i=1}^{n}|Xi.Yi| \quad (16)$$

$$\mathrm{MARE} = \frac{1}{n}\sum_{i=1}^{n}\left|\frac{\mathrm{Yi.Xi}}{\mathrm{Yi}}\right| \quad (17)$$

$$\mathrm{RMSE} = \sqrt{\frac{1}{n}\sum_{i=1}^{n}(\mathrm{Xi.Yi})^2} \quad (18)$$

$$\mathrm{R}^2 = 1 - \frac{\sum_{i=1}^{n}(xi.Yi)^2}{\sum_{i=1}^{n}(\bar{Y}.Yi)^2} \quad (19)$$

Where *Xi* is the observation data, *Yi* is the estimation/interpolation result, $\bar{X}$ is the average of all observation data, and n is the total number of data points or observations. The MAE, RMSE, and MAPE values can be interpreted based on the ranges shown in Table 1, while the R^2 value can be interpreted according to the ranges in Table 2, as an indicator of the model's accuracy in representing real data [40].

Table 1. Interpretation of MAE, MAPE, and RMSE values

Range of values	Interpretation
< 10	High level of prediction
10 – 20	Acceptable prediction
20 – 50	Tolerable prediction
> 50	Unacceptable prediction

Table 2. Interpretation of R^2 values

Range of values	Interpretation
0	No correlation
0 < R2 ≤ 0.25	Very weak correlation
0.25 < R2 ≤ 0.50	Fair correlation
0.50 < R2 ≤ 0.75	Strong correlation
0.75 < R2 ≤ 0.99	Very strong correlation
1.00	Perfect correlation

3. Results and Discussion

3.1 Rescaled Adjusted Partial Sums (RAPS) Test

The results of the RAPS test on rainfall data from six stations in Denpasar City during the 2013–2022 period are presented in Table 3. The statistical values show that the data is relatively consistent and there is no significant trend, so it can be used for further analysis.

Table 3. RAPS Test Results

Station name	RAPS Test					
	Q_{count}	Q_{table}	Information	R_{count}	R_{table}	Information
Buagan Station	0.41	1.05	Consistent	1.13	1.21	Consistent
Penatih Station	0.58	1.05	Consistent	1.11	1.21	Consistent
Ubung Station	0.56	1.05	Consistent	0.88	1.21	Consistent
Sumerta Station	0.53	1.05	Consistent	0.95	1.21	Consistent
Sanglah Station	0.68	1.05	Consistent	0.12	1.21	Consistent
Suwung Station	0.34	1.05	Consistent	0.32	1.21	Consistent

3.2 Design Rainfall

Design rainfall was obtained from processing daily rainfall data for the 2013–2022 period at six rainfall stations in Denpasar City using the Log Pearson Type III method. This method is used to calculate extreme rainfall at several return periods: 2, 5, 10, 15, 20, 25, and 50 years. The results of the design rainfall calculations for each return period are presented in Table 4.

3.3 Design Rain Distribution Mapping

Based on the design rainfall values at each station for each return period, an interpolation analysis was performed to map the distribution of rainfall in the Denpasar City area. This analysis was conducted to accurately depict spatial variations in rainfall and provide information that can be used as a basis for hydrological planning and flood mitigation strategies. The map presentation focuses on the 2-year return period, as shown in Figure 3, Figure 4, and Figure 5, which show the results of interpolation using the IDW, Kriging, and Spline methods, respectively.

Table 4. Design rainfall for 2-50 yr return period in Denpasar City

Station name	Design rainfall (mm)						
	2-yr	5-yr	10-yr	15-yr	20-yr	25-yr	50-yr
Buagan	129	185	228	244	262	281	337
Penatih	119	158	184	194	205	217	240
Ubung	118	147	1601	166	170	175	184
Sumerta	133	168	187	194	200	207	220
Sanglah	118	154	154	184	192	201	219
Suwung	90	104	112	115	118	121	126

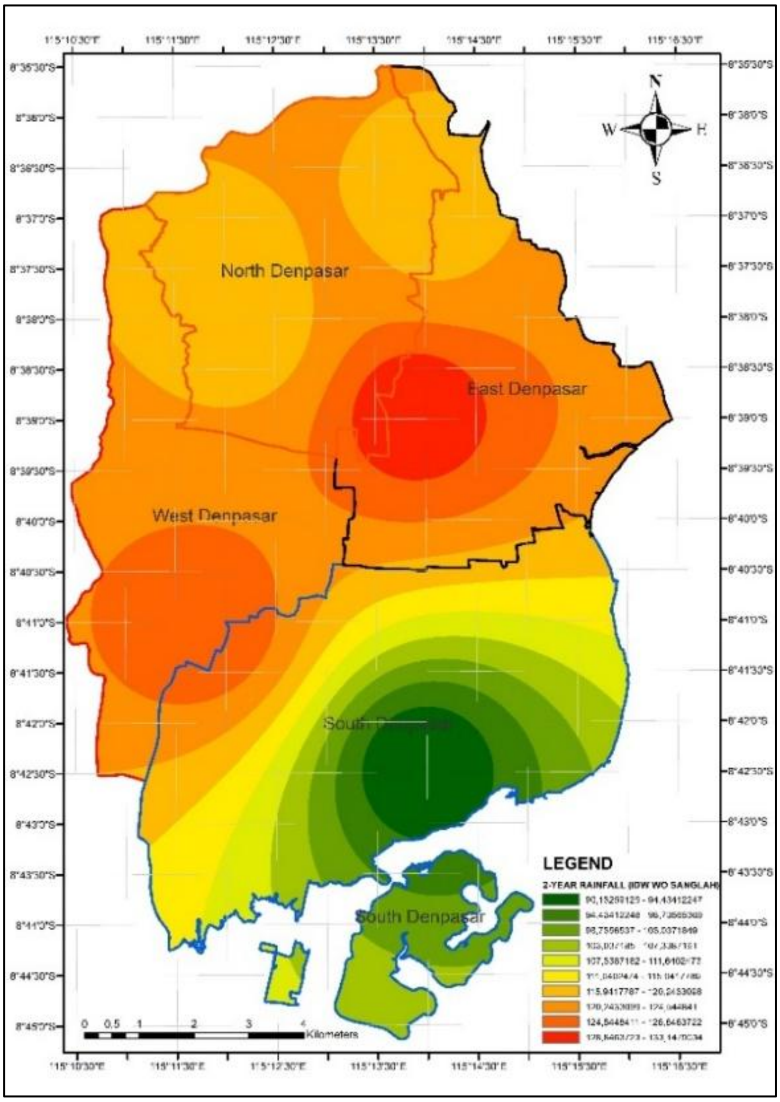

Figure 3. Map of rainfall distribution with a 2-year return period in Denpasar City using the IDW method

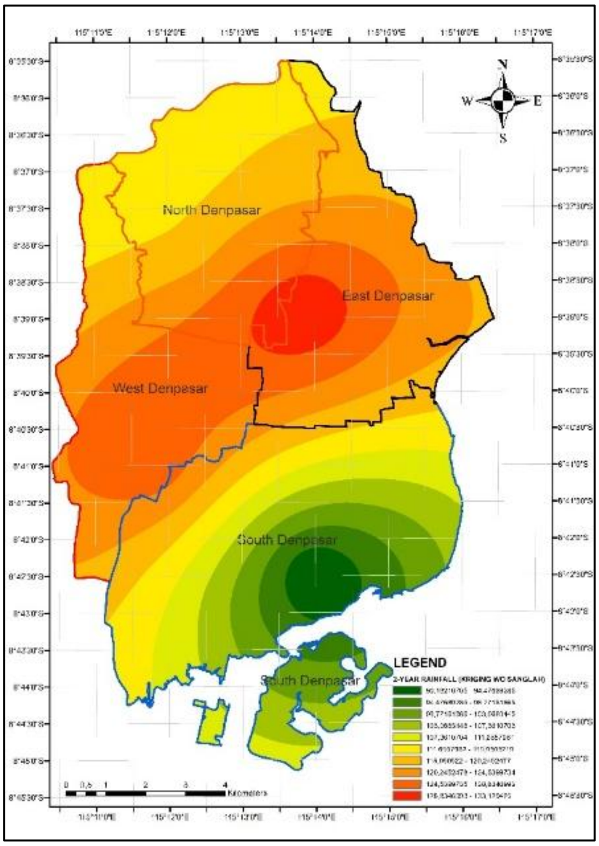

Figure 4. Map of rainfall distribution with a 2-year return period in Denpasar City using the Kriging method

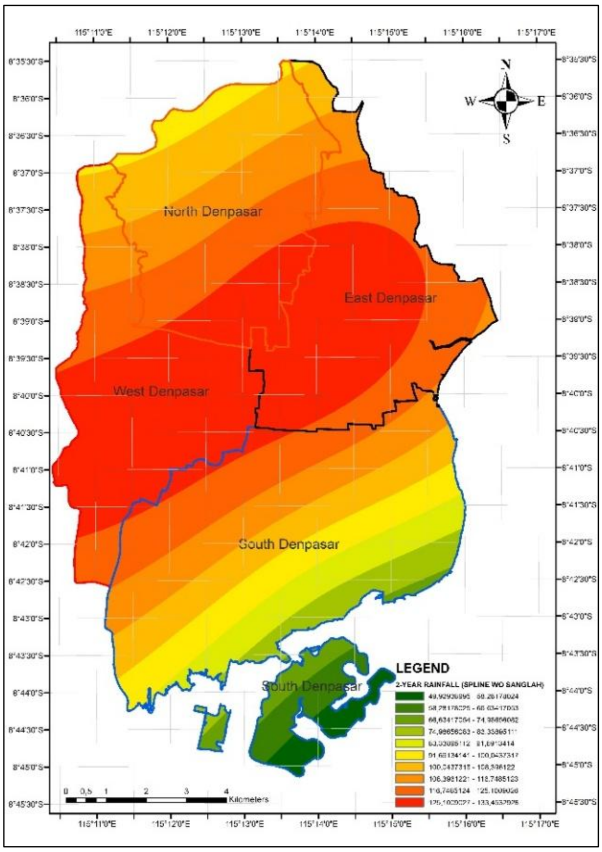

Figure 5. Map of rainfall distribution with a 2-year return period in Denpasar City using the Spline method

Table 5. Mean Absolute Error (MAE) value of the design rainfall interpolation results

Method	Return Period						
	2 yr	5 yr	10 yr	15 yr	20 yr	25 yr	50 yr
IDW	12.888	23.736	39.262	39.634	44.797	50.082	66.660
Kriging	13.283	23.478	37.740	38.356	42.857	48.613	59.146
Spline	22.433	37.707	55.679	57.297	62.753	68.628	88.806

3.1 Performance Comparison of Design Rainfall Interpolation Methods

To evaluate the performance differences between interpolation methods in mapping the design rainfall distribution, a comparative analysis was conducted based on several relevant statistical indicators, namely Mean Absolute Error (*MAE*), Mean Absolute Percentage Error (*MAPE*), Root Mean Squared Error (*RMSE*), and R^2. This analysis aims to assess how well each method is able to represent the observation data and to determine the most effective method in describing the spatial variation of rainfall in the Denpasar City area. The evaluation results of each indicator are presented in Table 5 for MAE, Table 6 for MAPE, Table 7 for RMSE, and Table 8 for R^2.

Based on Table 5, the Mean Absolute Error (*MAE*) value shows that Kriging has the lowest average error at most return periods, ranging from 13.283 mm at the 2 year return period to 59.146 mm at the 50 year return period. The IDW MAE value is slightly above Kriging, ranging from 12.888 mm at 2 year to 66.660 mm at 50 year. Meanwhile, Spline shows the highest MAE value, ranging from 22.433 mm at 2 year to 88.806 mm at 50 year, indicating a relatively less accurate estimate compared to the other two methods.

Table 6. Mean Absolute Percentage Error (*MAPE*) values from design rainfall interpolation results

Method	Return Period						
	2 yr	5 yr	10 yr	15 yr	20 yr	25 yr	50 yr
IDW	11.944%	17.797%	26.113%	24.983%	27.035%	28.938%	34.636%
Kriging	12.195%	17.379%	24.754%	23.822%	25.516%	27.603%	30.386%
Spline	19.840%	26.979%	35.834%	35.476%	37.529%	39.661%	46.811%

Table 7. Root Mean Square Error (*RMSE*) value of the design rainfall interpolation results

Method	Return Period						
	2 yr	5 yr	10 yr	15 yr	20 yr	25 yr	50 yr
IDW	16.364	30.726	46.783	48.685	54.820	61.117	81.906
Kriging	17.231	30.591	45.364	47.531	53.157	60.347	79.042
Spline	23.601	40.744	59.820	64.567	71.571	79.384	102.224

Table 8. Coefficient of Determination (R^2) values for the interpolated rainfall data

Method	Return Period						
	2 yr	5 yr	2 yr	15 yr	2 yr	25 yr	2 yr
IDW	0.937	0.915	0.885	0.873	0.864	0.858	0.833
Kriging	0.887	0.905	0.896	0.886	0.883	0.861	0.929
Spline	0.030	0.336	0.263	0.238	0.239	0.231	0.205

Analysis of the Mean Absolute Percentage Error (*MAPE*) values in Table 6 shows a similar trend to MAE. Kriging produces the smallest percentage error, ranging from 12.195% at 2 yr return periods to 30.386% at 50 yr. IDW has a slightly lower MAPE value at short return periods (11.944% for 2 yr) but increases to 34.636% at 50 yr. Spline has the highest MAPE, ranging from 19.840% to 46.811%, confirming that this method is less precise.

Table 7 shows the Root Mean Squared Error (*RMSE*) values, where Kriging and IDW have lower RMSE than Spline. Kriging has an RMSE of 17.231 mm at a 2yr return period and 79.042 mm at 50 yr, while IDW is slightly higher, ranging from 16.364 mm to 81.906 mm. Spline shows the highest RMSE, ranging from 23.601 mm at 2 yr to 102.224 mm at 50 yr, indicating a larger deviation from the observed values.

Based on Table 8, the Coefficient of Determination (R^2) values show a strong correlation between the interpolation results and the observed data for IDW (0.937–0.833) and Kriging (0.887–0.929) across all return periods. In contrast, Spline has low R^2 values, ranging from 0.030 to 0.205, especially at short return periods, indicating poor spatial representation capabilities.
The evaluation of the four statistical indicators (*MAE*, *MAPE*, *RMSE*, and R^2) shows varying performance patterns for the interpolation methods. IDW provides more accurate estimates at short return periods, particularly 2 yr, with relatively low error values and a high coefficient of determination. Kriging demonstrates superiority at medium to long return periods (5–50 yr), producing stable predictions that closely match the observed data. Spline tends to have higher error and a low R^2, especially at long return periods. Overall, this evaluation confirms that the effectiveness of the interpolation method is highly dependent on the return period and data characteristics at each station, so the choice of method must be adjusted to the needs of the hydrological analysis.

To further strengthen the interpretation of these results, a comparison with previous studies is necessary. Several studies have reported varying performance of interpolation methods depending on spatial characteristics and data distribution. For instance, research conducted in the Upper Brantas Sub-watershed showed that the IDW method produced the highest accuracy, particularly due to its ability to capture localized rainfall variability in areas with relatively uniform station distribution [17]. This finding is consistent with the results of this study, where IDW demonstrates superior performance at short return periods, indicating its effectiveness in representing local rainfall patterns in urban environments.

On the other hand, studies in the Abab Sub-watershed indicated that Kriging tends to produce larger errors under certain conditions, particularly when spatial homogeneity assumptions are not fully met [18]. However, in this study, Kriging shows better performance at medium to long return periods. This difference may be influenced by the spatial autocorrelation structure of rainfall in Denpasar City, where urban morphology, land use change, and drainage patterns create more structured spatial relationships that can be better captured by geostatistical methods such as Kriging.
Furthermore, research conducted in North Sumatra found

that the Spline method can provide good interpolation results under specific conditions, especially when data distribution is smooth and continuous [22]. In contrast, the results of this study show that Spline performs poorly, particularly at longer return periods, as indicated by higher error values and lower R^2. This discrepancy suggests that Spline may be less suitable for areas with high rainfall variability and complex spatial patterns, such as Denpasar, where rapid urbanization significantly influences hydrological processes.

These differences highlight that the performance of interpolation methods is not universal but strongly influenced by regional characteristics, including station density, spatial variability of rainfall, and urban landscape complexity. Therefore, the selection of interpolation methods should not be generalized, but must be adapted to local conditions. In the case of Denpasar City, the combination of IDW for shortterm analysis and Kriging for longterm estimation provides a more reliable approach for supporting hydrometeorological disaster mitigation planning, particularly in urban flood risk assessment. This finding reinforces the importance of integrating spatial analysis with urban hydrological characteristics to improve the accuracy of rainfall-based disaster mitigation strategies.

4. Conclusion

From the overall analysis, it can be concluded that IDW and Kriging are the most reliable interpolation methods to represent the design rainfall distribution in Denpasar City, with IDW superior at short return periods and Kriging superior at medium to long return periods. Spline does not provide optimal results, especially at long return periods. This finding emphasizes the importance of selecting the right interpolation method to support hydrological planning and mitigation strategies for hydro-meteorological disasters such as floods. In practical terms, the use of IDW can support short-term flood risk identification, particularly for early warning systems and rapid response planning, while Kriging is more suitable for long-term flood mitigation planning, including drainage system design, retention basin development, and urban water management strategies. Therefore, accurate rainfall mapping generated from appropriate interpolation methods can assist local governments and planners in identifying flood-prone areas, optimizing infrastructure planning, and improving the effectiveness of flood mitigation measures in urban environments such as Denpasar City.

References

[1] Badan Meteorologi Klimatologi dan Geofisika, "Cuaca ekstrem masih mengintai, BMKG ingatkan kesiapsiagaan nasional," *Badan Meteorologi, Klimatologi, dan Geofisika*, 2025. https://www.bmkg.go.id/siaran-pers/cuaca-ekstrem-masih-mengintai-bmkg-ingatkan-kesiapsiagaan-nasional?utm_source=chatgpt.com (accessed Sep. 20, 2025).

[2] Badan Penanggulangan Bencana Daerah Provinsi Bali, "Tujuh wilayah Provinsi Bali terdampak banjir dan longsor," *Badan Penanggulangan Bencana Daerah Provinsi Bali*, 2025. https://www.bnpb.go.id/berita/update-tujuh-wilayah-provinsi-bali-terdampak-banjir-dan-longsor (accessed Sep. 20, 2025).

[3] F. N. Ulya and D. Prabowo, "BNPB ungkap 120 titik banjir di Bali, paling banyak di Denpasar," *Kompas.com*, 2025. https://nasional.kompas.com/read/2025/09/11/13114321/bnpb-ungkap-120-titik-banjir-di-bali-paling-banyak-di-denpasar (accessed Sep. 20, 2025).

[4] Z. P. Andreas, R.-V. Virginia, and M. Péter, "Understanding flood triggering mechanisms and flood risk changes." 2021. doi: 10.48350/151728.

[5] N. M. L. K. Putri, "Ini pemicu hujan deras penyebab banjir di Denpasar Bali," *detinews*, 2025. https://news.detik.com/berita/d-8104645/ini-pemicu-hujan-deras-penyebab-banjir-di-denpasar-bali (accessed Sep. 20, 2025).

[6] A. Tribhuwana, F. Rohman, and O. Farhan, "Surface flow analysis as an efforts flood mitigation," *J. Green Sci. Technol.*, vol. 8, no. 1, 2024, doi: 10.33603/jgst.v8i1.144.

[7] I. G. Y. Wisnawa, I. G. N. Y. Jayantara, and D. G. D. Putra, "Pemetaan lokasi rawan banjir berbasis sistem informasi geografis di Kecamatan Denpasar Barat," *J. ENMAP.*, vol. 2, no. 2, pp. 18–28, 2021, doi: 10.23887/em.v2i2.39841.

[8] N. Irmayanti, I. Lanya, and N. W. F. Utami, "Zonasi kawasan perkotaan berbasis mitigasi bencana banjir (Studi kasus Kota Denpasar)," *J. Arsit. Lansek.*, vol. 6, no. 2, p. 190, 2020, doi: 10.24843/jal.2020.v06.i02.p06.

[9] M. Hemmati, K. Kornhuber, and A. Kruczkiewicz, "Enhanced urban adaptation efforts needed to counter rising extreme rainfall risks," *npj Urban Sustain.*, vol. 2, no. 1, pp. 1–5, 2022, doi: 10.1038/s42949-022-00058-w.

[10] B. Arellano, Q. Zheng, D. Martínez, C. Serra, and J. Roca, "Assess the effect of heavy rainfall through the integration of remote sensing and in situ measurements," 2025. doi: 10.1117/12.3069961.

[11] M. K. Thakur, "Exploring the rainfall data from satellites to monitor rainfall induced landslides – A case study," *Adv. Sp. Res.*, vol. 66, no. 4, pp. 887–894, 2020, doi: 10.1016/J.ASR.2020.05.015.

[12] N. Peleg, "Mapping storm spatial profiles for flood impact assessments," *Adv. Water Resour.*, vol. 166, p. 104258, 2022, doi: 10.1016/j.advwatres.2022.104258.

[13] D. Fitriani, E. Suhartanto, and U. Andawayanti, "Studi pemetaan daerah rawan banjir berbasis sistem informasi geografis sebagai upaya mitigasi bencana pada DAS Welang," *J. Teknol. dan Rekayasa Sumber Daya Air*, vol. 4, pp. 1323–1337, 2024, doi: 10.21776/ub.jtresda.2024.004.02.135.

[14] H. Rakuasa and P. C. Latue, "Analisis spasial daerah rawan banjir di DAS Wae Heru, Kota Ambon," *J. Tanah dan Sumberd. Lahan*, vol. 10, no. 1, pp. 75–82, 2023, doi: 10.21776/ub.jtsl.2023.010.1.8.

[15] V. Ruiz-Ortiz, H. M. Fernandez, F. Martins, M. Vélez-Nicolás, J. M. G. P. Isidoro, and S. García-López, "A multimethod interpolation approach for mapping the spatial distribution of rainfall in southwest Iberian Peninsula," *Hydrol. Sci. J.*, 2024, doi: 10.1080/02626667.2024.2387805.

[16] I. Arianti, Soemarno, H. A. W, and S. R, "Rainfall estimation by Using Thiessen Polygon, Inverse Distance Wighted, Spline, and Kriging Methods: A Case Study in Pontianak, West Kalimantan," *Int. J. Educ. Res.*, vol. 6, no. 11, pp. 301–310, 2018.

[17] A. F. I. Marthadyanti, D. Harisuseso, and J. S. Fidari, "Pemetaan sebaran hujan rancangan pada berbagai kala ulang menggunakan metode interpolasi spasial di Sub DAS Brantas Hulu," *J. Teknol. dan Rekayasa Sumber Daya Air*, vol. 3, no. 2, pp. 113–124, 2023, doi: 10.21776/ub.jtresda.2023.003.02.010.

[18] A. G. F. M. Fiqri, D. Harisuseno, and J. S. Fidari, "Mapping of design rainfall at multiple return periods using spatial interpolation in Abab Sub-Watershed, Blitar Regency," vol. 14, no. 1, pp. 38–52, 2023, doi: 10.21776/ub.pengairan.2023.014.01.4.

[19] S. Susanto, H. Pratikto, S. Winarto, and E. Siswanto, "Pemetaan curah hujan dengan Metode Interpolasi Invers Distance Weighting (IDW) Kabupaten Kediri," *J. Eng.*, vol. 15, no. 1, pp. 44–55, 2024, doi: 10.24905/jureng.v15i1.7.

[20] Y. P. A. Wardana, D. Harisuseno, and S. Wahyuni, "Pemetaan sebaran hujan rancangan menggunakan Interpolasi Kriging di DAS Kali Lamong," *J. Teknol. dan Rekayasa Sumber Daya Air*, vol. 04, no. 01, pp. 239–249, 2024.

[21] W. Vimelia, C. Azis, and S. Purwani, "Prediction of rainfall data in the DKI Jakarta area using Cubic Spline Interpolation," *WSN An Int. Sci. J.*, vol. 192, no. March, pp. 76–87, 2024, [Online]. Available: www.worldscientificnews.com

[22] D. A. Putri, E. Octaviani, V. S. Saragih, L. Alyani, R. M. Badri, and F. D. Irawati, "Evaluasi kinerja metode interpolasi spasial untuk estimasi curah hujan (Studi kasus di Sumatera Utara pada kuartal I tahun 2025)," vol. 2025, no. Senada, pp. 241–252, 2025.

[23] M. Pasek *et al.*, "Penerapan metode Analytical Hierarchy Process (AHP) dalam pemetaan ancaman banjir di Kota Denpasar," *J. ENMAP (Environment Mapping) ENMAP*, vol. 5, no. 1, pp. 1–11, 2024.

[24] E. Lewis, "Quality control of a global hourly rainfall dataset," *Environ. Model. Softw.*, vol. 144, p. 105169, 2021, doi: 10.1016/J.ENVSOFT.2021.105169.

Bon, "Estimated Spline in Nonparametric Regression with a Generalized Cross Validation and Unbiased Risk Approach," 2021. doi: 10.46254/an11.20210684.

[37] A. R. Khlefha, "Comprehensive Review of Interpolation Techniques Using B-Spline," *Int. Acad. J. Sci. Eng.*, vol. 11, no. 1, pp. 304–311, 2024,

[25] A. Yuliana, J. Sujono, and Karlina, "Analysis of extreme rainfall in the Mt. Merapi Area," *J. Civ. Eng. Forum*, vol. 10, no. 1, pp. 73–84, 2024, doi: 10.22146/jcef.10084.

[26] B. Đurin, "Application of rescaled adjusted partial sums (RAPS) method in hydrology – an overview," pp. 58–72, 2022, doi: 10.13167/2022.25.6.

[27] T. H. Pamungkas, M. I. Yekti, and I. G. A. A. Putra, "Perencanaan sistem pemanenan air hujan dalam memenuhi kebutuhan air di Nusa Penida," *J. Penelit. Pengelolaan Drh. Aliran Sungai*, vol. 7, no. 1, pp. 59–76, 2023, doi: 10.59465/jppdas.2023.7.1.59-76.

[28] M. K. Amin, "Evaluation of Design Rainfall Intensity using Frequency Analysis." 2024. doi: 10.13140/rg.2.2.33592.56328.

[29] R. Wittmanová, I. Marko, M. Šutúš, and Š. Stanko, "Development of design rainfalls: A review," *IOP Conf. Ser. Mater. Sci. Eng.*, vol. 1209, no. 1, p. 012028, 2021, doi: 10.1088/1757-899x/1209/1/012028.

[30] T. H. Pamungkas, M. I. Yekti, P. D. H. Ardana, K. B. Warsana, and I. K. Kembarajaya, "Infiltration well design for environmental conservation: assessing watershed and groundwater depth in Denpasar City," *J. Presipitasi Media Komun. dan Pengemb. Tek. Lingkung.*, vol. 22, no. 1, pp. 168–182, 2025, doi: 10.14710/presipitasi.v22i1.168-182.

[31] R. Bahtiar, Y. Wijayanto, S. A. Budiman, and T. W. Saputra, "Perbedaan karakteristik sebaran spasial hujan di Kabupaten Jember menggunakan metode Inverse Distance Weighted (IDW) dan Poligon Thiessen," *Berk. Ilm. Pertan.*, vol. 5, no. 1, pp. 1–5, 2022, doi: 10.19184/bip.v5i1.34423.

[32] T. H. Tong, "Development of method to optimize rain gauge station location in da rang river basin using spatial interpolation technique," *J. Sci. Tech.*, 2023, doi: 10.56651/lqdtu.jst.v6.n02.736.sce.

[33] Z. Li, "An enhanced dual IDW method for high-quality geospatial interpolation," *Sci. Rep.*, vol. 11, no. 1, p. 9903, 2021, doi: 10.1038/S41598-021-89172-W.

[34] Z. Liu and T. Yan, "Comparison of spatial interpolation methods based on ArcGIS," 2021, vol. 1961, no. 1, p. 12050. doi: 10.1088/1742-6596/1961/1/012050.

[35] A. R. Chandrarien, D. Harisuseno, and S. Wahyuni, "Pemetaan sebaran hujan rancangan menggunakan Metode Interpolasi Kriging di DAS Rejoso," *J. Teknol. dan Rekayasa Sumber Daya Air*, vol. 4, no. 1, pp. 956–968, 2024, doi: 10.21776/ub.jtresda.2024.004.01.081.

[36] A. Tripena, A. Prabowo, Y. Lianawati, and A. T. doi: 10.9756/iajse/v11i1/iajse1135.

[38] J. Zhan *et al.*, "A generalized spatial autoregressive neural network method for three-dimensional spatial interpolation," *Geosci. Model Dev.*, vol. 16, no. 10, pp. 2777–2794, 2023, doi: 10.5194/gmd-16-2777-2023.

[39] D. Chicco, M. J. Warrens, and G. Jurman, “The coefficient of determination R-squared is more informative than SMAPE, MAE, MAPE, MSE and RMSE in regression analysis evaluation,” *PeerJ Comput. Sci.*, vol. 7, pp. 1–24, 2021, doi: 10.7717/PEERJ-CS.623.

[40] C. D. Lewis, *Industrial and business forecasting methods: Apractical guide to exponential smoothing and curve fitting*. London; Boston, 1982.

E-ISSN: 2528-388X
P-ISSN: 0213-762X

Addition of Alkali Activator and Substitution of GGBFS in Hydraulic Cement for High Early Flexural Strength and High Slump Concrete

Maria Apolonia Palan Keron[1], Iman Satyarno[1*], Suprapto Siswosukarto[1], Ratna Dwiyani Nawangsasi[2], and Muhammad Hasan Taufiq[2]

[1)] Department of Civil and Environmental Engineering, Universitas Gadjah Mada, Yogyakarta, 55281, Indonesia
[2)] PT. Solusi Bangun Indonesia Tbk, Bogor, 16820, Indonesia

Keywords:
Hdraulic Cement
GGBFS
Alkali Activator
Flexural Strength
Workability

ABSTRACT

To lower CO_2 emissions, the construction sector is increasingly adopting sustainable practices, such as cutting back on clinker usage in cement manufacturing. Hydraulic cement is an environmentally friendly cement material because it uses a smaller amount of clinker. The amount of industrial waste, including materials like Ground Granulated Blast Furnace Slag (GGBFS), keeps rising each year. Because of this, it is frequently used as an alternative to cement. However, concrete with GGBFS substitution generally experiences a delay in early strength development due to its low reactivity to water. To overcome this, adding an alkali activator in NaOH and Na_2SiO_3 is necessary. In this study, the dosage of alkali activator was varied at 0%, 2.5%, 5% and 7.5% by weight of GGBFS with *R* and *A* values set at 1.5 and 0.45. In addition, using GGBFS can also reduce the workability of concrete, so it is necessary to use a superplasticizer in the form of Sika® Viscocrete®-1050 to improve concrete flow properties. The dosage of superplasticizer used was 0.75% by weight with a target slump of 20 cm for ease of working. The amount of GGBFS used was 30% by weight. To evaluate the materials performance, test were carried out to measure the concrete workability, compressive strength of paste and concrete flexural strength after 3 days of curing. The results show that increasing the dosage of alkali activator can increase the paste compressive strength by more than 24 MPa according to the requirements of using hydraulic cement and concrete flexural strength by more than 3 MPa in 3 days. Concrete with a 7.5% alkali activator dosage can achieve a concrete flexural strength of 4.81 MPa at 3 days and has a slump value of 20 cm. This research can be a solution to reduce CO_2 emissions and is useful for construction projects that require high flexural strength values at early ages and high slump.

1. Introduction

The demand for concrete production continues to increase every year [1], this has led to a steady increase in cement production. However, cement production generates large CO_2 emissions, accounting for around 6% of greenhouse gas emissions [2]. Therefore, the industry construction must in innovate to engineer materials that are kinder to the environment. One of the most widely used methods is to substitute green materials for normal clinker during the cement production process, thereby reducing clinker usage and lowering CO_2 emissions [3] or commonly known as hydraulic cement. Following ASTM C1157 standards [4], hydraulic cement usually contains normal clinker mixed with renewable or green materials such as fly ash [5] and limestone [6]. Hydraulic cement in the construction industry is considered more environmentally friendly because its production process generates lower carbon emissions due to using less clinker than conventional cement, reducing CO_2 emissions [7].

*Corresponding author.
E-mail: imansatyarno@ugm.ac.id

https://doi.org/10.21831/inersia.v21i2.87888
Received 01 July 2025; Revised 29 April 2026; Accepted 30 April 2026
Available online 01 May 2026

Another significant industrial byproduct is Ground Granulated Blast Furnace Slag (GGBFS), which continues to increase year after year and contributes to CO_2 emissions [8]. GGBFS is a by-product generated from the smelting of iron ore and rapidly cooled using water or steam [9]. In concrete applications, GGBFS can replace cement to its comparable chemical makeup to ordinary portland cement [10]-[11]. The chemical composition of GGBFS, such as silica, calcium, and alumina, can effectively increase the compressive strength of concrete [12]-[13]. Previous studies have shown that substituting GGBFS in OPC cement at a substitution rate of 30-45% can increase the compressive strength and flexural strength of concrete [14]-[15]. However, other researchers attempted to compare the strength of normal concrete and concrete with GGBFS substitution at 3, 7, and 28 days of age. The results showed that concrete with GGBFS substitution had lower strength at an early age compared to normal concrete [16]. This occurs because OPC contains C_3S and C_3A, which react quickly with water to produce high concrete strength at an early age, while GGBFS requires an alkali activator to accelerate the hydration reaction in concrete, thereby increasing concrete strength at an early age [17]. Although GGBFS has a slow reaction initially, it has high strength over a longer time. To overcome this problem, GGBFS requires an alkali activator solution [18] which can accelerate the reaction rate to produce high early strength concrete.

Sodium hydroxide (NaOH) and sodium silicate (Na_2SiO_3) represent the most frequently employed alkaline activators in practice [19]. A mixture of NaOH and Na_2SiO_3 as an alkali activator has been proven to significantly improve the mechanical properties of concrete because it creates an alkaline environment that allows GGBFS to react more quickly [20]. Several factors must be considered in the alkali activator solution, such as; the ratio of Na_2SiO_3 and NaOH (R), the concentration of the NaOH solution (molarity), the ratio of alkali activator to cement (A), and the percentage of alkali activator solution to the amount of cement used. Several studies have found that the ideal ratio for R is 1.5–2.5, the ideal molarity is 10–16 M, and the value of A used is 0.45 to achieve concrete high early strength [21] - [22] - [18] and [23]. The amount of alkali activator solution greatly affects the hydration properties of concrete, this leads to changes in the concrete structural strength. Therefore, testing is necessary to determine the most effective dose of alkali activator to activate the chemical properties of the amount of GGBFS used in this study.

The demand for high early-strength concrete is increasing in line with developments in construction, as it can accelerate project implementation and reduce project costs [24]. However, using large amounts of cement to achieve this strength increases CO_2 emissions. Hydraulic cement and GGBFS are used as alternatives to reduce this. Although effective, GGBFS reduces the workability of concrete, which affects the ease of construction in the field. [25]. Since the slump target was 20 cm, Sika® Viscocrete®-1050 *HE* superplasticizer was added to improve workability without increasing the amount of water.

This study used HE (High Early) type hydraulic cement, which complies with ASTM C1157 [4]. The concrete is required to reach a compressive strength of 24 MPa within 3 days, which corresponds to a flexural strength of about 3 MPa. By incorporating GGBFS and using an alkali activator to accelerate hydration, it's anticipated that the flexural strength at 3 days can surpass 3 MPa due to the improved early-age strength development. This research is expected to reduce CO_2 emissions by using hydraulic cement with minimal clinker content, which is then substituted with 30% GGBFS, an industrial waste material. It is hoped that the combination of these two cementitious materials can produce high concrete strength at an early age by varying the dose of alkali activator and adding superplasticizer to obtain the best mechanical properties of concrete, thereby enabling its use in various constructions requiring high early flexural strength and high slump concrete.

2. Methods

2.1 Material

Hydraulic cement and GGBFS served as the fundamental materials in this study. Hydraulic cement and GGBFS were referred to as cement. The hydraulic cement used was sourced from PT. SBI with a specific gravity of 3.15. GGBFS was sourced from PT. Krakatau Indonesia has a specific gravity of 2.77, and the chemical content of GGBFS can be seen in the Table 1. Preliminary testing revealed that a 70:30 blend of hydraulic cement to GGBFS yielded the best performance.

The superplasticizer used is Sika® Viscocrete®-1050 HE type E, which reduces water usage and accelerates the initial setting process of concrete. This type of superplasticizer is suitable for application requiring rapid strength development concrete and can increase the slump value with a 30% reduction in water quantity [26].

Table 1. Chemical content of GGBFS

Components	Content (%)
Aluminium Trioxide (Al_2O_3)	15.75
Silicon Dioxide (SiO_2)	37.03
Iron Trioxide (Fe_2O_3)	0.67
Calcium Oxide (CaO)	42.61
Sulfur Trioxide (SO_3)	1.83
Potassium Oxide (K_2O)	0.30

Sodium hydroxide (NaOH) and sodium silicate (Na_2SiO_3) are mixed to create the alkaline activator solution. NaOH pellets with a content of 98.5% have a specific gravity of 1.34, and Na_2SiO_3 has a specific gravity of 1.65. NaOH pellets are dissolved in distilled water at a concentration of 10 molar. After the NaOH has dissolved, the NaOH solution is left to stand for 24 hours. The NaOH solution is then mixed with Na_2SiO_3 in a ratio of R (Na_2SiO_3/NaOH) of 1.5 and cooled for one hour or until it reaches room temperature before use. The ratio of alkali activator to cement (A) is 0.45. The variations in the percentage of alkali activator in this study are 0%, 2.5%, 5%, and 7.5% of the weight of GGBFS, and the amount of alkali activator is reduced from the amount of water. The 10 Molar NaOH concentration, R ratio, and A ratio are the results of previous research on geopolymer paste, mortar, and concrete, which produced high mechanical strength in concrete [22]-[27].

The fine aggregates used are silica sand and Optima sand. Silica sand is sourced from Tayan with a specific gravity of 2.66 and a unit weight of 1390. Optima sand is sourced from Rumpin, Bogor, with a specific gravity of 2.53 and a unit weight 1430. Silica sand and Optima sand are used together in concrete mixtures at a ratio of 70:30. For coarse aggregate, crushed stone from Rumpin, Bogor, is used with a size of 10-20 mm, a specific gravity of 2.58, and a unit weight of 1480. Fine aggregate and coarse aggregate are prepared in the Saturated Surface Dry (*SSD*) condition, in accordance with the guidelines outlined in ASTM C136 [28].

2.2 Mix Design

In this research, the absolute volume method was employed to calculate paste, mortar, and concrete mixtures, as standardized guidelines for geopolymer concrete formulations are currently unavailable. This approach determines mix proportions by converting each material's absolute volume into the total volume of 1 m³ of the final mixture [29]. The calculation of absolute volume starts from paste, mortar, to concrete in the following order:

The calculation of the proportion of the paste mixture based on absolute volume can be done using Equation (1).

$$V_s + V_{ggbfs} + V_{sv} + V_a + V_{ac} = 1m^3 \quad (1)$$

where, V_s is absolute volume of hydraulic cement, V_{ggbfs} is absolute volume of GGBFS, V_{sv} is absolute volume of Sika® Viscocrete®-1050, V_a is absolute volume of water, V_{ac} is absolute volume of alkali activator.

Equation (1) can be expanded into Equation (2) to calculate the weight of each material:

$$\frac{W_s}{G_{ss}\gamma_w} + \frac{W_{ggbfs}}{G_{sggbfs}\gamma_w} + \frac{W_{sv}}{G_{ssv}\gamma_w} + \frac{W_a}{G_{sa}\gamma_w} + \frac{W_{ac}}{G_{sac}\gamma_w} = 1m^3 \quad (2)$$

The above equation can then be further translated into Equation (3) with a cementitious weight (weight of hydraulic cement and GGBFS) of 70:30. The cementitious FAS (F_AS_m) is the weight of water and the weight of alkali activator to cementitious weight is 0.25

$$\frac{(1-X)W_{sm}}{G_{ss}\,\gamma_w} + \frac{XW_{sm}}{G_{sggbs}\,\gamma_w} + \frac{YW_{sm}}{G_{ssv}\,\gamma_w} + \frac{(FAS_m - ZAX)W_{sm}}{G_{sa}\,\gamma_w} + \frac{ZAXW_{sm}}{G_{sac}\,\gamma_w} = 1m^3 \quad (3)$$

where, X is percentage of GGBFS, Y is weight of Sika® Viscocrete®-1050, Z is percentage of alkali activator to GGBFS, F_AS_m is water cementitius ratio, A is Alkali activator/cement ratio, W_{sm} is weight of cementitius, Gss is specific gravity of hydraulic cement, G_{sggbfs} is specific gravity of GGBFS, G_{ssv} is specific gravity of Sika® Viscocrete®-1050, G_{sa} is specific gravity of water, G_{sac} is specific gravity of alkali activator, γw is density of water.

In the mortar mix design, the effect of the ratio between the absolute volume of paste to the absolute volume of fine aggregate voids (R_m) was set at 1.4 based on previous research [19]. The volume of fine aggregate voids (V_{ragh}) in 1 m³ can be determined based on the unit weight of fine aggregate (B_{sagh}), the SSD specific gravity of fine aggregate (G_{sagh}) and the unit weight of water (γ_w). Then it can be calculated with Equation (4):

$$V_{ragh} = 1 - \frac{B_{sagh}}{G_{sagh}}\gamma_w \quad (2)$$

Furthermore, if V_{ragh} is known, the weight of cement (W_s), weight of GGBFS (W_{ggbfs}), weight of Sika® Viscocrete®-1050 (W_{sv}), weight of water (W_a) and weight of alkali activator ($W_{a}c$) required in 1 m³ of mortar mix can be calculated with Equation (5):

$$\frac{(1-X)W_{sm}}{G_{ss}\,\gamma_w} + \frac{XW_{sm}}{G_{sggbs}\,\gamma_w} + \frac{YW_{sm}}{G_{ssv}\,\gamma_w} + \frac{(FAS_m - ZAX)W_{sm}}{G_{sa}\,\gamma_w} + \frac{ZAXW_{sm}}{G_{sac}\,\gamma_w} = R_mV_{ragh} \quad (5)$$

Furthermore, the weight of fine aggregate can be calculated with Equation (6):

$$V_{ragh}R_m + \frac{W_{agh}}{G_{sagh}\gamma_w} = 1m^3 \tag{3}$$

The research evaluates effect of the ratio between the absolute volume of mortar to the absolute volume of coarse aggregate voids (R_b) of 1.4 based on previous research [19] - [22]. The volume of voids between grains of coarse aggregate (Vragk) in 1 m^3 can be determined based on the unit weight of coarse aggregate (B_{sagk}), SSD specific gravity of coarse aggregate (G_{sagk}) and unit weight of water (γ_w). Then it can be calculated with Equation (7):

$$V_{ragk} = 1 - \frac{B_{sagk}}{G_{sagk}}\gamma_w \tag{4}$$

Furthermore, if Vragk is known, the weight of cement (W_s), weight of GGBFS (W_{ggbfs}), weight of Sika® Viscocrete®-1050 (W_{sv}), weight of water (W_a) and weight of alkali activator (W_{ac}) required in 1m^3 of concrete mix can be calculated with Equation (8):

$$\frac{(1-X)W_{sm}}{G_{ss}\,\gamma_w} + \frac{XW_{sm}}{G_{sggbs}\,\gamma_w} + \frac{YW_{sm}}{G_{ssv}\,\gamma_w} + \frac{(FAS_m - ZAX)W_{sm}}{G_{sa}\,\gamma_w} + \frac{ZAXW_{sm}}{G_{sac}\,\gamma_w} = R_m V_{ragh} R_b V_{ragk} \tag{8}$$

Furthermore, the weight of fine aggregate can be calculated with Equation (9):

$$V_{ragh}R_m\, V_{ragk}\, R_b + \frac{W_{agh}}{G_{sagh}\gamma_w} = V_{ragk}\, R_b \tag{5}$$

To calculate the coarse aggregat mass, apply the Equation (10):

$$V_{ragk}\, R_b + \frac{W_{agk}}{G_{sagk}\gamma_w} = 1m^3 \tag{6}$$

The results of material quantity calculations for 1 m^3 of concrete are available in Table 2. Material Requirements. Mix ID is a variation of the test variable, with *B* as the symbol for concrete, AG as the symbol for alkali activator and the numbers 0, 2.5, 5, and 7.5 are the percentage of alkali activator used.

2.3 Mixing and Casting

The process begins with the dry mixing of hydraulic cement and GGBFS until they become uniform. At this stage, it is recommended to wear a mask because fine particles of dry material can fly and endanger breathing. Then pour water that has been mixed with superplasticizer slowly while stirring for ± 3 minutes until evenly mixed, and there are no lumps, then pour the alkali activator and stir again until evenly mixed. The process continues by adding fine aggregate in the form of silica sand and optima sand in SSD (Saturated Surface Dry) and stirring again for ± 3 minutes until well blended.

To make the beam specimens, the fresh concrete mixture is then poured into a 150 x 150 x 600 mm steel beam mold and compacted to prevent air bubbles from being trapped in the concrete. Once the concrete has hardened, the steel beam mold is removed, and the specimen is ready for testing. To make cube specimens paste, use a 50 x 50 x 50 mm mold.

2.4 Testing

After the mixing process is complete, a slump test is carried out according to SNI 1972-2008 [30] to evaluate the workability of fresh concrete. Compressive strength testing of paste based on ASTM C109 [31] to determine the compressive strength of paste at 3 days of age before further testing of concrete specimens.

Flexural strength testing of concrete beams was conducted at 3 days of age. The flexural strength test was performed using a two-point loading method based on SNI 4431-2011 [31]. The beam specimens were placed on the testing machine with two-point loading along the horizontal axis and perpendicular to the testing machine. After testing the beam specimens for each test variable, the flexural strength values were calculated using the formula corresponding to the beam's fracture surface.

Table 2. Material requirements (1m^3)

Mix ID	Variable	Concrete Mix Design Proportion (kg/m^3)								
		HC	GGBFS	Water	SV	SS	SH	PS	PO	CA
BAG0	H70GGBFS30SV0.75AG0	463.1	198.5	165.4	5.0	-	-	382.1	163.7	1040
BAG2.5	H70GGBFS30SV0.75AG2.5	464.0	198.9	163.5	5.0	1.3	0.9	382.1	163.7	1040
BAG5	H70GGBFS30SV0.75AG5	465.0	199.3	161.6	5.0	2.7	1.8	382.1	163.7	1040
BAG7.5	H70GGBFS30SV0.75AG7.5	465.9	199.7	159.7	5.0	4.0	2.7	382.1	163.7	1040

3. Results and Discussion

The results of testing the workability of concrete, compressive strength of paste, and flexural strength of concrete are explained in the following points:

3.1 Workability

The test results showed that adding an alkali activator decreased the slump value of concrete. This can be seen in Figure 1, Concrete without the use of alkali activator (BAG0) has a slump of 23 cm, concrete with the use of 2.5% alkali activator (BAG2.5) has a slump value of 22.5 cm, concrete with the use of 5% alkali activator has a slump value of 22 cm. Concrete using 7.5% alkali activator has a slump value of 20 cm. Of the four test variables, the one that meets the target with a slump of 20 cm is the concrete with 7.5% alkali activator, indicating a 13% decrease in slump compared to concrete without alkali activator. It is observed that the slump value of concrete exceeds 20 cm with the use of superplasticizer, and there is a decrease in slump as the amount of alkali activator increases. According to Cornelis [27] Using Na_2SiO_3 and NaOH as alkali activators can affect the workability properties of fresh concrete and shorten the hardening time of concrete. Concrete with a high slump value of more than 20 cm can be used for precast prestressed concrete [32].

From this study, it can also be concluded that each addition of alkali activator percentage can make the consistency of concrete more homogeneous and prevent segregation, even though it has a high slump value when compared to concrete without the use of alkali activator [21]. As can be seen in Figure 2, concrete without alkali activator (BAG0) experienced segregation, where separation occurred between the paste and aggregate in the concrete. When 2.5% alkali activator (BAG2.5) was added, the concrete mixture still experienced segregation but not as much as BAG0 concrete. The concrete mixture begins to appear more homogeneous when 5% alkali activator (BAG5) is added, and the concrete mixture with 7.5% alkali activator (BAG7.5) is the most homogeneous and does not experience segregation despite having a slump value of 20 cm. Concrete with a high slump value can make work easier.

This slump test's results can also align with the function of Sika® Viscocrete®-1050 type HE as a superplasticizer with high workability. Sika® Viscocrete®-1050 type HE is a polycarboxylate-based superplasticizer that can improve the workability of concrete [33].

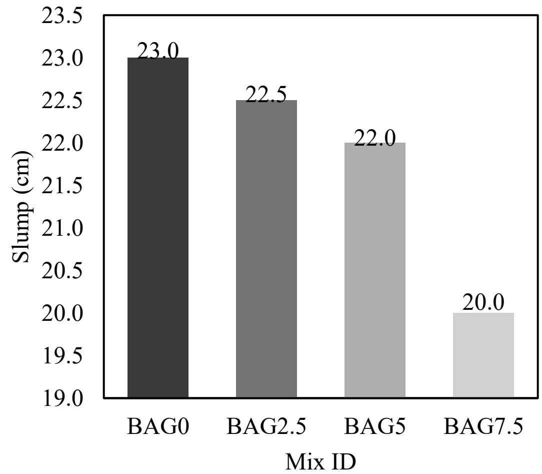

Figure 1. Percentage of alkali activator to concrete slump value

(a) (b) (c) (d)

Figure 2. Concrete Slump Value Measurement **(a)** Without the use of alkali activator (BAG0); **(b)** Use of 2.5% alkali activator (BAG2.5); **(c)** Use of 5% alkali activator (BAG5); **(d)** Use of 7.5% alkali activator (BAG7.5)

3.2 Compressive Strength of Paste

Before making concrete, compressive strength testing is first carried out on the paste to determine the effect of using GGBFS and alkali activators on hydraulic cement, because, in general compressive strength and flexural strength have consistent results [34]. The results of the paste compressive strength test can be seen in Figure 3. Based on ASTM C1157 on hydraulic cement, the compressive strength requirement for HE type hydraulic cement paste after 3 days is 24 MPa [4]. The results of compressive strength testing of paste with 30% GGBFS substitution and the addition of alkali activator at 3 days of age in this study proved to increase compressive strength by up to 68.3% at 3 days of age. These test results indicate that adding 30% GGBFS and alkali activator significantly increases the compressive strength of hydraulic cement paste to over 24 MPa at the early age of 3 days.

3.3 Flexural Strength of Concrete

Figure 4. illustrates the flexural strength of concrete. At three days of curing, the flexural strength exhibits an upward trend as alkali activators are introduced. This improvement in strength results from the alkali activation process, where the reaction between the alkaline solution and GGBFS produces calcium silicate hydrate (C-S-H) gel and sodium alumino-silicate hydrate (N-A-S-H) gel, enhancing the concrete's structural integrity [35]. This reaction creates strong bonds within the concrete aggregate, making the concrete mixture more homogeneous as the alkali activator is added [36]. As can be seen in Figure 5, segregation occurred in concrete that did not use an alkali activator (BAG0). In concrete with 2.5% (BAG2.5) and 5% (BAG5) alkali activator, segregation was minimal, and in concrete with 7.5% (BAG7.5) alkali activator, there was no segregation, resulting in higher concrete strength.

Alkali activators are very helpful in accelerating the rate of concrete strength gain in the early age because the chemical components in GGBFS become more reactive when mixed with alkali activators [37]. However, using less alkali activator may not react optimally with the amount of pozzolan used, which can cause segregation. Using too much alkali activator can also affect the workability of concrete and make it denser and more difficult to work with [36]. In addition, the CaO content in GGBFS also makes the concrete matrix denser, resulting in high concrete flexural strength [38]-[39]. The flexural strength of concrete with 7.5% alkali activator increased by 38% compared to concrete without alkali activator. The flexural strength of concrete increased with the addition of alkali activator, and the pattern of increase in concrete strength was similar to the results of previous paste tests, the inclusion of alkali activators has been shown to enchance concrete early strength development.

This study, the high flexural strength of concrete at an early age depends on the amount of alkali activator used and the amount of GGBFS used. The more alkali activator used, the higher the flexural strength of concrete, but it can reduce the workability of concrete [40]. Conversely, using a small alkali activator cannot react effectively with GGBFS. It cannot bind the aggregates well, which can cause segregation and reduce the flexural strength of the concrete.

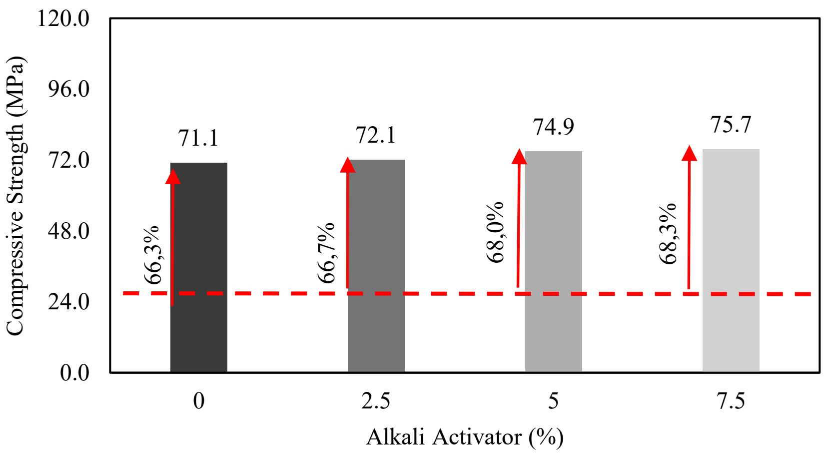

Figure 3. Percentage of alkali activator to compressive strength of paste at 3 days

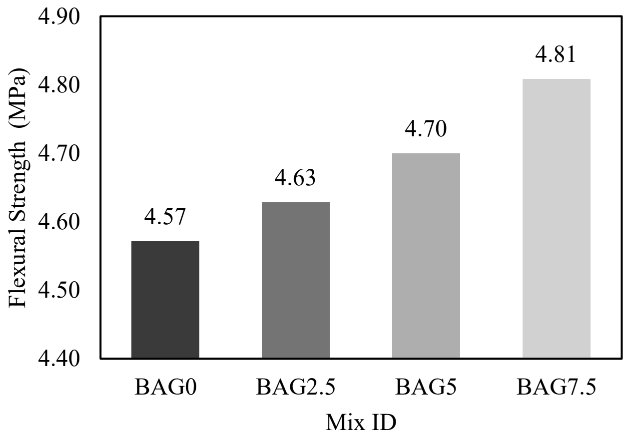

Figure 4 Flexural strength of concrete at 3 days

(a) (b) (c) (d)

Figure 5 Concrete specimens **(a)** Without the use of alkali activator (BAG0); **(b)** Use of 2.5% alkali activator (BAG2.5); **(c)** Use of 5% alkali activator (BAG5); **(d)** Use of 7.5% alkali activator (BAG7.5)

4. Conclusions

The study's results indicate that using hydraulic cement with a 30% substitution of GGBFS can produce concrete with high flexural strength at an early age of 3 days. Concrete mixtures containing alkali activator show changed workability characteristics along with improved early strength. The higher the percentage of alkali activator used, the higher the flexural strength of the concrete achieved. However, the amount of alkali activator used must be limited to ensure the concrete's workability, thereby not impairing its performance. The optimal percentage of alkali activator to activate the pozzolanic properties of 30% GGBFS is 7.5%, as it results in a homogeneous mixture with good workability and high flexural strength. Concrete using 7.5% alkali activator has a slump value of 20 cm and high flexural strength up to 4.81 MPa at early age, making it suitable for precast prestressed concrete that requires high early-age concrete strength with a high slump. This research demonstrates the potential for more environmentally friendly concrete by reducing the use of OPC and utilizing industrial waste as an alternative cement substitute in concrete.

Acknowledgments

We extend our sincere appreciation PT. Solusi Bangun Indonesia, for providing the data and materials such as; hydraulic cement and GGBFS and other materials required for this research. We would also like to express sincere gratitude to LPDP for the financial support provided for this research.

References

[1] A. Minhajuddin and A. Saha, “Performance evaluation of geopolymer concrete with waste granite powder as a sustainable alternative to sand,” *J. Mater. Sci. Mater. Eng.*, vol. 20, no. 1, 2025, doi: 10.1186/s40712-025-00227-6.

[2] A. L. Almutairi, B. A. Tayeh, A. Adesina, H. F. Isleem, and A. M. Zeyad, “Potential applications of geopolymer concrete in construction: A review,” *Case Stud. Constr. Mater.*, vol. 15, no. September, p. e00733, 2021, doi: 10.1016/j.cscm.2021.e00733.

[3] A. R. Mazumdar, “Journal of Thailand Concrete Association HYDRAULIC CEMENT (TIS 2594) AND ORDINARY PORTLAND,” vol. 9, no. 1, pp. 1–6, 2021.

[4] C. ASTM, "iTeh Standards iTeh Standards," *Des. E 778 – 87 (Reapproved 2004)*, vol. i, no. Reapproved, pp. 3–5, 2018, doi: 10.1520/C1157.

[5] A. A. Adam, "The Effects of Water to Solid Ratio, Activator to Binder Ratio, and Lime Proportion on the Compressive Strength of Ambient-Cured Geopolymer Concrete," *J. Civ. Eng. Forum*, vol. 5, no. 2, p. 161, 2019, doi: 10.22146/jcef.43878.

[6] W. Petchgate, S. Pongsivasathit, J. Tangpagasit, S. Piyaphipat, K. Pinpatthanapong, and P. Thongindam, "Case Studies in Construction Materials Sustainable soil stabilization : Evaluating the feasibility of hydraulic cement in the deep mixing method," *Case Stud. Constr. Mater.*, vol. 22, no. September 2024, p. e04394, 2025, doi: 10.1016/j.cscm.2025.e04394.

[7] T. Proske, S. Hainer, M. Rezvani, and C. Graubner, "Cement and Concrete Research Eco-friendly concretes with reduced water and cement contents — Mix design principles and laboratory tests," vol. 51, pp. 38–46, 2013.

[8] V. Johnpaul, N. Balasundaram, and M. Natarajan, "Environmental impact of dumping ggbfs on lands in Coimbatore," *Int. J. Eng. Adv. Technol.*, vol. 8, no. 2, pp. 332–334, 2019.

[9] Y. Esen and E. Orhan, "Investigation of the effect on the physical and mechanical properties of the dosage of additive in self-consolidating concrete," *KSCE J. Civ. Eng.*, vol. 20, no. 7, pp. 2849–2858, 2016, doi: 10.1007/s12205-016-0258-2.

[10] J. Pradhan, S. Panda, R. Kumar Mandal, and S. Kumar Panigrahi, "Influence of GGBFS-based blended precursor on fresh properties of self-compacting geopolymer concrete under ambient temperature," *Mater. Today Proc.*, no. xxxx, 2023, doi: 10.1016/j.matpr.2023.06.338.

[11] J. Pradhan, S. Panda, S. Dwibedy, P. Pradhan, and S. K. Panigrahi, "Production of durable high-strength self-compacting geopolymer concrete with GGBFS as a precursor," *J. Mater. Cycles Waste Manag.*, vol. 26, no. 1, pp. 529–551, 2024, doi: 10.1007/s10163-023-01851-0.

[12] A. I. Ruiz, M. A. de la Rubia, J. Massana, F. Alonso Peralta, A. Moragues, and E. Reyes, "Sustainable low-cement blends featuring blast furnace slag, metakaolin and nanosilica show remarkable long-term durability against chlorides for one day curing age," *Case Stud. Constr. Mater.*, vol. 22, no. March, p. e04511, 2025, doi: 10.1016/j.cscm.2025.e04511.

[13] P. Nath and P. K. Sarker, "Effect of GGBFS on setting, workability and early strength properties of fly ash geopolymer concrete cured in ambient condition," *Constr. Build. Mater.*, vol. 66, pp. 163–171, 2014, doi: 10.1016/j.conbuildmat.2014.05.080.

[14] Z. Qu, Z. Liu, R. Si, and Y. Zhang, "Effect of Various Fly Ash and Ground Granulated Blast Furnace Slag Content on Concrete Properties: Experiments and Modelling," *Materials (Basel).*, vol. 15, no. 9, 2022, doi: 10.3390/ma15093016.

[15] D. A. F. Hashmi, M.S. Khan, M. Bilal, M. Shariq, and A. Baqi, "Green Concrete: An Eco-Friendly Alternative to the OPC Concrete," *Construction*, vol. 2, no. 2, pp. 93–103, 2022, doi: 10.15282/construction.v2i2.8710.

[16] N. Puspita, Y. Arti, and Febryandi, "Flexural Strength Analysis of Concrete With the Addition B3 Waste as an Additive to Ordinary Portland Cement," *Proc. 4th Forum Res. Sci. Technol.*, vol. 7, pp. 343–348, 2021, doi: 10.2991/ahe.k.210205.057.

[17] B. Lothenbach, K. Scrivener, and R. D. Hooton, "Supplementary cementitious materials," *Cem. Concr. Res.*, vol. 41, no. 12, pp. 1244–1256, 2011, doi: 10.1016/j.cemconres.2010.12.001.

[18] R. Prakash, S. Srividhya, P. Neelamegam, K. Mukilan, R. Premkumar, and M. V. Kumar, "Fresh and hardened characteristics of a novel alkali-activated geopolymer concrete with GGBFS," *Mater. Prot.*, vol. 65, no. 2, pp. 294–306, 2024, doi: 10.62638/ZasMat1121.

[19] R. Cornelis, H. Priyosulityo, I. Satyarno, Rochmadi, and I. Rustendi, "Effect of the Mortar Volume Ratio on the Mechanical Behavior of Class CI Fly Ash-Based Geopolymer Concrete," *Civ. Eng. J.*, vol. 8, no. 9, pp. 1920–1935, 2022, doi: 10.28991/CEJ-2022-08-09-012.

[20] S. Zhang and D. Niu, "Hydration and mechanical properties of cement-steel slag system incorporating different activators," *Constr. Build. Mater.*, vol. 363, no. January 2022, 2023, doi: 10.1016/j.conbuildmat.2022.129981.

[21] G. S. Ryu, Y. B. Lee, K. T. Koh, and Y. S. Chung, "The mechanical properties of fly ash-based geopolymer concrete with alkaline activators," *Constr. Build. Mater.*, vol. 47, no. 2013, pp. 409–418, 2013, doi: 10.1016/j.conbuildmat.2013.05.069.

[22] Hanani, "Mix Design of Ambient Cured Geopolymer Concrete with Fly Ash , GGBFS , and Borax," vol. 20, no. 2, 2024.

[23] H. Zhang, H. Li, H. Guo, Y. Li, and L. Wei, "Mechanical properties of alkali activated geopolymer cement mortar for non vibratory compacted trench backfilling," pp. 1–15, 2025.

[24] M. Li and V. C. Li, "High-early-strength engineered cementitious composites for fast, durable concrete repair-material properties," *ACI Mater. J.*, vol. 108, no. 1, pp. 3–12, 2011, doi: 10.14359/51664210.

[25] F. Hussain, I. Kaur, and A. Hussain, "Reviewing the influence of GGBFS on concrete properties," *Mater. Today Proc.*, vol. 32, pp. 997–1004, 2020, doi: 10.1016/j.matpr.2020.07.410.

[26] P. D. Sheet, "Sika ® ViscoCrete ® -1050 HE," no. November, pp. 1–3, 2017.

[27] R. Cornelis, H. Priyosulistyo, I. Satyarno, and Rochmadi, "The Investigation on Setting Time and Strength of High Calcium Fly Ash Based Geopolymer," *Appl. Mech. Mater.*, vol. 881, pp. 158–164, 2018, doi: 10.4028/www.scientific.net/amm.881.158.

[28] ASTM C 136, "SNI ASTM C136:2012. Metode uji untuk analisis saringan agregat halus dan agregat kasar," *Badan Stand. Nas.*, pp. 1–24, 2012.

[29] I. Satyarno, A. P. Solehudina, C. Meyartoa, D. Hadiyatmokoa, P. Muhammada, and R. Afnana, "Practical method for mix design of cement-based grout," *Procedia Eng.*, vol. 95, no. Scescm, pp. 356–365, 2014, doi: 10.1016/j.proeng.2014.12.194.

[30] SNI-1972, "Cara Uji Slump Beton," 2008.

[31] B. S. N. SNI 4431, "SNI 4431-2011 Cara Uji Kuat Lentur Beton Normal dengan Dua Titik Pembebanan," *Badan Standar Nas. Indones.*, pp. 1–16, 2011.

[32] C. Lee, S. Lee, and N. Nguyen, "Modeling of Compressive Strength Development of High-Early-Strength-Concrete at Different Curing Temperatures," *Int. J. Concr. Struct. Mater.*, vol. 10, no. 2, pp. 205–219, 2016, doi: 10.1007/s40069-016-0147-6.

[33] E. Anggarini and D. P. Hardiani, "Comparison of Addition of Sika-Viscocrete 1050 He and Sika-Visco Flow for High Strength Concrete SCC Fc'45 Mpa (Case Study: Replacement of Sei. Alalak Bridge)," *Eng. Appl. Technol.*, vol. 1, no. 1, p. 2023, 2023.

[34] J. Vincent, B. Natarajan, D. Das Amaladas, and D. Cruze, "An Evaluation of Mechanical Properties of Nano GGBFS in Concrete with Statistical Validation," *Buildings*, vol. 13, no. 12, 2023, doi: 10.3390/buildings13123060.

[35] M. I. Khan, V. V. Ram, and V. I. Patel, "Strength, Environmental Impact and Cost Assessment of Alkali-Activated Concrete with Pre-treated Coarse Recycled Aggregates," *Int. J. Concr. Struct. Mater.*, vol. 19, no. 1, 2025, doi: 10.1186/s40069-025-00768-2.

[36] S. Chen and S. Wang, "Effect of activator dosage and mass ratio of GGBFS to FA on 3D printing performance of kenaf geopolymer," pp. 0–17, 2024.

[37] G. Fahim Huseien, J. Mirza, M. Ismail, S. K. Ghoshal, and A. Abdulameer Hussein, "Geopolymer mortars as sustainable repair material: A comprehensive review," *Renew. Sustain. Energy Rev.*, vol. 80, no. April, pp. 54–74, 2017, doi: 10.1016/j.rser.2017.05.076.

[38] I. Ismail, S. A. Bernal, J. L. Provis, R. San Nicolas, S. Hamdan, and J. S. J. Van Deventer, "Modification of phase evolution in alkali-activated blast furnace slag by the incorporation of fly ash," *Cem. Concr. Compos.*, vol. 45, pp. 125–135, 2014, doi: 10.1016/j.cemconcomp.2013.09.006.

[39] S. Sasui, G. Kim, J. Nam, T. Koyama, and S. Chansomsak, "Strength and microstructure of class-C fly ash and GGBS blend geopolymer activated in NaOH & NaOH + Na2SiO3," *Materials (Basel).*, vol. 13, no. 1, 2020, doi: 10.3390/ma13010059.

[40] W. Chen and H. J. H. Brouwers, "The hydration of slag, part 1: Reaction models for alkali-activated slag," *J. Mater. Sci.*, vol. 42, no. 2, pp. 428–443, 2007, doi: 10.1007/s10853-006-0873-2.

E-ISSN: 2528-388X
P-ISSN: 0213-762X

INERSIA
Vol. 22, No. 1, May 2026

Effects of Square Body Openings in Castellated Steel Beams on Stiffness and Natural Frequencies

Guntur Nugroho* and Fayza Aughitri

Civil Engineering Program, Universitas Muhammadiyah Yogyakarta, Yogyakarta 55183, Indonesia

Keywords:
Castella beams
Natural Frequency
Abaqus CAE
Moment of Inertia

ABSTRACT

Castella beams are one of the steel structural innovations that have the advantage of reducing weight without sacrificing bending stiffness, so they are widely used in long-span structures. This study aims to analyze how square-shaped openings affect the natural frequency of castellated beams, considering different numbers of openings and various support conditions. The research was conducted numerically using Abaqus CAE software and theoretically using Stokey's theory. Five models were tested with the number of openings between 9 and 19 and three different support conditions: fixed-fixed, fixed-pinned, and pinned-pinned. Results show that increasing the number of openings significantly decreases the mass and stiffness of the beam, which impacts the natural frequency values of the structure. The analysis results using Stokey's theory yield natural frequency values that tend to be higher than the numerical analysis because it does not consider the local weakening effect due to the openings. The difference between the results of the two approaches reaches 7-904 Hz, depending on the configuration and vibration mode analyzed. The difference is more striking at higher vibration modes because the concentration of local deformation is more dominant. Modifying Stokey's formula by adding an inertial correction coefficient proved to predict the downward trend of the natural frequency more accurately. The results show that the natural frequency values at low vibration modes are in high agreement. Therefore, it is recommended to use this approach, especially in low-vibration mode analysis.

1. Introduction

One type of steel beam that is increasingly popular in the construction world and is widely used in various structural projects is the castellated beam. Steel beams with openings in the body were first applied in construction during World War II to reduce the cost of building steel structures [1]. Castellated beams are designed with various shapes of body openings, including circular, hexagonal, rectangular, diamond, and pentagonal. Body openings in beams extend pipes, cables, and other services across the beam. In modern structural applications, castellated steel beams (CSBs) are used for long-span construction [2] - [3]. Castella steel beams are widely used because they offer excellent structural performance, with advantages such as light weight, ease of construction, adequate strength, and economical use of materials [4]. Lighter beams are easier to handle and install, thus reducing construction time and cost [5] - [6]. With a higher body geometry yet still light mass, castellated beams can resist bending loads more effectively than conventional steel beams. This feature improves structural efficiency and makes it a more economical solution as it can reduce overall construction costs [7]. Structural engineers are not only responsible for designing the safety and serviceability of a structure but also for ensuring that the structure functions according to the needs of its use [8].

The conducted a research analytical study on the behavior of cellular steel beams subjected to lateral torsional buckling to evaluate the effect of various loading conditions on structural stability. Simulations were carried out using ABAQUS software [9]. Researched to analyze the performance of castella composite beams as multi-story buildings carried out experimentally through cyclic loads on beam-column portal models [10]. Research

*Corresponding author.
E-mail: guntur.nugroho@umy.ac.id

https://doi.org/10.21831/inersia.v21i2.87871
Received 01 July 2025; Revised 04 May 2026; Accepted 06 May 2026
Available online 10 May 2026

conducted aims to analyze stress in castella steel beams at web joints with beam plates with hexagonal, octagonal, and diamond openings [7].

The conducted this study investigating the instability of castellated beams under bending and analyzing the interaction between bending modes using the Direct Strength Method (DSM) with a hexagon-shaped opening type [11]. The conducted a study to evaluate the effect of CFRP stiffeners on the load capacity of beams with diamond and hexagonal shaped openings [12]. Research focused on determining the load-carrying capacity and deflection values by comparing hexagonal, circular, square, and diamond openings was conducted by [13]-[14]. Research analyzed the effect of opening height variations on castellated beams using the Reduced Beam Section (RBS) method. This study focused on determining the optimal opening height based on the evaluation of stress, strain, deflection, and structural stiffness [15]. A study aimed at determining the use limit between string and beam-string theory through the ratio parameter of moment of inertia to cable length (I/L), and to identify the effect of bending stiffness on the natural frequency of the cable. The analysis was carried out using numerical methods and experimental testing [16].

Research conducted [17] - [18] discussed the effect of deformation on natural frequency values and rotary inertia in the dynamic response of castella beams. The study found that at higher vibration modes, the influence of shear deformation on frequency reduction becomes increasingly dominant. This indicates that the contribution of shear force cannot be ignored, especially when the structure is subjected to excitation at high frequencies. Meanwhile, rotary inertia is known to decrease the value of vibration frequency. However, the negative influence of the rotary inertia can be compensated by openings in the beam body, which generate additional shear effects that stabilize the frequency. This finding confirms the importance of considering the interaction between swivel inertia and opening configuration in the dynamic analysis of castella beams [17] - [18]. This study examines the effect of the moment of inertia in castella steel beams on natural frequency values by considering circular body openings. The methods used include a numerical approach using software and theoretical analysis based on Stokey Theory. The results showed a difference between the natural frequency values obtained from the two methods [19].

This indicates that the numerical approach could capture the effect of opening geometry details more accurately than the theoretical calculation. Based on previous studies, this research aims to analyze the effect of square-shaped openings in the body of castella beams on the natural frequency values under different boundary conditions, namely fixed-fixed, fixed-pinned, and pinned-pinned. In addition, this study also aims to compare the results of natural frequencies obtained through theoretical approaches using the Stokey formula with the results of finite element-based numerical simulations conducted using Abaqus CAE software.

2. Research Methods

2.1 Materials

In this study, IWF steel material with cross-sectional dimensions of 200 × 100 × 8 × 5.5 mm and a length of 5 meters was used. The openings used are square with a size of 100 mm × 100 mm placed on the body of the profile, according to the illustration shown in Figure 1. The steel material used has an elastic modulus (E) of 200,000 MPa, a density (ρ) of 7850 kg/m³, and a Poisson's ratio (v) of 0.3. This study tested five model variations: a model without openings and body openings with a spacing distance of 155 mm, 200 mm, 325 mm, and 410 mm, and the number of body openings ranging from 9 to 19 openings. All models were compared under three support conditions: fixed-fixed, fixed-pinned, and pinned-pinned. Each model's steel weight per meter decreased as the number of openings increased, from 21.3 kg/m (without openings) to 6.00 kg/m (for 19 openings). Complete data on the model configurations are shown in Table 1.

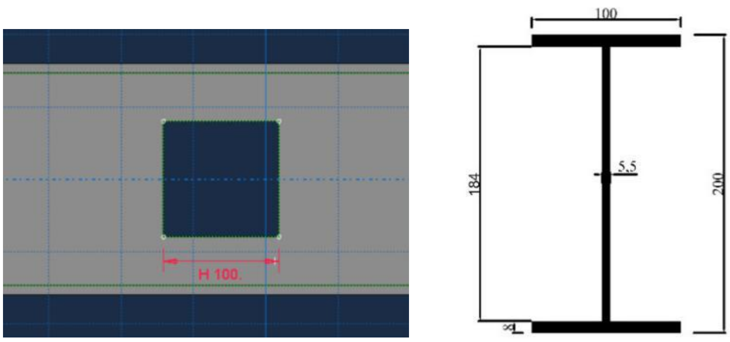

Figure 1. Typical beam section details.

Table 1. Detail of specimens

Support	Modelling	Distance Between Openings (mm)	Opening Diameter (mm)	Number of Openings	Steel Weight (Kg/m)
Fixed - Fixed	M1	-	-	-	21.3
	M2	410	100	9	14.05
	M3	325	100	11	12.44
	M4	200	100	16	8.42
	M5	155	100	19	6.00
Fixed - Pinned	M1	-	-	-	21.3
	M2	410	100	9	14.05
	M3	325	100	11	12.44
	M4	200	100	16	8.42
	M5	155	100	19	6.00
Pinned - Pinned	M1	-	-	-	21.3
	M2	410	100	9	14.05
	M3	325	100	11	12.44
	M4	200	100	16	8.42
	M5	155	100	19	6.00

2.2 Method

This study conducted a numerical analysis using Abaqus CAE software to obtain accurate and detailed results. The model geometry was constructed based on the dimensions of a steel profile with a square-shaped opening placed right in the center of the beam body to evaluate its effect on the dynamic response of the structure. Before the analysis was performed, a convergence test was applied to the element size to ensure the results' stability and the model's suitability. The convergence test results showed the stability of the frequency value in the first mode, so the meshing process was carried out with a distance of 150 mm and resulted in 1,514 elements. The elements used are tetrahedral, which is known to be effective in representing complex geometries. In the analysis stage, natural frequency comparisons were made of the five main vibration modes, ranging from mode shape 1 to mode shape 5, to examine changes in dynamic characteristics due to openings in the beam body.

Stokey theory is a mathematical approach in structural dynamics analysis used to determine the natural frequencies and vibration modes of a system. The proposed a formulation for calculating the natural frequency of structural elements as shown in Formula (1) [20].

$$f_n=\frac{k^2}{2\pi L^2}\sqrt{\frac{EI}{m}}\sqrt{1\pm\frac{FL^2}{EI\pi^2 n^2}} \qquad (1)$$

Where f_n is the natural frequency (*Hz*), *L* is the steel length (*m*), *F* is the force (*N*), n is the mode number, *K* is a parameter based on the type of support used, *EI* is the flexural strength (Nm²), and m is the mass (kg/m).

3. Results and Discussion

This study was conducted to analyze the effect of the opening configuration on the castellated profile on the natural frequency of the structure. Based on Table 1, there are 15 models categorized based on the types of fixed-fixed, fixed-pinned, and pinned-pinned support, as well as variations in the number and distance between openings. Model M1 is a beam without openings, so it has the largest steel weight of 21.3 kg/m. Meanwhile, the model with the largest number of openings M5 has the lightest weight of 6.00 kg/m. The distance between openings also plays an important role in determining the dynamic characteristics of the beam. The results of the analysis on the fixed-fixed, fixed-pinned, and pinned-pinned pedestals can be seen in Figure 2 to Figure 4.

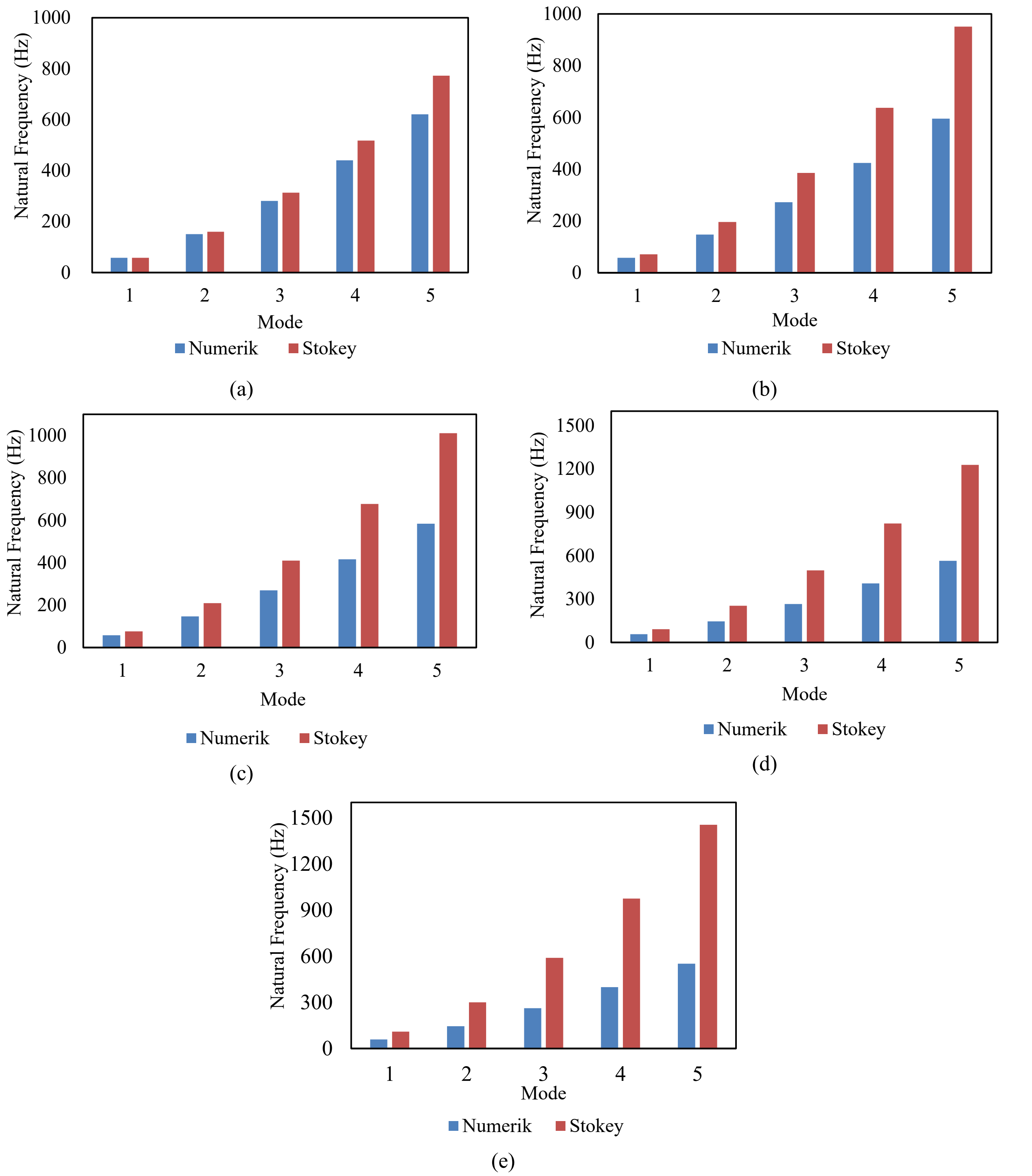

Figure 2. (a) M1, (b) M2, (c) M3, (d) M4, and (e) M5 comparison of numerical results and stokey theory on castellated steel beams with varying web openings using fixed-fixed boundary condition

Model M1 shows the same natural frequency value in the first mode between the results of numerical analysis and Stokey's theoretical calculations. This similarity occurs because model M1 has no openings in the profile body, so there is no change in mass or stiffness.

Meanwhile, models M2 to M5 show differences in natural frequency values between the results of numerical analysis and theoretical calculations. The difference in natural frequency values from mode 1 to mode 5 was recorded as 9 Hz to 904 Hz in the fixed-fixed support.

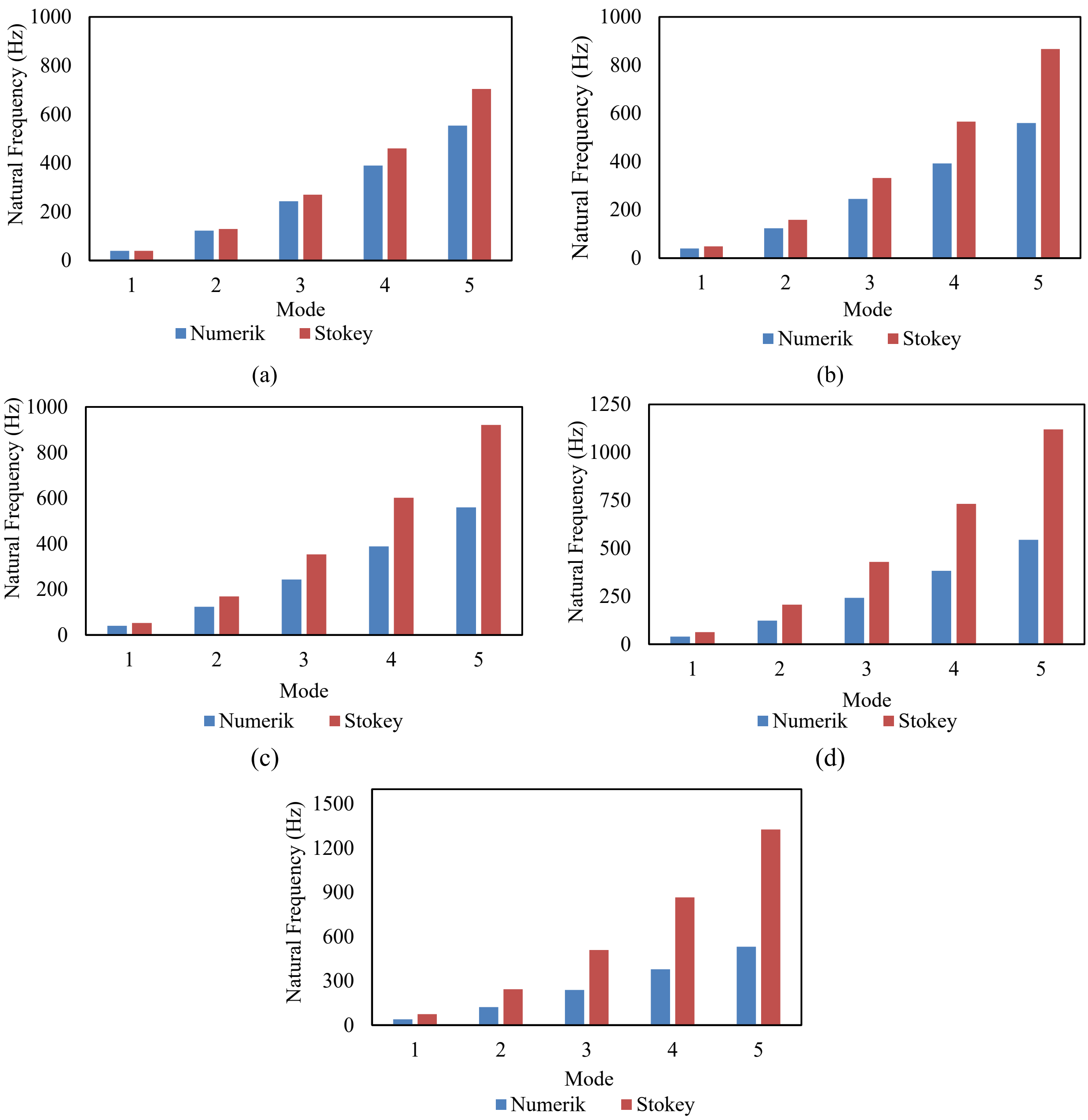

(e)

Figure 3. (a) M1, (b) M2, (c) M3, (d) M4, and (e) M5 comparison of numerical results and stokey theory on castellated steel beams with variations in web openings using fixed-pinned boundary condition

Models M2 to M5 show a difference in natural frequency values between the results of numerical analysis and theoretical calculations using the Stokey approach. The difference was recorded to vary from 9 Hz to 904 Hz under fixed-pinned pedestal conditions. Among all the models tested, model M5 produced the largest difference in natural frequency values.

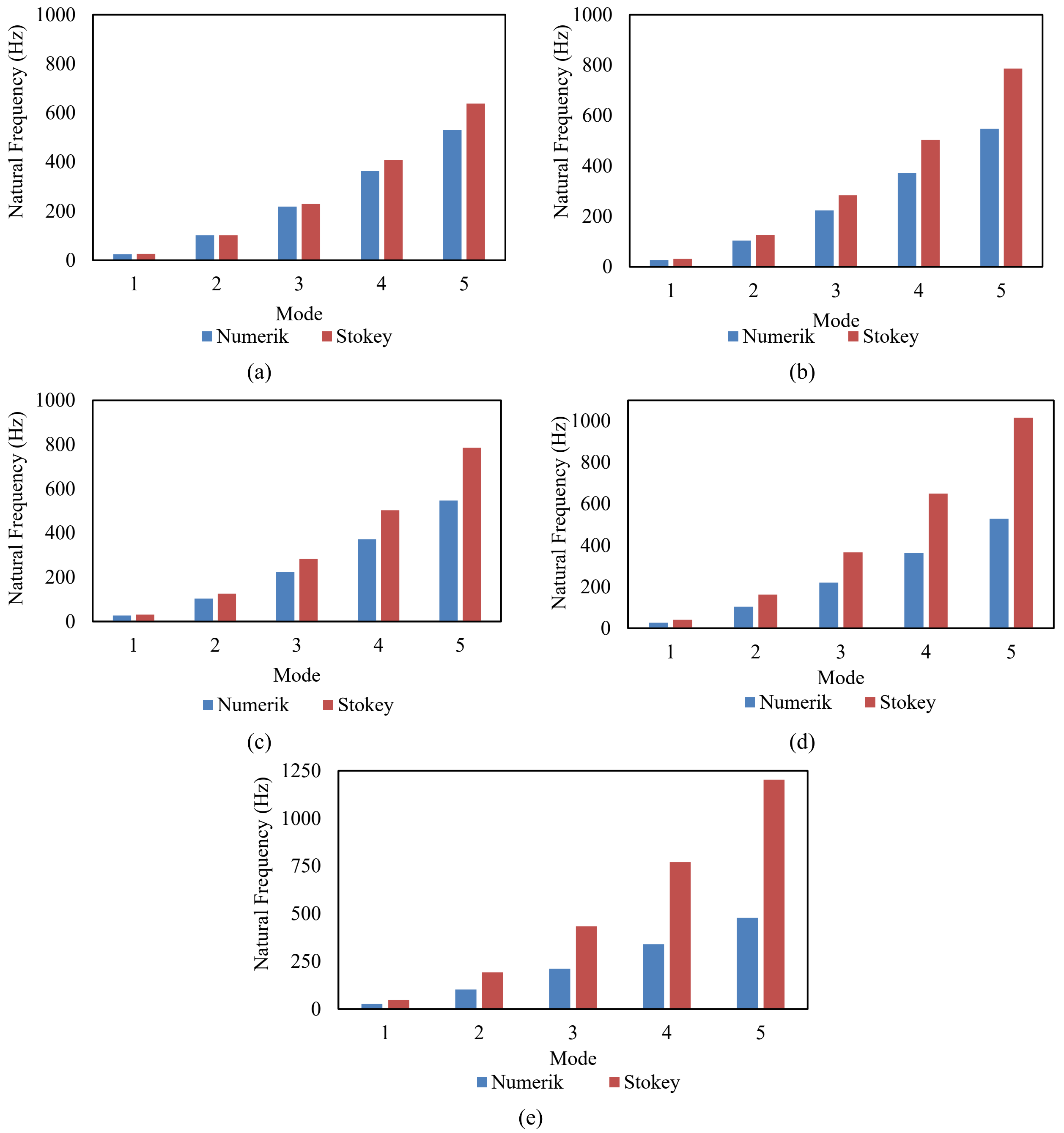

Figure 4. (a) M1, (b) M2, (c) M3, (d) M4, and (e) M5 comparison of numerical results and stokey theory on castellated steel beams with variations in web openings using pinned-pinned boundary condition

The pinned-pinned boundary condition exhibits the lowest natural frequency among the three support types when compared to fixed-fixed and fixed-pinned configurations. This is primarily due to the limited ability of the pinned support to resist structural vibrations, resulting in reduced dynamic stiffness. The difference in natural frequency values for models M2 to M5 under this support condition ranges between 11 Hz and 487 Hz.

The analysis based on Stokey's theory resulted in higher natural frequency values than the numerical simulation results for all vibration modes analyzed. Stokey's theory calculates the natural frequencies based on the assumption of uniform distribution of stiffness and mass along the beam length.

This model does not take into account the weakening of the structure due to the presence of openings in the beam body. In contrast, numerical simulations in Abaqus consider geometric influences, including the effects of stress concentration and redistribution of internal forces around openings. In addition, in the numerical model, the steel mass lost due to the openings is also taken into account, resulting in an uneven mass distribution. This condition contributes to the decrease in the resulting natural frequency value. From the mode shape analysis results, it is known that the natural frequency value increases as the mode order increases. However, the difference between theoretical and numerical results also increases at higher modes. This indicates that the influence of local deformation due to the presence of openings is more significant at higher modes of vibration. In the first mode, the vibration is still evenly distributed along the structural element, while in the subsequent modes, the vibration pattern becomes more complex with larger deformations occurring around the opening area.

In addition, based on Stokey's theory, models with smaller spacing between openings, such as M5, tend to have higher natural frequency values than models with larger spacing between openings, such as M2. This phenomenon arises because a larger number of openings in theory is considered not to change the stiffness significantly, while in reality, the local weakening effect is more dominant.

The numerical analysis results show relatively similar natural frequency values between models due to considering the actual stiffness degradation caused by the dense openings. Thus, the results of this discussion confirm that using numerical models provides a more realistic estimation of the exact condition of the structure. Therefore, numerical approaches are highly recommended for designing structures involving complex geometries to obtain more accurate predictions of dynamic behavior.

The difference in values between the results of numerical analysis and calculations using Stokey's theory can be calculated using the formula found in this study. This formula can consider the value of mass and stiffness loss in beams subjected to body openings. Stokey's theoretical approach calculates the reduction in moment of inertia using a coefficient representing the relationship between the percentage reduction in inertia due to the shape and number of openings and the resulting natural frequency value. The percentage reduction in moment of inertia is obtained through calculations based on a specific formula that considers the profile's geometry, the openings' location, and the volume of material lost due to the openings. The percentage reduction in moment of inertia is calculated based on the Formula (2).

$$I_n = I_x - (k \times n) \quad (2)$$

It is the moment of inertia value of the castella beam, *Ix* is the moment of inertia value of the solid steel, *k* is the coefficient 6,664E-07, and *n* indicates the number of openings. The value 6,664E-07 is the coefficient obtained to calculate the moment of inertia for the circular web opening shape. The results of the calculation of the moment of inertia of the castella beam can be seen in Table 2.

After systematically considering and analyzing the correction coefficient values used in Formula (2), the natural frequency values calculated based on modifying the Stokey formula were obtained. This modification helped predict the decreasing trend of the natural frequency in response to the effect of the aperture. The difference between the theoretical calculation based on Stokey's formula and the numerical results obtained from the Abaqus CAE simulation is that the graphs displayed in the analysis show a unidirectional trend pattern.

The theoretical and numerical approaches showed a similar trend in the direction of natural frequency change concerning the variation of the number of openings. The similarity of this pattern confirms that the theoretical approach used is representative enough to describe the general behavior of the structure. In addition, the stiffness correction coefficient *K*, which is included in the calculation through Formula (2), has an important role and is closely related to the applied opening configuration. The geometry of the openings in the primary structural system directly influences the stiffness correction value, which in turn impacts the natural frequency calculation results. Validation of this can be visually observed in Figure 5, which show comparisons between the theoretical and numerical results for various web openings and castellated beam supports.

Table 2. Calculation of moment of inertia of square body opening

Modelling	Number of Openings	Inertia Value of Solid Steel	Coefficient	Castella Steel Inertia Value
M1	-	1.761E-05	6.664E-07	-
M2	9	-	6.664E-07	1.161E-05
M3	11	-	6.664E-07	1.028E-05
M4	16	-	6.664E-07	6.946E-06
M5	19	-	6.664E-07	4.947E-06

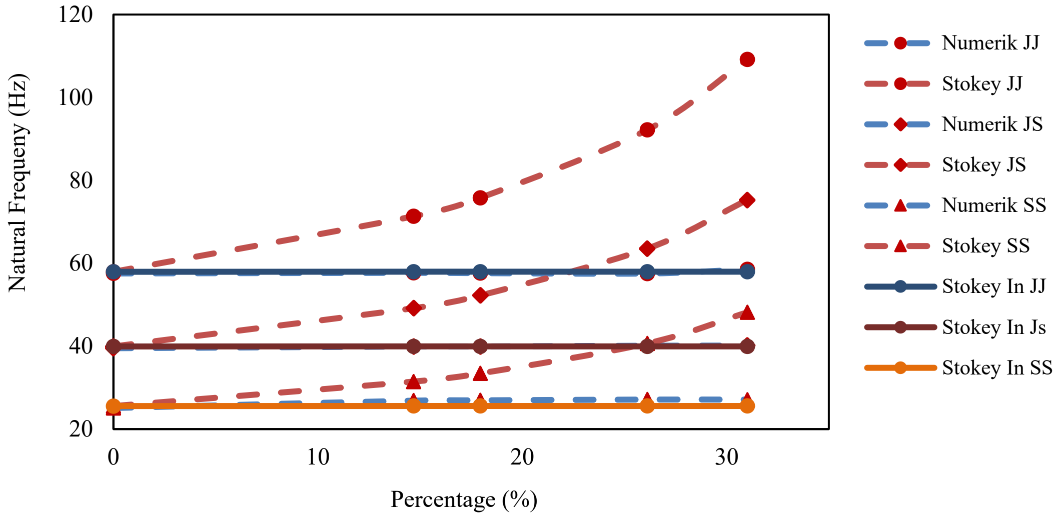

Figure 5. Effect of moment of inertia analysis calculation

The analysis done by [19] found that changing the Stokey theory calculation with coefficients related to the shape and size of the opening affected the natural frequency value. Each variation of opening shape and size has a different effect on the weight and stiffness of the beam. Therefore, it is essential to adjust the analysis to make the results more accurate and represent the actual structural conditions.

4. Conclusions

This study analyzes the effect of square openings in castellated beams on changes in dynamic characteristics, especially natural frequency values, by considering various types of supports. Comparison of natural frequency results was obtained through two approaches, namely numerical methods and theoretical calculations using the Stokey formula.

The openings' configuration significantly affects the castellated beams' mass and stiffness. The more the number of openings, the lighter the mass of the beam and the less the stiffness. This is evident from the comparison between the model without openings (M1), which weighs 21.3 kg/m, and the model with 19 openings (M5), which weighs only 6.00 kg/m. The analysis shows that the natural frequency increases as the number of openings in the beam increases. This increase is more evident and significant in the calculations using Stokey's theory than in the numerical analysis results. The difference is due to Stokey's theoretical approach that does not consider local effects due to the presence of openings, such as mass reduction due to openings. In contrast, the numerical simulation can capture these effects in more detail and more thoroughly.

The natural frequency values based on the numerical analysis show an almost uniform trend in each model. This is due to the ability of numerical analysis to systematically calculate changes in mass and stiffness due to openings in the beam body. Meanwhile, Stokey's theoretical approach cannot thoroughly calculate the mass and stiffness reduction, resulting in significant differences. The numerical simulation results show that the natural frequency values are lower than the theoretical calculation results. The difference between the two methods ranges from 9 Hz to 904 Hz at the fixed-fixed support, 7 Hz to 794 Hz at the fixed-pinned support, and 11 Hz to 487 Hz at the pinned-pinned support. This difference increases at higher vibration modes, indicating the structure's sensitivity to local deformation due to openings.

Modifying Stokey's formula by introducing correction coefficients into the moment of inertia significantly improves the accuracy of natural frequency predictions for castellated beams. By accounting for the number and geometry of web openings, the proposed correction reflects the associated mass and stiffness reductions more realistically. Validation through finite element simulations using Abaqus confirms a strong agreement, particularly in the lower vibration modes. Therefore, this approach is recommended for reliable analytical estimation of natural frequencies in castellated beam design, especially in low-mode vibration analyses.

References

[1] S. G. Morkhade and L. M. Gupta, "Behavior of Castellated Steel Beams: State of the Art Review," Electron. J. Struct. Eng., vol. 19, no. 1, pp. 39–48, 2019.

[2] V. N. Jadhav, R. R. Kurlapkar, and A. P. Patil,

"Assessment of Lateral-Torsional Buckling Capacity of Mild Steel Castellated Beam with Sinusoidal Web Openings," Asian J. Civ. Eng., vol. 25, no. 5, pp. 4081–4090, 2024, doi: 10.1007/s42107-024-01032-w.

[3] S. M. Hadeed and A. J. H. Alshimmeri, "Comparative Study of Structural Behaviour for Rolled and Castellated Steel Beams with Different Strengthening Techniques," Civ. Eng. J., vol. 5, no. 6, pp. 1384–1394, 2019, doi: 10.28991/cej-2019-03091339.

[4] T. Theopuspitasari Lu and Y. Afriado, "Analisis Perbandingan Struktur Komposit Pelat Beton Balok Baja Sebelum dan Sesudah Kastela," vol. 9, no. 1, 2026.

[5] S. Mathur, M. Senthilpandian, and K. Karthikeyan, "Static and Dynamic Analysis of Steel Beams with Web Openings," J. Phys. Conf. Ser., vol. 1716, no. 1, 2021, doi: 10.1088/1742-6596/1716/1/012016.

[6] A. J. Mehetre and R. S. Talikoti, "Castellated Steel Beams A Torsional Analysis," Int. J. Eng. Adv. Technol., vol. 9, no. 5, pp. 536–540, 2020, doi: 10.35940/ijeat.e9606.069520.

[7] V. W. Yustisia, B. Suswanto, D. Irawan, and D. Iranata, "The Structural Behavior of Castellated Beam with Shape Variation Using Finite Element Methods," IOP Conf. Ser. Mater. Sci. Eng., vol. 930, no. 1, 2020, doi: 10.1088/1757-899X/930/1/012051.

[8] H. El-Dehemy, "Static and Dynamic Analysis Web Opening of Steel Beams," World J. Eng. Technol., vol. 05, no. 02, pp. 275–285, 2017, doi: 10.4236/wjet.2017.52022.

[9] F. P. V. Ferreira, A. Rossi, and C. H. Martins, "Lateral-Torsional Buckling of Cellular Beams According to the Possible Updating of EC3," J. Constr. Steel Res., vol. 153, pp. 222–242, 2019, doi: 10.1016/j.jcsr.2018.10.011.

[10] M. Junus, "Castella Composite Beam Testing to be Used as A Structural Element of Multistorey Buildings in Eastern Indonesian Region," ARPN J. Eng. Appl. Sci., vol. 11, no. 1, pp. 731–736, 2016.

[11] C. M. Weidlich, E. D. Sotelino, and D. C. T. Cardoso, "An Application of the Direct Strength Method to the Design of Castellated Beams Subject to Flexure," Eng. Struct., vol. 243, no. April, p. 112646, 2021, doi: 10.1016/j.engstruct.2021.112646.

[12] S. S. Mali and P. D. Kumbhar, "Comparative Study on Behaviour of Castellated Beams with Diamond- and Hexagonal-Shaped Openings Using CFRP Stiffeners," Asian J. Civ. Eng., vol. 25, no. 1, pp. 939–952, 2024, doi: 10.1007/s42107-023-00823-x.

[13] S. S. Patil and P. D. Kumbhar, "Comparative Study on the Behaviour of Castellated Beams Provided With Hexagonal, Circular, and Diamond-Shaped Web Openings," Asian J. Civ. Eng., vol. 25, no. 1, pp. 359–369, 2024, doi: 10.1007/s42107-023-00780-5.

[14] A. Sayyad and A. Shaikh, "Estimation of Deflections in Cantilever and Fixed Castellated Beams with Hexagonal, Square and Circular Openings," Tec. Ital. J. Eng. Sci., vol. 64, no. 1, pp. 118–127, 2020, doi: 10.18280/ti-ijes.640118.

[15] N. H. Aswad, D. Pongsimpin, T. Asikin, R. M. Rachman, Tachrir, and M. Tumpu, "Analysis of the Effect of High Opening Variation on the Performance of Castellated Beams using the Reduced Beam Section Method," Eng. Technol. Appl. Sci. Res., vol. 15, no. 2, pp. 22059–22064, 2025, doi: 10.48084/etasr.10260.

[16] G. Nugroho, "Natural Frequency of Tension Cable Based on Moment Inertia to Span Ratio: Determination Using Analytical, Numerical and Experimental Study," Int. J. Sustain. Constr. Eng. Technol., vol. 11, no. 2, pp. 89–100, 2020, doi: 10.30880/ijscet.2020.11.02.010.

[17] J. K. Chen, B. Kim, and L. Y. Li, "Analytical approach for transverse vibration analysis of castellated beams," Int. J. Struct. Stab. Dyn., vol. 14, no. 3, pp. 1–10, 2014, doi: 10.1142/S0219455413500715.

[18] J. Z. Gu, "Free Vibration of Castellated Beams with Web Shear and Rotary Inertia Effects," Int. J. Struct. Stab. Dyn., vol. 14, no. 6, pp. 19–21, 2014, doi: 10.1142/S0219455414500114.

[19] F. Aughitri, G. Nugroho, and A. Jamadin, "Dynamic Behavior of Castella Beams : Effect of Web Openings on Stiffness at Natural Frequencies," vol. 28, no. 1, pp. 77–89, 2025.

[20] W. . Stokey, Vibration of systems having distributed mass and elasticity: chapter. 1988.

E-ISSN: 2528-388X
P-ISSN: 0213-762X

Priority Analysis of Community Preparedness for Megathrust Earthquakes Using Analytic Hierarchy Process (AHP): A Case Study of Warungboto Village, Yogyakarta

Adi Setiabudi Bawono* and Muhamad Nur Huda

Civil Engineering Department, Universitas Teknologi Yogyakarta, Yogyakarta 55285, Indonesia

Keywords:
Community preparedness,
Earthquake,
Megathrust,
Analytic Hierarchy Process (AHP),
Disaster mitigation

ABSTRACT

The Special Region of Yogyakarta is highly vulnerable to megathrust earthquakes due to its proximity to an active subduction zone, posing significant risks to communities. While structural mitigation is important, community preparedness is critical to disaster risk reduction. This study aims to identify and prioritise factors influencing preparedness using the Analytic Hierarchy Process (AHP), with a case study in Warungboto Village. Data were collected from 30 respondents using pairwise-comparison questionnaires. Four main criteria were evaluated: Public Education and Awareness, Infrastructure Resilience, Emergency Response Management, and Social and Psychological Factors. The results show that Public Education and Awareness is the most influential factor (35.81%), followed by Infrastructure Resilience (24.10%), Emergency Response Management (20.20%), and Social and Psychological Factors (20.00%). Key sub-criteria include disaster drills, education programs, and awareness levels. All Consistency Ratio (CR) values are below 0.1, indicating reliable results. These findings highlight the importance of education-based strategies in enhancing community preparedness.

1. Introduction

Indonesia lies at the convergence of three major tectonic plates: the Indo-Australian Plate, the Eurasian Plate, and the Pacific Plate. This unique geological setting makes the country one of the most seismically active regions in the world, with frequent earthquakes along plate boundaries. The interaction between these plates, particularly through subduction processes, generates significant seismic energy that can result in large-magnitude earthquakes. One of the most critical and potentially catastrophic types of seismic events in this context is the megathrust earthquake, which originates from the rupture of large segments along subduction zones.

Megathrust earthquakes are characterised by their extremely large magnitudes and their potential to trigger secondary hazards, such as tsunamis, which can cause widespread destruction in coastal areas. Based on global earthquake records over the past 25 years, Indonesia has experienced several major megathrust events, including those on December 26, 2004; March 28, 2005; and October 25, 2010 [1]–[3]. These events not only resulted in significant loss of life and infrastructure damage but also highlighted the urgent need for comprehensive disaster risk reduction strategies, particularly in regions located along active subduction zones.

Most of Indonesia's southern coastal regions lie directly above active subduction interfaces, making them highly vulnerable to megathrust earthquakes and associated tsunami hazards. This includes the Special Region of Yogyakarta (Daerah Istimewa Yogyakarta/DIY), which is situated near the Java subduction zone. The vulnerability of this region has been clearly demonstrated by past seismic events, particularly the 2006 Yogyakarta earthquake, as well as by updated national earthquake hazard maps that indicate a high level of seismic risk [4]. Given these conditions, it is essential not only to focus on

*Corresponding author.
E-mail: adi.setiabudi@uty.ac.id

https://doi.org/10.21831/inersia.v21i2.95716
Received 5 February 2026; Revised 4 May 2026; Accepted 4 May 2026
Available online 10 May 2026

structural mitigation measures but also to strengthen non-structural measures, especially community preparedness.

Disaster risk reduction efforts have increasingly emphasised the importance of integrating both structural and non-structural approaches. While structural measures, such as earthquake-resistant buildings and infrastructure, are crucial in reducing physical damage, non-structural aspects—particularly community preparedness—play a vital role in minimising casualties and enhancing response effectiveness during disaster events. Communities with higher preparedness tend to respond more quickly, make better decisions, and adapt more effectively under emergency conditions, thereby significantly reducing potential losses. However, community preparedness is a complex, multidimensional concept influenced by interrelated factors, including education, infrastructure, governance, social dynamics, and individual perceptions of risk.

To analyse complex, multi-criteria problems, the Analytic Hierarchy Process (AHP) has been widely used as a decision-making tool. AHP is a structured multi-criteria decision-making method that allows researchers to decompose complex problems into a hierarchical framework consisting of objectives, criteria, and sub-criteria. Through pairwise comparisons, AHP enables the systematic evaluation of both qualitative judgments and quantitative data, yielding priority weights that support informed decision-making [5]. The flexibility and robustness of AHP make it particularly suitable for disaster management studies, where multiple interdependent factors must be considered simultaneously.

Previous studies have demonstrated the applicability of AHP in various disaster-related contexts. For instance, Wibowo and Khilmi [6] applied AHP to determine priority strategies for earthquake mitigation in Semarang City, while Pamungkas et al. [7] used the method to assess community preparedness levels in Cisarua District. Similarly, Hadi et al. [8] utilised AHP to map earthquake vulnerability in Bengkulu City, and Jena et al. [9] applied an integrated approach to assess earthquake risk in Aceh. On an international scale, Yariyan et al. [10] employed AHP to evaluate earthquake risk in Sanandaj, Iran. These studies highlight the versatility of AHP in addressing disaster-related decision-making problems across different spatial contexts.

Despite the growing body of literature, most studies have focused primarily on hazard assessment, structural vulnerability, and large-scale risk mapping. Relatively limited attention has been given to the quantitative prioritisation of community preparedness factors, particularly at the local or village level. In addition, many studies are conducted at regional or national scales, which may not fully capture the unique socio-demographic characteristics and local dynamics that influence preparedness at smaller spatial units.

Recent studies have further emphasised that megathrust earthquakes in Indonesia present not only significant structural challenges but also substantial non-structural risks, particularly in densely populated urban areas. The southern part of Java, including the Special Region of Yogyakarta, lies near an active subduction interface capable of generating large-magnitude earthquakes and tsunamis. Despite this high level of hazard exposure, preparedness at the community level often remains uneven, with variations in knowledge, awareness, and response capacity among different groups.

In this context, Warungboto Village represents a highly relevant case study. As an urban village characterised by relatively high population density and complex social interactions, Warungboto is exposed to significant earthquake risks and faces challenges in evacuation, communication, and coordination during emergencies. Understanding the priority factors that shape community preparedness in such settings is essential for designing targeted, context-specific disaster risk reduction strategies.

Therefore, this study aims to address the identified research gap by applying the Analytic Hierarchy Process (AHP) to systematically identify and prioritise the key factors influencing community preparedness for megathrust earthquakes at the village level. By focusing on Warungboto Village as a case study, this research seeks to provide both theoretical and practical contributions to disaster risk reduction, particularly in enhancing community-based preparedness strategies in earthquake-prone urban areas.

2. Methods

This study employs a quantitative approach using the Analytical Hierarchy Process (AHP) to determine community preparedness priorities for megathrust earthquakes. AHP was selected for its ability to evaluate complex decision-making problems involving multiple criteria systematically and to incorporate expert judgment in determining priority weights. Data analysis methods are the process of converting raw data into meaningful information through various statistical and non-statistical techniques to support decision-making or hypothesis testing [12].

2.1 Study Area and Data Collection

The study was conducted in Warungboto Village (Figure 1), an urban area in Yogyakarta City characterised by dense settlements and potential exposure to seismic hazards. The selection of this location was based on its vulnerability to earthquake risks and its relevance to urban disaster preparedness planning.

Primary data were collected through structured questionnaires distributed to respondents within the study area. The questionnaire was designed to obtain pairwise comparisons of criteria and sub-criteria related to community preparedness using the AHP scale.

2.2 Research Respondents

The study involved 30 respondents, consisting of 23 academics (76.7%) and 7 community representatives (23.3%). Respondents were selected through purposive sampling, targeting individuals with relevant knowledge and experience in disaster management and familiarity with local conditions.

The inclusion of academic respondents was intended to ensure analytical rigour, while community representatives contributed practical insights into local preparedness conditions. This combination is considered appropriate for AHP-based studies, where expert judgment plays a critical role in the evaluation process.

2.3 Development of AHP Hierarchical Structure

The AHP model in this study is structured into three hierarchical levels: objective, criteria, and sub-criteria.

1. Objective Level

The primary objective is to determine priority factors influencing community preparedness for megathrust earthquakes. Disaster preparedness policies have been established to strengthen Indonesia's disaster management system and increase capacity across various regulations and community guidelines, which were used to determine the criteria and sub-criteria in this article.

2. Criteria Level

The criteria were developed through a review of relevant policies and literature on disaster management in Indonesia, including:

Figure 1. Research Location [11].

- Law No. 24 of 2007 concerning Disaster Management [13]
- Disaster Preparedness Campus Guidelines by the Indonesian Red Cross (PMI), 2012 [14]
- Regulation of the Minister of Education and Culture (Permendikbud) No. 33 of 2019 concerning the Disaster-Safe Education Unit (SPAB) Program [15]
- Supporting literature from peer-reviewed journals and official policy documents [16]–[18]

Based on this review, four main criteria (N) were identified as: Infrastructure Resilience (A); Public Education and Awareness (B); Emergency Response Management (C); Social and Psychological Factors (D).

3. Sub-Criteria Level

Each criterion is further divided into several sub-criteria identified through content analysis of the selected references. The first sub-criterion is building structure, which refers to the structural condition and earthquake resistance of buildings. The second is evacuation routes and warning signals, which encompass the availability and accessibility of evacuation paths and early warning systems. Technology for mitigation is also considered, focusing on the use of technology to support disaster risk reduction and early warning mechanisms. In addition, disaster education programs are included to assess structured educational activities aimed at improving disaster-related knowledge within the community. Disaster drills and simulations represent practical exercises designed to train community responses during emergency situations.

Another important aspect is the level of public awareness, which reflects the community's understanding and awareness of disaster risks. Emergency response policy examines the existence of regulations and procedures related to disaster response, while coordination with stakeholders highlights collaboration among government agencies, communities, and relevant institutions. The availability of emergency facilities includes the provision of shelters, medical services, and logistical support during disasters. Community participation is also emphasized, referring to the involvement of local communities in preparedness activities. Furthermore, disaster risk perception evaluates how communities perceive earthquake risks and potential impacts. Finally, post-disaster psychosocial support addresses the availability of mental and emotional recovery assistance for affected communities after a disaster event.

2.4 Data Analysis Using AHP

The data processing in this study used the Analytic Hierarchy Process (AHP), which systematically evaluates decision-making problems through pairwise comparisons and priority weighting. The analysis stages are described as follows [5].

Preparation of a pairwise comparison matrix between criteria and subcriteria

The first step involves constructing a pairwise comparison matrix between criteria and sub-criteria based on respondents' judgments using Saaty's scale (1–9). This matrix reflects the relative importance of each element. The results of the pairwise comparison between the criteria examples are presented in Table 1.

Table 1. Example of a Pairwise Comparison Matrix of Criteria from Respondent 1

Criteria	A	B	C	D
A	1	1/3	5	9
B	3	1	3	7
C	1/5	1/3	1	5
D	1/9	1/7	1/5	1

Aggregation of Respondents' Judgments

Since the data were obtained from multiple respondents, the pairwise comparison values were combined using the Geometric Mean (GM), as shown in Equation 1.

$$GM = \sqrt[n]{(X_1)(X_2) \dots . (X_n)} \qquad (1)$$

which *GM* as geometric mean, X_1 as Respondent 1, X_2 as Respondent 2, X_3 as Respondent 3, *GM* is to obtain a representative value for each comparison, which is shown in Table 2.

Table 2. Geometric Mean of Criteria

Criteria	A	B	C	D	Total
A	1.000	0.717	1.326	1.126	4.169
B	1.395	1.000	2.572	1.360	6.326
C	0.754	0.389	1.000	1.501	3.644
D	0.888	0.735	0.666	1.000	3.290
Total	4.037	2.841	5.564	4.987	14.429

Normalization of the Matrix

The aggregated matrix is then normalised by dividing each element by the column's total. This step aims to standardise the values for subsequent calculations. The normalized matrix is presented in Table 3.

Table 3. Matrix normalization

Criteria	A	B	C	D	Total
A	0.248	0.252	0.238	0.226	0.964
B	0.345	0.352	0.462	0.273	1.432
C	0.187	0.137	0.180	0.301	0.804
D	0.220	0.259	0.120	0.201	0.799
Total	1.000	1.000	1.000	1.000	4.000

Priority Weight Calculation

The priority weights are calculated by averaging the values in each row of the normalized matrix. These weights represent the relative importance of each criterion. The results of the priority weights are shown in Table 4.

Table 4. Matrix Normalization

Criteria	Code	Weight	Presentase
Infrastructure Resilience	A	0.241	24.10%
Public Education and Awareness	B	0.358	35.81%
Emergency Response Management	C	0.201	20.1%
Social and Psychological Factors	D	0.200	20%
Total		1.000	100%

Eigenvalue (λ_{max}) Calculation

The maximum eigenvalue (λ_{max}) is calculated to assess the consistency of the pairwise comparison matrix. This is obtained by multiplying the pairwise matrix with the priority vector and averaging the results as Equation 2. The calculated λ_{max} was 4.099.

$$\lambda_{max} = \sum matriks \frac{\sum value\ of\ n\ row\ element}{N} \quad (2)$$

Consistency Test (CI and CR)

To ensure the reliability of the judgments, the Consistency Index (CI) and Consistency Ratio (CR) are calculated using Equation 3 and Equation 4.

$$CI = \frac{\lambda_{max} - n}{n-1} \quad (3)$$

$$CR = \frac{CI}{RI} \quad (4)$$

Based on the calculation results, the CI value is 0.0365 (3.65%), which is less than the acceptable threshold of 10%. Therefore, the pairwise comparison matrix is considered consistent, and the analysis can proceed to the next stage.

Final Priority Analysis

The final step involves combining the priority weights across all hierarchical levels. This is done by multiplying the sub-criteria's weights by their respective parent criteria to obtain the global weights. The hierarchical structure and final weights are illustrated in Figure 2.

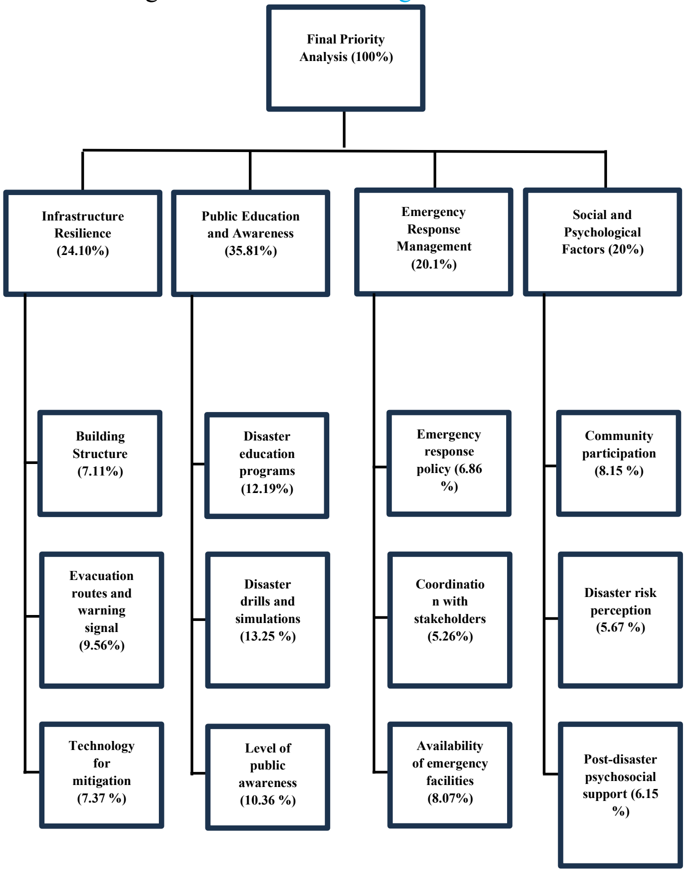

Figure 2. The hierarchical structure and final weights

2.4 Research Procedure

The overall research procedure, including data collection, AHP model development, analysis, and interpretation, is illustrated in Figure 3.

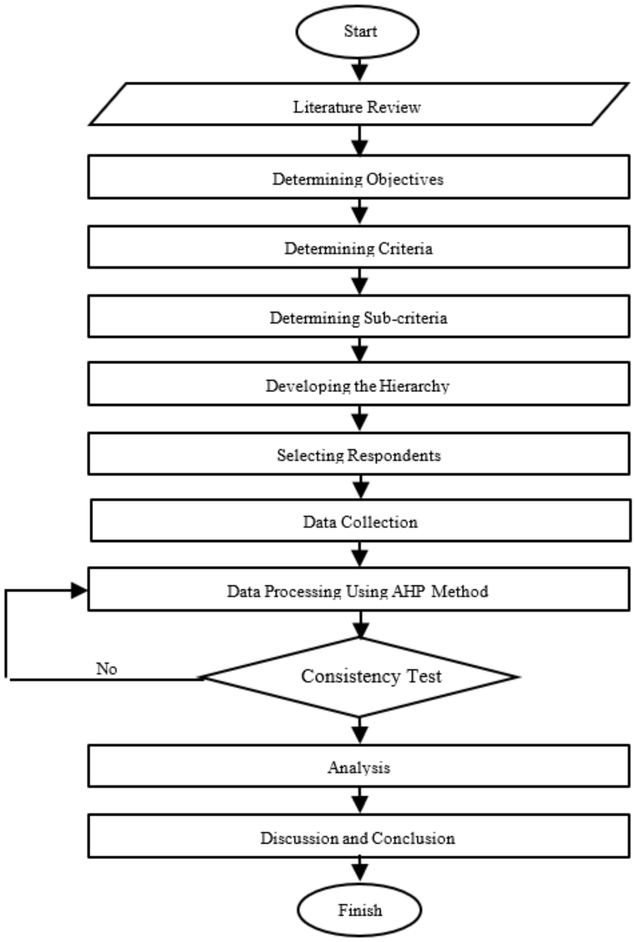

Figure 3. Research Flowchart

3. Results and Discussion

3.1 Main Criteria Weighting Results

The results of the weighting calculation for the main community preparedness criteria are presented in Figure 2. These results indicate that public education and awareness emerge as the most dominant factors in enhancing preparedness for megathrust earthquakes. With the highest weighting among all criteria, this finding demonstrates that knowledge-based and awareness-driven aspects play a central role in shaping the community's overall preparedness capacity.

A more detailed interpretation of these results suggests that the ability of individuals and communities to understand disaster risks, recognise early warning signs, and respond appropriately is strongly influenced by their level of education and exposure to disaster-related information. Public education and awareness not only improve individual preparedness but also facilitate collective action, which is essential in emergencies. In densely populated areas such as Warungboto Village, where rapid response and coordination are critical, the role of education becomes even more significant.

In comparison, other criteria such as infrastructure resilience, emergency response management, and social and psychological factors, although still important, have relatively lower weighting values. This does not imply that these factors are less relevant; rather, it indicates that their effectiveness is closely dependent on the community's level of awareness and understanding. For example, well-developed infrastructure may not function optimally if the community lacks the knowledge to utilise it during an emergency. Therefore, the dominance of public education and awareness highlights the foundational role of non-structural capacity in disaster preparedness..

3.2 Sub-Criteria Weighting Results

Based on the calculation of the total sub-criteria weights, the highest priority sub-criteria include: disaster drills and simulations, disaster education programs, and public awareness level. These sub-criteria are all associated with the Public Education and Awareness criterion, further emphasising the critical importance of strengthening non-structural aspects in disaster mitigation efforts. The prominence of these sub-criteria indicates that practical, continuous learning processes are essential for building an effective preparedness system at the community level.

Disaster drills and simulations, which rank as the highest priority, play a crucial role in providing hands-on experience and improving response readiness. Through simulation activities, community members can practice evacuation procedures, understand their roles during emergencies, and identify potential challenges in real-time scenarios. This experiential approach enhances not only technical skills but also confidence and decision-making capabilities under pressure.

Similarly, disaster education programs serve as a fundamental component in increasing knowledge and awareness. These programs can take various forms, including formal education, community training, workshops, and public campaigns. When implemented consistently and inclusively, such programs can significantly improve the community's understanding of disaster risks and appropriate response strategies.

The level of public awareness, as another key sub-criterion, reflects the extent to which individuals are conscious of potential hazards and motivated to take preventive actions. High levels of awareness are often associated with proactive behaviour, such as preparing emergency kits, participating in training activities, and disseminating information within the community. Therefore, enhancing awareness is not only about information dissemination but also about fostering a culture of preparedness.

Overall, the dominance of these sub-criteria underscores the strategic priority of strengthening human capacity through education, training, and awareness-building initiatives to improve disaster preparedness, particularly in urban village contexts.

3.3 Consistency Ratio (CR) Test

The Consistency Ratio (CR) for each pairwise comparison matrix in this study is below the acceptable threshold of 0.1. This indicates that respondents' judgments are consistent and reliable, and that the resulting priority weights can therefore be considered valid for decision-making purposes.

In the Analytic Hierarchy Process (AHP), consistency is a critical aspect that ensures the logical coherence of pairwise comparison judgments. A CR value below 0.1 suggests that the comparisons made between criteria and sub-criteria are not random or contradictory, but rather reflect a structured and rational evaluation process. This strengthens the credibility of the analysis and supports the robustness of the findings.

Furthermore, achieving a satisfactory level of consistency indicates that the respondents have a clear understanding of the criteria being evaluated. This is particularly important in studies involving subjective judgments, such as perceptions of preparedness and risk. The consistency of the results also implies that the prioritisation outcomes can be confidently used as a basis for developing disaster risk reduction strategies.

In addition, the acceptable CR values obtained in this study demonstrate that the AHP method has been properly applied, following standard procedures for pairwise comparisons and consistency testing. This reinforces the methodological validity of the research and enhances its contribution to the field of disaster preparedness analysis.

3.4 Discussion

The results of the Analytic Hierarchy Process (AHP) analysis clearly indicate that public education and awareness constitute the most influential factors in enhancing community preparedness, with a weighting value of 35.81%. This finding demonstrates that, among all evaluated criteria, education-related aspects have the highest priority in shaping the community's preparedness capacity. In particular, the results suggest that levels of knowledge, understanding, and prior experience in disaster management play a critical role in determining how individuals and communities respond to the potential threat posed by megathrust earthquakes. This is especially relevant in the context of Warungboto Village, where variations in educational exposure and access to disaster-related information may significantly influence preparedness levels.

A deeper interpretation of these findings reveals that individuals who possess adequate knowledge and understanding of disaster risks are more likely to take appropriate preventive actions, respond effectively during emergencies, and participate actively in preparedness programs. Prior experience with disaster events or training activities further strengthens this capacity, as experiential learning enables individuals to internalise response procedures and develop situational awareness. Therefore, education and awareness are not only theoretical constructs but also practical components that directly influence behavioural responses in disaster situations.

This finding is consistent with a growing body of literature indicating that well-informed and educated communities tend to respond more quickly, effectively, and appropriately during disaster events. Previous studies have highlighted that disaster education programs, public awareness campaigns, and community-based training activities are essential tools for improving preparedness and resilience [19]. Such programs are particularly effective when they incorporate participatory approaches, simulations, and continuous engagement, allowing community members to actively develop and reinforce their understanding of disaster risks and response mechanisms.

Furthermore, the results of this study indicate that infrastructure resilience and emergency response management remain important supporting factors in enhancing community preparedness. Although these factors do not rank as highly as education and awareness, their roles are nonetheless critical, particularly in facilitating evacuation processes, enabling efficient emergency response, and supporting post-disaster recovery. Infrastructure resilience, including the availability of safe evacuation routes, shelters, and communication systems, provides the physical foundation necessary for effective disaster response. Meanwhile, well-organised emergency management systems ensure coordination among stakeholders and enable timely intervention during critical situations.

In addition to structural and managerial aspects, social and psychological factors also contribute significantly to shaping community preparedness. Elements such as community participation, risk perception, awareness, trust, and social cohesion play a crucial role in influencing how individuals and groups respond to disaster threats. Communities with strong social networks and high levels of trust are generally better able to coordinate collective action, share information, and support one another during emergencies. These social dynamics enhance not only preparedness but also the community's overall resilience.

Several empirical studies have demonstrated that communities with higher levels of disaster knowledge and participation in preparedness training tend to exhibit faster and more effective responses, thereby reducing the adverse impacts of disasters. Training-based interventions, including evacuation drills, simulation exercises, and structured disaster education programs, have been shown to significantly improve response behaviour, decision-making capabilities, and overall preparedness levels [20]. Moreover, integrating local knowledge with formal disaster education further strengthens community capacity by ensuring that preparedness strategies are contextually relevant and culturally appropriate.

In addition, effective risk communication and public awareness strategies have been identified as key drivers of improved preparedness behaviour. Clear, consistent, and accessible communication enables communities to understand potential hazards better and take proactive measures to mitigate risks. Studies have shown that communities exposed to regular information dissemination and awareness campaigns tend to demonstrate higher levels of preparedness and a greater willingness to engage in disaster risk reduction activities [21]. This highlights the importance of not only providing information but also ensuring it is communicated and understood effectively by diverse segments of the population.

The dominance of public education and awareness as the highest-priority factor in this study indicates that non-structural factors play a crucial, and often decisive, role in enhancing community preparedness. This finding suggests that efforts to improve knowledge, understanding, and practical experience through education and training may yield more immediate and sustainable impacts than relying solely on physical infrastructure improvements. While infrastructure remains important, its effectiveness depends heavily on the community's capacity to utilise it appropriately during disasters.

In the specific context of Warungboto Village, this result is particularly significant due to its urban characteristics, including high population density, limited open spaces, and complex spatial arrangements. These conditions can complicate evacuation processes and increase the potential risks associated with disaster events. As a result, the community's ability to respond quickly and effectively depends heavily on its level of awareness, preparedness, and familiarity with emergency procedures. Education and simulation-based preparedness programs are therefore essential to ensuring that residents can act decisively and appropriately during emergencies.

The findings of this study are generally consistent with previous research indicating that disaster education and training significantly improve response capacity and reduce disaster impacts. However, compared with studies conducted in other regions, this study places greater emphasis on the role of education relative to infrastructure.

This difference may be attributed to specific local conditions, including socio-demographic characteristics, levels of access to information, and the existing state of infrastructure development in urban environments such as Warungboto Village. In areas where basic infrastructure is already relatively available, the marginal benefit of improving education and awareness may be more pronounced.

Nevertheless, infrastructure resilience and emergency response management should not be overlooked. Although they rank lower in priority, their contributions remain essential for supporting evacuation, facilitating emergency operations, and enabling effective recovery. This underscores the importance of adopting an integrated approach to disaster risk reduction, in which both structural and non-structural strategies are implemented in complementary ways.

Finally, social and psychological factors, including community participation, collective awareness, and social cohesion, continue to play a significant role in shaping preparedness behaviour. Communities characterised by strong interpersonal relationships and active participation are generally more resilient, as they are better able to coordinate actions, provide mutual support, and adapt to changing conditions during disasters. These findings reinforce the importance of fostering community engagement and strengthening social capital as part of comprehensive disaster preparedness strategies.

4. Conclusions

At the sub-criteria level, disaster drills and simulations, disaster education programs, and the level of public awareness are identified as the top priorities. These findings highlight that strengthening non-structural aspects, particularly through continuous education and training, is crucial to enhancing community preparedness for potential megathrust earthquakes.

The results of this study provide practical implications for policymakers and stakeholders in designing effective community-level disaster risk reduction strategies. Specifically, efforts should focus on implementing sustainable disaster education programs, conducting regular simulation exercises, and improving risk communication to increase public awareness.

Overall, this study confirms that a comprehensive approach integrating educational, technical, and social dimensions is essential to improving disaster preparedness and reducing potential impacts in earthquake-prone areas.

Further research is recommended to involve a larger number of respondents and a more representative proportion of the community, to combine the AHP method with other methods to enrich the analysis, to assess the implementation of priority outcomes through concrete programs, and to evaluate their effectiveness.

This study contributes to the existing body of knowledge by providing a structured prioritisation of community preparedness factors using the AHP method at the village level. Unlike previous studies that focus on broader scales, this research highlights the importance of local context in shaping preparedness strategies.

However, this study has several limitations, including a relatively small sample size and the dominance of academic participants over community representatives. Future research is recommended to involve a more balanced and larger sample, integrate additional decision-making methods, and evaluate the implementation of recommended strategies in real-world settings.

References

[1] USGS, "Significant Earthquakes 1900-2026," *https://earthquake.usgs.gov/*, 2026. [Online]. Available: https://earthquake.usgs.gov/earthquakes/browse/significant.php. [Accessed: 05-Feb-2026].

[2] BNPB, "Mengungkap Ancaman Megathrust di Indonesia," *bnpb.go.id*, 2024. [Online]. Available: https://sejarah.dibi.bnpb.go.id/artikel/mengungkap-ancaman-megathrust-di-indonesia-1/84. [Accessed: 05-Feb-2026].

[3] P. Supendi *et al.*, "On the potential for megathrust earthquakes and tsunamis off the southern coast of West Java and southeast Sumatra, Indonesia," *Nat. Hazards*, vol. 116, no. 1, pp. 1315–1328, 2023.

[4] A. R. Bramantya, Sugiharto, and Lillyana Mulya, "Documenting disaster in Yogyakarta: A case study of earthquake on May 27 th, 2006," *Rec. Libr. J.*, vol. 10, no. 2 SE-Research Paper, pp. 247–260, Dec. 2024.

[5] T. L. Saaty, "What is the Analytic Hierarchy Process?," in *Mathematical Models for Decision Support*, vol. 48, Berlin, Heidelberg, Heidelberg: Springer Berlin Heidelberg, 1988, pp. 109–121.

[6] S. R. Wibowo, Muhammad Nanang Khilmi; Cholil, "Analisis Penanganan Bencana di Kota Semarang 2024 menggunakan Metode AHP dan VIKOR,"

Kementeri. Pendidikan, Kebudayaan, Riset, dan Teknol., vol. 30, pp. 82–91, 2025.

[7] E. Pamungkas, T.D., Aliyan, S.A., Nurfalah, I., Ningrum, E. & Maryani, "Preparedness of the community in facing disasters like earthquakes (Case : Cisarua , Indonesia)," *Jàmbá - J. Disaster Risk Stud.*, pp. 1–9, 2022.

[8] A. I. Hadi, M. Farid, B. Harlianto, N. Hudayat, and M. Krisbudianto, "Pemetaan Potensi Kerentanan Gempabumi Pada Kota Bengkulu Menggunakan Data Mikrotremor dan Metode Analytical Hierarchy Process," vol. 18, pp. 105–118, 2021.

[9] R. Jena, B. Pradhan, and G. Beydoun, "Geoscience Frontiers Integrated model for earthquake risk assessment using neural network and analytic hierarchy process : Aceh province , Indonesia," *Geosci. Front.*, vol. 11, no. 2, pp. 613–634, 2020.

[10] P. Yariyan, H. Zabihi, I. D. Wolf, M. Karami, and S. Amiriyan, "Earthquake risk assessment using an integrated Fuzzy Analytic Hierarchy Process with Artificial Neural Networks based on GIS: A case study of Sanandaj in Iran," *Int. J. Disaster Risk Reduct.*, vol. 50, no. February, p. 101705, 2020.

[11] Google Maps, "Satelite View of Warungboto Village," 2025. [Online]. Available: https://maps.app.goo.gl/nG3aoz9VhPgx7YJi9. [Accessed: 02-Jun-2025].

[12] J. W. Creswell, *Research Design: Qualitative, Quantitative, and Mixed Methods Approaches*, 6th ed. SAGE Publications, 2022.

[13] U. No.24/2007, *Undang-Undang Republik Indonesia Nomor 24 Tahun 2007 Tentang Penanggulangan Bencana*. 2007.

[14] F. M. Dheni Prasetyo, "Panduan Kampus Siaga Bencana." PMI (Palang Merah Indonesia, 2012.

[15] Disaster Resilient Education, *Disaster Resilient Education*, 1st ed. Jakarta: National Secretariat For Disaster-Safe Education Unit Ministry Of Education And Culture Directorate-General Of Primary And Secondary Education Directorate Of Special Education Development, 2019.

[16] L. Judijanto, N. Nofirman, R. Yusuf, and M. Marjan, "Tinjauan Upaya Pemerintah dalam Mitigasi Risiko Gempa Megathrust dengan Analisis Kesiapan Infrastruktur dan Edukasi Masyarakat," vol. 2, no. 03, 2024.

[17] A. N. Gadeng, E. Maryani, E. Ningrum, and I. Setiawan, "The Implementation of Disaster Curriculum Toward Disaster Preparedness Campus at Syiah Kuala University," *Geosfera Indones.*, vol. 7, no. 3, p. 304, 2022.

[18] R. F. Nasution and E. B. Lestari, "Peran Pendidikan Kesiapsiagaan Bencana dalam Meningkatkan Kesadaran pada Remaja," vol. 3, 2025.

[19] L. Guo, M. Fang, L. Liu, H. Chong, W. Zeng, and X. Hu, "The development of disaster preparedness education for public: a scoping review," *BMC Public Health*, vol. 25, no. 1, p. 645, 2025.

[20] W. Addiarto, M. G. R. Pandin, A. Yusuf, and R. Yunita, "Disaster education and training programs for enhancing community preparedness: a systematic review from the nursing perspective," *medRxiv*, pp. 2009–2025, 2025.

[21] M. Watanabe and T. Fujimi, "Causal effects of time-sensitive risk communication on disaster preparedness," *Int. J. Disaster Risk Reduct.*, vol. 126, p. 105598, 2025.

E-ISSN: 2528-388X
P-ISSN: 0213-762X

INERSIA
Vol.22, No.1, May 2026

Integrated Infiltration Runoff Drainage Assessment for Urban Pluvial Flooding at a Campus Scale in a Tropical Environment

Aiun Hayatu Rabinah, Suparman*, Jamal Mahbub, Parhadi, Dian Sukma Larassati, Baiq Heny Sulistiawati, and Rizky Aji Kusdiyanto

Civil Engineering Department, Politeknik Negeri Semarang, Semarang 50275, Indonesia

Keywords:
Green–Ampt model
Unsaturated soil
Hydraulic conductivity
Low Permeability

ABSTRACT

Urban pluvial flooding frequently occurs in semi-urban tropical environments where intense rainfall exceeds local infiltration and drainage capacity. This study presents an integrated infiltration runoff drainage assessment at the campus scale to evaluate surface water inundation risk at Politeknik Negeri Semarang, Indonesia. Soil physical and hydraulic properties were characterized through laboratory testing, and infiltration behavior was simulated using the physically based Green–Ampt model under 2, 5, 10, and 20-year return period rainfall. Runoff was estimated using the Rational Method based on rainfall intensity corresponding to the time of concentration, while drainage storage capacity was quantified through field-based geometric measurements. The results indicate that the site is dominated by fine-grained soils (OH/MH; A-7-5) with very low saturated hydraulic conductivity (4.209×10^{-6} mm/s), limiting infiltration effectiveness to the early stage of rainfall. Infiltration rates rapidly decline toward saturated conductivity values, causing increasing rainfall increments to be converted directly into surface runoff. Estimated runoff volumes increase from 341.308 m³ (2-year) to 527.498 m³ (20-year return period). Although total drainage storage capacity (1270.38 m³) exceeds runoff volume, the storage margin decreases significantly under higher return periods, indicating increasing susceptibility to drainage surcharge. The integrated framework provides a process-based explanation of pluvial flooding driven by limited infiltration and drainage capacity utilization in tropical campus environments.

1. Introduction

Urban drainage systems in rapidly developing areas are increasingly challenged by intense rainfall events that generate surface runoff exceeding local storage and conveyance capacity. When rainfall-induced runoff cannot be accommodated by drainage networks and available infiltration capacity, temporary surface water inundation occurs, commonly referred to as urban pluvial flooding. This type of flooding is not associated with river overflow but is instead driven by the interaction between rainfall intensity, soil infiltration behavior, land surface characteristics, and drainage system performance [1][2].

In tropical regions, flooding caused by heavy rainfall is becoming more frequent due to high rainfall intensity combined with progressive land-use changes that reduce effective infiltration areas. Increasing urban development and heavy rainfall contribute to increasing urban flood volume and increasing drainage loads [3]. The expansion of impervious surfaces and the limited capacity of urban drainage systems often result in localized inundation even during relatively short rainfall events. Similar conditions have also been reported in urban areas experiencing rapid land-use change and increasing runoff concentration [4]. Previous studies have shown that such flooding is strongly controlled by the exceedance of drainage storage capacity and transient soil saturation rather than catchment-scale hydrological processes [5][6].

Semarang City, Central Java, Indonesia, represents a typical tropical urban environment where pluvial flooding frequently occurs. The Politeknik Negeri Semarang (Polines) campus, located in the Tembalang area, experiences recurrent surface water inundation during

*Corresponding author.
E-mail: suparman@polines.ac.id

https://doi.org/10.21831/inersia.v21i2.96113
Received 27 February 2026; Revised 13 May 2026; Accepted 14 May 2026
Available online 18 May 2026

heavy rainfall events despite the presence of an established drainage network. Several buildings within the campus are situated in local topographic depressions, which further increase vulnerability to water ponding when drainage capacity is exceeded. Previous investigations in the surrounding Tembalang area have reported similar drainage-related inundation driven by rainfall-induced runoff [7][8].

The generation of surface runoff in such environments is closely linked to soil infiltration characteristics. Infiltration governs the partitioning of rainfall into subsurface flow and surface runoff, particularly during the early stages of rainfall. Fine-grained soils with moderate to high plasticity typically exhibit low permeability and limited infiltration capacity, leading to rapid saturation and increased runoff generation under intense rainfall conditions [9][10]. Numerous studies have shown that infiltration rates are initially high due to matric suction effects but decline rapidly as the soil approaches saturation, highlighting the transient nature of infiltration processes [11][12]. Wei et al. also observed a similar trend, where an increase in soil moisture during rainfall resulted in a reduced infiltration rate [13].

Physically based infiltration models provide a valuable framework for representing these processes. Zhang et al. also reported that rainfall infiltration behavior in unsaturated geomaterials is strongly influenced by transient hydraulic boundary conditions [14]. The Green–Ampt model has been widely applied to simulate infiltration under rainfall conditions because it explicitly accounts for soil hydraulic properties and wetting front advancement [15]. When combined with rainfall frequency analysis and runoff estimation methods, infiltration modeling enables a more realistic assessment of runoff generation and drainage surcharge potential. For small to medium urban catchments such as campus areas, the Rational Method remains a practical approach for estimating peak runoff, particularly when rainfall intensity is derived from the time of concentration [16][17].

In addition to runoff generation, drainage storage capacity plays a critical role in controlling surface water inundation. Drainage channels act as temporary storage that can attenuate runoff peaks; however, when their capacity is exceeded, water is forced onto the surface, resulting in localized flooding. Studies on urban drainage systems emphasize that pluvial flooding often arises not from insufficient total storage volume alone but from the combined effects of limited infiltration, reduced effective drainage capacity, and local hydraulic bottlenecks [1][18].

Despite increasing attention to pluvial flooding, integrated studies that explicitly link soil infiltration behavior, rainfall characteristics, runoff generation, and drainage storage capacity at the campus scale remain limited, particularly in Indonesian contexts. Many existing studies focus on regional flooding or evaluate drainage systems without incorporating detailed soil infiltration analysis [19][20]. Consequently, there is a need for an integrated assessment that captures the coupled hydrological and geotechnical controls governing surface water inundation in semi-urban environments. This evaluation is essential for adapting urban drainage under changing rainfall conditions [21].

This study investigates rainfall infiltration and surface runoff at the Polines campus as an integrated approach to understanding and reducing pluvial flood risk caused by drainage capacity exceedance. The objectives are to (i) characterize soil physical and hydraulic properties, (ii) evaluate infiltration behavior using the Green–Ampt model under different rainfall return periods, (iii) estimate runoff based on rainfall intensity corresponding to the time of concentration, and (iv) assess the adequacy of existing drainage storage capacity. By integrating infiltration analysis with runoff and drainage evaluation, this study provides a scientifically grounded basis for improving stormwater management strategies in campus-scale and similar urban environments.

Unlike many previous studies that evaluate urban flooding mainly through rainfall–runoff relationships or drainage hydraulics alone, this study integrates soil infiltration behavior, runoff generation, and drainage storage capacity within a unified campus-scale framework. The novelty lies in explicitly linking transient infiltration dynamics, represented by the physically based Green–Ampt model, with drainage storage exceedance as the mechanism controlling surface water inundation.

Instead of treating infiltration losses as a lumped parameter, this study demonstrates how limited soil permeability and rapid saturation restrict runoff reduction during intense rainfall, even when total drainage storage appears sufficient. By combining laboratory-based soil characterization, rainfall frequency analysis, time-of-concentration–based runoff estimation, and detailed drainage storage evaluation, the proposed framework provides a process-oriented explanation of pluvial flooding in tropical semi-urban environments.

2. Methods

2.1. Study Area

This study was conducted at the Politeknik Negeri Semarang (Polines) campus, located in the Tembalang area, Semarang City, Central Java, Indonesia. The campus represents a semi-urban catchment characterized by mixed land use, including academic buildings, paved surfaces, and limited green open spaces. Several facilities are situated within shallow topographic depressions, making the area susceptible to surface water inundation during intense rainfall events. Stormwater drainage is provided by an open-channel network that functions both as a conveyance system and temporary storage during rainfall.

2.2. Soil Sampling and Laboratory Testing

Soil samples were collected from representative locations within the campus area. Disturbed samples were used to characterize soil physical and hydraulic properties governing infiltration behavior. Laboratory testing was conducted at the Soil Mechanics Laboratory of Polines following relevant ASTM standards.

The tests included grain size distribution analysis (sieve and hydrometer), Atterberg limits tests, and specific gravity tests. Soil classification was performed using the Unified Soil Classification System (USCS) and the AASHTO classification system. Saturated hydraulic conductivity (Ks) was determined through laboratory permeability tests using constant-head or falling-head methods depending on soil gradation.

2.3 Rainfall Data and Frequency Analysis

Daily maximum rainfall data over a ten-year period were obtained from the nearest rainfall station serving the Tembalang area. The data were screened for consistency and completeness, and annual maximum rainfall values were extracted. Frequency analysis was conducted to estimate design rainfall depths for return periods of 2, 5, 10, and 20 years. The selected return periods represent typical design conditions for evaluating urban drainage performance.

2.4. Infiltration Analysis

Infiltration behavior was evaluated using the physically based Green–Ampt model, which represents infiltration in unsaturated soils as the downward movement of a sharp wetting front. The infiltration rate *f(t)* is expressed as Equation 1.

$$f(t) = K_s\left(1+\frac{\psi_f(\theta_s-\theta_i)}{F(t)}\right) \tag{1}$$

Where K_s as the saturated hydraulic conductivity, ψ_f as the the wetting front suction head, θ_s *and* θ_i as the saturated and initial volumetric water contents, respectively, and *F(t)* as the cumulative infiltration at time *t*. In addition, Cumulative infiltration is obtained by solving Equation 2.

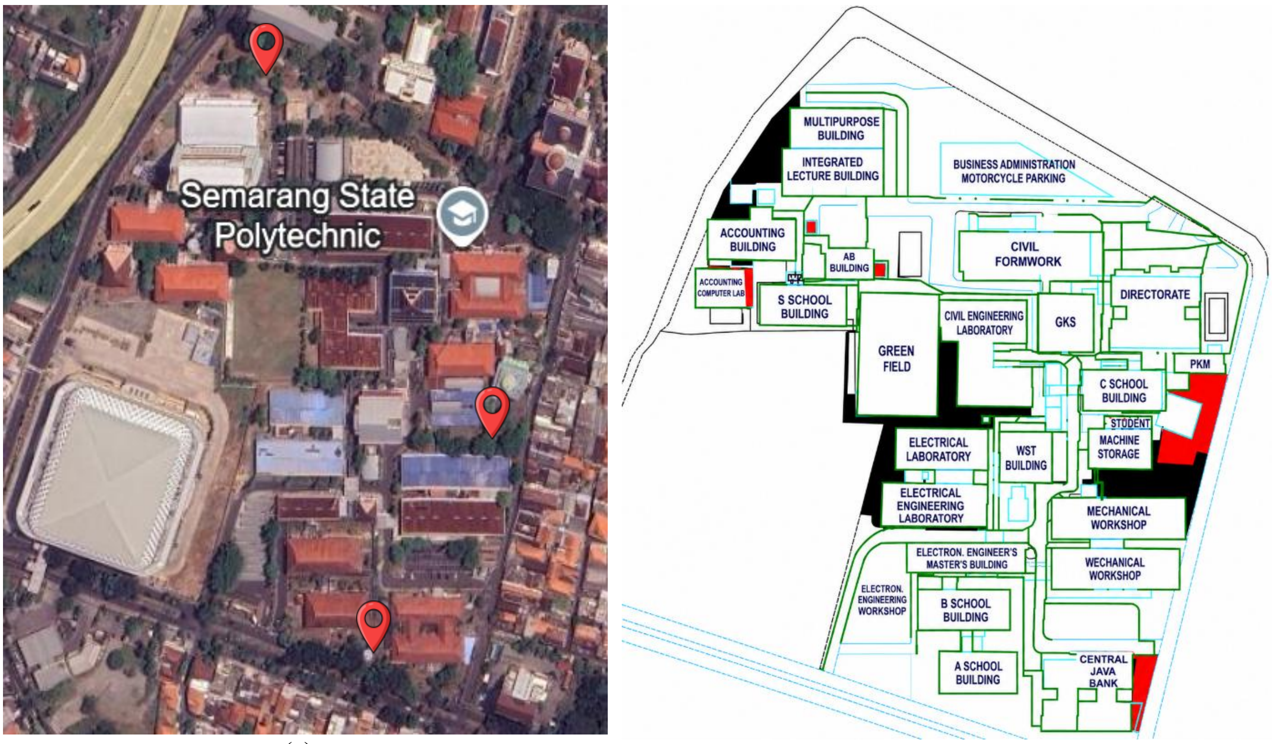

(a) (b)

Figure 1. Location of the study area (a) and layout of the existing campus drainage network (b)

$$F(t) = K_s t + \psi_f(\theta_s - \theta_i)\ln\left(1+\frac{F(t)}{\psi_f(\theta_s-\theta_i)}\right) \quad (2)$$

Model parameters were derived from laboratory test results and estimated soil water characteristic properties. The analysis focused on the temporal evolution of infiltration capacity and the transition from unsaturated to near-saturated soil conditions during rainfall events.

2.5. Time of Concentration

The time of concentration (T_c) was estimated using the Kirpich (Equation 3) , which is commonly applied to small urban catchments.

$$T_c = 0.0195\ L^{0.77} S^{-0.385} \quad (3)$$

where L represent the length of the longest flow path and S represent the average slope of the catchment. The calculated T_c was used to determine the critical rainfall duration for runoff estimation.

2.6. Runoff Estimation

Surface runoff was estimated using the Rational Method, which is suitable for small urban catchments such as campus areas. Peak runoff discharge Q was calculated as Equation 4.

$$Q = C\ I\ A \quad (4)$$

where C represents the runoff coefficient representing land-use and surface characteristics, I represents the rainfall intensity corresponding to the time of concentration, and A represents the catchment area.

Runoff coefficients were selected based on observed land cover and surface conditions within the campus. Rainfall intensity values were derived from the design rainfall depth divided by the critical rainfall duration equal to T_c.

2.7. Drainage Storage Capacity Assessment

The drainage network was inventoried through field observation and dimensional measurements of channel cross sections and lengths. The storage volume of each drainage segment was calculated geometrically, and the total drainage storage capacity was obtained by summing individual segment volumes.

Drainage performance was evaluated by comparing runoff volumes and peak discharges with the available drainage storage capacity. Conditions where runoff exceeded storage capacity were interpreted as drainage surcharge, leading to surface water inundation.

2.8. Integrated Assessment Framework

An integrated assessment framework was applied to evaluate urban pluvial flooding driven by drainage capacity exceedance. The framework links rainfall characteristics, transient infiltration behavior, runoff generation, and drainage storage capacity within a unified process-based analysis. This approach enables identification of critical conditions under which surface water inundation occurs despite the presence of drainage infrastructure, highlighting the combined influence of limited infiltration and drainage surcharge at the campus scale.

3. Results and Discussion

3.1. Soil Characteristics and Hydraulic Implications

The soil characterization results indicate that the study area is dominated by fine-grained soils with moderate to high plasticity. As summarized in Table 1, the soil is classified as OH/MH according to the Unified Soil Classification System and A-7-5 under the AASHTO classification. The measured saturated hydraulic conductivity is 4.209×10^{-6} mm/s, which falls within the category of very low permeability soil.

Table 1. Physical and hydraulic properties of soil in the study area

Parameter	Unit	Value
Specific Gravity (*Gs*)	–	2,65
Liquid Limit (*LL*)	%	> 50
Plasticity Index (*PI*)	%	19,35
Soil classification (USCS)	–	OH / MH
Soil classification (AASHTO)	–	A-7-5
Saturated hydraulic conductivity (K_s)	mm/s	$4{,}209 \times 10^{-6}$

3.2. Soil Water Retention Characteristics

The unsaturated hydraulic behavior of the soil is further illustrated through the Soil Water Characteristic Curve (SWCC), as presented in Figure 2. The curve represents the relationship between matric suction and volumetric water content and provides quantitative insight into moisture retention and desaturation behavior of the fine-grained soil in the study area.

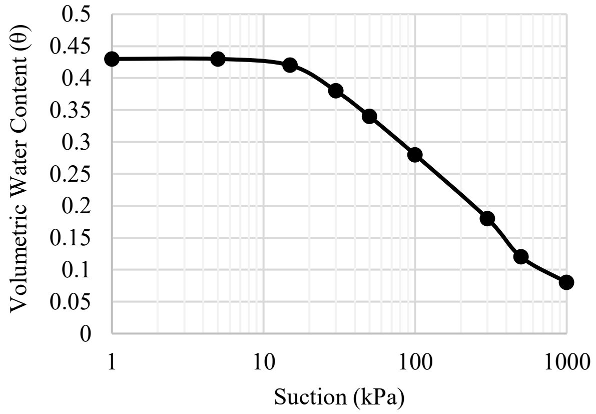

Figure 2. Soil Water Characteristic Curve (SWCC) for the study area

As shown in Figure 2, the saturated volumetric water content (θ_s) is approximately 0.43, while the residual volumetric water content (θ_r) is approximately 0.08. The air entry value (AEV) is approximately 15 kPa, indicating the suction threshold at which desaturation begins. The dominant transition zone extends from approximately 15 kPa to 300 kPa, reflecting gradual moisture redistribution within the soil matrix. The relatively low air entry value confirms the fine pore structure typical of high-plasticity soils. Once matric suction decreases during rainfall infiltration, hydraulic conductivity rapidly approaches its saturated value, limiting additional increases in infiltration capacity.

3.3. Infiltration Dynamics under Design Rainfall

The infiltration behavior simulated using the Green–Ampt model exhibits a distinct transient pattern, as illustrated in Figure 3. At the onset of rainfall, infiltration rates are relatively high due to the influence of matric suction in unsaturated soil conditions. However, infiltration rates decline rapidly with time as the soil approaches saturation, eventually converging toward a quasi-steady value close to the saturated hydraulic conductivity.

Differences among return periods are evident during the initial phase of rainfall, where higher rainfall intensity produces higher initial infiltration rates. However, as rainfall continues, the infiltration curves tend to converge, indicating similar infiltration behavior at later stages.

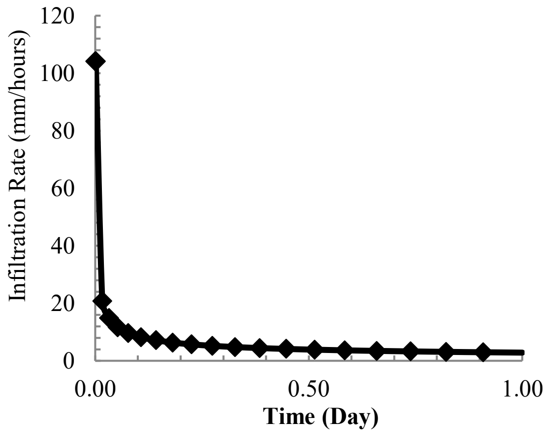

(a) 2-year return period rainfall

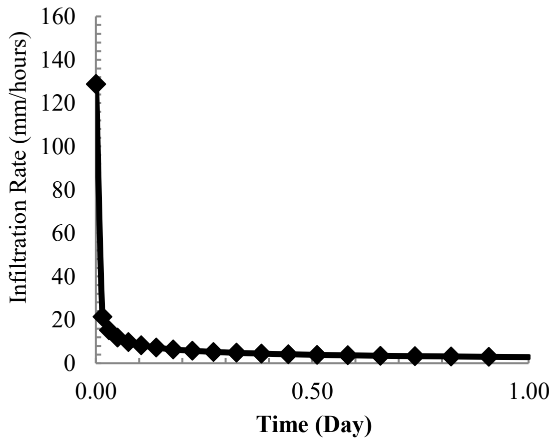

(b) 5-year return period rainfall

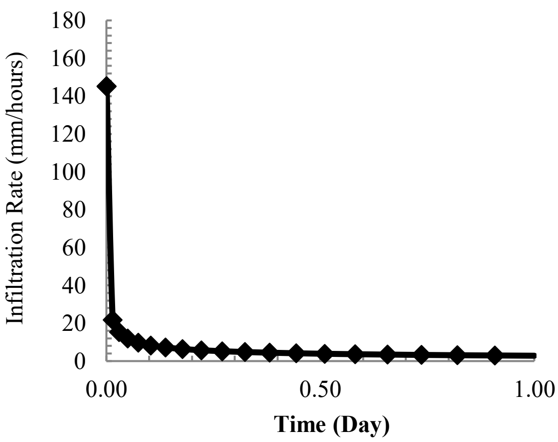

(c) 10-year return period rainfall

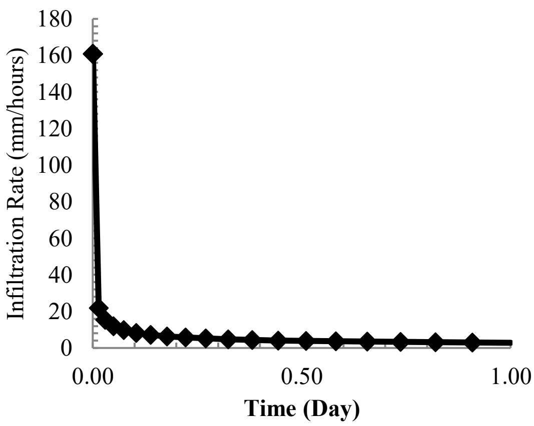

(d) 20-year return period rainfall

Figure 3. Temporal variation of infiltration rate simulated using the Green–Ampt model under different rainfall return periods

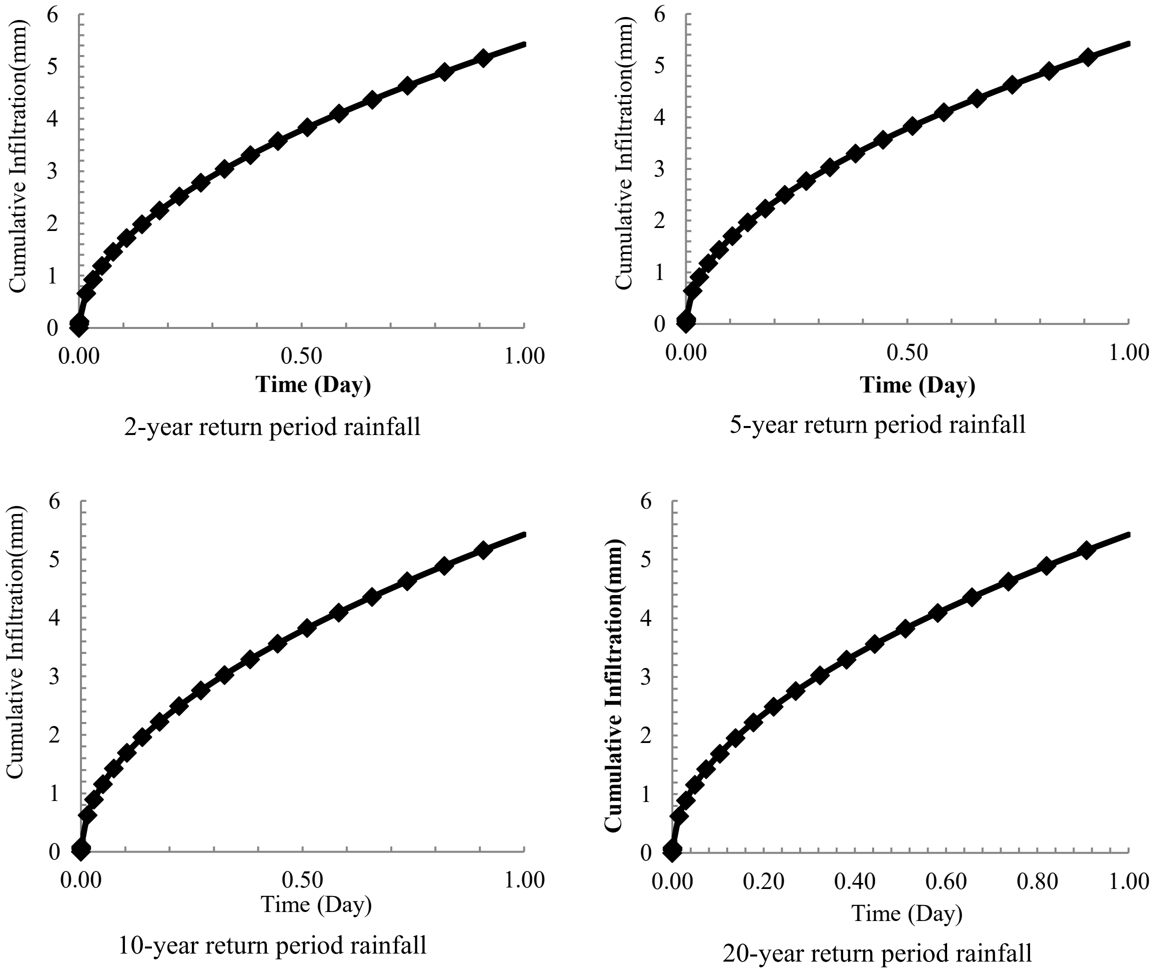

Figure 4. Cumulative infiltration as a function of time simulated using the Green–Ampt model for different rainfall return periods.

Table 2. Comparison between runoff volume and drainage storage capacity for different rainfall return periods

Return period (years)	Design rainfall (mm/day)	Estimated runoff volume (m³)	Drainage storage capacity (m³)	Storage margin (m³)
2	104.123	341.308	1270.38	928.692
5	128.767	422.090	1270.38	847.910
10	145.125	475.710	1270.38	794.290
20	160.924	527.498	1270.38	742.502

Cumulative infiltration (Figure 4) increases nonlinearly with time. Higher return periods produce larger cumulative infiltration values during early and intermediate rainfall durations. At longer durations, the cumulative infiltration curves evolve with similar slopes, indicating that infiltration increments become relatively uniform across return periods.

3.4. Rainfall Characteristics and Runoff Response

Rainfall frequency analysis using the Log-Pearson Type III distribution produced design rainfall depths ranging from 104,123 mm (2-year return period) to 160,924 mm (20-year return period). This increase in rainfall depth directly translates into higher runoff volumes and peak discharges, as estimated using the Rational Method. Runoff volumes were calculated using the Rational Method based on rainfall intensity corresponding to the time of concentration. The results are summarized in Table 2.

The results indicate a progressive increase in runoff volume with increasing rainfall return period. The estimated runoff volume increases from 341.308 m³ for the 2-year return period to 527.498 m³ for the 20-year return period.

3.5. Hydrological Partitioning and Rainfall Excess Transformation

To provide a clearer interpretation of rainfall–runoff behavior at the campus scale, the design rainfall input was conceptually partitioned into infiltration and rainfall excess components. At the beginning of rainfall events, water is partially absorbed into the soil profile under unsaturated conditions, driven by matric suction and surface hydraulic gradients. However, as infiltration capacity progressively declines toward the saturated hydraulic conductivity (K_s), the proportion of rainfall converted into surface runoff increases.

The results indicate that infiltration effectiveness is temporally constrained. During the early stage of rainfall, a portion of rainfall is accommodated within the soil matrix. As the soil approaches near-saturation conditions, additional rainfall increments exceed infiltration capacity and are transformed into rainfall excess. This transition occurs more rapidly under higher return period rainfall, where rainfall intensity surpasses the declining infiltration rate at an earlier stage.

The increase in runoff volume from 341.308 m³ (2-year return period) to 527.498 m³ (20-year return period) reflects this progressive shift in rainfall partitioning. Rather than demonstrating enhanced infiltration under higher rainfall intensity, the system exhibits increasing dominance of rainfall excess generation. Consequently, runoff response becomes primarily governed by surface hydrological processes once soil storage potential is exhausted.

This rainfall partitioning mechanism confirms that hydrological response in the study area is controlled by intrinsic hydraulic limitations rather than by total rainfall volume alone.

3.6. Discussions

Role of Soil Water Retention Behavior in Infiltration Limitation

The Soil Water Characteristic Curve (SWCC) provides a fundamental explanation of the transient infiltration behavior observed in this study. The identified air entry value of approximately 15 kPa indicates that desaturation begins at relatively low suction levels, which is characteristic of fine-grained soils with small pore throats and high plasticity. Such soils initially retain water effectively under moderate suction; however, capillary resistance diminishes rapidly as wetting progresses.

During the early stage of rainfall, matric suction enhances the hydraulic gradient between the soil surface and the advancing wetting front. This suction-controlled regime explains the elevated initial infiltration rates simulated using the Green–Ampt model. Classical infiltration theory has long established that early infiltration is dominated by suction effects before gradually transitioning to a conductivity-controlled regime [10][11]. Recent experimental investigations on unsaturated soils further confirm that matric suction significantly influences early infiltration but becomes progressively less dominant as the soil approaches saturation [12].

As suction decreases, hydraulic conductivity converges toward the saturated value (K_s). In the present study, the measured K_s (4.209×10^{-6} mm/s) is extremely low, indicating severe limitations in vertical percolation once near-saturation is reached. Although the SWCC shows a relatively wide suction transition zone (15–300 kPa), moisture redistribution within this range does not substantially increase infiltration capacity under sustained rainfall. Similar findings have been reported where infiltration under design storm conditions becomes strongly bounded by intrinsic soil hydraulic parameters rather than rainfall intensity alone [9].

The SWCC therefore clarifies why infiltration in the study area functions only as a short-duration buffer. Once suction effects are exhausted, additional rainfall increments are converted predominantly into surface runoff. This transition from suction-controlled to conductivity-limited flow represents a critical mechanism governing pluvial flood susceptibility at the campus scale.

Influence of Soil Hydraulic Properties on Infiltration Limitation

The results demonstrate that the study area is dominated by fine-grained soils (OH/MH; A-7-5) with very low saturated hydraulic conductivity (4.209×10^{-6} mm/s). Such hydraulic characteristics impose a fundamental limitation on infiltration capacity, particularly during prolonged rainfall events.

Fine-grained soils with high plasticity are known to exhibit low pore connectivity and reduced effective permeability, which significantly restrict vertical water movement [9][10]. The measured hydraulic conductivity in this study falls within the range typically associated with clayey soils where infiltration transitions rapidly from suction-controlled flow to conductivity-controlled flow. This behavior is consistent with the theoretical framework established by Green and Ampt [11], where infiltration capacity progressively declines as the wetting front advances and soil suction effects diminish.

Recent experimental investigations on unsaturated soils confirm that matric suction initially enhances infiltration rates but becomes progressively less influential as saturation increases [12][19]. The convergence of infiltration rates toward a quasi-steady value close to Ks observed in this study directly reflects this hydraulic control mechanism. Therefore, even under higher rainfall intensities associated with larger return periods, infiltration is ultimately bounded by intrinsic soil properties rather than rainfall magnitude.

These findings reinforce the interpretation that infiltration losses in the study area cannot be treated as a flexible or scalable parameter during extreme rainfall. Instead, infiltration acts as a rapidly exhausted buffer, after which additional rainfall is converted predominantly into surface runoff.

Transient Infiltration Dynamics and Return Period Effects

The simulated infiltration curves indicate that rainfall return period influences infiltration primarily during the early stage of rainfall events. Higher rainfall intensities produce higher initial infiltration rates due to increased hydraulic gradients at the soil surface. However, as rainfall duration increases, infiltration rates for different return periods converge.

This behavior aligns with classical infiltration theory, which predicts that infiltration under ponded or near-ponded conditions becomes governed by saturated hydraulic conductivity once soil suction is dissipated [11][15]. Beven further emphasized that cumulative infiltration in fine-grained soils is constrained by soil hydraulic properties rather than rainfall intensity alone [22].

The cumulative infiltration curves obtained in this study exhibit similar long-term slopes across return periods, indicating a hydraulic upper bound. Comparable results were reported by Rawls et al. (1983), who demonstrated that Green–Ampt parameters derived from soil properties strongly dictate infiltration limits under design storm conditions [9].

From a flood risk perspective, this convergence is critical. It implies that under high-return-period rainfall, infiltration does not proportionally increase to offset additional rainfall input. Consequently, incremental rainfall depth is translated almost directly into increased runoff volume.

Rainfall–Runoff Response in Semi-Urban Catchments

Rainfall frequency analysis shows a substantial increase in design rainfall depth from 104.123 mm/day (2-year) to 160.924 mm/day (20-year). The Rational Method results indicate a corresponding increase in runoff volume. In semi-urban environments such as campus areas, runoff generation is strongly influenced by impervious surfaces and limited infiltration capacity. Brattebo and Booth demonstrated that surface sealing significantly increases runoff response even when partial permeable areas exist [18]. Similarly, Mardiah et al. reported that infiltration-based mitigation in campus environments becomes less effective when soil permeability is inherently low [19].

The runoff behavior observed in this study supports the classification of flooding as urban pluvial flooding, which is primarily driven by local rainfall–runoff imbalance rather than riverine overflow [1][2]. The results confirm that runoff generation is controlled by short-duration rainfall intensity exceeding infiltration and drainage response capacity. Furthermore, studies in Indonesian urban contexts have highlighted similar mechanisms, where localized drainage exceedance rather than watershed-scale processes dominates flood occurrence [5][6][7][8].

Drainage Storage Capacity and Inundation Risk

The total available drainage storage capacity within the study area is approximately 1270,38 m³, as summarized in Table 2. When compared with effective runoff volumes, the drainage system appears capable of accommodating runoff for all analyzed return periods in terms of total volume balance. However, the safety margin between runoff volume and drainage storage decreases substantially with increasing rainfall return period.

Specifically, the storage margin decreases from approximately 928,69 m³ for the 2-year return period to 742,50 m³ for the 20-year return period. This reduction indicates that the drainage system operates increasingly close to its capacity threshold during extreme rainfall events. Similar patterns have been reported in urban drainage studies, where localized inundation occurs despite sufficient total storage due to temporal concentration of runoff and hydraulic bottlenecks within the drainage network [1][5]. Thus, the results suggest that pluvial flooding in the study area is governed not merely by total volume balance, but by the interaction between transient infiltration exhaustion, rapid runoff concentration, and drainage surcharge dynamics.

Influence of Drainage Geometry Variability on Hydraulic Performance

The heterogeneous distribution of drainage storage capacity introduces potential hydraulic imbalance within the network. Even when total system storage appears adequate, localized segments with limited cross-sectional capacity may experience surcharge earlier than others.
Urban drainage literature emphasizes that bottlenecks within drainage networks can trigger surface ponding despite sufficient aggregate capacity [1]. Flow concentration from impervious surfaces may rapidly load downstream segments, particularly those situated in micro-topographic depressions.

In the present study, the spatial variability of channel dimensions suggests that pluvial flooding risk is not solely dependent on total storage volume but also on the geometric configuration of individual segments. This finding supports the argument that drainage system evaluation should incorporate spatial distribution analysis rather than relying exclusively on cumulative capacity. The interaction between concentrated runoff input and heterogeneous storage distribution further amplifies vulnerability during high-intensity rainfall events.

Integrated Infiltration–Runoff–Drainage Interaction

The integrated framework adopted in this study highlights the coupled hydrological and geotechnical controls on pluvial flooding. Infiltration is initially governed by matric suction but quickly transitions to conductivity-controlled flow. Once infiltration capacity is exceeded, additional rainfall contributes directly to runoff generation. The drainage system then functions as temporary storage, but its safety margin diminishes with increasing return period.

Beven emphasized the necessity of process-based rainfall–runoff modeling to capture such nonlinear interactions [22]. Similarly, Butler and Davies argued that urban flood mitigation requires integration of hydrological losses and drainage hydraulics rather than treating them independently [1]. The results demonstrate that limited infiltration capacity in fine-grained tropical soils constrains the effectiveness of natural infiltration as a mitigation mechanism. As rainfall intensity increases, the system response becomes dominated by runoff concentration and drainage storage utilization. This integrated interpretation provides a mechanistic explanation for recurrent pluvial flooding at the campus scale and reinforces the importance of coupling infiltration enhancement strategies with drainage capacity optimization in semi-urban tropical environments.

Engineering Implications for Campus-Scale Stormwater Management

The hydraulic characteristics identified in this study indicate that stormwater mitigation in the investigated campus environment cannot rely solely on natural infiltration. The very low saturated hydraulic conductivity limits sustained vertical percolation once near-saturation conditions are reached. Although matric suction enhances infiltration at the onset of rainfall, this effect diminishes rapidly as the wetting front advances, a transition consistent with classical infiltration theory [11] and subsequent experimental findings on unsaturated soils [12].

Similar limitations have been reported in semi-urban environments where infiltration-based measures become less effective in fine-textured soils [19]. Under such conditions, rainfall excess generation increases rapidly once infiltration capacity is exceeded, leading to higher hydraulic loading on drainage systems. The present results confirm that runoff amplification under higher return periods is primarily governed by intrinsic soil permeability rather than rainfall magnitude alone, which aligns with process-based rainfall–runoff interpretations [22].

From a drainage perspective, the declining storage margin suggests that system resilience depends not only on total volumetric capacity but also on hydraulic continuity and segment configuration. Urban drainage studies emphasize that localized surcharge may occur despite adequate aggregate storage due to flow concentration and network bottlenecks [1]. Consequently, improvement strategies at the campus scale should prioritize distributed storage enhancement, conveyance optimization, and localized geometric adjustments rather than exclusively expanding total storage volume. Qin et al. showed that distributed stormwater management measures can help reduce runoff accumulation during high-intensity rainfall conditions [23].

These findings highlight the importance of integrating soil hydraulic characterization with drainage system evaluations in tropical, semi-urban environments. Consistent with Peng et al. [24], this study confirms that pairing drainage management with low-impact development is superior for runoff reduction, highlighting the crucial need to understand infiltration limitations.

Study Limitations and Research Outlook

Several limitations should be acknowledged. The infiltration analysis was based on the Green–Ampt model, which assumes a sharp wetting front and homogeneous soil conditions. While suitable for representing transient infiltration processes, this assumption may simplify actual field heterogeneity. In addition, runoff estimation was performed using the Rational Method, which emphasizes peak discharge and does not simulate full hydrograph routing within the drainage network.
The rainfall analysis was derived from a ten-year data record, which may not fully capture long-term climate variability or potential intensification trends. Future studies could incorporate longer rainfall datasets, dynamic hydraulic routing models, and two-dimensional surface flow simulations to improve predictive capability. More detailed hydraulic simulations may also support future urban drainage adaptation under changing rainfall conditions [21]. Despite these limitations, the integrated

framework developed in this study provides a consistent and physically grounded basis for evaluating pluvial flooding at the campus scale.

4. Conclusions

This study shows that pluvial flooding at the Politeknik Negeri Semarang campus is mainly controlled by limited infiltration capacity and increasing surface runoff during high-intensity rainfall. The investigated soil is dominated by fine-grained material classified as OH/MH and A-7-5 with a saturated hydraulic conductivity of only 4.209×10^{-6} mm/s. Such conditions cause infiltration capacity to decrease rapidly once the soil approaches saturation.

The Green–Ampt analysis indicates that infiltration is effective only during the initial stage of rainfall. Afterward, most additional rainfall is converted into surface runoff because the infiltration rate gradually approaches the saturated hydraulic conductivity. This condition is reflected by the increase in runoff volume from 341.308 m^3 for the 2-year return period to 527.498 m^3 for the 20-year return period.

The existing drainage system still has a total storage capacity of 1,270.38 m^3, which is larger than the estimated runoff volume for all analyzed return periods. However, the available storage margin decreases from 928.692 m^3 under the 2-year return period to 742.502 m^3 under the 20-year return period. This trend indicates that the drainage system will experience higher hydraulic loading during extreme rainfall events, particularly in drainage segments located near local topographic depressions.

Based on these results, flood mitigation at the campus scale should focus on preserving the effective performance of the existing drainage network. Routine sediment cleaning and maintenance are necessary to prevent reduction of channel storage capacity. In addition, drainage sections with relatively small dimensions and located in areas with lower ground elevation should be prioritized for hydraulic improvement because these locations are more susceptible to temporary surcharge during peak runoff conditions.

The results also suggest that future campus development should maintain existing permeable areas and avoid reducing green areas that could increase runoff contributions to the drainage network. The integrated infiltration–surface flow–drainage approach used in this study provides a practical framework for evaluating potential rainfall-induced flooding in tropical semi-urban environments with low-permeability soils.

Acknowledgments

This work was supported by the DIPA of Politeknik Negeri Semarang (No. 139.03.2.693471/2025; dated 2 December 2024) under the Applied Research Grant for Academic Staff (Contract No. 161/PL4.7.4.2/PT/2025).

References

[1] D. Butler, C. Digman, C. Makropoulos, and J. W. Davies, *Urban Drainage*, 5th ed. Boca Raton: CRC Press, 2024. doi: 10.1201/9781003408635.

[2] P. Luo *et al.*, "Flood inundation assessment for the Hanoi Central Area, Vietnam under historical and extreme rainfall conditions," *Sci Rep*, vol. 8, no. 1, p. 12623, Aug. 2018, doi: 10.1038/s41598-018-30024-5.

[3] [3] Q. Zhou, G. Leng, J. Su, and Y. Ren, "Comparison of urbanization and climate change impacts on urban flood volumes: Importance of urban planning and drainage adaptation," Sci. Total Environ., vol. 658, pp. 24–33, Mar. 2019, doi: 10.1016/j.scitotenv.2018.12.184.

[4] Y. Sun, W. Sumelka, and Y. Gao, "Reformulated fractional plasticity for soil-structure interface," Mech. Res. Commun., vol. 108, p. 103580, Sep. 2020, doi: 10.1016/j.mechrescom.2020.103580.

[5] Suripin, R. Pujiastuti, and Widjonarko, "The Initial Step for Developing Sustainable Urban Drainage System in Semarang City-Indonesia," *Procedia Engineering*, vol. 171, pp. 1486–1494, 2017, doi: 10.1016/j.proeng.2017.01.478.

[6] A. N. Anna, "Spatial modelling of local flooding for hazard mitigation in Surakarta, Indonesia," GEOMATE, vol. 21, no. 87, Nov. 2021, doi: 10.21660/2021.87.j2306.

[7] W. A. B. N. Sidiq, F. Hanafi, D. Priakusuma, W. Haruman, M. Y. Sumarso, and N. Setyowati, "Analisis banjir genangan di kawasan Tembalang dan sekitarnya," RIPTEK, vol. 16, no. 2, pp. 137–144, Dec. 2022, doi: 10.35475/riptek.v16i2.159.

[8] A. S. Pambudi, "Problems of local floods and their relation to Bogor city drainage infrastructure system," IJAR, vol. 3, no. 1, pp. 10–22, Apr. 2022, doi: 10.30997/ijar.v3i1.178.

[9] W. J. Rawls, D. L. Brakensiek, and N. Miller, "Green-ampt Infiltration Parameters from Soils Data," *J.*

Hydraul. Eng., vol. 109, no. 1, pp. 62–70, Jan. 1983, doi: 10.1061/(ASCE)0733-9429(1983)109:1(62).

[10] D. Hillel and A. W. Warrick, Environmental Soil Physics. Amsterdam, The Netherlands: Academic Press, 2009.

[11] W. H. Green and G. A. Ampt, "Studies on soil physics," J. Agric. Sci., vol. 4, no. 1, pp. 1–24, May 1911, doi: 10.1017/S0021859600001441.

[12] C. Gu *et al.*, "Study on rainfall infiltration characteristics and instability mechanism of a lateritic soil landslide in Yunnan, China," *Front. Earth Sci.*, vol. 12, p. 1478570, Nov. 2024, doi: 10.3389/feart.2024.1478570.

[13] L. Wei et al., "Experimental investigation of relationship between infiltration rate and soil moisture under rainfall conditions," Water, vol. 14, no. 9, p. 1347, Apr. 2022, doi: 10.3390/w14091347.

[14] J. Zhang et al., "Evaluation of the effects of rainfall infiltration boundaries on the stability of unsaturated soil slopes using the particle flow code," Water, vol. 16, no. 24, p. 3704, Dec. 2024, doi: 10.3390/w16243704.

[15] V. T. Chow, D. R. Maidment, and L. W. Mays, Applied Hydrology. New York, NY, USA: McGraw-Hill, 1988.

[16] Sri Harto Br., Hidrologi: Teori, Masalah, dan Penyelesaian. Yogyakarta, Indonesia: Nafiri Offset, 1993.

[17] B. Triatmodjo, Hidrologi Terapan, 2nd ed. Yogyakarta, Indonesia: Beta Offset, 2010.

[18] B. O. Brattebo and D. B. Booth, "Long-term stormwater quantity and quality performance of permeable pavement systems," Water Res., vol. 37, no. 18, pp. 4369–4376, Nov. 2003, doi: 10.1016/S0043-1354(03)00410-X.

[19] A. M. Mardiah, C. N. Ainy, M. Bagus, and D. Harlan, "Study on the Effectiveness of Infiltration Wells to Reduce Excess Surface Run Off In ITB," *MATEC Web Conf.*, vol. 147, p. 03008, 2018, doi: 10.1051/matecconf/201814703008.

[20] A. Mansida, F. Gaffar, M. A. Zainuddin, and A. M. Syamsuri, "Analysis of infiltration and surface runoff using rainfall simulator with variation of rain intensity and vegetation," *IOP Conf. Ser.: Mater. Sci. Eng.*, vol. 1088, no. 1, p. 012108, Feb. 2021, doi: 10.1088/1757-899X/1088/1/012108.

[21] K. V. Murali, "Urban flood risk under climate change: Modeling and LID-based solutions," CES, vol. 2, no. 1, pp. 11–21, Jun. 2025, doi: 10.37446/ces/ra/2.1.2025.11-21.

[22] K. Beven, Rainfall-Runoff Modelling: The Primer, 2nd ed. Chichester, U.K.: Wiley-Blackwell, 2012. doi: 10.1002/9781119951001.

[23] H. Qin, Z. Li, and G. Fu, "The effects of low impact development on urban flooding under different rainfall characteristics," J. Environ. Manage., vol. 129, pp. 577–585, Nov. 2013, doi: 10.1016/j.jenvman.2013.08.026.

[24] Z. Peng, K. Jinyan, P. Wenbin, Z. Xin, and C. Yuanbin, "Effects of low-impact development on urban rainfall runoff under different rainfall characteristics," Pol. J. Environ. Stud., vol. 28, no. 2, pp. 771–783, Dec. 2018, doi: 10.15244/pjoes/85348.

E-ISSN: 2528-388X
P-ISSN: 0213-762X

INERSIA
Vol. 22, No. 1, May 2026

The Mediation of City Branding Identity: An Analysis of Aesthetic Elements in Surakarta's Iconic Architecture

Marinda Noor Fajrina Noviana Putri*, Retna Hidayah and Pita Asih Bekti Cahyani

Architecture Study Program, Department of Civil Engineering and Planning, Universitas Negeri Yogyakarta, Yogyakarta 55281, Indonesia

Keywords:
Iconic architecture
Visual appeal
City branding
Surakarta

ABSTRACT

Landmark buildings often serve as the most powerful visual representations of a city. However, the ways in which the visual qualities of architecture operate in shaping *city branding* remain insufficiently examined. Recent scholarship increasingly highlights the importance of architecture in constructing urban identity. Nevertheless, specific investigations into the aesthetic criteria of iconic buildings—particularly colour, ornament, and form—as factors that influence visitors' perceptions and place memory are still relatively limited. This study addresses this gap by proposing an analytical framework that connects architectural aesthetics to the core dimensions of city branding. Using a qualitative digital etnographic approach, this research develops an Aesthetic–Branding Analysis Framework to map particular visual attributes to branding outcomes, including identity, representation, and experiential quality within the digital dimension. The findings indicate that aesthetic elements are not merely decorative features, but actively communicate meaning and shape visitors' expectations of a place. Building on these results, the study proposes a Conceptual Model of Aesthetic-Based Branding Formation, illustrating how architectural visuals interact with collective perceptions and urban narratives through ongoing reciprocal processes, ultimately producing shared meanings over time. Theoretically, this study reinforces the argument that aesthetic decisions—often treated as secondary or supportive aspects—can function as key drivers in forming urban character and reputation. Practically, the findings encourage more strategic investment in iconic architecture as a tool for city brand communication, strengthen the rationale for heritage preservation beyond cultural considerations alone, and support the systematic integration of aesthetic factors as essential components of urban planning and development.

1. Introduction

These days city branding is really important for the sustainable of cities. Cities need to make themselves more interesting to get people to visit and invest in them [1] - [2]. The awareness to build the strategies increase aware that the built environment especially iconic architectural landmarks significantly influences public perception and strengthens a city's appeal to both tourists and potential investors [3], [4], and [5]. Building with iconic and symbolic qualities of architecture are now closely intertwined with the wider narrative of urban identity, serving as a key medium through which cultural values and representations are communicated [6] - [7].

Surakarta, also known as "Solo," is widely recognized for its rich cultural heritage in Central Java, Indonesia, and is promoted through the branding tagline "Solo, the Spirit of Java." This identity is strongly supported by the city's heritage architecture, particularly traditional landmarks such as Keraton Kasunanan and Pura Mangkunegaran, which serve as key historical and cultural site [5], [8] Nevertheless, while iconic newly developed structures like the Sheik Zayed Grand Mosque and revitalized heritage sites like Lokananta and Pracima Tuin began to emerge in Surakarta in 2022, the city still faces challenges in translating the architectural significance into an effective and coherent city branding strategies [5], [9].

*Corresponding author.
E-mail: marindanoorfajrina.np@uny.ac.id

https://doi.org/10.21831/inersia.v22i1.82029
Received 6 January 2025; Revised 19 May 2026; Accepted 30 May 2026
Available Online 31 May 2026

Research about the relationship between architecture and city branding is well-established. Yet, the specific mechanisms through which visual aesthetic elements such as colour, ornament, and form contribute to the formation of city brand identity, image, and experience remain insufficiently theorized [10]. This gap represents a critical oversight, as aesthetic attributes are often the primary means through which audiences encounter and interpret iconic buildings, particularly in the digital age where represent on social media platforms.

While Surakarta possesses numerous iconic architectural structures after the priority project, the city's branding strategy has not systematically leveraged the aesthetic dimensions of these buildings. Currently the branding of Surakarta efforts to emphasize cultural narratives and historical significance without adequately addressing how specific visual elements contribute to brand perception. This represents a missed opportunity, as empirical research demonstrates that aesthetic attributes of architectural elements directly influence visitor perception and urban memory formation [11]. The aesthetics and materiality of iconic buildings serve as powerful meaning generators that inform perceptions of both physical visitors and digital audiences about the unique character of a city [11]. Furthermore, architecture has been established as one of the most effective tools in formulating and communicating distinctive city images, functioning as both an identity definer and a promotional instrument that shapes cultural meanings of urban places [12]. More specifically, this paper help to understand the mechanisms through which color, ornament, and form influence the three primary dimensions of city branding: identity, image, and experience.

This research aims to achieve two primary objectives. Developed an aesthetic branding analysis framework that systematically maps the relationship between visual aesthetic attributes of iconic architecture and their impacts on city brand dimensions. Than formulated a conceptual model of aesthetic based on branding formation that explains the process through which visual elements dialectically shape public perception and urban narratives, thereby contributing to overall city brand development. Finally, the findings offer guidance for urban planners, architects, and city administrators in strategically designing and promoting iconic buildings as effective branding assets. Furthermore, the conceptual model can be applied to other heritage cities seeking to strengthen their urban identity through architectural intervention.

2. Methods

This research used qualitative thematic analysis of online reviews as an approach to examine how visual aesthetic elements of iconic architecture contribute to city branding formation [13]. This method is particularly suited to the present study because it allows researchers to access authentic, spontaneous expressions of visitor perceptions and emotional responses to architectural spaces as documented in social media platform.

Due to the limited availability of structured social media datasets, purposive sampling was employed, the data was collected with a purposive sampling strategy from visitor reviews in the online travel platform called TripAdvisor. This platform was chosen because of: (1) its extensive repository of user-generated content provides a large sample size for robust analysis; (2) its focus on travel experiences ensures that reviews contain detailed narratives about visitor perceptions of architectural sites; and (3) its global reach allows for the inclusion of diverse perspectives from both domestic and international visitors. There are three procedure of data analyse the data refer in Figure 1.

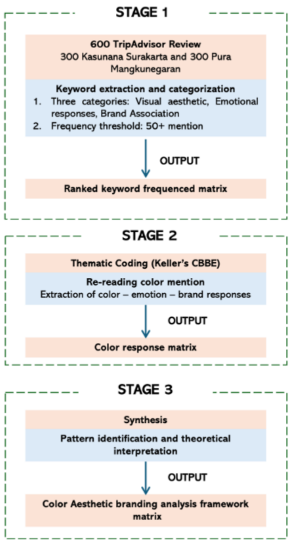

Figure 1. Method Stage 1

Based on Kozinet, the method of netnography approach that are some criteria for data selection. The criteria are public account and have relevant and meaningful review to the research context, enabling a deeper representation of the practices, narratives, and experiences being analyzed [14].

2.1 Sample and Time Period

This paper used 600 review from the platform and equally divided between the two case study sites: Keraton

Kasunanan Surakarta and Pura Mangkunegaran. All reviews were collected from January 1, 2012, to December 31, 2024 and collect in data excel, This sample size was deemed sufficient to achieve data saturation, where additional reviews no longer yield new themes or insights.

2.2 Selection Criteria

The screening process was set the inclusion and exclusion criteria were designed to filter for reviews that contained rich, descriptive data related to architectural aesthetics and brand perception after collecting the data. The criteria are summarized in Table 1.

Table 1. Inclusion And Exclusion Criteria for Review Selection

Criteria Type	Specification
Inclusion	1. Minimum Length of 50 Words
	2. Explicit Mention of Architectural or Aesthetic Elements
	3. Reviews in English or Indonesian
	4. Reviews from Individual travelers
Exclusion	1. Reviews Shorter than 50 Words
	2. Service-Only Focus
	3. Duplicate or Bot-Generated Content
	4. Ambiguous or Irrelevant Content

2.3 City Branding in the Context of Tourism and Urban Development

City branding is a planned by cities to create and share unique identities that set them apart in competitive global markets. As described in urban discussion, city branding is the intentional construction of a unique story, visual identity, and experience that make a city an attractive place for tourists, residents, and investors to visit [15], [16].

City branding have multifaceted objective. First, it serves a differentiation function, enabling cities to distinguish themselves from competitors by highlighting unique cultural, historical, or architectural attributes [17]. Second, it establishes emotional connections with audiences through the creation of memorable experiences and narratives. Finally, loyalty relationship was created with positive associations. In the context of urban tourism, city branding increasingly aligns with the broader vision of sustainable tourism development [18] - [19].

To achieve this, city branding typically involves multiple stakeholders including government agencies, private developers, cultural institutions, and local communities who collectively shape and communicate the city's public image. Within tourism, city branding functions not only to generate positive perceptions, but also to frame authentic experiences that encourage repeat visits and longer stays, ultimately contributing to tourism revenue and cultural exchange.

2.4 Iconic Architecture as a Branding Asset

The discussion of architecture have many field of study, so it's necessary to understand and know what kind of iconic architecture are being considered. Many experts in architecture define iconic architecture as buildings that are not only recognized for their unique and memorable forms but are also rich in powerful symbolic meaning [3]. However, in the context of tourism, iconic architecture is simply a structure that typically has a silhouette different from what is usually seen in everyday life. Based on this, the definition of iconic architecture already differs depending on the context, but when viewed functionally, the iconic architectural approach has similarities where a building is not just a building but must go beyond its functional purpose. From there, it then developed into a symbol of the city's identity, cultural pride, and shared memory for the community.

When viewed in the urban context, iconic architecture serves as a key to the success of the city regeneration process. The successful development of iconic architecture can be considered a catalyst in the economic and cultural sectors [3]. This clearly demonstrates that iconic architecture can also serve as a city landmark closely tied to the city's values. Moreover, they used it as an asset to generate tangible economic benefits thru increased tourism, rising property values, and expanded business opportunities [20].

The Kasunanan Hadiningrat Palace, the Mangkunegaran Palace, and the Syeikh Zayed Grand Mosque, built in 2022, are some of the architectural buildings in Surakarta, serving as a catalyst to support tourism. Based on previous research, this building reflects diverse building characteristics [5]. This diversity shows the complex iconic form of the city, so this iconic asset needs to collectively communicate an identity in accordance with Surakarta's city branding.

2.5 Visual Aesthetic Characteristic in Architecture: Colour, Form and Ornament

After discussing the definition, it is necessary to identify the visual characteristics of iconic architecture so that the observation's unit of analysis can be easily determined. As is known, the visual aspect is an important aspect in the iconicity of a building, making it important to discuss this aspect. How visual aspects can interact and be interpreted.

This subsection will explain how the visual characteristics related to color, ornament, and building shape can serve as image stimuli. As per the background, these elements function as visitor attractions in UGC; the intensity of color, shape, and ornament can be used as content and shared by visitors [21], [22]. Based on the interaction between elements and visitors in the digital platform, it can expand the reach of a city's branding image [23].

Color is one of the characteristics of iconic architecture. The presence of color is often the first stimulus felt by visitors, making it a powerful element in the affective process of shaping experience. Color can provide the initial stimulus before the building's form, details, and function are further understood by visitors [24]. Therefore, it is concluded that the presence of color in buildings can be felt emotionally, not just cognitively. The initial impression that arises can be lasting and create an emotional bond with a person. In the case study of existing buildings in the city of Surakarta itself, color is related to the traditions present in the city of Surakarta. For example, in the Kasunanan Solo Palace building, the choice of colors reflects local identity and cultural uniqueness, often referred to as local color [25].

Kraton and Pura Mangkunegaraan in Surakarta city have facades dominated by the color blue. Symbolically, the blue and white colors on the Surakarta kraton represent the balance between heaven and earth. Not only in Indonesia, a similar phenomenon is also found in India. India is also a country rich in culture. One of the buildings named Hawa Mahal uses orange as the color for its facade. Orange is a strong color that reflects the local cultural character [26] - [27].

Visual characteristics as markers of a building's iconic status, beside color, are ornaments. Ornament is a visible marker that can be seen directly. Ornaments not only serve to enhance esthetic value but also enrich the local cultural value [28]. The presence of ornaments on a building's facade can influence visitors' perceptions, ranging from their association with authenticity, historical value, and esthetic sophistication. Ornaments rich in symbolic value serve as distinctive markers in supporting city branding strategies [29]. The intended markers can be present due to their complex shapes.

The more complex and unique the shape of the ornament, the closer the observation it can encourage and make it a photo or content background [30]. In the realm of digital tourism activities, ornaments can appear as photo backgrounds [30]. A previous study showed that ornamentation on buildings significantly affects the spread of photos on social media, particularly Instagram [31]. So, what happens on social media has become part of modern tourism activities.

Its silhouette, scale, and spatial configuration are indicators of a building's form and mass elements. These three indicators can clearly represent the dimensions architecturally. Buildings with unusual structural typologies and strong symbolic value can influence visitor perception [32]. Examples of monumental-scale buildings like the Burj Khalifa and the Burj Al Arab in Dubai.

The visual elements of the building indirectly symbolize Dubai as a modern and advanced place [21]. This is also in line with what is happening in the city of Surakarta, where the form of iconic architectural silhouettes reflects certain perceptions. The palace building has a symmetrical facade silhouette with the characteristic silhouette of traditional Javanese buildings. Meanwhile, the Mangkunegaran temple uses construction elements that emerge from the textual meaning of concepts and language [33]. The appeal of the Sunanate palace buildings is partly due to their unique architectural form, which features a cultural blend of Javanese and European silhouettes [34]. The intricate and magnificent pillar shapes in the palace create an impression that is both grand and esthetic. This blend of styles offers tourists a unique and complex visual experience.

2.6 Dimension of City Branding: Identity, Image and Experience

City branding operates across three interconnected dimensions: Identity refers to the distinctive characteristics and values that define a city. It is the "essence" of what the city represents, communicated through its cultural heritage, architectural heritage, and contemporary aspirations [35]. Iconic architecture contributes to identity formation by embodying and visually representing core urban values [21]. Image refers to the collective perceptions held by external audiences about the city.

City Image based on tourist activities is formed through multiple channels direct experience, media representation, social media narratives, and word-of-mouth communication. Iconic architecture shapes image by providing visual content that circulates through these channels, creating consistent visual associations with the city [36]. The affective process; the direct sensory and emotional encounters that audiences have with the city [35]. This includes physical visits to iconic sites as well as digital experiences through photographs, videos, and social media content. The aesthetic qualities of iconic architecture directly affect the visual sensory quality and memorability of these experiences.

2.7 Customer Based Brand Equity Framework

Branding is a strategy used by manufacturers with the ultimate goal of customer loyalty. That goal can be achieved if the strategic communication process is delivered well. In the context of this research, the producers are the government and the consumers are tourists. The Surakarta city government has a branding strategy to make Solo the soul of Javanese culture, or with the tagline "Solo, the Spirit of Java".

As is known, visual elements can influence the experience and perception of tourism. Therefore, it is necessary to know the extent to which this phenomenon is accepted, whether it is still in line with what was conceptualized by stakeholders, or whether it has changed. A theoretical approach is needed to interpret what is happening in the digital tourism phenomenon. The Customer-Based Brand Equity Framework (CBBE) is needed to address this. Branding generally originates from discussions in management science, but is beginning to be adapted into an urban context. There are 4 stages to achieve consumer loyalty, starting with brand identity, brand meaning, brand response, and finally, brand relationship [37]. Figure 2 shows a further explanation related to CBBE.

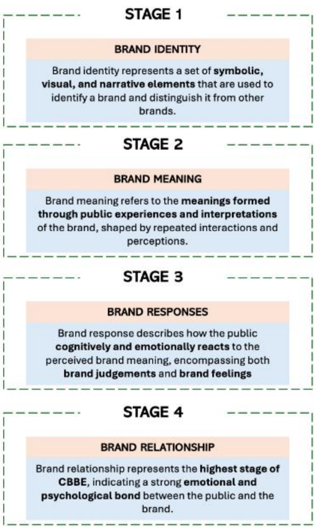

Figure 2. CBBE Stages

Based on CBBE, popularized by Keller, the strength of a brand lies in what can be seen, felt, and learned over time. The model developed by Keller provides a framework aimed at understanding how brands are built and developed to build brand equity.

3. Result and discussion

This chapter will discuss the results of the analysis related to the analysis of tourist comments on the Tripadvisor platform. The discussion will reveal how the visual elements of iconic architectural characteristics (color, ornament, form, and mass) are perceived by tourists and whether they align with the branding concept desired by the government. Based on the existing comments, they will be translated according to how brand equity is formed.

Table 2 shows some example of the findings organized according to Keller's Customer-Based Brand Equity (CBBE) framework, explaining the CBBE concept on the cases consecutively based on the level.

Table 2. Response on the CBBE level

CBBE Level	Definition	Observable Indicators in Reviews	Example Review Excerpt
Brand Response (Judgements)	Cognitive evaluations	Mentions of "beautiful", "impressive", "authentic", "elegant"	"The architecture is truly impressive and authentic..."
Brand Response (Feelings)	Emotional reactions	Mentions of "peaceful", "awed", "fascinated", "connected"	"I felt a deep sense of peace and connection to history..."

The findings indicate that the visual aspect of tourism assets, specifically iconic buildings, plays a crucial role in building brand equity. This is demonstrated in the comments from the two objects used as the unit of analysis. Pura Mangkunegaran shows a stronger brand identity, with 42.7% supported by the visual elements of its ornaments. Meanwhile, the Kasunanan Surakarta palace is superior in brand perception by 27%. The history and culture of the palace tend to contribute to how architectural elements can contribute to its image.

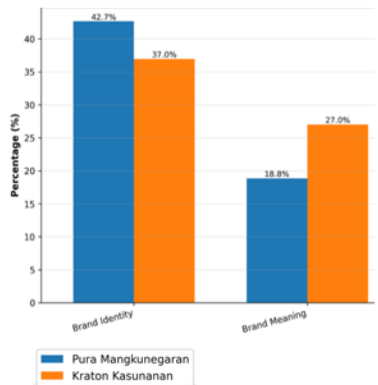

Figure 3. Overall Result of Brand Identity and Meaning

3.1 Colour as Visual Element in Customer-Based Brand Equity

In the literature review, these results support the idea that color plays a role in the fundamental layers of identity formation for a brand. Color-related comments appeared 26 times in the observation unit of Pura Mangkunegaran. Gold is the most frequently mentioned color in the references, with 19 reviews directly mentioning its association with brand identity recognition. The gold color present at the Mangkunegaran Palace is a distinctive color palette that contributes to the visual impression for visitors. As one visitor noted, "The gold decoration throughout the palace creates an unforgettable first impression," highlighting how color directly influences the formation of brand salience.

The Kasunanan Surakarta Palace provided different data results, with a more diverse chromatic vocabulary. Gold appeared 38 times (28 mentions of identity), while blue (biru) was mentioned 14 times (10 mentions of identity), and white (putih) appeared 9 times (7 mentions of identity). The color blue is highly significant in the identity of the Kasunanan Palace, as it represents a deliberate architectural choice that distinguishes this palace from other heritage sites. Visitor comments illustrate this: "The blue and white facade of the Kasunanan Palace immediately identifies it as a place of historical significance and cultural importance".

Although gold is the most frequently mentioned color in the reviews. However, based on the results of further analysis that looked at more than just the number of words that appeared. The use of blue by the Kasunanan Palace as a secondary color creates a more complex visual identity. The chromatic complexity of the blue color presented by this palace contributes to a stronger brand identity differentiation, as visitors can more easily distinguish the Kasunanan Palace from other architectural landmarks thru its unique color combination.

The role of color in fostering brand loyalty and repeat visit intention is evident in the mention of relationship levels. For the Mangkunegaran Temple, the mention of gold in the context of brand relationships appears in 8 meanings (diagram 4) associated with recommendations and the intention to revisit. Visitors expressed statements such as "The golden beauty of this palace makes it worth recommending to friends and family" and "I will definitely return to experience the grandeur again."

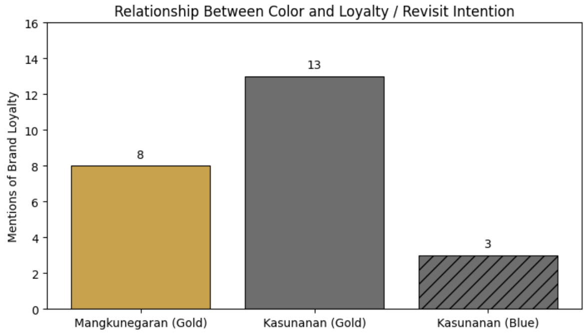

Figure 4. Color Contribution on Loyality

In Figure 4, the relationship between colors in the Surakarta palace and colors in the context of loyalty or relationships can be seen (13 for gold, 3 for blue, slightly lower, indicating that although color contributes to initial appeal, other factors (such as condition and accessibility) may be more influential in determining loyalty. However, visitors who specifically appreciate the symbolic meaning of colors express a stronger intention of loyalty, as reflected in visitor reviews such as "Understanding the meaning of blue and white deepened my connection to this place and made me want to return".

3.2 Ornaments as Visual Elements Based on Customer-Based Brand Equity

At the cognitive stage, the stimulus provided by the ornament is slightly different from color. Color operates on the macro visual aspect, while the ornament operates on the micro aspect. Closer and more detailed observation of the ornaments on the building is needed. Ornaments represent expression. Based on the analysis of UGC, the mention of ornaments found in reviews of Pura Mangkunegaran is categorized into 35 categories. 21 out of 25 reviews directly contribute to the direct mention of identity. The presence of this ornament certainly makes a substantial contribution, reflecting the complexity of the ornament.

Meanwhile, reviews related to ornaments for the Surakarta palace are slightly lower. There were only 12 direct mentions of ornamentation out of a total of 15 mentions. However, there are reviews that use specific mentions of ornaments such as relief works and sculptures. Reviews that are direct, like sentences. The reliefs tell the story of Javanese history and culture, making them a key introduction to the significance of this palace. Based on this, it is concluded that the ornaments found in the Mangkunegaran temple play a role in shaping identity due to the complexity of the carvings. When linked to CBBE, the ornamentation at Mangkunegaran Temple holds additional value for brand identity. Meanwhile, the ornaments in the Surakarta Palace provide more meaning from the story behind their presence. Therefore, ornamentation serves as the primary vehicle for communicating cultural meaning, historical narratives, and philosophical principles. The symbolic content embedded in the ornamental forms creates layers of meaning that distinguish heritage architecture from contemporary buildings.

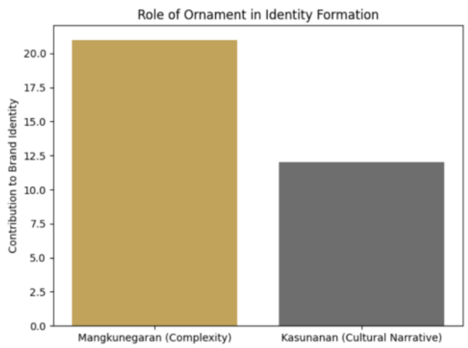

Figure 5. Ornament Contribution on Loyalty and Identity

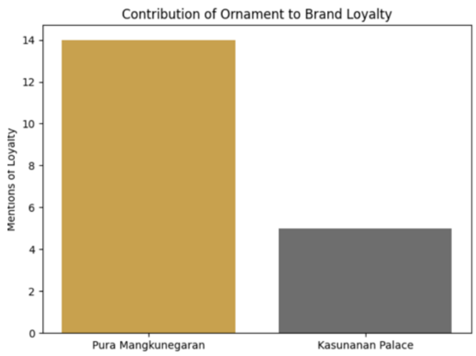

Figure 6. Ornament Contribution on Loyalty and Identity

The analysis results in Figure 5 and Figure 6show that the visual elements of the ornament contribute to brand loyalty by creating a memorable esthetic experience and facilitating deeper cultural engagement. Based on the data, the expressions indicating loyalty to Pura Mangkunegaran related to ornaments total 14, with 6 mentions of the ornaments and 8 details. Reviews indicating loyalty are expressed with phrases like "I want to come back to see the details of the ornaments." Slightly lower than Pura Mangkunegaran, the results of loyalty to the Kasunanan Palace only have 5 reviews. The reviews do show that ornaments alone are not enough to drive loyalty. For the case of the kraton, complementary factors are needed, such as improved accessibility or interpretive programs

3.3 Form and Massing Based on Customer-Based Brand Equity

Compared to the previous two elements, which tend to be two-dimensional, the elements of form and mass represent the quality of space in three dimensions in architectural design. Therefore, the operational analysis of reviews includes architectural elements as well as the spatial organization of the building. In this context, the architectural forms referred to are specific elements such as doors, columns, and roofs.

The overall architectural form and the specific elements (doors, columns, roofs) serve as the main identifiers in shaping the brand identity of both palaces. There are 75 architectural review data points for the Mangkunegaran Temple, 49 of which directly contribute to brand identity. This proportion highlights the strong role of the palace silhouette, roof profile, and overall massing as easily recognizable visual markers. Drawn deeper into the discussion of architecture, it is also revealed with more specific language. Mentions related to specific elements also strengthen identity, especially doors, windows, and komom, which were mentioned 16 times (10 times related to identity). The specific mention of curved elements enriches the formal visual vocabulary in architectural aspects.

At the Kasunanan Palace, the data shows that mentions related to architecture appear more frequently. The 87, with 69 directly related to brand identity, indicates a stronger reliance on the overall form. The complex silhouette with double pavilions and layered spaces forms a more elaborate formal identity. The specific element of the door is the most dominant element, mentioned 36 times, with 21 of those mentions contributing to brand identity. Based on this data, when viewed from the perspective of brand meaning and cultural associations, Pura Mangkunegaran recorded 24 mentions of meaning, reflecting a synthesis of Javanese architectural principles influenced by European styles. This is evident from the symmetrical massing geometry, balanced proportions, and spatial hierarchy. Conversely, the Kasunanan Palace exhibits an intensity of meaning that is almost twice as high, with 45 mentions. In the unit of analysis, the kraton is discussed more extensively in reviews that mention its hierarchical spatial organization and the procession's spatial arrangement, which communicate many reviews linking it to Javanese cosmology. Narrowed down to examine the emotional responses, the data source from the Mangkunegaran Palace recorded a total of 28 mentions of responses, the majority of which were positive, related to the harmony of proportions, the balance of massing, and the well-maintained condition of the buildings. Specific elements such as doors (6 mentions in responses) and curved elements (1 mention in responses) trigger esthetic appreciation. The Kasunanan Kraton records 45 mentions of responses, indicating a more complex reaction. Thus, the architectural form is appreciated for its grandeur and historical value, but issues of physical condition and accessibility have led to criticism. The door (12 response mentions) received mixed responses, with some praising its monumentality and others criticizing its maintenance. Regarding the brand relationship and loyalty aspect, Pura Mangkunegaran recorded 21 mentions, primarily related to repeat visit intentions and recommendations based on esthetic appreciation. The Kasunanan Palace records 23 mentions, with loyalty more often driven by cultural significance and historical awareness, including visitors' commitment to preservation.

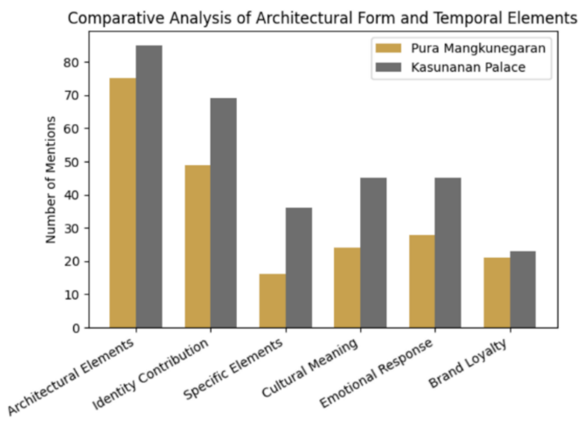

Figure 7. Comparative Element of Mass and Shape Between Two Case Study

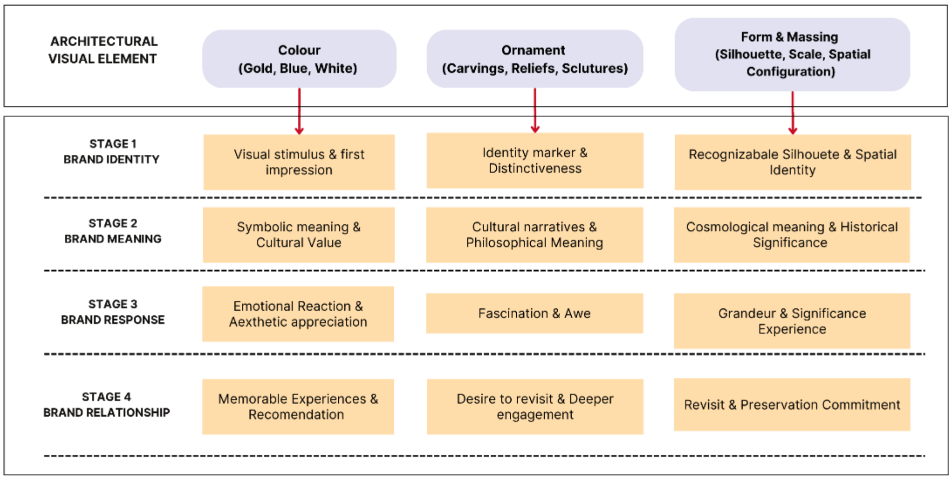

Figure 8. Contribution of Architectural Visual Elements to Customer-Based Brand Equity (CBBE) Levels

3.4 Comparative Analysis: Visual Elements and CBBE Integration

Integrated analysis of color, ornament, and form shows that visual elements work as a unified system in shaping architectural brand equity at both palaces in Figure 8.

These elements do not operate in isolation, but rather mutually reinforce each other in building a coherent brand perception. Pura Mangkunegaran represents a visual strategy oriented toward esthetic excellence, characterized by the dominance of gold color, rich ornamentation, and refined formal proportions. The integration of these three elements results in a brand identity that emphasizes visual beauty and quality craftsmanship, which further elicits a consistently positive brand response from visitors.

Conversely, the Kasunanan Surakarta Palace showcases a visual strategy that focuses on cultural meaning and historical significance. The use of symbolic colors (blue and white), meaningful ornaments, and complex spatial organization builds a brand identity rooted in cultural authenticity and historical narratives. This approach resulted in strong brand associations with Javanese philosophical and civilizational values. Overall, the findings confirm that the brand equity of heritage architecture is not determined by the strength of a single visual element, but rather by the overall coherence of the visual system and its alignment with brand positioning strategies, visitor expectations, and cultural values

4. Conclusion

This research concludes that the visual elements of architecture, particularly color, ornamentation, and form and massing, play a key role in shaping the brand equity of heritage destinations in Surakarta. The findings indicate that visitors do not perceive aesthetic elements solely as decoration, but rather as a system of signs that build identity, produce cultural meaning, trigger emotional responses, and foster brand relationships such as recommendations and repeat visit intentions. Thus, brand strengthening does not rely on a single specific visual element, but rather on the integration and coherence between visual elements as a unified strategy. Moreover, this study novelty is a conceptual model that elucidates how the aesthetic elements of iconic architecture namely colour, ornament, and formcontribute to the formation of city brand equity through two distinct branding strategies, which subsequently generate outcomes in the form of a coherent city image, enriched visitor experience, and enhanced heritage preservation value. Furthermore, the model demonstrates that this process operates as a continuous reciprocal cycle, wherein the outcomes reinforce and reshape the perception of the architectural visual elements over time in Figure 9.

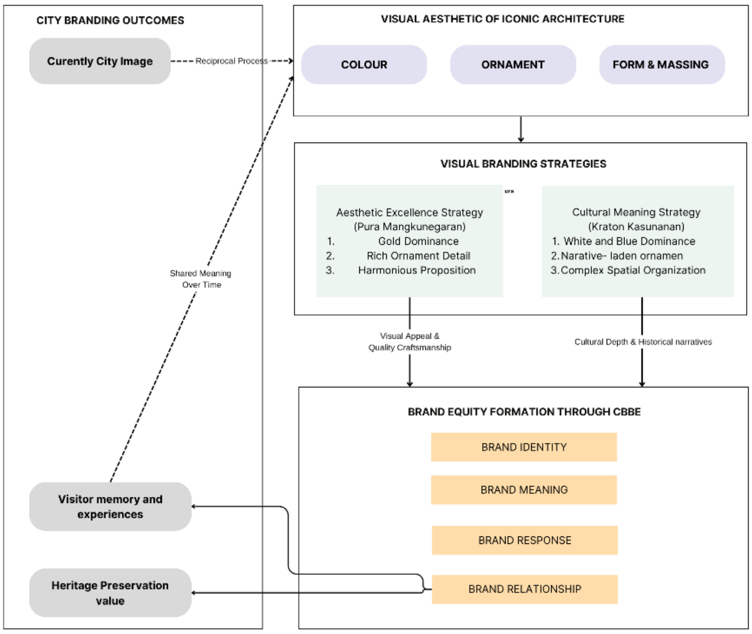

Figure 9. Conceptual Model of Aesthetic-Based Brand Equity Formation in Heritage Architecture

At the Mangkunegaran Palace, visual strategies tend to be oriented toward esthetic excellence and formal elegance. The striking color palette, the richness of ornamental detail, and the harmonious proportions create a visually recognizable identity that consistently elicits a positive response from visitors. The esthetic experience in this place serves as the main trigger for forming impressions, feelings of awe, and the desire to return, thus brand equity develops through the power of visual appeal and perceived quality of craftsmanship.

Meanwhile, the Kasunanan Surakarta Palace showcases a visual strategy more centered on cultural meaning and historical significance. The color choices rich in symbolism, the narrative-laden ornaments, and the complex spatial organization create an identity rooted in cultural authenticity and historical memory. As a result, visitors tend to link their experiences with philosophical meanings and Javanese civilization values. However, emotional responses to the Kraton are also more diverse because visitors' experiences are influenced by aspects of physical condition and accessibility, which in some cases enhance or diminish the quality of the experience.

Comparatively, both palaces equally demonstrate that visual elements can be a primary driver of brand equity formation, but through different paths. Pura Mangkunegaran is more effective at building equity through aesthetic consistency and visual quality that elicit positive responses, while Kraton Kasunanan is stronger at building equity through the depth of cultural meaning and historical narratives that strengthen brand associations and value attachment. Therefore, this research confirms that the success of heritage architecture-based city branding is not determined solely by visual grandeur or uniqueness, but rather by how these visual elements are coherently orchestrated to shape an experience, meaning, and city image that aligns with visitor expectations and local cultural values

References

[1] M. Grębosz-Krawczyk, "Place branding (r)evolution: the management of the smart city's brand," Place Branding and Public Diplomacy, vol. 17, Mar. 2021, doi: 10.1057/s41254-020-00167-2.

[2] M. N. F. N. Putri and T. M. Sunarharum, "Tinjauan Literatur Peran Smart Visual Identity dalam Membangun Branding Smart City," Jurnal Lingkungan Binaan Indonesia, vol. 14, no. 2, Jun. 2025, doi: 10.32315/jlbi.v14i2.448.

[3] R. El Messeidy, "Architecture and City Branding: Role of Iconic buildings," 2019.
[4] B. H. H. Al-Majidi and A. samari Ibrahim, "Role of iconic architecture in sustainable tourism development," Al-Esraa University College Journal for Engineering Sciences, vol. 3, no. 3, pp. 167–196, Jun. 2021, doi: 10.70080/2790-7732.1017.
[5] A. Della Puspitasari, D. C. Natalia, M. Marsudi, and S. Marmoah, "Pura Mangkunegaran dan Keraton Kasunanan Surakarta sebagai Sarana Wisata Edukasi Sejarah," Jurnal Abdimas Pariwisata, vol. 6, no. 1, pp. 55–70, 2025, doi: 10.36276/jap.v5i2.481.
[6] A. Mengoni, "Visual Semiotics," in The Palgrave Handbook of Image Studies, 2021, pp. 641–654. doi: 10.1007/978-3-030-71830-5_39.
[7] A. A. Amini and B. Adibzadeh, "The role of visual preferences in architecture views," Journal of Architecture and Urbanism, vol. 44, no. 2, pp. 122–127, Sep. 2020, doi: 10.3846/jau.2020.12582.
[8] A. D. Ipmawati and O. Hodijah, "Analisis Semiotika Roland Barthes Pada Arsitektur Masjid Raya Sheikh Zayed Solo Sebagai Destinasi Wisata Religi Roland Barthes ' Semiotic Analysis of the Architecture of the Sheikh Zayed Grand Mosque Solo as a Religious Tourism Destination," JICN: Jurnal Intelek dan Cendikiawan Nusantara, vol. 1, no. 5, pp. 8065–8075, 2024, [Online]. Available: https://jicnusantara.com/index.php/jicn/article/view/1446/1597
[9] O. P. Angga Purnama, "EVALUASI PENERAPAN ARSITEKTUR TIMUR TENGAH PADA MASJID RAYA SHEIKH ZAYED SOLO Dalam Menghadapi Tantangan Iklim Tropis dan Konteks Budaya Setempat," Jurnal SENTHONG, vol. 8, no. 2, pp. 520–529, 2025.
[10] Y. N. Al-Betawi and H. B. Abu Ehmaid, "Branding Cities Through Architecture: Identify, Formulate, and Communicate the City Image of Amman, Jordan," Architecture, vol. 5, no. 3, Sep. 2025, doi: 10.3390/architecture5030050.
[11] A. Zamparini, G. Gualtieri, and F. Lurati, "Iconic buildings in the making of city identity: The role of aspirational identity artefacts," Urban Studies, vol. 60, no. 12, pp. 2474–2495, 2023, doi: 10.1177/00420980221144157.
[12] Y. N. Al-Betawi and H. B. Abu Ehmaid, "Branding Cities Through Architecture: Identify, Formulate, and Communicate the City Image of Amman, Jordan," Architecture, vol. 5, no. 3, Sep. 2025, doi: 10.3390/architecture5030050.
[13] R. Kozinets V, "Netnography : The Essential Guide to Qualitative Social Media Research," Netnography: Redefined, no. 416, pp. 1–52, 2020.
[14] P.-Y. Kozinets, Robert V. Earley, Dolbec and Amanda, "Netnographic Analysis: Understanding Culture through Social Media Data," in Handbook of Qualitative Research, Sixth., Sage Publication, 2023, p. 262.
[15] S. Anholt, Competitive Identity: Brand Management for Nations. 2007.
[16] M. Kavaratzis, "From city marketing to city branding: Towards a theoretical framework for developing city brands," 2004.
[17] B. 'Baker, Destination Branding for small City (the essential for succesful place branding). Orgeon: Creative Leap book, 2007.
[18] M. Kavaratzis and G. J. Ashworth, "CITY BRANDING: AN EFFECTIVE ASSERTION OF IDENTITY OR A TRANSITORY MARKETING TRICK?," 2005.
[19] S. Gönüllüoğlu and S. Arslan Selçuk, "City branding in the context of architecture, tourism, culture, and cultural identity interaction—bibliometric analysis of literature," Place Branding and Public Diplomacy, 2024, doi: 10.1057/s41254-024-00365-2.
[20] B. Plaza, M. Esteban, I. Aranburu, and J. Johny, "Iconic Architecture As a Catalyst for Wine Tourism: a Case Study of Marques De Riscal," European Countryside, vol. 16, no. 1, pp. 168–182, 2024, doi: 10.2478/euco-2024-0010.
[21] K. Elhagla, D. M. Nassar, and M. A. Ragheb, "Iconic buildings' contribution toward urbanism," Alexandria Engineering Journal, vol. 59, no. 2, pp. 803 – 813, 2020, doi: 10.1016/j.aej.2020.01.020.
[22] N. Li, F. Meng, and D. Martin, "The Distorted Gaze? Travel Photo Editing in the Social Media Era," J. Travel Res., 2024, doi: 10.1177/00472875241274562.
[23] S. Jojic, "City Branding and the Tourist Gaze: City Branding for Tourism Development," European Journal of Social Science Education and Research, vol. 5, no. 3, pp. 150–160, 2019, doi: 10.2478/ejser-2018-0066.
[24] J. Outram, "Iconic Engineering: Reflections on the subject of colour in architecture, ornament and city planning," Colour for Architecture Today, pp. 99–105, 2020, doi: 10.4324/9781315881379-23.
[25] M. S. Zuhri and I. P. Wardhana, "Symbolic Meaning in Tradition The Malem Selikuran of Keraton Kasunanan Surakarta Hadiningrat, Indonesia," Sabdasastra : Jurnal Pendidikan Bahasa Jawa, vol. 8,

no. 2, p. 124, Sep. 2024, doi: 10.20961/sabpbj.v8i2.91464.

[26] J. Pallasmaa, The eyes of the skin : architecture and the senses, 3rd ed. Chichester: John Wiley & Sons Inc, 1988.

[27] C. Morganti, "Contemporary-Temporary Lexicon: Lifeguard Towers of Miami," in Springer Tracts in Civil Engineering, vol. Part F3500, 2024, pp. 173–187. doi: 10.1007/978-3-031-65104-5_9.

[28] F. Zahra and S. B. Shahir, "Spiritual Aesthetics of Islamic Ornamentation and the Aesthetic Value in Islamic Architecture," Journal of Islamic Thought and Civilization, vol. 12, no. 1, pp. 164–175, 2022, doi: 10.32350/jitc.121.08.

[29] M. Wang and Z. Jia, "Investigating the correlation between building façade design elements and tourist satisfaction - Cases study of Italy and the Netherlands," Habitat Int., vol. 144, Feb. 2024, doi: 10.1016/j.habitatint.2024.103001.

[30] M. Nastasi and D. Ponzini, "Toward a photographic urbanism?," 2018, pp. 217–231. doi: 10.4324/9781315163956-17.

[31] V. López-Chao and V. Lopez-Pena, "Aesthetical appeal and dissemination of architectural heritage photographs in instagram," Buildings, vol. 10, no. 12, pp. 1–15, Dec. 2020, doi: 10.3390/buildings10120225.

[32] A. H. Alganawi and A. Ibrahim, "The Role of Mayadeen (Roundabouts) in City Branding: The Case of Jeddah," The International Research &Innovation Forum, 2023, doi: 10.1007/978-3-031-44721-1_20.

[33] Sunarmi, "Puro Mangkunegaran Building as a Representation of the Javanese Palace, Indonesia," 2022.

[34] H. Bagja Prasthia, A. P. Agustiananda, and R. B. Santosa, "Akulturasi dalam arsitektur jawa di Yogyakarta Fasad berpedimen dalam arsitektur jawa di Kraton Yogyakarta dan Dalem Notonegaran," 2023.

[35] K. Lynch, The Image of the City. London: MIT Publisher, 1960.

[36] J. Urry and J. Larsen, "The Tourist Gaze 3.0," 2011.

[37] L. K. Keller, Strategic brand management, vol. 5, no. 6. 2013. doi: 10.1057/bm.1998.36.

.

E-ISSN: 2528-388X
P-ISSN: 0213-762X

INERSIA
Vol. 22, No. 1, May 2026

Assesment of Construction Safety Management System (CSMS) In Confined Space Tunnel Construction: A Case Study Of Jragung Dam

Indah Wahyuni[1*] and Shabrina Nur Hamidah[2]

[1)] Department of Civil Engineering and Education Planning, Faculty of Engineering, Universitas Negeri Yogyakarta, Yogyakarta 55281, Indonesia
[2)] Department of Civil Engineering, Faculty of Vocational, Universitas Negeri Yogyakarta, Yogyakarta 55281, Indonesia

Keywords:
CSMS,
Confined Spaces,
Bypass Tunnels,
Construction Safety,
Dam Construction.

ABSTRACT

Construction work on bypass tunnels involves work in confined spaces that pose high-risk hazards, such as toxic gases, noise, electrical hazards, and limited mobility; therefore, the implementation of a Construction Safety Management System (CSMS) is essential to minimize the risk of workplace accidents. Previous research on CMS implementation has primarily focused on open-space construction projects, while studies on confined-space construction—particularly bypass tunnels—remain limited. Additionally, several safety compliance issues were identified during the Jragung Dam project. This study aims to analyze CMS implementation, identify barriers to its adoption, and propose corrective measures in accordance with applicable regulations. The research method used is quantitative with a descriptive approach. Data were obtained through questionnaires, observations, and interviews at the Jragung Dam bypass tunnel construction project in Semarang Regency. The results of the study indicate that seven out of nine components of SMKK implementation fall into the “good” and “effective” categories, while the remaining two components fall into the “fairly good” category. The highest percentage was found in traffic signs and accessories as well as consultation with construction experts at 88%, while the lowest percentage was found in construction safety risk control activities at 75%. This study suggests that the implementation of SMKK in confined spaces needs to be carried out more effectively and in accordance with regulations so that the risk of workplace accidents can be minimized and worker safety better ensured.

1. Introduction

Diversion tunnels are an important part of dam construction that aims to direct the flow of rivers during the construction process of the main dam. The construction of the diversion tunnel for the Jragung Dam was carried out using the NATM (New Austrian Tunneling Method) approach. NATM is not just a construction method but a strategy to ensure the smooth implementation of construction activities, prioritizing safety and economy as the main principle [1]. Construction using NATM must comply with the agreed specifications, contract documents, work instructions, and other requirements. In addition, there is a need for quality assurance and occupational health safety (OHS) assurance [2]. The use of this method allows for adaptation to different geological conditions along the tunnel work site. Without proper adaptation of geological conditions, it can lead to the risk of accidents, structural failure, and delays in the implementation of construction. Structural safety assessment of tunnel layers is known that the safety factors of layers with cavities underneath based on a fuzzy comprehensive evaluation model are strongly influenced by changes in the classification of surrounding rocks, cavity locations, and depths. In contrast, changes in cavity length do not significantly affect the safety of the coating [3].

The construction of diversion tunnels is under the construction of limited space. Confined space is a work

*Corresponding author.
E-mail: indahwahyuni@uny.ac.id

https://doi.org/10.21831/inersia.v21i2.95138
Received 17 January 2026; Revised 29 May 2026; Accepted 31 May 2026
Available online 31 May 2026

area that workers can enter under certain conditions, features limited entry and exit points and is not designed for continuous occupancy. Working in confined spaces has environmental limitations that can trigger hazards, such as limited oxygen, increased concentrations and contamination of toxic gases, noise, structural instability, high temperatures, equipment failure, electrical risks such as exposure to electrical sources, and limited movement [4]. If left untreated, hazards in confined space work can significantly increase the risk of workplace accidents. The construction sector is the largest contributor to work accidents. From 2011 to 2019, there were 1,030 reported deaths due to confined space work accidents. For tunnel work in confined spaces, 129 deaths were reported, mainly caused by collapse and inhalation of hazardous substances [5].

Based on observations, on-site workers are still entering and exiting diversion tunnels without wearing full personal protective equipment (PPE), there are no access restrictions for individuals entering confined spaces, there are no barriers separating confined spaces from open areas, and not all workers in confined spaces have communication devices such as walkie-talkies. The high accident rate in construction work, limited space and low awareness of worker safety demand proactive measures to minimize accidents. These steps can be achieved by implementing an ideal construction safety management system (CSMS). Every service provider and construction service user are required to implement a CSMS in the implementation of construction service activities [6]. A Construction Safety Management System (CSMS) is an integral component of overall management that includes the organizational structure, planning, responsibilities, analysis, procedures, processes, and resources necessary to implement, achieve, and maintain occupational safety and health policies [7]. The ideal CSMS includes CSMS document preparation, socialization, promotion, training, personal protective equipment (PPE), work protective equipment (WPE), insurance and permits, construction safety personnel, facilities, and medical equipment, signage and traffic equipment, consultation with construction experts, and environmental inspections [8].

As previously described, in the practice of implementing CSMS in limited space in the Jragung Dam diversion tunnel construction project, there are still some shortcomings in meeting the construction safety aspect. Given the specific hazards in confined spaces, which are different from open spaces, ignoring these shortcomings in meeting the safety aspects of construction can significantly increase the risk of construction accidents in confined spaces. Additionally, non- compliance with CSMS in the space can damage the company's reputation and reduce the trust of project owners and other stakeholders. Remedial measures and increased oversight are required to ensure that the construction of the Jragung Dam diversion tunnel is aligned with the specific specifications for the CSMS Analysis component.

In line with that, from 2012 to 2022 in China, it was obtained that the concept of safety management was not implemented in the chemical industry in China. This can be seen in a study that observed that 14 major chemical accidents in China had poor safety cultures, inadequate accident investigations, inadequate training, and a lack of poor safety personnel, deliberate violations [9]. Therefore, the effectiveness of CSMS is highly dependent on the involvement of all stakeholder's interests, policy support, and adoption of safety technology and culture. The implementation of OHSMS in South Korea has shown significant success, with a 67% reduction in accidents and a 10.3% decrease in fatal accidents in the period 2006–2011. However, the difference in perception between general managers and K3 managers towards these systems shows the importance of harmonized understanding in safety management [10].

Hong Kong has implemented the Safety Management System (SMS) through formal regulations since 1999. The system integrates 14 safety elements and is closely supervised by the Labour Department, making Hong Kong a successful regulatory model in the implementation of construction safety [11]. Malaysia has not had comprehensive regulations for construction safety since the pre-construction stage. Recent studies highlight the need for safety indicators at the preconstruction stage as a preventive measure [12]. Norway sees good overall management of construction projects as having a positive impact on safety management. The results advocate the implementation of safety management as an integral aspect of all management activities within a project rather than as a disconnected subsystem. This work is new by empirically demonstrating the impact of the project management aspect on safety management in construction projects [13].

This study was conducted with the aim of analyzing the CSMS analysis in the limited space of the diversion tunnel construction project at the Jragung Dam and providing recommendations to improve CSMS compliance and reduce the risk of work accidents. The study not only seeks to protect workers' welfare but also aims to improve the overall efficiency and sustainability of the project. The findings of this study are expected to provide insight into the ideal CSMS Analysis in confined spaces for similar projects in accordance with applicable regulations [6] and [4]. The novelty of this research lies in its focus on the construction of confined spaces, while other research has been conducted on the construction of open spaces. In addition, evaluations are conducted on nine elements of the CSMS as set forth in the specific CSMS specification CSMS is a part of construction project management designed to ensure safety during the execution of work. Occupational Health and Safety (K3) in the construction sector encompasses all measures taken to protect workers from the risk of accidents and illnesses associated with their work. This effort involves preventive measures to prevent work incidents and maintain the health of workers during construction projects [14]. According to the safety management system as an increase in the speed of the safety management system in the form of external and internal inspections of the safety management process is the core of process safety management (PSM) and is an important opportunity to improve operational solutions [15]. To ensure the realization of construction safety, it is necessary to apply targets in the implementation of CSMS in construction projects. The following are the objectives in the implementation of construction safety [16]:

a) Ensuring the fulfillment of safety, safety, health, and sustainability standards in the study, planning, design, and implementation of construction projects;
b) Maintaining the health and safety of workers and other individuals at the construction site;
c) Ensure the safety, health, efficiency, and effectiveness of any materials and tools used;
d) Ensure the smooth completion of construction work;
e) Ensure safe and efficient use and maintenance of construction products.

In the implementation of CSMS, there are several components that must be met. The following are the components of CSMS implementation activities in accordance with a) CSP (Construction Safety Plan), containing CSMS management, project safety targets and programs, internal and external challenges in the implementation process, communication schedule, risk analysis, CSMS implementation costs, emergency response procedures, work stoppage steps when there is a threat, all aspects of safety control in construction, and monitoring and inspection schedules; b) CSU (Construction Safety Unit) In the implementation of CSMS, construction service providers must form UKK. UKK gets a mandate from the department that manages safety in construction, which is part of the service provider's highest management structure. UKK consists of leaders and members who are responsible for it; c) CSMS Implementation Fee. Service users need to ensure that the entire budget for the implementation of the CSMS has been prepared and allocated appropriately by the service provider. The CSMS implementation budget includes costs related to the implementation of CSMS in construction projects as well as costs for construction consulting services [6].

Specification of CSMS Implementation Components the components of CSMS [8] implementation activities are further explained as follows:

a) Preparation of CSMS implementation documents, including the creation of CWP (Construction Work Plan), CWQP (Construction Quality Plan), EMMWP (Environmental Management and Monitoring Work Plan), and RMLLP (Work Traffic Management Plan) documents. Creation of procedures and work instructions. Preparation of reporting on the implementation of CSMS (daily, weekly, monthly, final);
b) Socialization, promotion, and training;
c) Work protective equipment and personal protective equipment;
d) Insurance and licensing;
e) Construction safety personnel;
f) Medical facilities, infrastructure, and equipment;
g) Signs and necessary traffic or traffic management equipment;
h) Consultation with experts related to construction safety; and
i) Activities and equipment related to safety risk control.

The application of CSMS varies greatly between countries depending on regulations, work culture, and technology used. The United States uses data-driven approaches, such as predictive analytics and BIM, under OSHA oversight. Standards such as ANSI/ASSE Z10 are widely applied, with quantitative indicators such as the Total Recordable Incident Rate (TRIR) used for safety performance evaluation [17]. Systems in the UK are controlled by the Health and Safety Executive (HSE) through the Construction (Design and Management) Regulations (CDM). This model emphasizes the principle of Prevention through Design (PtD), ensuring risks are minimized from the planning stage [18]. A dedicated management framework has been developed to support construction clients to ensure their projects are safe and healthy for construction workers. Examples include the Model Client Framework in Australia [18] and the operational excellence model for OHS client engagement in the US [19]. PSM systems from jurisdictions in Asia, Australia, Europe, and North America, as well as approaches to the development of process safety performance indicators, are analyzed. The core process safety concept of an inherently safer design, the introduction of warning signs, a process safety culture, and dynamic risk assessment are also considered from the perspective of their integration in PSM [20].

In addition to technical and managerial aspects, human factors also play a crucial role in the successful implementation of construction safety management systems in confined-space tunnel projects. Several studies indicate that unsafe behavior among workers remains one of the primary causes of construction accidents, particularly in high-risk work environments such as tunnels and underground structures. Workers often underestimate the dangers due to monotonous work patterns, lack of supervision, time pressure, and low awareness of workplace safety procedures. Unsafe actions such as failing to wear complete personal protective equipment, entering confined spaces without permission, and disregarding communication procedures can increase the likelihood of fatal accidents during tunnel construction activities [21].

Human behavior regarding construction safety is greatly influenced by an organization's safety culture. Safety culture refers to the attitudes, perceptions, competencies, and collective behavioral patterns that determine a commitment to occupational health and safety management to [22]. A positive safety culture can encourage workers to follow regulations, actively participate in hazard reporting, and improve communication between supervisors and workers. Conversely, a weak safety culture can lead to negligence, rule violations, and low compliance with established safety procedures. In confined space construction work, a safety culture becomes even more critical because emergency situations can develop rapidly and potentially lead to serious consequences if preventive measures are not properly implemented.

Research conducted on underground construction projects shows that communication and monitoring systems have a significant impact on worker safety performance. Effective communication between supervisors, operators, and workers is crucial in tunnel construction because environmental conditions such as limited visibility, high noise levels, dust exposure, and restricted movement can hinder coordination during work activities [23]. Communication devices such as walkie-talkies, warning systems, emergency alarms, and monitoring equipment are essential for ensuring worker safety. Inadequate communication systems can hinder emergency response and exacerbate the consequences of accidents during operations in confined spaces.

In addition, the implementation of CSMS in tunnel construction also requires a continuous hazard identification and risk assessment process. Tunnel construction involves dynamic geological conditions that can change during the excavation process. Changes in rock structure, groundwater conditions, and excavation stability can give rise to new hazards that were not identified during the planning stage. Therefore, periodic risk assessments are necessary to ensure that control measures remain effective throughout the project's implementation [24]. Continuous monitoring systems, geotechnical instrumentation, and environmental inspections are key components of tunnel safety management for detecting potential failures at an early stage.

Management commitment is another key factor influencing the effectiveness of CSMS implementation. Strong commitment from project owners, contractors, and supervisors can improve compliance with safety procedures and encourage the allocation of adequate resources for safety programs. Management commitment can be demonstrated through regular safety evaluations, the provision of safety facilities, the enforcement of safety regulations, and the implementation of training programs for workers [25]. In large-scale infrastructure projects such as dam construction, management support is essential to ensure that safety objectives are integrated into every stage of construction.

Technological advancements have also helped improve safety management practices in construction projects. Digital technologies such as Building Information Modeling (BIM), real-time gas monitoring systems, wearable safety devices, and automated warning systems are increasingly being implemented to reduce the risk of accidents in confined spaces [11]. These technologies help project managers monitor environmental conditions, worker locations, and potential hazards more effectively. In tunnel construction projects, monitoring technologies can provide early warnings regarding hazardous gas concentrations, oxygen deficiency, excessive vibrations, or structural instability. Integrating these technologies into CSMS implementation can improve decision-making processes and enhance overall project safety performance.

Although there have been advances in safety regulations and technology, the implementation of CSMS in developing countries still faces various challenges. Limited safety budgets, inadequate training, weak enforcement, and a lack of worker participation often hinder the effectiveness of safety management systems [18]. In some cases, safety programs are implemented solely to meet administrative requirements, rather than to foster a genuine safety culture. As a result, safety procedures may not always be followed during project implementation. Therefore, evaluating the implementation of CSMS in actual construction projects is crucial for identifying gaps between regulatory standards and on-site practices.

Based on these considerations, an evaluation of the implementation of the Confined Space Management System (CSMS) in the Jragung Dam diversion tunnel project is essential, as this project involves high-risk construction activities in confined spaces using the New Austrian Tunneling Method (NATM). The findings of this study are expected to contribute to the development of more effective construction safety practices, particularly for tunnel and underground construction projects in Indonesia. Additionally, this study is expected to provide recommendations for enhancing safety awareness, strengthening oversight systems, and optimizing the implementation of CSMS in accordance with applicable regulations and international best practices.

3. Methods

This study uses a quantitative method with a descriptive approach. According to [20], quantitative methods are research methods used to study certain populations or samples, where data collection is carried out using research instruments and the analysis is quantitative/statistical. Meanwhile, the descriptive approach, as defined [4], aims to describe the phenomena that occur in the object of research.

The research was carried out at the construction site of the Jragung Dam diversion tunnel package III. Geographically, the Jragung Dam is located in Candirejo Village, Pringapus, Semarang, Central Java. The sampling technique used is saturated sampling, where all members of the population are taken as samples. The sample and population in this study consisted of all workers involved in the diversion tunnel construction project, including SQM (Site QHSE Manager), QHSE staff, administrative staff, technical staff, and operational staff.

The needs analysis in this study is divided into two types: primary data and secondary data. Primary data were obtained through questionnaires, which were developed based on the components of the CSMS Analysis activities as set out in the CSMS-specific guidelines. Secondary data is collected through observation and interviews to gather additional information.

The analysis of the questionnaire results was carried out by measuring the success rate for each indicator outlined in the questionnaire. The measurement scale used in this study is the Likert scale. The Likert scale is used to measure an individual's opinion of a particular phenomenon). The criteria in Table 1 for evaluating success are presented in the table below [16].

Table 1. Classification of CSMS analysis success

Classification	Score
Very Precise	4
Quite Precise	3
Less Accurate	2
Inappropriate	1

The scores obtained for each questionnaire point were then processed using univariate analysis. Univariate analysis is a type of data analysis that involves only one variable at a time. To assess the success of the Construction Safety Management System Analysis (CSMS) in the confined space of the Jragung Dam tunnel construction project, a central tendency measurement formula was applied, calculating the average value as follows [23].

Table 2. Classification of success in CSMS analysis

No	Total Value Range	Description
1	$Y_r >$ Mi + 1.5 Sbi	Good and effective
2	Mi < ≤ Million Mr . 1,5 SbiY_r	Quite good and effective
3	Miss 1,5 Sbi < ≤ MiY_r	Poorly implemented
4	$Y_r \leq$ Mi – 1.5 Sbi	Unsuccessful/failed
5	$Y_r >$ Mi + 1.5 Sbi	Good and effective

$$Y = \Sigma yi = Y1 + Y2 + Y3 \ldots + Yn \quad (1)$$

The results of the univariate analysis are then categorized based on a predetermined range. Table 2 is a success range for the Construction Safety Management System Analysis (CSMS).

3. Results and Discussion

3.1 Construction Safety Management System (CSMS) Analysis

Based on the analysis of the questionnaire results, the percentage and category of success of the CSMS (Construction Safety Management System) Analysis component in the construction of the Jragung Dam diversion tunnel are presented in the Table 3.

Based on the results, the Construction Safety Management System (CSMS) Analysis in the construction project of the limited space of the Jragung Dam diversion tunnel is included in the good and effective category. Seven components were categorized as good and effective, while two items were classified as quite good and effective. The highest percentage of 88% is observed in indicators for traffic signs and additional traffic devices, as well as consultation with relevant construction experts. In contrast, the lowest percentage of 75% is recorded in the indicators for activities and equipment related to construction safety risk control.

3.2 Shortcomings and Obstacles Along with Solutions for CSMS

This study also aims to identify the shortcomings and constraints of the Construction Safety Management System (CSMS) Analysis in the limited space of the Jragung Dam diversion tunnel construction project. Table 4 are some of the shortcomings and solutions obtained from observations and interviews. The practical implications for addressing shortcomings and obstacles in the implementation of CSMS are in

line with applicable regulations and standards. This means that every step taken must be in accordance with the norms and standards set by the relevant authorities. One of the measures that can be adopted is to conduct daily inspections to ensure that all workers perform their duties according to established procedures and wear complete Personal Protective Equipment (PPE). In this way, the safety of workers can be maintained while on the job site. In addition, it is also important to document all components of the CSMS according to the forms provided, which include entry clearance forms for restricted areas, CSMS audits, inspections conducted, and documents stating that workers are free from exposure to hazards. Proper and systematic documentation not only aids in regulatory compliance but also serves as an important record for future evaluations and improvements.

Table 3. Components of CSMS analysis success

Not	Indicator	Percentage	Success Categories
1	CSMS Analysis Document	86%	Good and effective
2	Socialization, Promotion, and Training	87%	Good and effective
3	Protective Equipment	84%	Good and effective
4	Insurance	82%	Good and effective
5	Construction Safety Personnel	85%	Good and effective
6	Health Facilities, Infrastructure, and Equipment	81%	Quite good and effective
7	Traffic signs and complementary Equipment	88%	Good and effective
8	Consultation with a Construction Expert	88%	Good and effective
9	Activities and Equipment Related to Construction Safety Risk Control	75%	Quite good and effective

Table 4. Disadvantages and constraints of CSMS analysis

No	Indicator	Disadvantages and Barriers	Solution
1	CSMS Analysis Document	Lack of special permissions to enter restricted spaces	Creating a work permit Conduct special training for workers in confined spaces
		CSMS reporting is only done weekly	Improve CSMS reporting on a daily, weekly, and monthly basis
2	Socialization, Promotion, and Training	Safety induction is still common; No special safety induction for workers inconfined spaces	Perform special safety induction for workers in confined spaces
		No socialization about HIV/AIDS	Providing socialization about HIV/AIDS to all workers, both in limited spaces and outside, with the help of related agencies
		Lack of enthusiasm among workers	Provide a comfortable atmosphere and facilities

No	Indicator	Disadvantages and Barriers	Solution
		to attend training	Offer challenges and competitions with attractive incentives or prizes
		Inadequate and outdated information media	Conducting audits of construction safety information media Replacing and updating inadequate and outdated information media
3	Personal protection equipment	Safety lines have not been installed around the tunnel excavation area: Workers still wear inadequate PPE	Install safety lines to delimit between elevated and lower areas: Evaluate this issue Replace inadequate PPE Conduct training on the importance of wearing PPE
		Workers do not use complete PPE	Socializing the importance of using PPE Sentencing Severe Check the completeness of the PPE before starting work in the tunnel
4	Insurance	Equipment, heavy equipment, electrical, and other inspections are only carried out occasionally, not routinely before starting work	Perform inspections of heavy equipment, electrical equipment, and other tools whenever work in confined spaces begins
5	Construction Safety Personnel	Insufficient safety personnel, especially environmental management.	Add personnel for environmental management and emergency respons
		Officers and emergency response personnel	Providing training and certification for safety officers
6	Health Facilities, Infrastructure, and Equipment	Sanitation facilities are not yet available in the work area	Provides sanitation facilities such as portable stations with running water, and waste disposal sites
7	Traffic Signs and Auxiliary Devices	Heavy equipment mobilization is sometimes not supervised by flag guards	Set flagmen according to the SOP. Flagmen must be certified and trained according to their job description and use communication devices for coordination.
		No roadblocks on the road access to diversion tunnel works	Installing roadblocks at high-risk points on access roads to diversion tunnel works
8	Consultation with Related Construction Experts	No consultation has been carried out with earthquake and electrical experts	Consult with an earthquake and electrical expert both before and during the diversion tunnel construction process
9	Activities and Equipment Related to Construction	Ambient air quality inspections are not routine due to limited equipment	Companies should coordinate further and target routine inspections in the morning, afternoon, and evening, both at the inlet and exit.
10	Safety Risk Control	Environmental vibration tests and tests on motor vehicle vibration levels are only carried out at the beginning of tunnel work	Apply periodic vehicle vibration and vibration tests throughout the project.
		Ambient air quality documentation and river water quality checks are still lacking	Improve documentation, especially the results of ambient air quality inspections. The results should be transparent, allowing workers to access them, so they can know which results are poor or that exceed threshold values.

4. Conclusions

Based on the calculations that have been made, the findings are obtained in accordance with the research problem and in the form of recommendations. Of the nine ideal components for CSMS implementation, there are seven that fall into the category of good and effective. The remaining two components, including the advisory component, infrastructure, and medical equipment as well as the components of construction safety risk control activities and equipment are included in the category of quite good and effective. From the results of the analysis, it was found that the largest percentage of CSMS implementation, which is 88%, is in traffic signs and complementary indicators as well as consultation with construction-related experts. Meanwhile, the lowest percentage of 75% is in activity indicators and equipment related to construction safety risk control. According to the results of interviews and observations, the majority of shortcomings and obstacles in the implementation of CSMS come from within, such as management and limited resources. The solutions used in overcoming shortcomings and obstacles are adjusted to applicable regulations. The implementation of CSMS implementation solutions can be in the form of daily inspections before work to check that workers have worked according to procedures and are wearing complete PPE. In addition, documenting the components of the CSMS according to the available forms such as admission forms, CSMS audits, inspections, and free exposures. This study highlights the importance of strengthening operational safety controls in confined space tunnel construction projects. Future improvements should focus on increasing routine environmental monitoring, improving worker compliance with PPE usage, enhancing emergency preparedness systems, and providing adequate safety personnel and supporting facilities. Strengthening these aspects can help minimize occupational accidents and improve the sustainability of construction safety management implementation in high-risk infrastructure projects.

References

[1] V. Phadke and N. Titirmare, "Construction of tunnels by New Austrian Tunneling Method (NATM) and by Tunnel Boring Machine (TBM)," *International Journal of Civil Engineering (IJCE)*, vol. 6, no. 6, pp. 25–36, 2017.

[2] K. Rahmawati, "Analisis New Austrian Tunneling Method dan rancangan pemeliharaan terowongan pengelak pada pembangunan Bendungan Bener Kabupaten Purworejo," Master's thesis, Dept. Civil Engineering, Universitas Gadjah Mada, Yogyakarta, Indonesia, 2023.

[3] Y. Wang and H. Wang, "Safety assessment of tunnel lining structure with underlying cavities based on fuzzy comprehensive evaluation in mudstone stratum," *Journal of Applied Engineering and Technological Science (JAETS)*, vol. 5, no. 2, pp. 772–790, 2024, doi: 10.37385/JAETS.V5I2.3690.

[4] Menteri Ketenagakerjaan Republik Indonesia, *Peraturan Menteri Ketenagakerjaan Republik Indonesia Nomor 11 Tahun 2023 tentang Keselamatan dan Kesehatan Kerja di Ruang Terbatas*, Jakarta, Indonesia, 2023.

[5] A. S. Septiningtias, T. Rakhmadi, and A. T. Subekti, "Identifikasi bahaya dan penilaian risiko (IBPR) di ruang terbatas dengan pendekatan literature study," *Bhamada Occupational Health and Safety Environment Journal*, vol. 1, no. 2, pp. 16–27, 2023.

[6] Kementerian Pekerjaan Umum dan Perumahan Rakyat, *Peraturan Menteri PUPR Nomor 10 Tahun 2021 tentang Pedoman Sistem Manajemen Keselamatan Konstruksi*, Jakarta, Indonesia, 2021.

[7] T. Mardakngo, "Analisis keselamatan pekerjaan (Job Safety Analysis), bagian dari RKK dan SMKK dalam suatu tender pemilihan pelaksana konstruksi," in *Seminar Nasional Insinyur Profesional (SNIP)*, vol. 1, no. 1, 2021.

[8] Kementerian Pekerjaan Umum dan Perumahan Rakyat, *Spesifikasi Khusus Sistem Manajemen Keselamatan Konstruksi (SMKK)*, Jakarta, Indonesia, 2022.

[9] M. Bai *et al.*, "Why do major chemical accidents still happen in China: Analysis from a process safety management perspective," *Process Safety and Environmental Protection*, vol. 176, pp. 411–420, 2023, doi: 10.1016/J.PSEP.2023.06.040.

[10] S. J. Yoon, H. K. Lin, G. Chen, S. Yi, J. Choi, and Z. Rui, "Effect of occupational health and safety management system on work-related accident rate and differences of occupational health and safety management system awareness between managers in South Korea's construction industry," *Safety and Health at Work*, vol. 4, no. 4, pp. 201–209, 2013, doi: 10.1016/J.SHAW.2013.10.002.

[11] N. S. N. Yiu, N. N. Sze, and D. W. M. Chan, "In-depth investigation of safety management system in Hong Kong construction industry – Literature review and research agenda," *International Journal of Advances in Mechanical and Civil Engineering*, vol. 5, no. 1, pp. 6–10, 2018.

[12] N. M. Saifullah and F. Ismail, "Integration of occupational safety and health during pre-construction stage in Malaysia," *Procedia - Social and Behavioral Sciences*, vol. 35, pp. 603–610, 2012, doi: 10.1016/J.SBSPRO.2012.02.127.

[13] K. W. Edwin, T. Kongsvik, and E. Albrechtsen, "An analysis of the relationship between project management and safety management in the Norwegian construction industry," *Safety Science*, vol. 180, Art. no. 106654, 2024, doi: 10.1016/j.ssci.2024.106654.

[14] B. Tepparit, N. Am-Eam, and K. Warunsin, "Examining factory process safety management

systems and studying lean improvement methods," *Journal of Applied Engineering and Technological Science (JAETS)*, vol. 6, no. 1, pp. 249–261, 2024.

[15] M. Siswanto, *Menyusun Risiko Keselamatan Konstruksi Kecil dalam Dokumen Sistem Manajemen Keselamatan Konstruksi (SMKK)*. Jakarta, Indonesia: Kementerian PUPR, 2022.

[16] J. Hinze, S. Thurman, and A. Wehle, "Leading indicators of construction safety performance," *Safety Science*, vol. 51, no. 1, pp. 23–28, 2013, doi: 10.1016/J.SSCI.2012.05.016.

[17] J. Hinze, S. Thurman, and A. Wehle, "Leading indicators of construction safety performance," *Safety Science*, vol. 51, no. 1, pp. 23–28, 2013, doi: 10.1016/J.SSCI.2012.05.016.

[18] H. Lingard, N. Blismas, T. Cooke, and H. Cooper, "The model client framework: Resources to help Australian Government agencies to promote safe construction," *International Journal of Managing Projects in Business*, vol. 2, no. 1, pp. 131–140, 2009, doi: 10.1108/17538370910930554.

[19] H. Liu, E. Jazayeri, and G. B. Dadi, "Establishing the influence of owner practices on construction safety in an operational excellence model," *Journal of Construction Engineering and Management*, vol. 143, no. 6, Art. no. 04017005, 2017, doi: 10.1061/(ASCE)CO.1943-7862.0001292.

[20] P. R. Amyotte and C. S. Lupien, "Elements of process safety management," in *Methods in Chemical Process Safety*, vol. 1. Amsterdam, Netherlands: Elsevier, 2017, pp. 87–148, doi: 10.1016/BS.MCPS.2017.01.004.

[21] Pemerintah Republik Indonesia, *Peraturan Pemerintah Nomor 14 Tahun 2021 tentang Perubahan atas Peraturan Pemerintah Nomor 22 Tahun 2020 tentang Peraturan Pelaksanaan Undang-Undang Nomor 2 Tahun 2017 tentang Jasa Konstruksi*, Jakarta, Indonesia, 2021.

[22] Sugiyono, *Metode Penelitian Kuantitatif, Kualitatif, dan R&D*. Bandung, Indonesia: Alfabeta, 2019.

[23] V. H. Pranatawijaya, W. Widiatry, R. Priskila, and P. B. A. A. Putra, "Penerapan skala Likert dan skala dikotomi pada kuesioner online," *Jurnal Sains dan Informatika*, vol. 5, no. 2, pp. 128–137, 2019.

[24] D. E. Wibowo, I. Wahyuni, A. D. Hastutiningsih, I. M. Nurshefa, and D. D. Rimbawati, "Occupational safety and health risk analysis using HIRARC and JSA methods in building projects construction," *AIP Conference Proceedings*, vol. 2629, no. 1, 2023.

[25] H. Lingard and P. Pirzadeh, "Workplace health and safety performance at the client-contractor interface: Measurement, management and behaviour," *Safety Science*, vol. 184, Art. no. 106753, 2025, doi: 10.1016/J.SSCI.2024.106753.

.

E-ISSN: 2528-388X
P-ISSN: 0213-762X

INERSIA
Vol.22, No.1, May 2026

Assessing the Effects of Building Mass Configuration and Form on Solar Radiation Gain: A Hypothetical Study

Wildan Muhammad Haikal* and Nedyomukti Imam Syafii

Department of Architecture and Planning, Faculty of Engineering, Universitas Gadjah Mada, Yogyakarta 55281, Indonesia

Keywords:
Mass Configuration
Mass Form
Solar Radiation
Ladybug
Subsidized Housing

ABSTRACT

Urbanization has continued to grow from year to year, leading to one of its major impacts—the rising population in urban areas. This population increase is directly proportional to the growing demand for housing, which in turn drives up property prices. Therefore, government support in the form of subsidized housing for low-income communities (MBR) becomes essential. However, subsidized housing is often criticized by the public for its unsatisfactory quality. Moreover, the development of such housing is feared to exacerbate the ongoing issue of global warming, as it has the potential to increase ambient temperatures in residential areas. The objective of this study is to identify the influence of changes in building mass configuration and form on the reception of solar radiation at outdoor site surface. A quantitative research method was applied by simulating hypothetical building mass models of subsidized housing using Rhinoceros – Grasshopper – Ladybug software. The findings indicate that modifications in building mass configuration and form can reduce the amount of solar radiation received by outdoor site surface. On sites oriented west–east, the best case modification was able to reduce radiation values by up to 32.5% compared to the base case, while on sites oriented north–south, the most effective modification achieved a reduction of up to 25.3% compared to the base case.

1. Introduction

Urban development, particularly in major cities, directly influences population growth and the expansion of urban activities [1]. This phenomenon, commonly referred to as urbanization, continues to shape demographic and spatial dynamics in Indonesia. According to [2], the proportion of the population residing in urban areas is projected to exceed half of the national total by 2035, reaching approximately 66.6%. The increasing urban population inevitably drives higher demand for housing, while simultaneously intensifying land requirements for residential purposes. This pressure often leads to escalating land and property prices in urban centers [3]. Rising costs disproportionately affect low-income households, making it difficult for them to access adequate housing. To address this challenge, government intervention has become essential, particularly through subsidized housing programs. For low-income groups, such programs serve as a critical avenue to achieve homeownership at affordable prices [4]. However, the provision of subsidized housing faces significant challenges beyond affordability, especially concerning construction quality and thermal comfort. These issues are frequently overlooked as the primary focus remains on cost reduction. Studies highlight that many subsidized housing projects are criticized for substandard building quality and inadequate energy efficiency, resulting in discomfort and higher long-term operational costs for residents [5][6]. Thus, while subsidized housing addresses accessibility, it raises important concerns about sustainability, resilience, and the overall well-being of its occupants.

The rising demand for housing also drives higher energy consumption in the residential sector [7]. Electricity is projected to dominate household energy use, with its share increasing from 60% in 2018 to nearly 90% by 2050, largely due to the growing reliance on appliances

*Corresponding author.
E-mail: wildanmuhammadhaikal@mail.ugm.ac.id

https://doi.org/10.21831/inersia.v21i2.90046
Received 29 September 2025; Revised 17 June 2026; Accepted 18 June 2026
Available online 20 June 2026

such as air conditioners, refrigerators, and water pumps [8]. As a result, urban areas have become major contributors to overall energy consumption [9], while buildings themselves account for about one-third of global energy use and nearly one-quarter of carbon dioxide emissions, positioning them as critical players in the climate change crisis [10]. Among building systems, HVAC represents one of the largest energy demands [11], and its energy use is highly sensitive to both indoor and outdoor temperatures, which directly influence heating and cooling needs [12]. In the tropical climate of Indonesia, high temperatures increase the demand for cooling systems to ensure indoor comfort, forcing HVAC systems to work against heat gains primarily caused by solar radiation [13]. This underscores the urgency of design strategies that minimize indoor heat loads to prevent escalating HVAC energy use. One effective passive design approach is modifying building configuration and form to reduce incident solar radiation (insolation). Since the amount of insolation received by building surfaces is a primary driver of cooling demand, it directly impacts energy consumption [14]. Previous studies confirm that urban building massing is a key determinant of energy use and solar energy potential [15]. Furthermore, there is strong evidence linking urban form, local climate conditions, and building energy consumption [12]. Local climate also plays a central role in shaping indoor thermal comfort levels, further highlighting the need for climate-responsive building design [16].

Urbanization brings positive impacts, particularly in the economic sector, but it also carries potential environmental drawbacks if not properly managed—especially within residential housing areas. In many cases, subsidized housing developments appear to be built with minimal considerations, often neglecting both indoor comfort and the quality of the surrounding environment. One of the main challenges in creating thermally comfortable subsidized housing is limited funding, which restricts investment in higher-quality design and materials. As a response, passive design strategies—such as modifying or adjusting building massing and configuration—offer a cost-effective approach to improving thermal performance and creating more livable environments.

Most existing studies on massing and configuration adjustments have been conducted at the urban scale, focusing on city blocks or larger clusters of buildings. In contrast, this study applies such design modifications at a smaller scale, namely within residential neighborhoods. Research on how variations in building massing influence solar radiation and outdoor thermal conditions at the scale of housing developments remains scarce, leaving a clear gap in the literature. This study aims to address that gap by identifying the influence of building mass configuration and form variations on solar radiation exposure at outdoor site surface through quantitative analysis, using simulation methods applied to a hypothetical case study.

2. Methods

This study employs a quantitative method using an experimental strategy supported by computer-based simulations conducted with *Rhinoceros–Grasshopper–Ladybug*. *Ladybug* functions as a plugin within *Grasshopper*, while *Grasshopper* itself is a plugin for the *Rhinoceros* software. The process begins with 3D object modeling in *Rhinoceros*, after which the model is transferred into the *brep* component in *Grasshopper* to run solar radiation simulations using the *Ladybug* plugin. The simulation requires local climate data in the form of an *EnergyPlus Weather* file (EPW). For this research, the EPW dataset is sourced from the Sultan Aji Muhammad Sulaiman Sepinggan International Airport weather station in Balikpapan City, East Kalimantan. Balikpapan City was selected to represent cities with similar geographical conditions, particularly those located near the equator. The solar radiation simulation is executed with input parameters covering a full 24-hour cycle, from 00:00 to 24:00, and across an entire year from January through December. The overall workflow of the simulation process is illustrated in Figure 1.

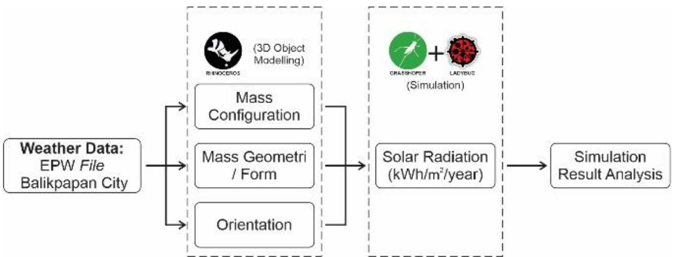

Figure 1. Simulation process.

Based on land use and building size regulations outlined in [17], the 3D object modeled in this study represents a subsidized housing unit with a building size of 36 m² on a land plot of 72 m² (type 36/72 house). The study site consists of eight plots, each with its own building mass. In total, the site measures 28.8 m x 26 m. A road runs through the center of the site, dividing it into two sections and creating four facing plots with opposing building masses. While the configuration and shape of each building mass vary, they are constrained to cover 50% of the plot area. All buildings share the same height of 5 meters, ensuring that each unit has identical footprint area, height, and volume despite differences in form. Three study groups are established for observation, as illustrated in Figure 2. The first group serves as the base case, representing the typical building mass commonly found in subsidized housing developments, while the second and third groups provide comparative alternatives. Case Study Group 1 had a building mass width of 7.2 m and no spacing between building masses. Case Study Group 2 had a building mass width of 6 m, while Case Study Group 3 had a building mass width of 4 m.

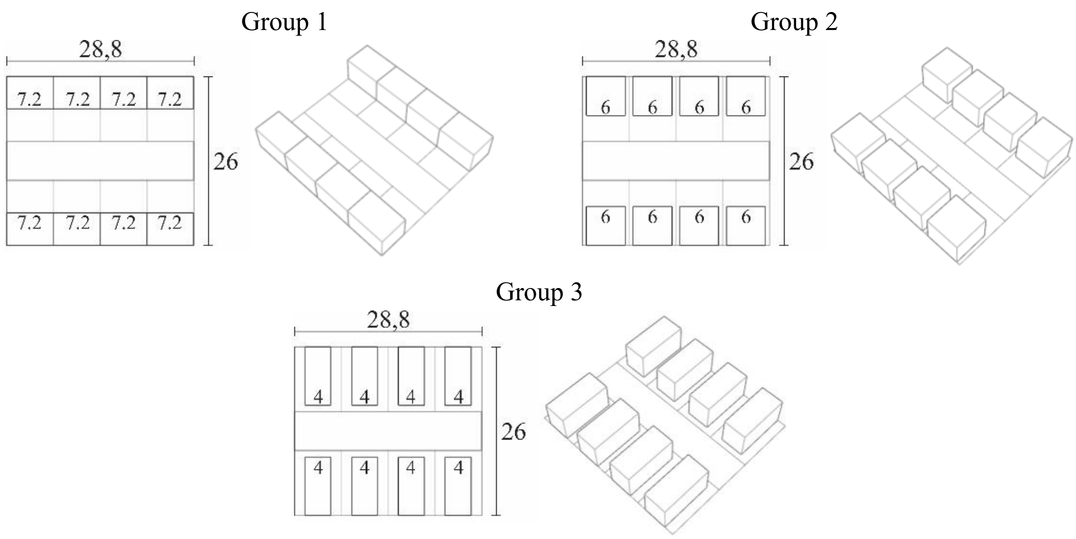

Figure 2. Floor Plan and Perspective of Three Case Study Groups.

Figure 3. Types of Building Mass Forms .

From the three study groups, each building mass will be transformed into three distinct variations, resulting in a total of nine simulated case studies. The modifications are derived from building mass forms commonly found in real housing developments (Figure 3), which are then simplified into 3D objects for the purpose of simulation and analysis.

Only the facade of the building mass facing the street was modified, while the other sides remained unchanged. Mass form A serves as the base case, representing the building's condition prior to any modifications. The three variations of modified building masses are presented in Figure 4.

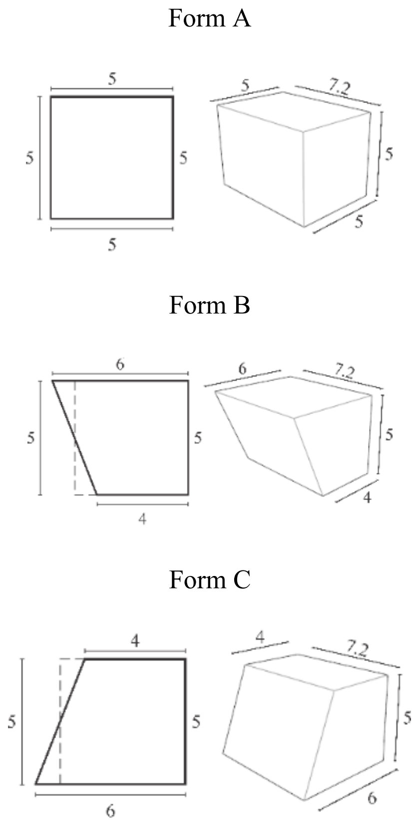

Figure 4. Side View and Perspective of Three Types of 3D Models of Building Mass Forms.

Subsidized Housing

Subsidized housing is one of the government's initiatives to provide decent and affordable homes for the public, particularly for low-income households (MBR) [4][6]. These houses are typically developed within residential complexes and supported by government incentives such as tax exemptions and low-interest mortgage schemes [18]. According to [17], regulations have set minimum land area and building floor area requirements for subsidized housing which can be seen in Table 1 .

Table 1. Land Area and Building Area of Subsidized Houses.

Type of House	Site Area (m^2)		Building Floor Area (m^2)	
	Lowest	Highest	Lowest	Highest
Subsidized Houses	60	200	21	36

Research exploring the relationship between subsidized housing, solar radiation, and building massing remains limited. Existing studies have primarily focused on the quality of physical elements in subsidized housing [6][4], the performance of existing buildings [16][5][19], sustainability aspects [20], and factors influencing the decision to purchase subsidized homes [21][22][23]. Most research on subsidized housing in Indonesia has relied on case studies of specific housing projects, with no studies identified that use hypothetical scenarios. Furthermore, no prior studies have specifically examined the role of building massing and configuration in subsidized housing. One relevant study on settlement-scale massing was conducted by [24], which analyzed its influence on microclimate conditions in residential areas. However, that research relied on existing buildings and field measurement methods, leaving significant gaps that this study aims to address.

Solar Radiation and Building Mass

Solar radiation is electromagnetic energy produced through nuclear fusion processes occurring in the core of the sun [25]. According to [26], solar radiation can be expressed in two main ways: as the density of energy flux or instantaneous power received on a surface (radiation, measured in W/m²), and as the total quantity of energy received per unit area over a given period (irradiance, measured in J/m² or Wh/m²). The cumulative amount of solar energy received by a surface per unit area within a specific timeframe is referred to as insolation, typically expressed in kWh/m² per day, month, or year.

Previous studies have revealed a strong correlation between insolation and the configuration or form of building massing. Compact or densely arranged building blocks tend to reduce the exposed surface area, thereby lowering insolation values, while more open configurations increase exposure to solar radiation. [15] emphasized that the form of urban building blocks is a crucial factor influencing both the utilization of solar energy potential and overall building energy consumption. Research on urban building massing has often been conducted using homogeneous block models, where a single type of block mass design is applied [27][28][29]. In contrast, other studies have adopted heterogeneous block models, which incorporate a combination of varied block massing designs to better represent urban complexity [30] [12][31].

3. Results and Discussion

The solar radiation simulation on the site surface was carried out under the assumption that the radiation values on each plane were influenced only by the building mass objects placed above it, without interference from other elements or objects. In addition, the site was tested under two different orientations (west–east and north–south) to evaluate their impact on solar radiation levels. Each case study, with its distinct building massing configuration, was analyzed to assess how variations in form affect the distribution and intensity of solar radiation received across the site. The simulation was first conducted on the west–east orientation, followed by the north–south orientation. The results of these simulations are presented in Table 2. Then, a bar chart of the simulation results presented in Figure 5.

Based on each group of building mass form categories, case study group 3 (3A, 3B, 3C) recorded the lowest solar radiation values compared to groups 1 (1A, 1B, 1C) and 2 (2A, 2B, 2C), as illustrated in Figure 6. Group 3 features elongated, slender masses oriented along the north–south axis, which create larger shaded areas than those in groups 1 and 2. In contrast, group 1 exhibited the highest radiation values among all groups. This is primarily because the masses in group 1 are directly adjacent to one another, unlike groups 2 and 3 where spacing between the buildings is present. The simulations demonstrate that as the distance between buildings increases, the level of solar radiation received decreases. This effect is most evident in group 3, which has the widest spacing among all cases. Moreover, the results confirm that even with identical footprint areas and building volumes, variations in massing that introduce wider inter-building spacing significantly reduce solar radiation exposure. In other words, the degree of shading produced by building separation plays a decisive role in shaping the overall radiation levels on the site surface.

Table 2. Average Annual Solar Radiation Value at Sites with West-East Orientation.

Case Study 1a (*Base Case*)	Case Study 1b	Case Study 1c
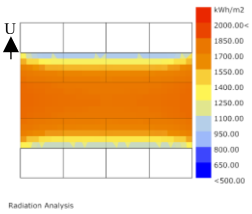	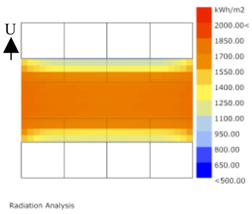	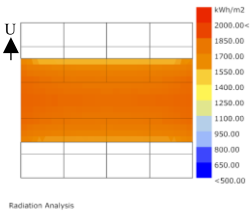
1,517.1 kWh/m²/year	1,310.7 kWh/m²/year	1,663.5 kWh/m²/year
Case Study 2a	Case Study 2b	Case Study 2c
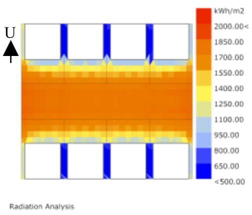	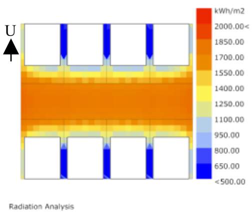	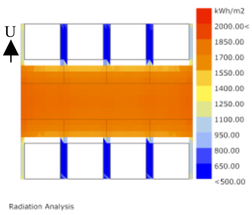
1,261.4 kWh/m²/year	1,126.5 kWh/m²/year	1,337.5 kWh/m²/year
Case Study 3a	Case Study 3b	Case Study 3c
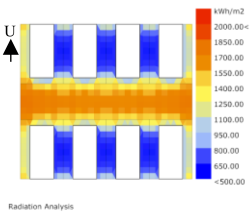	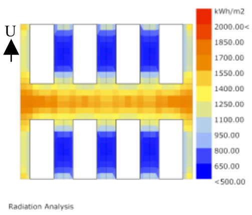	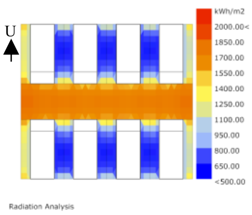
1,124.1 kWh/m²/year	1,024.4 kWh/m²/year	1,148.4 kWh/m²/year

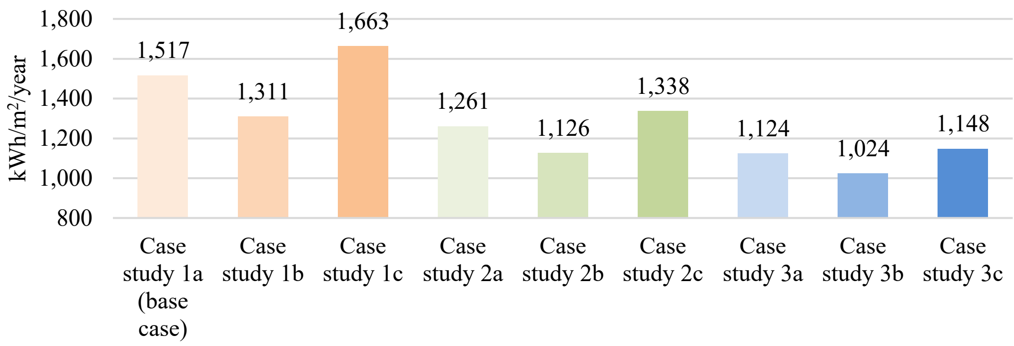

Figure 5. Average Solar Radiation Simulation Results / Year on West - East Site Orientation.

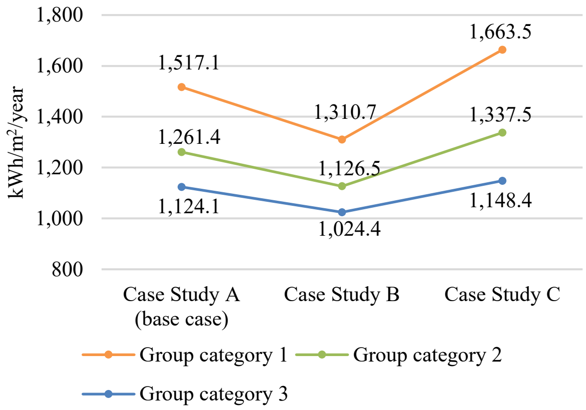

Figure 6. Average Solar Radiation Simulation Results / Year Based on Mass Form Category Groups in West - East Site Orientation.

As shown in Figure 6, building mass form B (1B, 2B, 3B) consistently produced the lowest solar radiation values compared to forms A (1A, 2A, 3A) and C (1C, 2C, 3C). The geometry of form B increases the extent of shaded areas, thereby reducing the site surface exposed to direct solar radiation and lowering the overall radiation levels. In contrast, form C recorded the highest solar radiation values, as its configuration reduces shaded areas and increases the portion of the site exposed to sunlight. This results in higher solar radiation intensity across the site surface. A similar study by [32], examined facade modifications by adjusting the tilt of building facades relative to solar angles. The findings demonstrated that the most optimized facade design reduced incident solar radiation, subsequently lowering cooling energy demand by approximately 20%–23%.

The simulation was then extended by reorienting the site from its initial west–east alignment to a north–south orientation, allowing for a comparative analysis between the two configurations. The results of the simulation for the north–south orientation are presented in Table 3.

A comparative analysis of the solar radiation simulations for both orientations revealed several consistent patterns alongside some notable differences. As illustrated in Figure 7, a similar trend is observed in case study group 1 (1A, 1B, 1C), which consistently recorded the highest solar radiation values compared to groups 2 (2A, 2B, 2C) and 3 (3A, 3B, 3C). Furthermore, when examining variations in building mass forms within each group, the results show that form B consistently produced the lowest radiation values, while form C recorded the highest.

Under the west–east orientation, Case Study 3B (1,024.4 kWh/m²/year) reduced solar radiation by 32.5% compared to the base case 1A (1,517.1 kWh/m²/year). In contrast, under the north–south orientation, Case Study 3B (1,036.7 kWh/m²/year) reduced solar radiation by 25.3% relative to the base case 1A (1,387.5 kWh/m²/year). These results indicate that site orientation also plays an important role in reducing solar radiation exposure on the site surface. This finding is consistent with the study conducted by [27], which identified site orientation as one of the most significant parameters affecting solar radiation exposure on buildings. The study likewise reported that the north–south orientation was the most effective in reducing solar radiation gain compared to other orientations.

Table 3. Average Annual Solar Radiation Value at Sites with North-East Orientation.

Case Study 1a (*Base Case*)	Case Study 1b	Case Study 1c
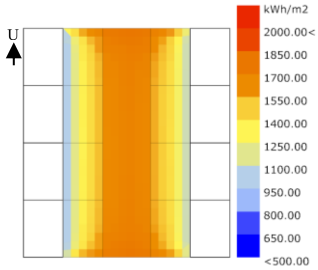	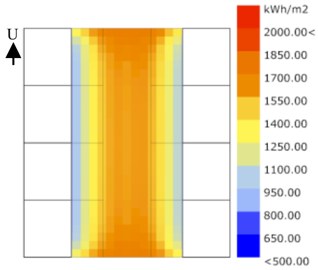	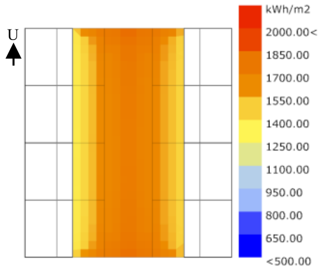
1,387.5 kWh/m^2/year	1,181.3 kWh/m^2/year	1,527.1 kWh/m^2/year
Case Study 2a	Case Study 2b	Case Study 2c
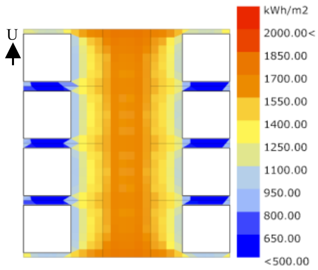	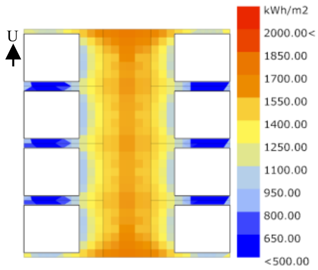	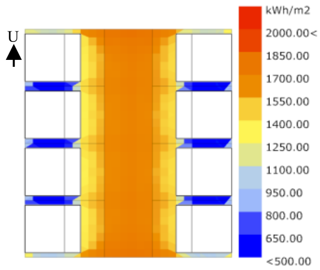
1,193 kWh/m^2/year	1,062.4 kWh/m^2/year	1,290.6 kWh/m^2 /year
Case Study 3a	Case Study 3b	Case Study 3c
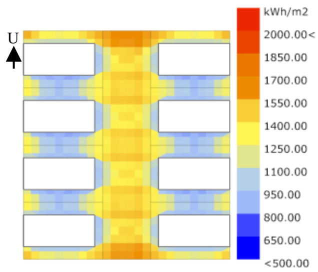	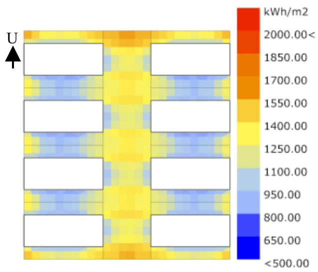	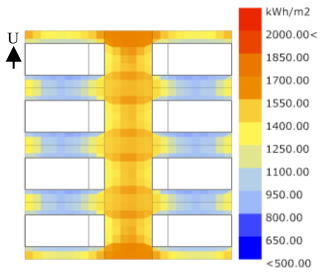
1,124.8 kWh/m^2/year	1,036.7 kWh/m^2/year	1,164.7 kWh/m^2/year

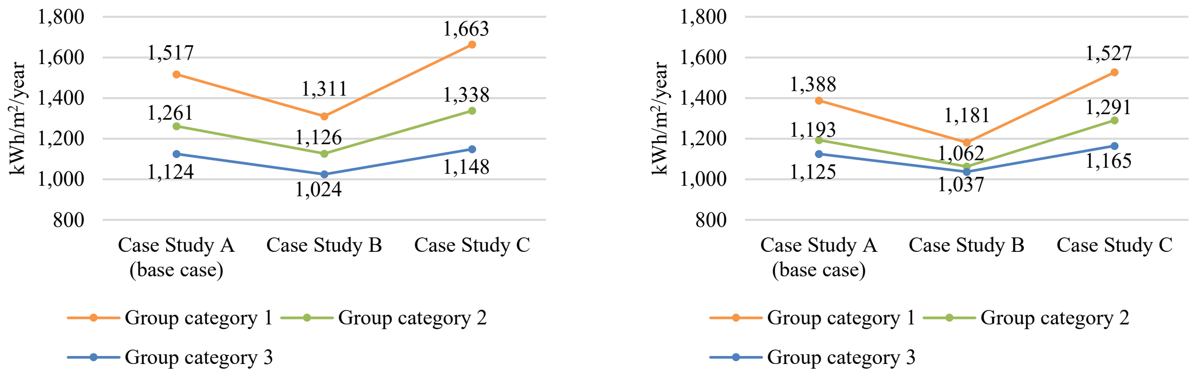

(a) (b)

Figure 7. Comparison of Average Solar Radiation Simulation Results per Year Based on Mass Form Category Groups in West - East (a) and North - South Site Orientations (b).

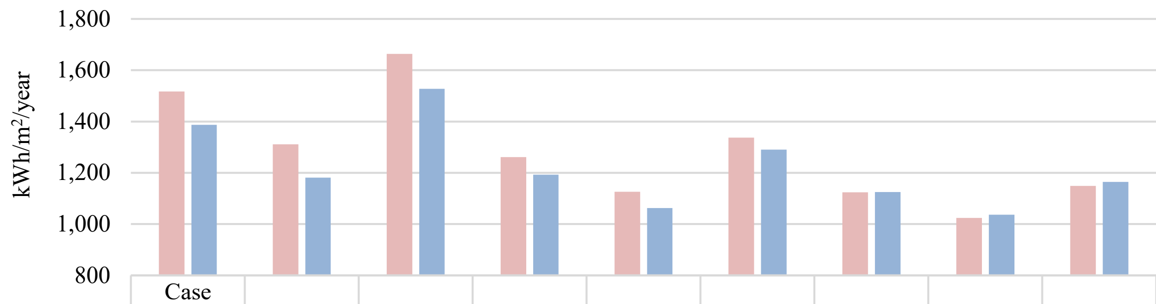

	Case study 1a (base case)	Case study 1b	Case study 1c	Case study 2a	Case study 2b	Case study 2c	Case study 3a	Case study 3b	Case study 3c
West-East	1517.11	1310.68	1663.47	1261.43	1126.49	1337.54	1124.12	1024.43	1148.41
North-South	1387.5	1181.3	1527.1	1193.0	1062.4	1290.6	1124.8	1036.7	1164.7

Figure 8. Comparison of Solar Radiation Simulation Results/Year at Sites with West-East and North-South Site Orientations.

Sites with a west–east orientation generally exhibited higher solar radiation values than those with a north–south orientation (WE > NS), as observed in Case Study Groups 1 and 2 (Figure 8). However, the opposite pattern was found in Case Study Groups 3, where the north–south orientation resulted in slightly higher solar radiation values than the west–east orientation (WE < NS), although the differences were relatively small. When Case Study Groups 3 were arranged on a west–east-oriented site, the elongated building masses were oriented north–south, resulting in larger shaded areas generated by the buildings. In contrast, when the same case study groups were arranged on a north–south oriented site, the elongated building masses became west–east oriented, producing smaller shaded areas. Theoretically, this phenomenon is closely related to the daily solar path, particularly during the morning and afternoon periods when the solar altitude angle is relatively low. These findings indicate that site orientation remains an important parameter in solar radiation control strategies for housing design in warm-humid tropical climates.

4. Conclusions

Based on the analysis and discussion, it can be concluded that building configuration and massing significantly influence the reduction of annual average solar radiation. Overall, the simulations indicate that greater spacing between buildings results in lower solar radiation values. In the west–east site orientation, case 3B recorded the lowest solar radiation, with 1,024.4 kWh/m²/year. This configuration reduced radiation by 32.5% compared to the base case, 1A, which recorded 1,517.1 kWh/m²/year. For the north–south orientation, Case 3B achieved the lowest radiation value at 1,036.7 kWh/m²/year, representing a 25.3% reduction compared to the base case, 1A, with 1,387.5 kWh/m²/year. The best performing modified cases in both orientations also demonstrated that increased shaded areas generated by building configurations and forms directly reduce solar radiation exposure. This study is expected to provide valuable insights and practical considerations for architects and other professionals in designing subsidized housing developments. By applying passive strategies through thoughtful massing and configuration, outdoor thermal comfort can be enhanced by mitigating solar radiation exposure.

References

[1] P. Melati, J. L. Pinassang, and S. A. Suwarlan, "Analisis Hunian Vertikal dengan Konsep Arsitektur Modular Sebagai Solusi Keterbatasan Lahan di Kota Batam," *J. Archit. Des. Dev.*, vol. 5, no. 1, pp. 89–99, Jun. 2024, doi: 10.37253/jad.v5i1.9283.

[2] Badan Pusat Statistik, Statistik Perumahan dan Permukiman Tahun 2022. Jakarta, Indonesia: Badan Pusat Statistik, 2023.

[3] F. A. Sabitha, "Analisis Pengaruh Tingkat Urbanisasi terhadap Ketersediaan Lahan Lahan Permukiman Perumahan di Kota Surabaya," *J. Lemhannas RI*, vol. 10, no. 1, pp. 19–26, 2022, doi: 10.55960/jlri.v10i1.268.

[4] B. Bramantyo, W. P. Tyas, and A. Argyantoro, "Aspek Kualitas Rumah Subsidi pada Program Rumah Murah Berdasarkan Perspektif Penerima Manfaat (Studi Kasus: Perumahan Subsidi Mutiara Hati Semarang)," *J. Permukim.*, vol. 14, no. 1, p. 1, 2019, doi: 10.31815/jp.2019.14.1-9.

[5] A. A. Soewarno, "Kinerja Lingkungan Rumah Subsidi di Indonesia (Studi Kasus Perumahan Kaba Residence Kendari)," *J. Ilmu Tek.*, vol. 2, no. 1, 2024, [Online]. Available: https://jurnal.unusultra.ac.id/index.php/juitek/index

[6] T. W. Wardani, Syahara, W. Terkelin, S. S. Indira, and C. Nuraini, "Analisis Perbandingan antara

Perumahan Subsidi dengan Perumahan Green Building," *JAUR (Journal Archit. Urban. Res.*, vol. 8, no. 1, pp. 121–128, 2024, doi: 10.31289/jaur.v8i1.12572.

[7] N. D. Reztrie, "Kriteria penilaian bangunan hijau pada hunian vertikal menurut preferensi masyarakat 1 1," *J. Archit. Des. Dev.*, vol. 04, no. 02, pp. 157–166, 2023, doi: 10.37253/jad.v4i2.8576.

[8] Dewan Energi Nasional, *Outlook Energi Indonesia 2019*. Sekretariat Jenderal Dewan Energi Nasional, 2019. [Online]. Available: https://www.esdm.go.id/assets/media/content/content-outlook-energi-indonesia-2019-bahasa-indonesia.pdf

[9] R. Bahgat, R. M. Reffat, and S. L. Elkady, "Analyzing the impact of design configurations of urban features on reducing solar radiation," *J. Build. Eng.*, vol. 32, no. 101664, 2020, doi: 10.1016/j.jobe.2020.101664.

[10] M. González-Torres, L. Pérez-Lombard, J. F. Coronel, I. R. Maestre, and D. Yan, "A review on buildings energy information: Trends, end-uses, fuels and drivers," *Energy Reports*, vol. 8, pp. 626–637, 2022, doi: 10.1016/j.egyr.2021.11.280.

[11] F. G. Ciampi, A. Rega, T. M. L. Diallo, F. Pelella, J. Y. Choley, and S. Patalano, "Energy consumption prediction of industrial HVAC systems using Bayesian Networks," *Energy Build.*, vol. 309, no. February, p. 114039, 2024, doi: 10.1016/j.enbuild.2024.114039 Received.

[12] K. Liu, X. Xu, R. Zhang, L. Kong, W. Wang, and W. Deng, "Impact of Urban Form on Building Energy Consumption and Solar Energy Potential: A Case Study of Residential Blocks in Jianhu, China," *Energy Build.*, vol. 280, no. 112727, 2023, doi: 10.1016/j.enbuild.2022.112727.

[13] A. Ahmed, A. Khalid, B. Ahmed, and G. S. Mohsin, "Impact of Solar Radiation on Building Envelope Using Energyplus Software," in *Proceedings of International Mechanical Engineering Conference (SIMEC-2017).*, 2017, pp. 24–25.

[14] S. Taleb, A. Yeretzian, R. A. Jabr, and H. Hajj, "Optimization of building form to reduce incident solar radiation," *J. Build. Eng.*, vol. 28, p. 101025, Mar. 2020, doi: 10.1016/j.jobe.2019.101025.

[15] P. Wang, Z. Liu, and L. Zhang, "Sustainability of compact cities: A review of Inter-Building Effect on building energy and solar energy use," *Sustain. Cities Soc.*, vol. 72, no. April, p. 103035, 2021, doi: 10.1016/j.scs.2021.103035.

[16] R. Mufida, A. Safyan, S. Olivia, E. Fahrizal, and Y. Novianti, "Pengaruh Orientasi Bangunan terhadap Kenyamanan Termal, Studi Kasus: Komplek Perumahan Griya Putri Grand Panggoi II," *J. Arsit. Zo.*, vol. 5, no. 2, pp. 361–368, 2022, [Online]. Available: http://ejournal.upi.edu/index.php/jaz-

[17] KEPMENPUPR NOMOR 689/KPTS/M/2023, "Tentang Batasan Luas Tanah, Luas Lantai, dan Batasan Harga Jual Rumah Umum Tapak dalam Pelaksanaan Kredit/Pembiayaan Perumahan Fasilitas Likuiditas Pembiayaan Perumahan, serta Besaran Subsidi Bantuan Uang Muka Perumahan," *Peratur. Mentri PUPR*, 2023, [Online]. Available: https://pu.go.id/assets/media/722223172permenpupr-no-08-tahun-2018.pdf

[18] G. A. P. P. Kamase, T. Handayani, and Z. Gazalba, "Penyuluhan dan Percontohan Desain Pengembangan Rumah Subsidi yang Sehat dan Nyaman Bagi Penghuni," *J. Abdi Insa.*, vol. 9, no. 4, pp. 1354–1365, 2022.

[19] R. Y. Riskillah, S. Olivia, A. Atthaillah, S. Husain, and E. Saputra, "Analisa Kenyamanan Termal Adaptif pada Rumah Tinggal Tipe 36 di Perumahan Ketaping Residence Padang Pariaman," *J. Arsitekno*, vol. 8, no. 1, p. 17, 2021, doi: 10.29103/arj.v8i1.3643.

[20] D. P. Retno, D. Syamsunur, T. R. Putri, and K. Pekanbaru, "Analisis Keberlanjutan Kinerja Energi dan Air pada Perumahan Bersubsidi dengan Pendekatan Bangunan Hijau di Kota Pekanbaru," *SIKLUS*, vol. 10, no. 1, pp. 1–11, 2024.

[21] S. R. Wati and H. Muthmainah, "Faktor - Faktor yang Mempengaruhi Konsumen untuk Melakukan Pembelian Perumahan Subsidi di Sukoharjo," *J. Ekobis Dewantara*, vol. 4, no. 3, pp. 144–155, 2021.

[22] I. N. Mbake, M. Bahantwelu, and I. G. N. W. Hardy, "Atribut Faktor yang Mempengaruhi Keputusan Pembelian pada Perumahan Subsidi oleh Konsumen," *J. Gewang*, vol. 3, no. 2, pp. 61–67, 2021.

[23] A. Lestari and M. Z. Hasibuan, "Pengaruh Lokasi dan Kualitas Produk terhadap Keputusan Pembelian Perumahan Subsidi Mulia Garden (Studi Kasus Perumahan Subsidi Mulia Garden Desa Naga Rejo)," *J. Mutiara Manaj.*, vol. 6, no. 1, pp. 46–56, 2021.

[24] C. N. Octarino, "Kajian Dampak Pola Massa Bangunan terhadap Iklim Mikro di Area Permukiman," *Rustic J. Arsit.*, vol. 2, no. 1, pp. 1–9, 2022.

[25] Y. Sianturi and C. M. Simbolon, "Pengukuran dan Analisa Data Radiasi Matahari di Stasiun Klimatologi Muaro Jambi," *Megasains*, vol. 12, no.

1, pp. 40–47, Apr. 2021, doi: 10.46824/megasains.v12i1.45.

[26] S. V. Szokolay, Introduction to Architectural Science: The Basis of Sustainable Design. Oxford, U.K.: Elsevier, 2004.

[27] S. Shareef, "The Impact of Urban Morphology and Building's Height Diversity on Energy Consumption at Urban Scale. The Case Study of Dubai," *Build. Environ.*, vol. 194, p. 107675, 2021, doi: 10.1016/j.buildenv.2021.107675.

[28] S. Mirzabeigi and M. Razkenari, "Design optimization of urban typologies: A framework for evaluating building energy performance and outdoor thermal comfort," *Sustain. Cities Soc.*, vol. 76, p. 103515, 2022, doi: 10.1016/j.scs.2021.103515.

[29] J. Li, Y. Wang, and Y. Xia, "A novel geometric parameter to evaluate the effects of block form on solar radiation towards sustainable urban design," *Sustain. Cities Soc.*, vol. 84, p. 104001, 2022, doi: 10.1016/j.scs.2022.104001.

[30] W. Wang, K. Liu, M. Zhang, Y. Shen, R. Jing, and X. Xu, "From simulation to data-driven approach: A framework of integrating urban morphology to low-energy urban design," *Renew. Energy*, vol. 179, pp. 2016–2035, 2021, doi: 10.1016/j.renene.2021.08.024.

[31] E. Rostami, N. Nasrollahi, and J. Khodakarami, "A Comprehensive Study of How Urban Morphological Parameters Impact the Solar Potential, Energy Consumption and Daylight Autonomy in Canyons and Buildings," *Energy Build.*, vol. 305, p. 113904, 2024, doi: 10.1016/j.enbuild.2024.113904.

[32] A. A. Y. Freewan, "Energy-Efficient Solutions Depending on Building Forms Design with Tilted South and North Facades," *Buildings*, vol. 12, no. 753, 2022, doi: 10.3390/buildings12060753.

.

E-ISSN: 2528-388X
P-ISSN: 0213-762X

INERSIA
Vol.22, No.1, May 2026
.

Revitalizing Heritage Districts at Tasikmalaya Station: Integrating Respectful Facade Articulation and Architectural Business Strategies

Fajar Rezandi*, Cut Sannas Saskia, Maria Immaculata Ririk Winandari, Teungku Nelly Fatmawati, Nisrina Rahma Ningsih

Department of Architecture, Faculty Civil of Engineering and Planning, Universitas Trisakti, Jakarta 11440, Indonesia

Keywords:
Heritage Architecture,
Adaptive Reuse,
TOD,
Respectful Façade,
Architecture Business Strategy.

ABSTRACT

The development of heritage transit districts ideally integrates respectful facade articulation design, adaptive architectural practices that respect historical values, and sustainability-oriented business strategies. This approach enables the preservation of cultural identity while generating new economic value through adaptive reuse and strategic place branding. Tasikmalaya Station is a heritage building that functions as a key transportation hub in East Priangan. However, the surrounding district faces challenges, including the degradation of heritage functions, suboptimal connectivity, and a lack of cohesive business models integrated with cultural potential. Revitalizing heritage areas like Tasikmalaya Station often faces a dilemma between preserving historic facades and meeting the demands for modern design and functionality. When innovative design is not aligned with business strategy, interventions risk becoming unsustainable and losing socio-economic relevance. This study explores how respectful facade articulation design, adaptive architectural reuse, and business strategies can be integrated to realize a sustainable and strategically valuable heritage-based TOD area. The study employs a literature review approach, synthesizing open-access scholarly journals on adaptive facades, reuse strategies, and architecture-driven business models. The selected literature is contextually aligned with the Tasikmalaya Station masterplan. Three interrelated dimensions respectful facade articulations, adaptive reuse, and business strategies mutually reinforce each other in shaping productive and relevant heritage districts. Respectful facade enhances visual identity and building performance; adaptive architecture maintains cultural continuity and contemporary function; while business strategies support sustainability through community branding and alternative funding models.

1. Introduction

The revitalization of train station districts as transportation hubs and public spaces demands architectural approaches that not only preserve historical value but also respond to contemporary challenges such as energy efficiency, regional competitiveness, and user experience. Tasikmalaya Station (Figure 1) is a designated heritage building located in the city center, with historical significance as a hub for distribution and trade since the colonial era. However, with urban development, the surrounding area has experienced spatial degradation and lacks optimal integration with public transport, commercial zones, and city tourism destinations.

The main issue in developing this area is how to design architectural interventions on heritage buildings such as the station without eroding their historical character, and how design can serve as a tool to generate added economic and social value. Modernization efforts through Transit Oriented Development (TOD) and new commercial functions often spark conflict between preserving

*Corresponding author.
E-mail: fajar.rezandi@trisakti.ac.id

https://doi.org/10.21831/inersia.v21i2.90323
Received 8 October 2025; Revised 7 July 2026; Accepted 11 July 2026
Available online 17 July 2026

architectural authenticity and meeting the demands of adaptive, productive, and modern uses.

This study aims to explore the integration of respectful facade articulation design, adaptive architectural reuse, and business strategies within the context of heritage-based TOD development. The specific objectives are: (1) to identify the potential of heritage facades as part of district identity, (2) to evaluate adaptive reuse practices through innovative architectural approaches, and (3) to formulate business strategies that support the sustainability of heritage districts.

Previous studies have discussed relevant aspects: reviewed adaptive facade technology for energy efficiency [1]; proposed a reuse management model for historic train stations [2]; and introduced the concept of community branding for heritage development [3]. However, there remains a gap in studies that fully integrate these three dimensions within a single architectural practice, particularly in the context of Indonesia's heritage-based TOD projects. This study presents originality by constructing an integrative framework that connects respectful facade articulation, adaptive reuse, and business strategies within a single case-based investigation at Tasikmalaya Station. The findings are expected to contribute both conceptually and practically to the development of similar districts in Indonesia.

This research applies a systematic literature review method, focusing on reputable open-access journals relevant to the three domains: respectful facade articulation, adaptive reuse architecture, and architectural business strategy. The literature is analyzed thematically and contextualized with the design and planning framework of the Tasikmalaya Station masterplan. The study is limited to the conceptual and strategic dimensions of architectural design and management. Technical aspects such as structural reinforcement and detailed cost analysis are not discussed. The analytical focus is on conceptual planning and urban design strategies. The significance of this research lies in its provision of an integrative conceptual model that can serve as a reference for architects, urban planners, and stakeholders in developing sustainable, adaptive, and economically viable heritage districts.

In designing a strategic area such as Tasikmalaya Station which serves both as a transportation hub and a heritage building architectural approaches are required to go beyond functionality and aesthetics. They must also be innovative, adaptive, and economically viable. The revitalization of this area demands the integration of three key domains: respectful facade articulation design to enhance building performance and visual identity; adaptive architectural practices that address the challenges of conservation and new functions; and architectural business strategies that ensure the sustainability of design implementation [1][3][4].

Figure 1. Area of PT. KAI land asset in Tasikmalaya Station

Tasikmalaya station will adapt the neoclassical architectural style of the second variant, third series [5]. This variant is found in the architectural style of station buildings during the construction period between 1875 and 1890. Tasikmalaya Station comes with the characteristics of the third series, stations from this variant are characterized by the use of large metal sheets to cover the emplacements built at the beginning of the station's establishment (Figure 2). Stations that fall into this category feature a regular geometric arrangement to emphasize a uniform design. The axis in the center of the facade shows the symmetry of the design. Adapting the roof to tropical conditions is not optimal. The roof slope is quite gentle with only a few eaves (extended roof). Columns, as the main structural element, become an aesthetic element of the building.

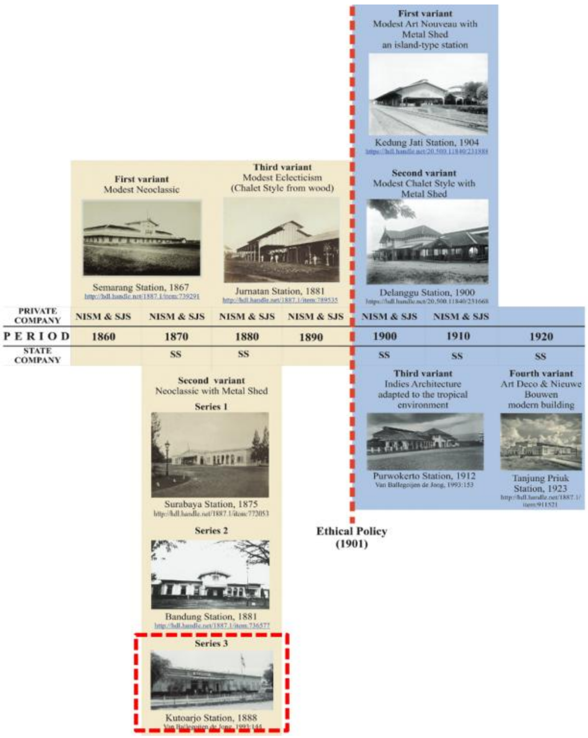

(a) Architectural Style Analysis of Tasikmalaya Station

(b) Elements of Neoclassical Architecture of Tasikmalaya Station

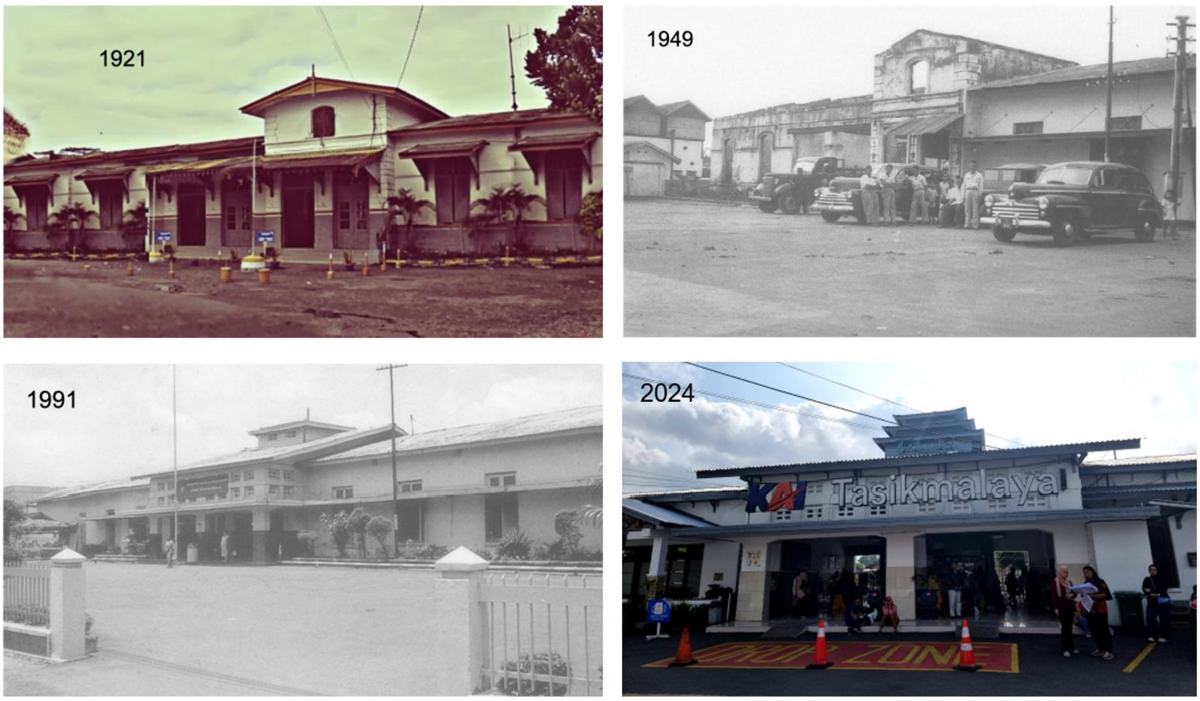

(c) Façade development of Tasikmalaya Station

Figure 2. Architectural Historical Analysis of Tasikmalaya Station

Figure 2 shows relation between architectural elements (2b), indicates the Architectural Style timeline (2a) and the development of the station façade through the years (2c). [5].

Facades serve not only as protective envelopes for buildings but also as mediums of cultural expression, architectural identity, and environmental performance. In the context of heritage buildings, respectful facade articulation must balance preservation with modernization, particularly in climates that demand responsiveness and energy efficiency. In a comprehensive review on adaptive facades, emphasize that facade systems can be designed to respond dynamically to external environmental changes, enabling energy efficiency and thermal comfort without compromising heritage aesthetics [1]. These systems may include kinetic elements, smart materials, and passive design integration. Similarly, traditional architecture already embodies local climate-responsive wisdom through thick walls, natural ventilation, and shaded overhangs [6]. This highlights that heritage facades can be sources of design innovation when reinterpreted sensitively. Furthermore, the role of new materials such as nano-coatings, self-cleaning surfaces, and energy-efficient glazing in conserving and enhancing the performance of historic buildings [7]. These technologies allow heritage buildings to be upgraded without damaging their cultural value. A study on colonial era residences in Bandung demonstrates that facade transformations in response to new functions do not necessarily erode heritage value [8]. On the contrary, preserving and showcasing the original facade elements can add commercial and symbolic value to revitalized buildings. While previous studies have examined façade performance at the building scale [9], limited research has explored how façade innovation can be integrated with heritage conservation and district-scale economic revitalization strategies. This study addresses that gap by examining façade innovation as part of a broader heritage-led urban regeneration framework.

Adaptive reuse is a design strategy that transforms heritage buildings to accommodate contemporary functions while maintaining their architectural integrity. It is increasingly employed in post-industrial and post-colonial contexts to revitalize obsolete but historically valuable structures. Exploration on reuse strategies in public heritage buildings across Asia and Europe, emphasizing that successful interventions are often supported by policy frameworks, design creativity, and stakeholder collaboration [10][11][12][13].

A study also shows sustainable management model for reusing disused railway stations, where balancing architectural preservation and socio-economic activation is crucial [2]. This aligns directly with the case of Tasikmalaya Station, where the original train depot and heritage facilities offer potential for commercial and cultural reuse.

A study on historic Jeddah presents an evaluation model that assesses adaptive reuse based on visual harmony, functional compatibility, and social relevance [14]. Such frameworks are particularly helpful in ensuring that the revitalization of heritage structures like those in Tasikmalaya does not result in architectural or cultural dissonance. Several success factors in adaptive reuse: technical adaptability, early expert involvement, community participation, and flexible financing [15]. These elements ensure that reuse projects are not only feasible but also supported by stakeholders, particularly in heritage-rich yet economically vulnerable urban areas.

The revitalization of heritage areas cannot rely solely on design interventions. Economic models, branding strategies, and stakeholder engagement are essential in ensuring long-term sustainability [13]. In context to local area, vernacular architecture contributes to city branding in Indonesia, demonstrating that heritage identity can strengthen tourism and small business ecosystems when aligned with inclusive governance [16]. A proposal suggests a shift from “place branding” to “community branding,” where identity is co-produced with residents and local enterprises [3]. Their model suggests that cultural heritage gains value not only from its physical attributes but also from its meaning and use within the community. An argument states that conventional business models are often incompatible with heritage projects. Instead, they recommend circular economy approaches, hybrid ownership schemes, and cross-subsidized financing [17]. These models support the economic viability of adaptive reuse while respecting conservation needs. Finally, a local case from Bandung where a colonial coffee house was transformed into a commercially successful café through adaptive reuse [18]. This transformation retained the building’s original architectural elements while integrating modern functions, showing that business and conservation can be mutually reinforcing.

In the context of the Tasikmalaya Station Masterplan, the three elements respectful facade articulation design, adaptive reuse practices, and business strategies are found to be interconnected. Facade innovation is employed to establish the area's visual identity and regulate local climatic performance [1][7]. Adaptive architectural practices are realized through the reuse of existing buildings for new functions aligned with TOD principles

[2]. Meanwhile, community-based business strategies position the area as both an economic catalyst and a symbol of local identity [3][4]. Vernacular settlements provide the foundation for city identity, which can be transformed into city branding through creative tourism and cultural activation programs [19][20]. The authors propose that heritage environments contribute unique visual, historical, and cultural characteristics that differentiate a city from competing destinations. Consequently, preservation efforts should be integrated with tourism development, place-making, and branding strategies to maximize both cultural and economic benefits. This holistic approach transforms a heritage district from a static historical relic into a dynamic ecosystem that unites cultural preservation, transportation connectivity, and economic vitality. Thus, the development of areas like Tasikmalaya Station can serve as a model of sustainable architectural practice that is locally grounded and globally progressive.

2. Methods

This research employs a qualitative, case-based methodology to explore how respectful facade articulation design, adaptive reuse strategies, and architectural business models are integrated into the revitalization of a heritage-based transit-oriented development (TOD) area. The study is descriptive in nature, combining theoretical insights from peer-reviewed literature with practical analysis of the Tasikmalaya Station Masterplan. The chosen case study Tasikmalaya Station in West Java, Indonesia serves as a relevant context due to its dual status as a transportation hub and cultural heritage site. Several of the buildings within the area, including the main station, old warehouse, station master's house, and auxiliary structures, have been officially designated as Cultural Heritage or Potential Cultural Heritage Objects (Cagar Budaya or ODCB). Data were collected through a combination of document analysis, spatial interpretation, and literature review. Primary design data were sourced from architectural drawings, zoning maps, and strategic planning documents related to the Tasikmalaya Station Masterplan. These were supplemented by secondary sources such as site photographs and spatial documentation. In parallel, an in-depth literature review was conducted using open-access academic databases (e.g., MDPI, SpringerOpen, SAGE Open) to identify scholarly studies published between 2015 and 2024. The literature review [21] focused on three key domains relevant to the study: respectful facade articulation, adaptive reuse of heritage buildings, and architectural business strategy. The research focuses on three analytical variables: (1) respectful facade articulation, assessed through the application of passive design techniques, materials, and visual coherence in the design of both old and new structures; (2) adaptive reuse, evaluated by examining how heritage buildings are programmatically and physically transformed while retaining their historical integrity; and (3) architectural business strategies, analyzed in terms of spatial programming, stakeholder engagement, and long-term economic sustainability. These variables were used as a framework for evaluating the design intentions and implementation strategies found in the masterplan [22]. Analysis was carried out using a thematic interpretation method [23], in which the theoretical concepts from the literature were used to interpret and assess the spatial, architectural, and economic interventions outlined in the masterplan. This interpretive process allowed for the identification of alignments, innovations, and gaps between the theoretical frameworks and the practical solutions applied in the case of Tasikmalaya Station. Ultimately, the method reveals how the intersection of respectful facade articulation, adaptive reuse, and business strategy supports a holistic and sustainable approach to heritage district revitalization.

3. Results and Discussion

Tasikmalaya Station is a historically significant railway facility in West Java, originally constructed during the Dutch colonial period. As part of the Java railway corridor, it served not only as a transportation hub but also as a catalyst for urban formation and economic activity in the region. Its architectural characteristics arched fenestrations, high-pitched roofing, symmetrical facades, and thick masonry walls are emblematic of tropical colonial railway typologies (Figure 3). Today, despite being preserved as a heritage building, its functional and spatial integration with the city has deteriorated due to urban sprawl, inadequate infrastructure, and disconnection from emerging economic activities. The Tasikmalaya Station Masterplan proposes a comprehensive spatial restructuring strategy that aims to re-establish the station as a Transit Oriented Development (TOD) node while preserving its heritage value. This strategy positions the station area as an intermodal hub, a civic landmark, and an economic district all within a walkable urban framework.

Figure 3. Tasikmalaya Station in 1949

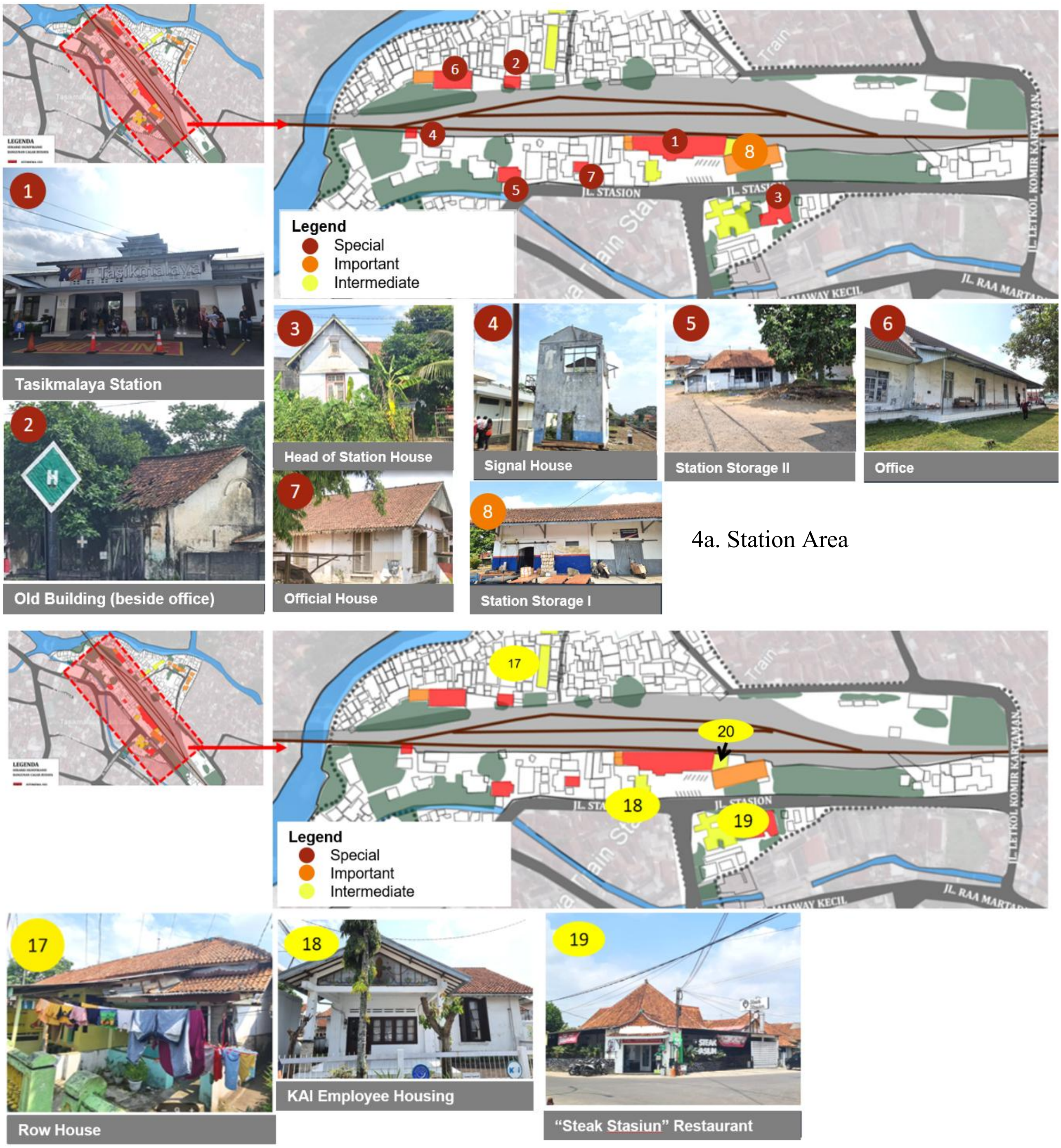

Figure 4a. Identification of Cultural Heritage (Cagar Budaya) or Potential Cultural Heritage Objects (ODCB)

Figure 5b. Identification of Cultural Heritage (Cagar Budaya) or Potential Cultural Heritage Objects (ODCB)

The analysis data in Figure 4a, 4b, and 4c indicates that the main station building, along with several supporting elements such as the old warehouse, the station master's house, and staff housing, possess significant historical value and have been classified as Cultural Heritage (Cagar Budaya) or Potential Cultural Heritage Objects (ODCB). On the other hand, analysis in Figure 5 shows that the area faces challenges such as limited pedestrian infrastructure, lack of integration with public transportation modes, and the overlapping circulation of logistics vehicles and passenger traffic. Therefore, a strategic approach to accessibility and circulation design is needed - one that is not only efficient but also inclusive.

Therefore, a strategic approach to accessibility and circulation design is needed—one that is not only efficient but also inclusive. Based on the site analysis, the proposed revitalization strategies were systematically classified according to the three analytical variables established in the research methodology. The first variable concerns respectful façade articulation, which examines how façade interventions can preserve the historical identity of heritage buildings while enhancing environmental performance. As shown in Table 1, each heritage asset is assigned a façade strategy code (F1–F7) that corresponds to its architectural characteristics, proposed intervention, supporting theoretical framework, and expected design outcome.

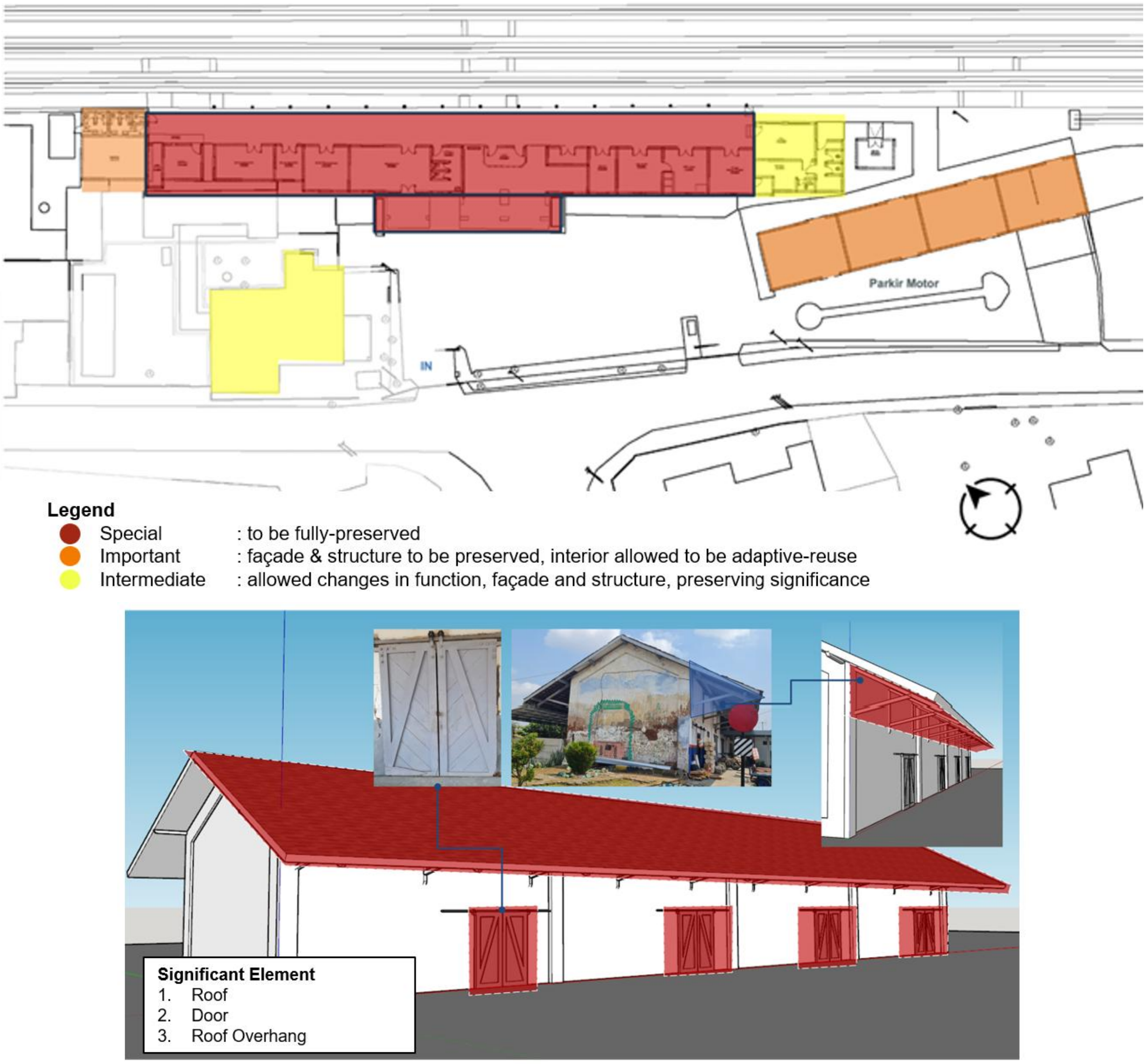

4c Significant Area of Tasikmalaya Station Building

Figure 6c. Identification of Cultural Heritage (Cagar Budaya) or Potential Cultural Heritage Objects (ODCB)

Table 1. Respectful Façade Articulation Strategies

Building	Code	Design Intervention	Supporting Theory	Expected Outcome
Main Station Building	F1	Preserve façade composition; introduce passive shading and climate-responsive envelope	[1]; [9]; [6]	Enhanced thermal performance while preserving heritage identity
Old Warehouse	F2	Retain industrial façade, brickwork and roof profile	[8]; [7]	Industrial heritage character retained
Station Master's House	F3	Restore original façade details and materials	[6]	Historical authenticity strengthened
Railway Office	F4	Upgrade envelope while maintaining façade rhythm	[1]	Improved building performance
Staff Housing	F5	Minimal façade intervention preserving vernacular identity	[8]	Living heritage preserved
New TOD Building	F6	Contemporary façade respecting heritage proportions	[1]	Visual continuity
Public Plaza	F7	Landscape articulation reinforcing heritage image	[3]	Improved place identity

Table 2. Adaptive Reuse Strategies

Building	Code	Design Intervention	Supporting Theory	Expected Outcome
Main Station Building	A1	Modernize passenger facilities while retaining railway function	[2]; [14]	Operational sustainability
Old Warehouse	A2	Creative hub, gallery and café	[2]; [12]	Economic activation
Station Master's House	A3	Museum / interpretation centre	[14]	Heritage education
Railway Office	A4	Library and mobility centre	[15]	Public service enhancement
Staff Housing	A5	Workshop / homestay	[12]; [15]	Community empowerment
Public Plaza	A6	Flexible civic programming	[3]	Public activation

As summarized in Table 1, the proposed façade articulation strategies (F1–F7) are designed according to the architectural significance and conservation requirements of each heritage asset. These interventions play a dual role in the revitalization of Tasikmalaya Station, functioning both as symbolic expressions of local identity and as adaptive responses to environmental performance. For the existing heritage building, the masterplan emphasizes restoration and visual amplification of key architectural details, such as ornamental cornices, arched windows, and ventilated roof eaves. At the same time, subtle insertions of passive design elements such as double-skin facades, high-performance glass, and overhang shading devices are proposed to improve thermal regulation [1][7]. Newly designed buildings in the TOD precinct are not generic insertions but reinterpretations of the colonial design language. They reflect the vertical rhythm, material warmth (e.g., clay bricks, wood, and natural stone), and tropical responsiveness of the heritage context. These respectful facade articulations not only ensure climatic responsiveness in a hot-humid environment but also establish architectural coherence across different building generations. Through this strategy, facade design becomes a storytelling device that reinforces cultural memory and place identity.

As presented in Table 2, adaptive reuse strategies (A1–A6) transform heritage buildings into productive urban assets through carefully selected functions that respond to both community needs and TOD principles. (Figure 6). For instance, the old freight warehouse is reimagined as a creative economy incubator, offering co-working spaces, cultural galleries, and artisan cafés. Meanwhile, the station's administrative wing is repurposed into a mobility information center and public library. These interventions are based on flexible internal layouts, sensitive retrofitting, and zoning that balances access, preservation, and safety.

The adaptive reuse process respects the original spatial hierarchy and circulation flows, while allowing for new programmatic overlays that enhance the station's civic relevance [2][13]. Importantly, the reuse strategy ensures that heritage buildings remain active contributors to contemporary urban life. By aligning architectural integrity with socio-economic functions, the masterplan avoids the risks of either fossilizing heritage or eroding its authenticity.

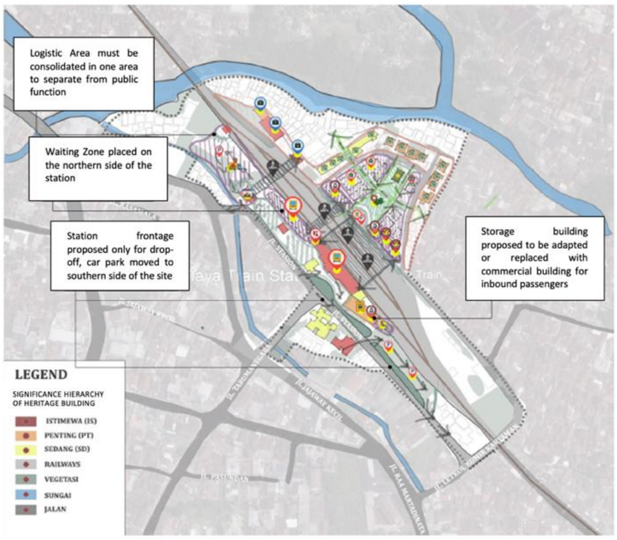

Figure 7. Urban and Heritage Context Analysis

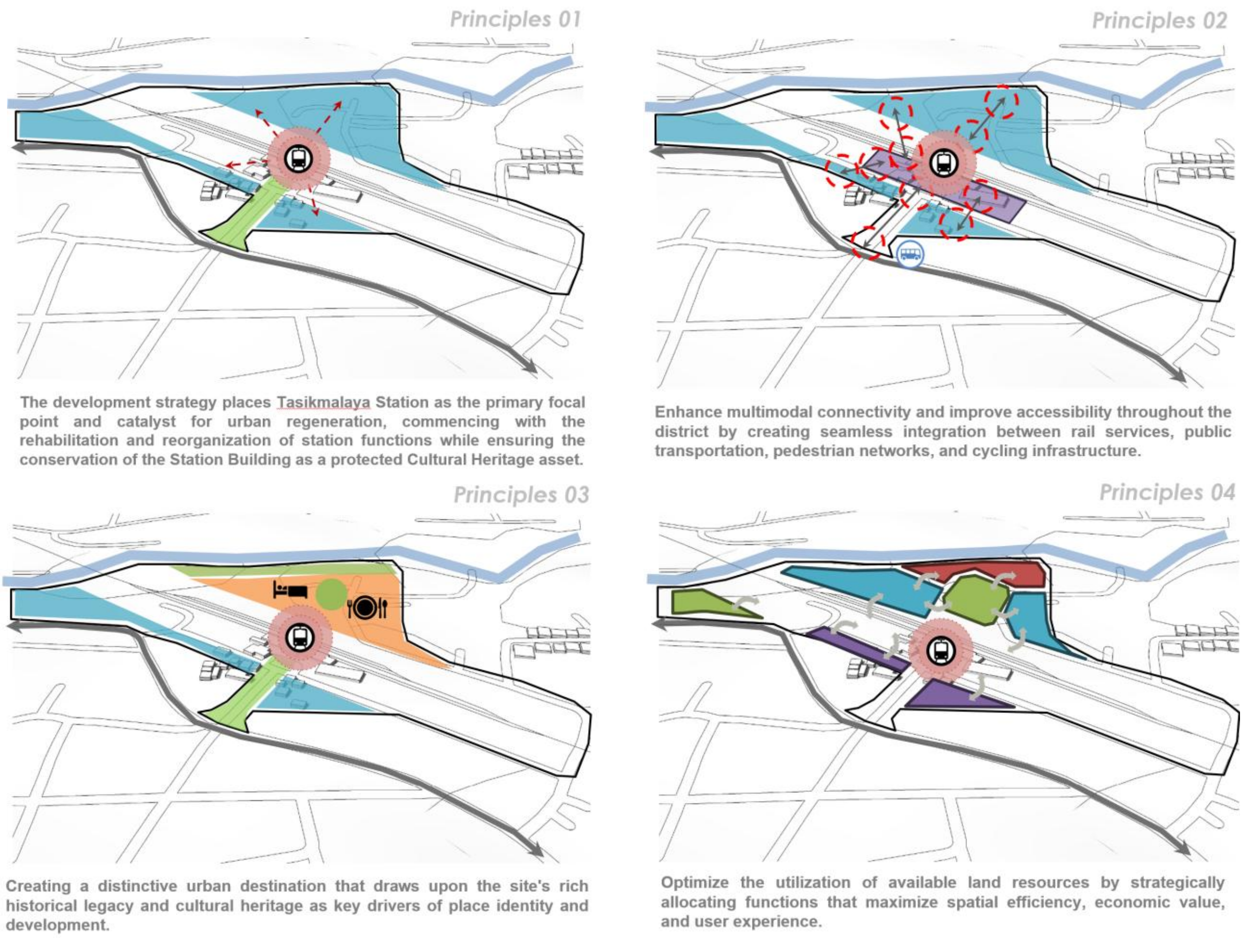

Figure 6. Masterplan Design Principles

Physical revitalization alone cannot ensure the long-term sustainability of heritage districts. Consequently, the third analytical variable examines architectural business strategies, which connect architectural interventions with economic activation, community participation, and destination branding. As presented in Table 3, each heritage asset is associated with a business strategy code (B1–B7) that identifies its value creation mechanism and target beneficiaries. The business strategies summarized in the table complement the physical design interventions by ensuring that each revitalized heritage asset contributes to the economic, social, and cultural sustainability of the district. The masterplan's long-term viability hinges on a robust architectural business strategy that incorporates both financial and social sustainability (Figure 7). This includes multi-stakeholder financing models, phased development, and asset management plans that prioritize adaptive reuse. Key to this strategy is a community-driven branding process, wherein the station's heritage value is actively promoted as part of a local identity narrative [3].

Table 3. Architectural Business and Value-Creation Strategies

Building	Code	Design Intervention	Supporting Theory	Expected Outcome
Main Station Building	B1	Heritage branding and destination gateway	[20]; [3]	Destination image and tourism revenue
Old Warehouse	B2	Creative economy incubator	[19]; [13]	SME growth and entrepreneurship
Station Master's House	B3	Museum-based tourism	[20]	Educational tourism
Railway Office	B4	Knowledge-based public services	[13]	Knowledge economy
Staff Housing	B5	Community enterprise	[3]	Local value creation
New TOD Building	B6	Mixed-use commercial development	[17]	Financial sustainability
Public Plaza	B7	Festivals and cultural activation	[20]; [3]	Place branding and social vitality

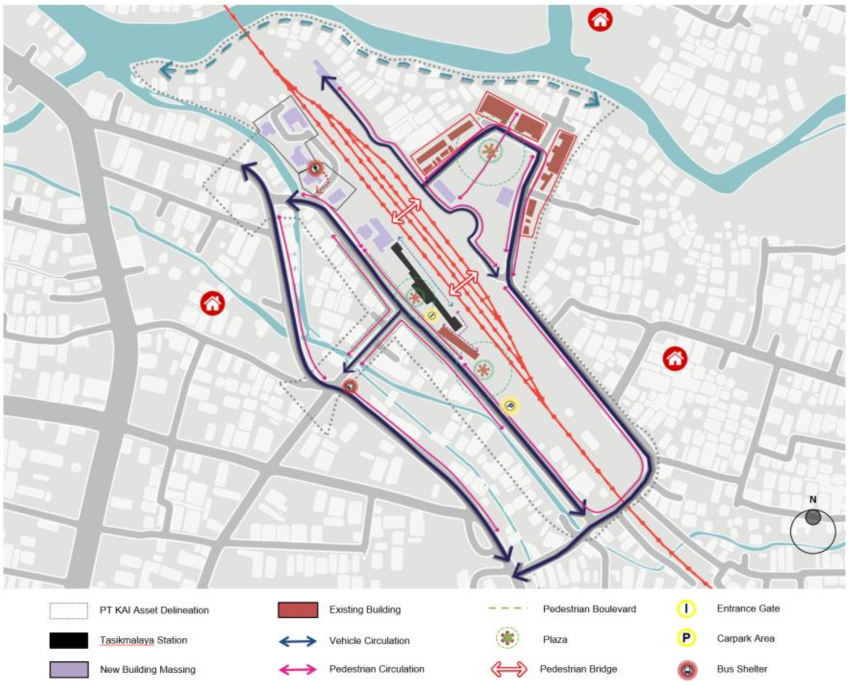

Figure 7. Urban Design Framework

(a) (b)

Figure 8. Pedestrian Accessibility (a) and Green Open Space Framework (b)

(a) (b)

Figure 9. New Building Zoning (a) & New Development Framework (b).

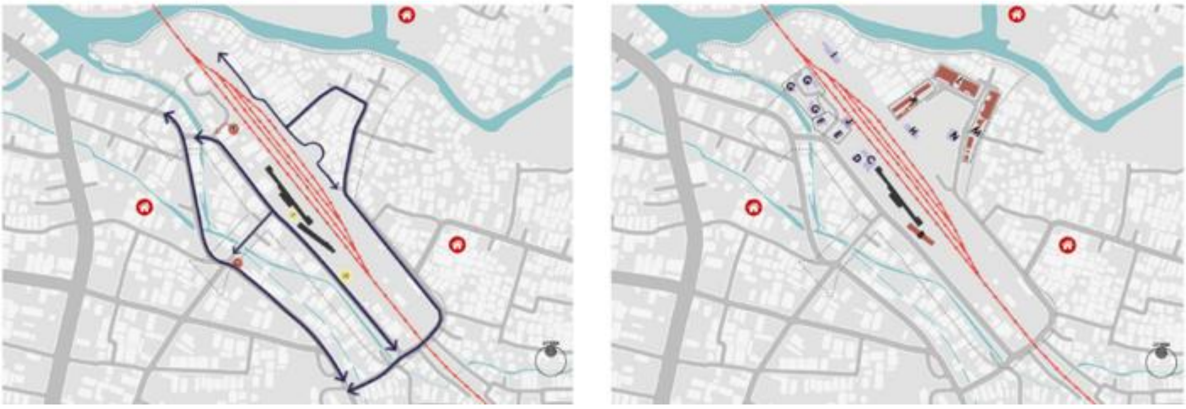

(a) (b)

Figure 8. Vehicle Accessibility (a) & Building Massing Framework (b).

Commercial spaces in heritage buildings are allocated to local SMEs and curated pop-up tenants that align with the station's cultural theme. Events such as heritage festivals, maker markets, and railway history tours are designed to activate the public realm while generating income.

These activities contribute not only to financial sustainability but also to the social reproduction of place, fostering a sense of ownership among residents and visitors alike. Furthermore, the business strategy integrates circular economy principles (Figure 8, Figure 9, Figure 10). Maintenance, material recycling, and lifecycle-based planning are embedded into the adaptive reuse framework. This approach enables long-term value creation, even as programmatic needs evolve [4].

The three analytical matrices presented in Table 1 to Table 3 demonstrate that the proposed revitalization is not based on isolated architectural interventions but on an integrated strategy in which façade articulation, adaptive reuse, and architectural business approaches are mutually reinforcing. Each heritage asset therefore combines physical conservation, functional adaptation, and economic activation to maximize its contribution to the overall development of the heritage district. The synthesis of the three analytical variables—respectful façade articulation, adaptive reuse, and architectural business strategy—constitutes the defining characteristic of the Tasikmalaya Station Masterplan. Rather than functioning independently, these interventions operate as an integrated framework in which façade enhancement strengthens heritage identity, adaptive reuse maintains functional relevance, and business strategies ensure long-term economic sustainability. This integrated approach transforms the heritage district from a passive historical asset into an active urban ecosystem capable of balancing conservation, mobility, and economic development. Each domain reinforces the other in a mutually supportive system: (1) Facade articulation enhances climatic performance and elevates the visual brand of the area, aligning heritage values with contemporary urban identity. (2) Adaptive reuse ensures functional resilience while preserving cultural and architectural continuity. (3) Business strategy secures long-term project sustainability, embedding community participation and economic regeneration into the design logic. This triadic integration transforms the heritage district from a passive historical asset into an active, living system that mediates between conservation and change. Tasikmalaya Station, in this framework, becomes a prototype for the revitalization of heritage-based TODs in Indonesia demonstrating how design can reconcile historical preservation with environmental stewardship and economic viability.

Figure 11 presents the proposed revitalization of the main station building and its extension, designed to harmonize modern functionality with the heritage character of the original structure. The new facade reflects the proportions, materials, and rhythmic openings of the historic building while introducing contemporary steel structural elements to signify modernization. The layout integrates key zones, including the ticket hall, waiting areas, passenger platforms, and a public terrace cafe, creating a seamless spatial sequence that enhances user comfort and circulation. The site plan emphasizes the connection between the heritage core, new extensions, green spaces, and supporting transport infrastructure, reinforcing the station's role as both a mobility hub and a culturally significant public space.

Legend:
A. Drop-off Area
B. Ticketing Area & Administration
C. Waiting Area
D. Tenant
E. ATM Center
F. PPKA Room
G. Director's Office
H. Staff Room
I. VIP Room
J. Nursery Room
K. Hall & Entrance Lobby
L. Toilet
M. Musholla (Prayer Room)
N. Intermodal
O. Generator Room
P. Parking Area
Q. Police Post
R. Extension Corridor

Figure 11. Proposed Revitalization of the Station: Main Station Building and Extension buildings with New Facade corresponds to heritage building.

Legend:
A. Drop-off Area
B. Ticketing Area & Administration
C. Waiting Area
D. Tenant
E. ATM Center
F. PPKA Room
G. Director's Office
H. Staff Room
I. VIP Room
J. Nursery Room
K. Hall & Entrance Lobby
L. Toilet
M. Musholla (Prayer Room)
N. Intermodal
O. Generator Room
P. Parking Area
Q. Police Post
R. Extension Corridor

Figure 12. Proposed Revitalization of the Station: Integration of Outdoor Space responding to TOD principles, pedestrian plaza and connectivity.

Figure 12 presents the proposed revitalization of the station area, emphasizing the integration of outdoor spaces that respond to Transit-Oriented Development (TOD) principles. The design introduces a pedestrian-friendly plaza that enhances accessibility and visual connectivity between the station building, surrounding public areas, and adjacent urban fabric. Open spaces are structured to support both circulation and social interaction, incorporating shaded walkways, green buffers, and gathering nodes that promote comfort and safety for users. The spatial arrangement also ensures seamless transitions between transport modes pedestrian, shuttle, and private vehicles while maintaining the historical context of the site. This approach reinforces the station's role as a multimodal hub and an inclusive public realm that encourages walkability and sustainable urban mobility.

Figure 13. Proposed Revitalization of the Station: Integration of heritage building facade with new extension building respectful facade articulation (ticketing on the left side, new small-micro enterprise on the right side).

(a) (b)

Figure 14. Proposed Facade Articulation for ticketing (a) and new small-micro enterprise (b).

Figure 13 presents the proposed revitalization of the station, emphasizing the integration of the heritage building facade with the new extension through a respectful and context-sensitive architectural articulation. The design maintains the symmetry and rhythm of the original colonial structure, ensuring visual continuity while introducing subtle contemporary interventions. The left side of the building accommodates the ticketing area, directly linked to the main circulation and waiting spaces, whereas the right side introduces new facilities for small and micro enterprises (SMEs), supporting local economic activities [19]. This balanced composition between preservation and adaptation strengthens the historical identity of the station while enhancing its functional capacity and inclusivity as a community-oriented transport hub.

Figure 14 presents the proposed facade articulation illustrating the integration between the ticketing area on the left and the new small–micro enterprise (SME) zone on the right. The design approach emphasizes harmony between the restored heritage elements and contemporary additions through the use of consistent material palettes, modular proportions, and rhythmic shading devices. The ticketing facade adopts subtle reinterpretations of the historical building's features, while the SME section introduces transparent and open frontages to encourage community interaction and commercial visibility. This balanced articulation not only respects the historical context of the station but also enhances its role as a dynamic and inclusive public interface. The proposed façade enhancement strategy should not be limited to preserving historical appearance but should also improve environmental performance. Façade characteristics have a measurable impact on energy efficiency and daylighting quality [9]. Therefore, the introduction of passive shading devices, climate-responsive openings, and high-performance glazing in the Tasikmalaya Station precinct could improve thermal comfort and natural lighting while preserving the heritage identity of the station buildings.

4. Conclusions

Revitalizing heritage areas based on Transit Oriented Development, as exemplified by the Tasikmalaya Station Masterplan, demands a holistic and integrative architectural approach. This study demonstrates that the success of such projects greatly depends on the synergy between respectful facade articulation design, adaptive reuse of buildings, and contextual, sustainable business strategies. Innovative facade design has been proven to strengthen the visual identity of the area while enhancing building performance in response to local climate conditions without compromising historical value. Adaptive reuse practices offer functional solutions for maintaining the usability of heritage buildings within the context of modern demands. Meanwhile, community-branding-based business strategies generate both economic and social value, extending the economic life of the district and reinforcing the cultural connection between communities and their environment. The findings support a study which identifies a strong relationship between heritage environments, city identity, city branding, and creative tourism [20]. The station complex, together with its historic warehouses, official residences, and supporting railway buildings, constitutes a distinctive heritage landscape capable of reinforcing the identity of Tasikmalaya. Through adaptive reuse interventions and public-space activation, these assets can be transformed into cultural attractions that strengthen the city's image while simultaneously generating economic opportunities.

Overall, these findings highlight the importance of an integrative approach in developing heritage areas. Physical preservation alone is not sufficient; spatial activation and community engagement are equally essential to transforming such districts into vibrant, relevant, and competitive urban destinations. This study offers both conceptual and practical contributions to the planning of other heritage areas and provides a foundation for developing design policies and management strategies for historic districts in Indonesia.

References

[1] Y. Zhang, W. Tian, L. Wang, T. Xu, and H. Song, "Adaptive facades: Review of designs, performance evaluation, and control systems," *Buildings*, vol. 12, no. 9, Art. no. 1442, 2022, doi: 10.3390/buildings 12091442.

[2] G. Bianchi and S. De Medici, "A sustainable adaptive reuse management model for disused railway cultural heritage to boost local and regional competitiveness," *Sustainability*, vol. 15, no. 10, Art. no. 8014, 2023, doi: 10.3390/su15108014.

[3] M. Cerreta, P. De Toro, and R. Papa, "From place-branding to community-branding: A collaborative decision-making process for cultural heritage enhancement," *Sustainability*, vol. 12, no. 15, Art. no. 6052, 2020, doi: 10.3390/su12156052.

[4] I. Vellecco and A. Martone, "Business models for cultural heritage adaptive reuse," in *Adaptive Reuse of Cultural Heritage*, F. Murru, Ed. Cham, Switzerland: Springer, pp. 185–202, 2024, doi: 10.1007/978-3-031-48682-5_10.

[5] H. Sulistyani, "The evolution of railway station architecture in Java," *J. Asian Archit. Build. Eng.*, pp. 1–9, 2023, doi: 10.1080/13467581.2023.1549961.

[6] V. Sanagustín-Fons, L. Herrera, and A. Vázquez, "Cultural heritage architecture and climate adaptation: A socio-environmental analysis of sustainable building techniques," *Land*, vol. 12, no. 3, Art. no. 654, 2023, doi: 10.3390/land12030654.

[7] F. Doni, G. Gazzaniga, and P. Mazzola, "Recent developments in materials science for the conservation and restoration of historic artifacts," *Appl. Sci.*, vol. 14, no. 1, Art. no. 219, 2024, doi: 10.3390/app14010219.

[8] M. A. Fadhlurrohman and S. Soewarno, "Perubahan elemen fasad bangunan cagar budaya eks kolonial," *J. Arsit. Itenas*, vol. 10, no. 2, pp. 103–113, 2022, doi: 10.26760/jati.10.2.2022.103-113.

[9] R. F. Madina, S. Tundono, F. Rezandi, A. P. Umara, and M. L. Nurrohman, "Correlation of facade characteristics on energy and daylighting performance optimization of office building (Case Study: Satrio Tower, Jakarta)," *Vitruvian*, vol. 14, no. 3, 2024, doi: 10.22441/vitruvian.2024.v14i3.003.

[10] M. Shi and X. Huang, "Reuse of public heritage buildings: Analysis of the successful practices and identification of the obstacle," *Open J. Soc. Sci.*, vol. 13, no. 1, 2025, doi: 10.4236/jss.2025.131020.

[11] X. Liu, X. Xiao, C. Tian, H. Li, and G. Zhu, "Multi-criteria decision-making in the adaptive reuse of historic buildings: A bibliometric and systematic review of practices in China," *J. Asian Archit. Build. Eng.*, pp. 1–26, 2025, doi: 10.1080/13467581.2025.2587384.

[12] B. Triratma, "Adaptive reused heritage building based

on sustainable development: A review," *ARTEKS: J. Tek. Arsit.*, vol. 8, no. 3, pp. 537–548, 2023, doi: 10.30822/arteks.v8i3.2635.

[13] E. Sulistyowati, M. Isa, and R. Fuadah, "Digital transformation and competitive advantage in architectural creative economy: A qualitative perspective," *Value Added: Maj. Ekon. dan Bisnis*, vol. 22, no. 1, 2026, doi: 10.26714/vameb.v22i1.20718.

[14] A. S. Alhojaly, O. Al-Hafith, and M. S. Alrubaih, "A proposed model of assessing the adaptive reuse of heritage buildings in Historic Jeddah," *Buildings*, vol. 12, no. 4, Art. no. 524, 2022, doi: 10.3390/buildings12040524.

[15] A. Savoie, R. Veilleux, and A. Gagnon, "Key factors for revitalising heritage buildings through adaptive reuse," *Buildings Cities*, vol. 4, no. 1, pp. 127–147, 2023, doi: 10.5334/bc.229.

[16] E. Nursanty, M. F. D. Husni, D. Rusmiatmoko, and W. Destiawan, "Balancing heritage preservation and city branding: Prospects and strategies for vernacular architecture in Indonesia," *ISVS e-J.*, vol. 10, no. 6, pp. 225–243, 2023.

[17] I. Vellecco and A. Martone, "Business models for cultural heritage adaptive reuse," in *Adaptive Reuse of Cultural Heritage*. Cham, Switzerland: Springer, 2024, doi: 10.1007/978-3-031-67628-4_17.

[18] S. M. K. Sajid, A. A. Yuwono, and A. Josephine, "Adaptive reuse of Antico Coffee heritage building in Bandung," *Serat Rupa J. Des.*, vol. 8, no. 2, 2024, doi: 10.28932/srjd.v8i2.7752.

[19] A. Gravagnuolo, "Heritage-led entrepreneurial ecosystems: Skills and role of social entrepreneurship for circular cultural heritage adaptive reuse," in *Adaptive Reuse of Cultural Heritage*. Cham, Switzerland: Springer, 2024, doi: 10.1007/978-3-031-67628-4_21.

[20] K. Kasemsarn, A. Sawadsri, and A. Kritsanaphan, "Employing creative tourism to produce city branding derived from vernacular settlements: A review," *ISVS e-J.*, vol. 11, no. 6, pp. 119–141, 2024.

[21] H. Snyder, "Literature review as a research methodology: An overview and guidelines," *J. Bus. Res.*, 2019, doi: 10.1016/j.jbusres.2019.07.039.

[22] B. Van Laar, A. Greco, H. Remøy, and V. Gruis, "What matters when?—An integrative literature review on decision criteria in different stages of the adaptive reuse process," *Developments Built Environ.*, 2024, doi: 10.1016/j.dibe.2024.100439.

[23] D. Byrne, "A worked example of Braun and Clarke's approach to reflexive thematic analysis," *Qual. Quant.*, vol. 56, pp. 1391–1412, 2021, doi: 10.1007/s11135-021-01182-y.

E-ISSN: 2528-388X
P-ISSN: 0213-762X

INERSIA
Vol.22, No. 01, May, 2026

Long-Term Rainfall Variability and Seasonal Shifts in Relation to Pranatamangsa in the Rongkop Karst Region, Indonesia

Qonaah Rizqi Fajriani*, Suwartanti Nayono, Satoto Endar Nayono, and Didik Purwantoro

Department of Civil Engineering and Planning, Faculty of Engineering, Universitas Negeri Yogyakarta, Yogyakarta 55281, Indonesia

Keywords:
Rainfall variability;
Seasonal onset;
Extreme precipitation;
Karst region;
Pranatamangsa

ABSTRACT

Climate change has altered rainfall characteristics and seasonal patterns. This matter affects mostly rainfed agricultural systems in karst regions. This study aims to analyze rainfall characteristics, extreme rainfall events, seasonal shifts, and the reliability of traditional seasonal knowledge *(pranata mangsa)* in the Rongkop karst area, Indonesia. The dataset used in this study are long-term daily rainfall data from Rongkop stations for the period 1986–2021. The rainfall data then convert to *dasarian* (10-day) temporal resolution. The daily rainfall was classified into intensity categories, while seasonal onset was determined based on rainfall thresholds. Trend analysis was conducted using the Mann–Kendall test and Sen's slope estimator. The results indicate that Rongkop has moderate annual rainfall, with an average of 2012 mm, and no significant trend in total rainfall. However, there is a significant increase in the frequency of heavy rainfall events (>50 mm/day), indicating a shift towards higher rainfall intensity. Seasonal analysis shows variability in the onset of the rainy season between late August and late December, and the dry season between early February and mid-May. Seasonal duration also varies significantly, with extended dry spells and increased rainfall during the dry season. The results indicate increasing inconsistencies between traditional and observed rainfall patterns, with very high rainfall occurring during the dry season and very low rainfall during the wet season. The onset of the wet and dry seasons also exhibits significant variability beyond the expected seasonal boundaries. These findings suggest that although traditional seasonal forecasts (*pranatamangsa*) still reflect general climate patterns, their reliability for agricultural planning has declined due to increasing rainfall variability, extreme events, and large-scale climate phenomena such as El Niño and La Niña, particularly in rainfed karst areas. Therefore, integrating traditional seasonal knowledge with modern climatological analysis is crucial to support adaptive agricultural management, particularly in karst areas.

1. Introduction

Climate change has become a major global issue that affect various environmental and socio-economic sectors. The Key indicators are include increasing average temperatures, sea level rise, extreme rainfall characteristics change, and long dry seasons. The agricultural sector had impacted from these changes, spesifically in tropical regions [1]–[3]. According to the World Meteorological Organization (WMO) [4], in 2015–2020 period was recorded as the six hottest years on record. Rising temperatures increase crop water requirements, while long dry seasons reduce the water availability [5]–[7]. Furthermore, the uncertainty about the onset of the rainy season make crop planning more complicated and reduces agricultural productivity.

Climate change also threatens global food security. The Food and Agriculture Organization (FAO) reports that approximately 25% of economic losses in developing countries are caused by climate-related disasters, such as droughts, floods, and storms [8]. One common form of adaptation by farmers is selecting crop varieties that are more tolerant to climate variability [9].

Regionally, the impact of climate change is increasingly severe on vulnerable ecosystems, such as karst areas. Gunungkidul Regency is characterized by karst geological formations composed of highly permeable limestone and underground channel systems [10]. Annual rainfall in this region ranges from 1,000–3,500 mm and is heavily influenced by large-scale climate phenomena such as El Niño [11]. Due to the characteristics of the karst system,

*Corresponding author.
E-mail: rizqifajriani@uny.ac.id

https://doi.org/10.21831/inersia.v21i2.95431
Received 27 January 2026; Revised 7 August 2026; Accepted 8 August 2026
Available online 12 August 2026

rainwater rapidly infiltrates into subsurface channels, limiting surface water availability. Consequently, agricultural activities in this region are highly dependent on rainfall.

Among the sub-districts in Gunungkidul Regency, Rongkop is one of the most vulnerable to severe agricultural droughts. Most agricultural land in this sub-district is rain-fed dryland, leaving farmers entirely dependent on seasonal rainfall due to the lack of irrigation facilities. Cassava is the main agricultural commodity cultivated in the region. However, farmers often experience significant losses due to the uncertainty of the onset of the rainy season. When rain falls later than expected or rainfall patterns become irregular, cassava tubers remain in the soil for longer periods, increasing the risk of rotting and reducing yields and quality.Farmers in Gunungkidul are dominated by the older generation. This generation cultivates according to the Javanese calendar, *Pranatamangsa*. *Pranatamangsa* is a traditional Javanese agricultural calendar system based on the solar cycle (*suryasengkala*), which divides the 365- or 366-day year into 12 periods *(mangsa)* with day lengths varying between 23 and 43 days. The twelve mangsa are *kasa* (first), *karo* (second), *katelu* (third), *kapat* (fourth), *kalima* (fifth), *kanem* (sixth), *kapitu* (seventh), *kawolu* (eighth), *kasanga* (ninth), *kasadasa* (tenth), *dhesta* (eleventh), and *sadha* (twelfth). Each mangsa has its own *candra* character or natural symbol based on bioclimatological signs, such as plant and animal behavior, wind direction, and specific constellations for navigation of seasonal changes. This calendar was historically inaugurated by Sri Susuhunan Paku Buwana VII of Surakarta on June 22, 1855 to provide a strong benchmark for regulating the work of farmers from year to year.

For Javanese farmers, the twelve seasons are grouped into four main time units that align with changes in planting time, namely the dry season or *mangsa katiga* (*mangsa kasa, karo, katelu*), *musim labuh* or the transitional rainy season (*mangsa kapat, kalima, kanem*), *mangsa rendheng* or the rainy season (*mangsa kapitu, kawolu, kasanga*), and *musim mareng* or the transitional dry season (*mangsa kasadasa, dhesta, sadha*). In addition to these four main seasons, farmers also recognize groupings based on transitional seasons that affect their living conditions as presented in Figure 1, namely the *mangsa terang* as the period between harvest and famine (*sadha and kasa*), the *mangsa semplah* which is interpreted as a season of hardship or despair (*karo, katelu, kapat, and kalima*), *mangsa udan* which is flanked by *semplah* and *pengarep-arep*, and *magsa pengarep-arep* as a time full of hope when animals and plants begin to reproduce (*kawolu, kasanga, kasadasa, and dhesta*). Through this periodic distribution, Javanese farmers were able to plan their lives wisely, such as learning to manage their finances and be frugal during difficult times and rejoice when welcoming a bountiful rice harvest. [12][13][14].

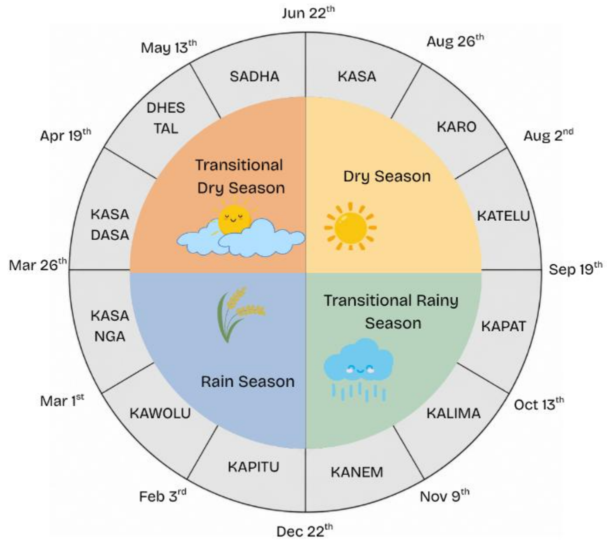

Figure 1. Pranatamangsa calendar [15]

This Prantamangsa were historically used to guide agricultural practices. However, climate change has significantly altered seasonal patterns. This shift has led to increased uncertainty in planting schedules, severe water scarcity during prolonged dry seasons, and escalating risks of total crop failure.

Despite numerous studies on rainfall variability and climate change in Gunungkidul, several critical gaps remain. Previous research in this karst region has mostly focused on regional-scale analysis, leaving a gap in localized studies. To date, there has been no specific, long-term rainfall analysis conducted specifically for the Rongkop karst area, despite its status as a drought-prone agricultural hub. Furthermore, existing literature is still limited by insufficient long-term observational data [16]. Most studies rely on monthly or annual rainfall. Dasarian temporal analysis, which is vital for precise agricultural planning, remains unexplored in this area. Additionally, the response of karst hydrological systems to extreme rainfall events under changing climate conditions is still poorly understood [17].

To address these gaps, this study aims to analyze rainfall characteristics, extreme rainfall events, and seasonal shifts specifically in the Rongkop karst area. By utilizing long-term, high-resolution rainfall data (1986–2021) at a dasarian temporal scale, this study provides the first localized climate analysis for Rongkop. The findings of this research are expected to serve as a crucial scientific foundation for local farmers to adjust their planting calendars and for policymakers to design targeted drought mitigation and climate adaptation strategies in water-scarce karst environments.

2. Methods

2.1 Study Area

This research was conducted in Rongkop District. Administratively, Rongkop District has 8 parts, namely: 1) Pucanganom; 2) Karangwuni; 3) Pringombo; 4) Semugih; 5) Petir; 6) Botodayakan; 7) Bohol; 8) Melikan. Agriculture in this area is strongly influenced by the geographical characteristics of the karst region (limestone hills) which have unique hydrological challenges. Rongkop is at an altitude of 100–300 meters above sea level with morphology in the form of conical hills, domes, valleys, and caves, but does not have underground rivers [13]. The usual planting calendar in one of the Districts in Rongkop (Karangwuni) presented in Table 1.

Table 1. Planting Calendar Estimation in Karangwuni, Rongkop [13]

Ward	Month											
	Wet					Dry			Lean		Wet	
Karangwuni	1	2	3	4	5	6	7	8	9	10	11	12
	Rice or corn					Intercropping: Corn, Cassava/Soybeans			Empty land/ Lean season			Rice or corn

According to Table 1, the wet season begins in late November. During this wet season in Karangwuni, Rongkop, farmers cultivate corn or rice. The dry season begins in June, and farmers plant less water-demanding field crops, such as corn or cassava.

2.2 Datasets

The daily rainfall data records covering the 1986–2021 period, with observations available for 27 years. These data obtained from the Department of Agriculture and Food of Gunungkidul Regency. The rainfall station location is in Rongkop to represent the study area (see Figure 2). The historical dataset originally dates back to 1952; however, the 1986–2021 period was specifically selected due to its superior data consistency and completeness.

Regarding data quality control, any missing data points within the observation period were left blank and strictly excluded from the statistical analysis to prevent artificial bias in trend detection. For temporal analysis, the daily rainfall records were aggregated into a dasarian resolution (10-day intervals), resulting in exactly three periods per calendar month (Dasarian I, II, and III). This high-resolution temporal framework allows for a more precise assessment of rainfall variability and seasonal transitions compared to standard monthly aggregations.

2.3 Rainfall Characteristics Analysis

Rainfall characteristics were analyzed based on daily rainfall data and classified into four categories as Light rainfall (<20 mm/day); Moderate rainfall (20–50 mm/day); Heavy rainfall (50–100 mm/day); and Very heavy rainfall (>100 mm/day). The frequency and percentage of each rainfall category were calculated annually to identify changes in rainfall patterns over time. In addition, the occurrence of heavy rainfall events (>50 mm/day) was analyzed to evaluate extreme rainfall behavior.

2.4 Seasonal Analysis (Onset of Rainy and Dry Seasons)

Seasonal analysis was performed using dasarian rainfall data to determine the onset of the rainy season (Awal Musim Hujan, AMH) and dry season (Awal Musim Kemarau, AMK). The criteria used in this study are defined as the onset of rainy season (AMH) occurs when rainfall exceeds 50 mm per dasarian for two consecutive periods and the onset of dry season (AMK) occurs when rainfall is less than 50 mm per dasarian for two consecutive periods. This method allows for a more detailed identification of seasonal transitions compared to monthly approaches, particularly in regions with high rainfall variability.

2.5 Analysis of Seasonal Variability

The variability of seasonal onset and duration was analyzed by examining the timing of AMH and AMK for each year. The duration of rainy and dry seasons was calculated based on the interval between onset and termination of each season.

Changes in seasonal patterns were evaluated to identify shifts in timing, duration, and variability of rainfall seasons, particularly in relation to climate variability.

2.6 Trend Analysis

Trend analysis was conducted to detect long-term changes in rainfall characteristics using the non-parametric Mann-Kendall test. This method is widely used for identifying monotonic trends in hydroclimatic time series without requiring normal data distribution.

The magnitude of the trend was estimated using Sen’s slope estimator, which calculates the rate of change over time. Positive slope values indicate increasing trends, while negative values indicate decreasing trends.

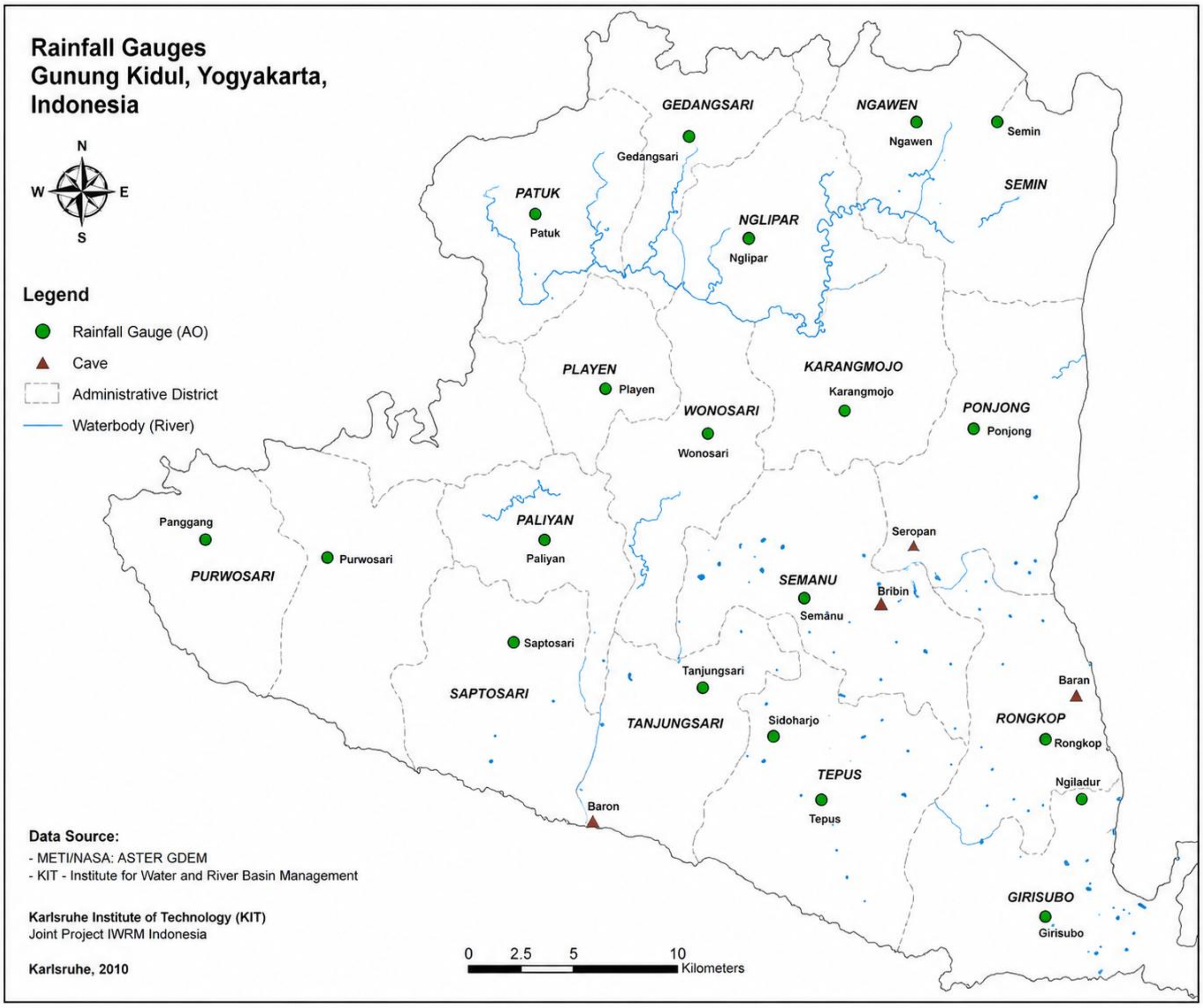

Figure 2. Distribution of rainfall stations in Gunungkidul Regency.

3. Results and Discussion

3.1 Rainfall Characteristics

The analysis of daily rainfall data in the Rongkop karst area shows that rainfall events are predominantly classified as light rainfall (<20 mm/day), followed by moderate rainfall (20–50 mm/day), heavy rainfall (50–100 mm/day), and very heavy rainfall (>100 mm/day).

The proportion of light rainfall dominates the annual rainfall distribution, indicating that most rainfall events occur at low intensity. However, an increasing tendency in the frequency of heavy and very heavy rainfall events is observed, particularly in the period after 2010. This suggests a shift in rainfall characteristics from low-intensity to high-intensity events.

Such changes in rainfall characteristics are important in karst regions, where rapid infiltration reduces surface water availability. Increasing rainfall intensity may enhance subsurface flow while also increasing the risk of soil erosion and land degradation.

3.2 Annual Rainfall Variability

The analysis of annual rainfall from 1986 to 2021 shows that the study area generally falls into the moderate rainfall category, with an average annual rainfall of approximately 2012 mm (Figure 3). Interannual variability is clearly observed, with several years classified as dry (e.g., 1997 and 2019) and wet (e.g., 2016 and 2021).

Trend analysis using the Mann-Kendall test indicates a positive trend in annual rainfall with Kendall's tau value of 0.088. However, the trend is not statistically significant at the 95% confidence level (p-value = 0.535). The magnitude of change estimated using Sen's slope is 5.48 mm/year, indicating a slight increase in annual rainfall over time.

This result suggests that total rainfall volume has not changed significantly, and rainfall variability in the study area is more influenced by interannual climate variability rather than long-term trends. Extreme dry years are associated with El Niño events, while wet years are linked to La Niña conditions, which influence rainfall patterns in Indonesia.

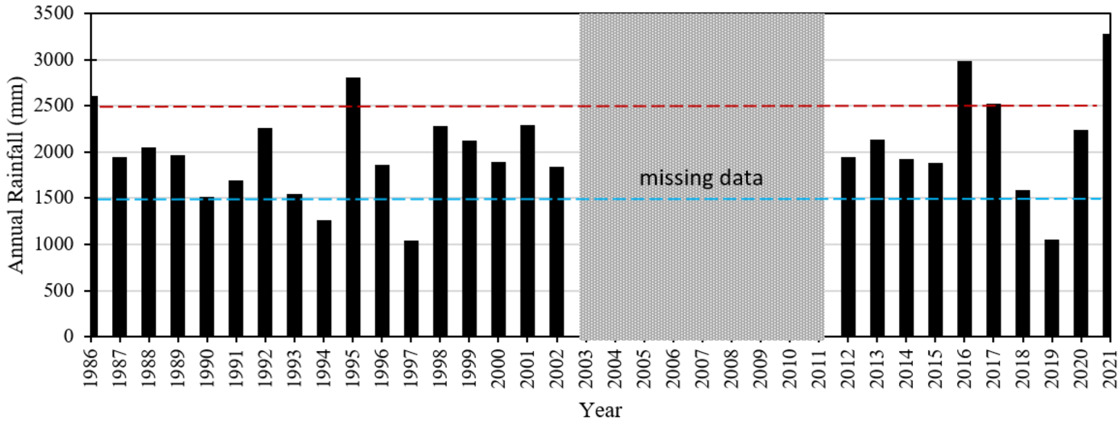

Figure 3. Annual rainfall

3.3 Trend of Extreme Rainfall Events

In contrast to annual rainfall, the analysis of heavy rainfall events (>50 mm/day) shows a significant increasing trend (Figure 4).

Based on the Mann-Kendall trend test, there is a statistically significant upward trend in the time series. This is supported by a calculated Kendall's tau of 0.465 and a positive statistic value. Because the computed two-tailed p-value of 0.001 is well below the 5% significance level, the null hypothesis of no trend is rejected in favor of the alternative hypothesis. Furthermore, Sen's slope estimator indicates a positive rate of change with a slope value of 0.200 (95% confidence interval: 0.083 to 0.308), confirming a steady, significant increase in the data over the analyzed period.

This finding highlights a shift in rainfall distribution, where total rainfall remains relatively stable, but rainfall intensity increases. Such a pattern is consistent with global climate change projections, which indicate an increase in extreme precipitation events rather than total rainfall volume.

In karst regions, increased rainfall intensity may lead to rapid infiltration into underground systems, reducing surface water availability while simultaneously increasing the risk of flash flooding and soil erosion in certain conditions.

Figure 5 indicates the dominance of low-intensity rainfall, with a gradual increase in the contribution of higher-intensity rainfall events over time.

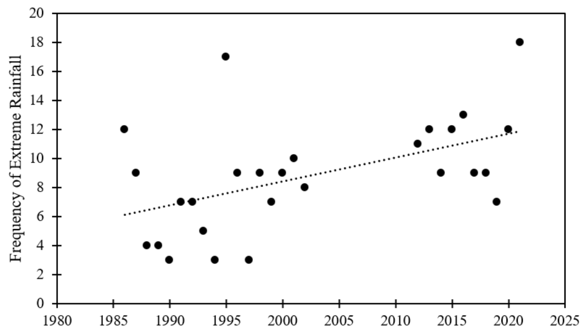

Figure 4. Annual number of extreme rainfall events (>50 mm/day) in the study area, showing an increasing trend over time.

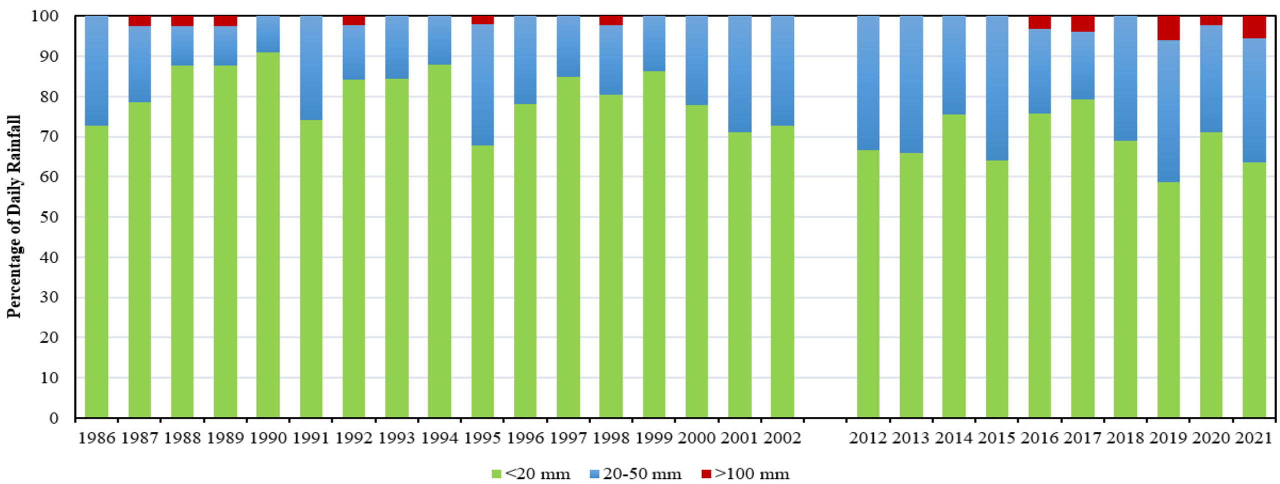

Figure 5. Percentage distribution of daily rainfall intensity (<20 mm, 20–50 mm, and >100 mm) in the Rongkop karst area from 1986 to 2021.

3.4 Monthly Rainfall Pattern

The average monthly rainfall pattern shows a clear seasonal distribution, with peak rainfall occurring in January and February, while the lowest rainfall occurs in July, August, and September (Figure 6). This pattern reflects the typical monsoonal climate of Southern Java.

However, variability in monthly rainfall is observed across years, indicating changes in seasonal distribution. In some years, rainfall occurs outside the typical rainy season, suggesting increasing irregularity in rainfall patterns.

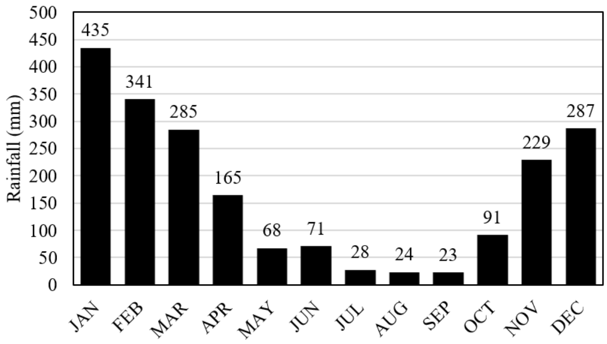

Figure 6. Monthly Rainfall Pattern

3.5 Seasonal Shift (Onset of Rainy and Dry Seasons)

The analysis of dasarian rainfall data reveals significant variability in the onset of rainy and dry seasons. The rainy season in the Rongkop karst area begins as early as the third ten-day period (dasarian) of August and as late as the third dasarian of December. Meanwhile, the dry season starts between the first dasarian of February and the second dasarian of May.

The duration of the dry season averages 212 days, while the rainy season lasts approximately 151 days. The longest dry seasons were recorded in 1997, 2013, and 2019, which are associated with El Niño events.

These results indicate that seasonal patterns are becoming increasingly irregular, which poses challenges for agricultural planning. Farmers who rely on traditional seasonal calendars such as *pranata mangsa* may face difficulties in adapting to these changes.

3.6 Implications for Karst Agriculture and Climate Variability

The findings of this study demonstrate that climate change impacts in the study area are not primarily reflected in changes in total rainfall, but rather in the increasing intensity and variability of rainfall events.

The significant increase in heavy rainfall events, combined with shifting seasonal patterns, may lead to increased hydrometeorological risks, including soil erosion, crop failure, and water management challenges. In karst regions, where water rapidly infiltrates into subsurface systems, these changes can exacerbate water scarcity during dry periods despite increased rainfall intensity.

These findings are consistent with previous studies indicating that climate change tends to increase rainfall variability and extreme events rather than total rainfall. Therefore, adaptation strategies in karst agricultural systems should focus on improving water management, adjusting planting calendars, and enhancing resilience to climate variability.

3.7 The Reability of Pranatamangsa

The accuracy of the Pranatamangsa is assessed by the stability of the rainfall amount during each mangsa period. Rainfall dynamics within the Pranatamangsa framework exhibit highly structured hydro-meteorological fluctuations, with shifting patterns that follow the apparent solar cycle and the monsoon wind system. Based on historical data for the 1986–2021 period, monthly and seasonal rainfall quantities divide 12 *mangsa* into four main groups that have a strong correlation with the cumulative rainfall thresholds of low (<100 mm/ mangsa), medium (100–300 mm/ mangsa), and high (>300 mm/ mangsa).

***Mangsa Katiga* (dry season)**

The dry season was identified in *Mongso Kasa*, *Karo*, and *Katelu*. Rainfall during this period is shown in Figure 7. The Dry Season is consistently in the Very Low rainfall category, with an average cumulative accumulation of only 75.3 mm. The dynamics of air and soil humidity dropped sharply starting from *Kasa* (41.3 mm) to reaching the driest point in *Karo* (16.5 mm) and *Katelu* (17.5 mm), where all three were well below the low threshold of 100 mm. This characteristic forces the agricultural sector to shift from high water deficit crops to secondary crops or leave the land in a fallow state to break the pest cycle. Although generally dry, this group has sharp anomalous dynamics, both in the form of wet dry phenomena and absolute drought. In years with a negative Indian Ocean dipole or coastal La Niña, such as 1986, 1992, and 2016, wet anomalies occurred with dry accumulations reaching 241–266 mm, *Katelu* alone contributed 249 mm of rain. Conversely, in 1991, 1994, 1997, 2012, 2015, 2018, and 2019, extreme dry anomalies occurred with accumulations of 0 mm for three consecutive years, triggering prolonged droughts and irrigation water crises.

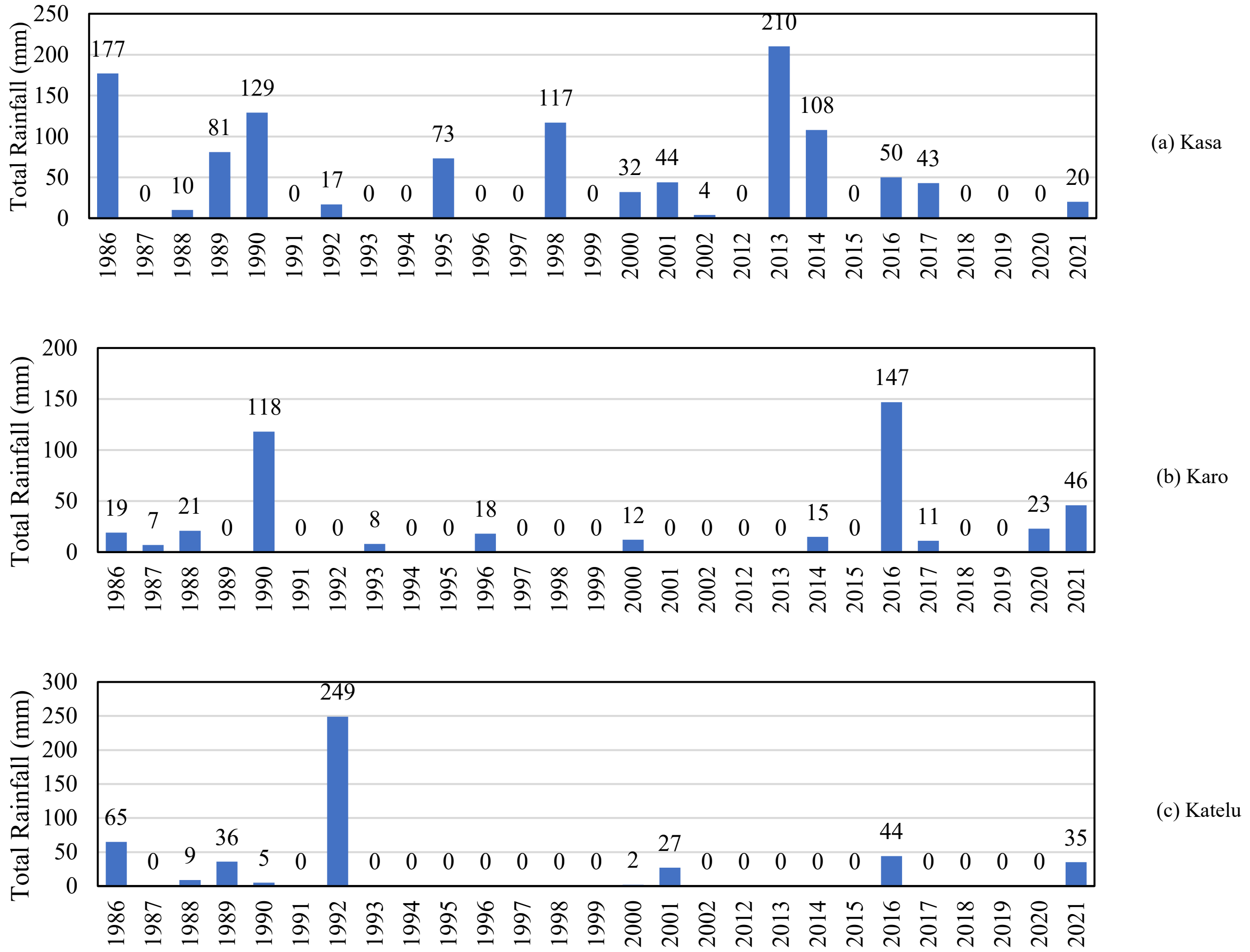

Figure 7. Total rainfall in *Mongso Ketigo* from 1986 to 2021

***Musim Labuh* (Transitional Rainy Season)**

Musim Labuh is identified by the *Kapat*, *Kalima*, and *Kanem*. Cumulative rainfall in these monsoons is shown in Figure 8.

Musim Labuh represents a transitional phase with high rainfall accumulation, a cumulative average of 517.9 mm, which increases from month to month. The dynamics begin with *Kapat* (34.2 mm), which falls into the Low category. Next, *Kalima* (112.1 mm) shifts to the Moderate category, marking the start of land cultivation, and culminates with *Kanem* (371.6 mm), which jumps to the High category, signaling the end of the transition period and the official start of the rainy season. Anomalies in this transitional group are crucial for the accuracy of the early-season planting schedule. In 2017 and 2021, very wet transitional anomalies occurred with cumulative totals reaching 1,145–1,177 mm. In 2021, *Kanem* recorded an extreme rainfall of 902 mm. On the other hand, due to the impact of strong El Niño in 1997 and 2019, this transition period experienced a failed transition with accumulated rainfall reaching only 36–40 mm, which caused a delay in the national simultaneous planting schedule.

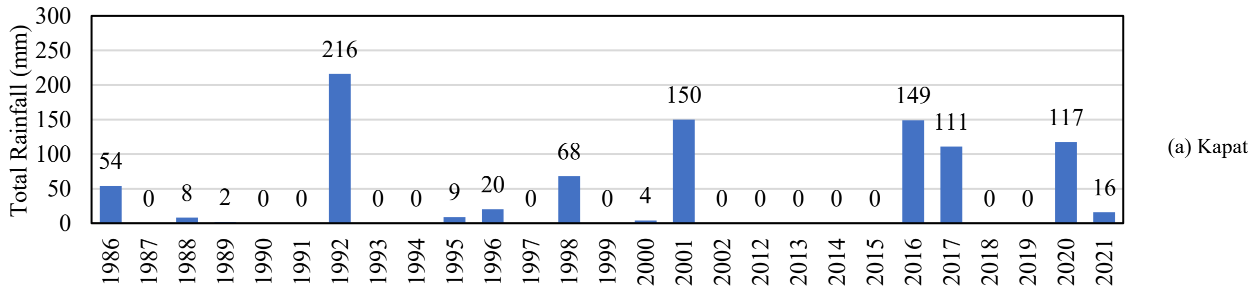

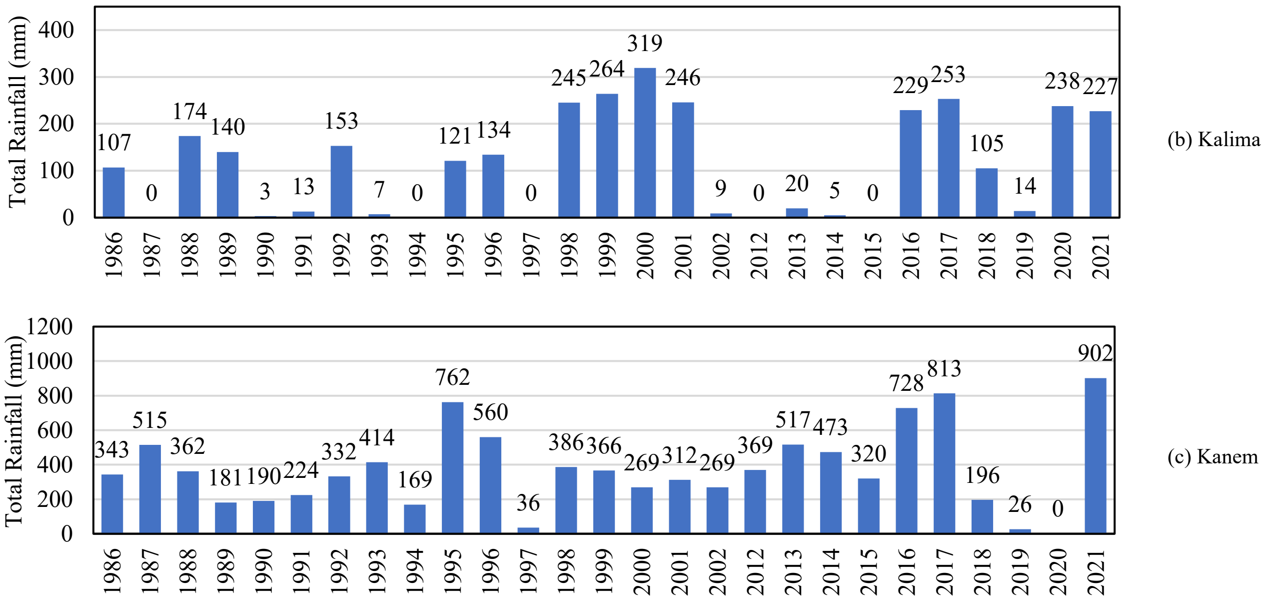

Figure 8. Total rainfall in *Mongso Ketigo* from 1986 to 2021

Mangsa rendheng (Rainy Season)

Mangsa rendheng was identified in the *Kapitu*, *Kawolu*, and *Kasanga* season. Rainfall in these period is shown in Figure 9.

Mangsa rendheng is characterized by a dominant Very High water accumulation, with a cumulative average reaching 1,073.9 mm per season. Rainfall dynamics during this period test land resilience due to the gradual, massive water supply, starting with the highest peak in *Kapitu* (average 528.7 mm), which is categorized as High, then gradually decreasing in *Kawolu* (314.9 mm) and *Kasanga* (230.3 mm), which are categorized as Medium. This excess water supply provides the main foundation for the rice planting phase (long-term drought), but also poses the risk of inundation and flooding in areas with poor catchment areas. These results are consistent with previous research which showed that Mangsa Kapitu was the period with the highest rainfall [18]. The anomaly in this mangsa is markedly contrasting due to the influence of global climate interactions such as La Niña and El Niño. In 2020, an extreme wet anomaly occurred with total seasonal rainfall reaching 1,700 mm, while *Kasanga*, which usually begins to subside, actually surged to 503 mm due to the strong La Niña phenomenon. Conversely, during El Niño events in 1997 and 2013, accumulated seasonal rainfall experienced a significant deficit, reaching a low of around 692–694 mm, drastically reducing water supplies during the vegetative growth period of rice plants.

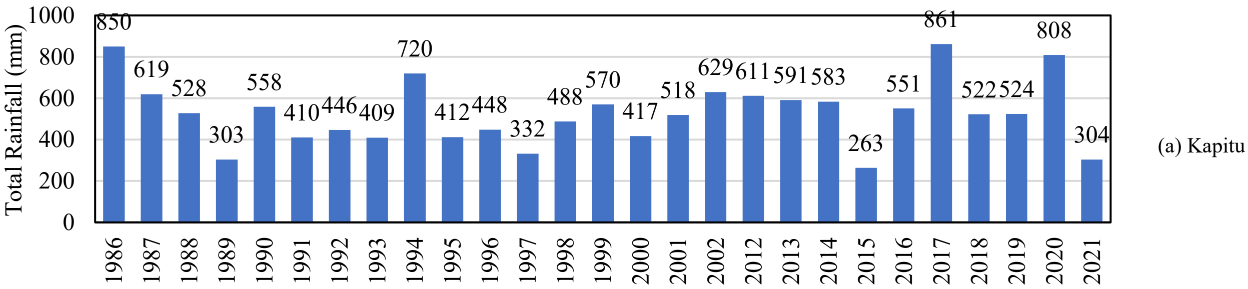

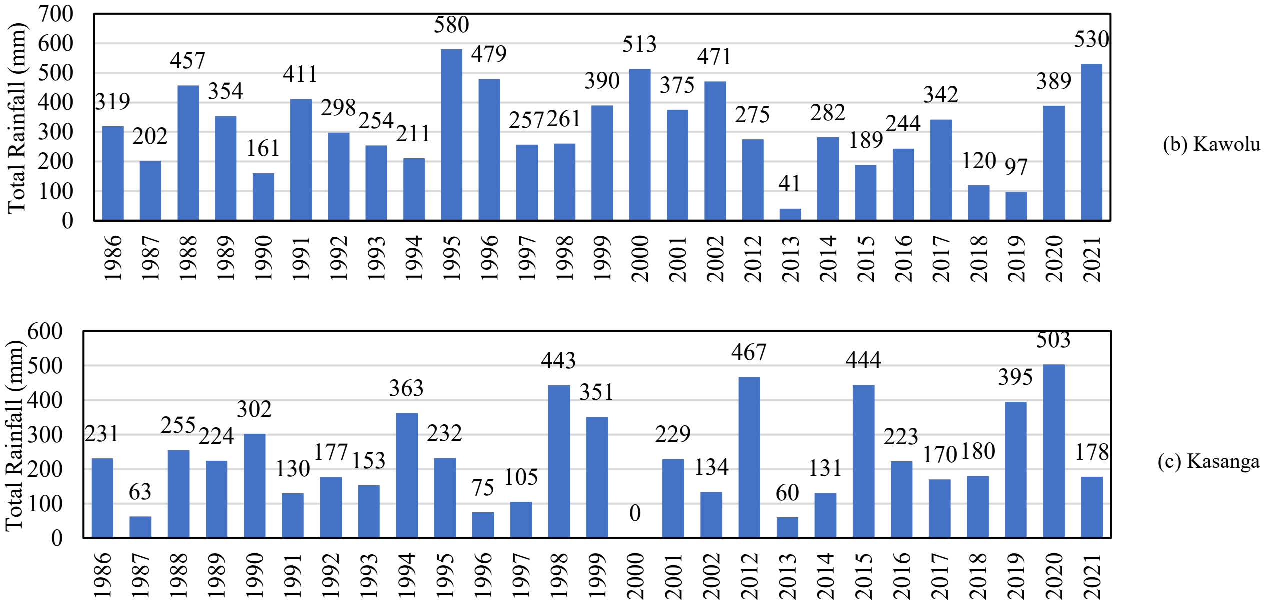

Figure 9. Total rainfall in *Mongso Udan* from 1986 to 2021

Mangsa Mareng (Transitional Dry Season)

Mangsa mareng was identified in *Kasasadasa*, *Dhestal*, and *Sadha*. Rainfall in these period is shown in Figure 10.

Mangsa mareng reflects a gradual moisture release phase, with accumulated rainfall in the Moderate category, with a cumulative average of 327.7 mm. Rainfall decreases steadily from *Kasasadasa* (161.6 mm) in the Moderate category, then decreases to *Dhestal* (67.6 mm) and *Sadha* (98.6 mm), both of which are in the Low category. Anomalies in *mangsa mareng* generally trigger crop uncertainty due to prolonged or abruptly shortened seasons. In 2016 (794 mm) and 2013 (600 mm), extreme wet Mareng anomalies occurred; in 2013, Sadha recorded up to 432 mm of rainfall, potentially disrupting the drying process of crops. In contrast, in 2019 (45 mm) and 2018 (85 mm), the transition to the dry season was very rapid and dry, which often made it difficult for farmers to utilize the remaining soil moisture.

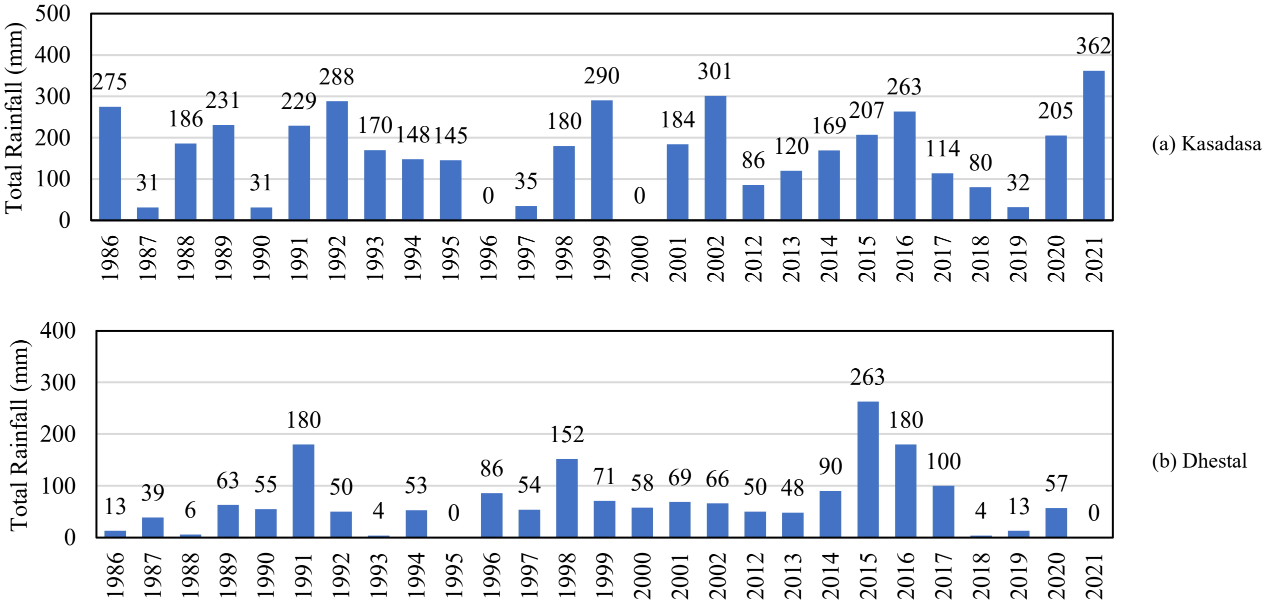

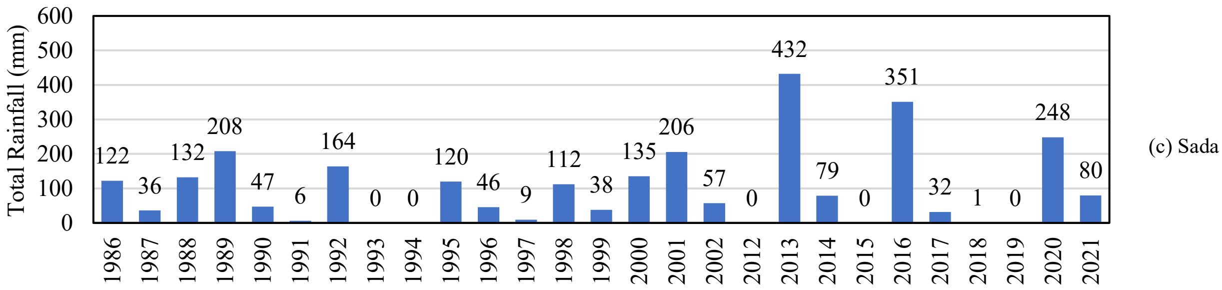

Figure 10. Total rainfall in *Mongso Udan* from 1986 to 2021

The analysis of rainfall distribution based on *pranatamangsa* indicates that the general seasonal pattern is still recognizable, where peak rainfall occurs during *Kanem* and *Kapitu*, while low rainfall is observed during *Karo*, *Katelu*, and *Kapat*. However, significant variability and anomalies are evident across the study period.

Several *mangsa* that are traditionally classified as dry exhibit unusually high rainfall, such as *Katelu* in 1992 and *Kapat* in 1992. Conversely, some wet *mangsa* show very low rainfall, such as *Kawolu* in 2013 and *Kasanga* in 2000 which is almost 0 . This indicates that rainfall distribution within traditional seasonal periods is becoming increasingly irregular. Figure 11 illustrates the Pranatamangsa calendar and the rainfall characteristics.

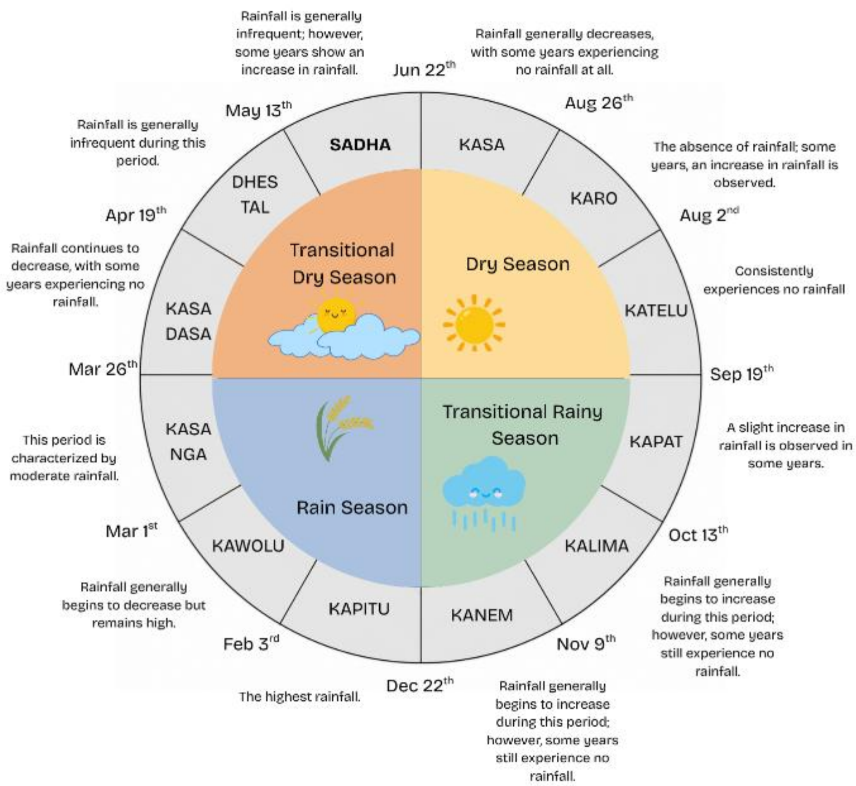

Figure 11. Pranatamangsa calendar and the rainfall characteristics.

The analysis of seasonal onset further supports this finding. The onset of the rainy season (AMH) does not consistently occur within the expected mangsa period, indicating a temporal shift in seasonal cycles. Similarly, the onset of the dry season (AMK) shows variability that deviates from traditional seasonal boundaries.

These inconsistencies suggest that while *pranatamangsa* still represents the general climatic pattern. However, according to the survey, only a third of farmers still consider paranata mangsa relevant, while the rest said it was not or needed to be re-evaluated [19]. its reliability has decreased due to increasing rainfall variability and extreme events. The observed increase in extreme rainfall events, as identified by the Mann-Kendall analysis, further supports this conclusion.

This condition reflects the impact of climate variability, particularly large-scale climate phenomena such as El Niño and La Niña, which influence rainfall distribution in the region. As a result, traditional seasonal indicators may no longer be sufficient for agricultural planning, especially in rainfed karst areas that are highly dependent on rainfall patterns [20].

4. Conclusions

This study demonstrates that the Rongkop karst area is characterized by moderate annual rainfall, with an average of approximately 2012 mm during the period 1986–2021. Although no significant trend is observed in total annual rainfall, there is a clear increase in the frequency and proportion of heavy (>50 mm/day) and very heavy (>100 mm/day) rainfall events. This shift toward higher rainfall intensity indicates an increasing risk of hydrometeorological hazards, which may negatively affect agricultural productivity in rainfed karst systems.

The analysis of dasarian rainfall reveals significant variability in seasonal patterns. The onset of the rainy season varies widely, occurring between the third ten-day period of August and the third ten-day period of December, while the dry season begins between the first ten-day period of February and the second ten-day period of May. The duration of both seasons is also highly variable, with prolonged dry seasons observed in 1997, 2013, and 2019, which are associated with El Niño events. In addition, the increasing occurrence of heavy rainfall during the typical dry season suggests growing seasonal irregularity, likely influenced by more frequent La Niña events.

The comparison between observed rainfall patterns and the traditional seasonal system (*pranata mangsa*) indicates that the general seasonal structure is still recognizable, particularly in distinguishing wet and dry periods. However, significant deviations are identified, including increased rainfall during traditionally dry mangsa and reduced rainfall during expected wet periods. These findings suggest that the reliability of *pranata mangsa* as a seasonal indicator has decreased due to increasing climate variability and extreme rainfall events.

Overall, this study highlights that climate change in the study area is manifested not through changes in total rainfall, but through increasing rainfall intensity and seasonal unpredictability. As a result, traditional seasonal knowledge alone is no longer sufficient for agricultural decision-making. Therefore, it is essential to integrate *pranatamangsa* with modern climatological analysis to improve the accuracy of seasonal prediction and enhance the resilience of agricultural systems in karst regions.

References

[1] A. Varga, "Climate change and its impact on agriculture," *Acta Hortic. Regiotect.*, vol. 24, no. s1, 2021, doi: 10.2478/ahr-2021-0010.

[2] J. P. Aryal, T. B. Sapkota, R. Khurana, A. Khatri-Chhetri, D. B. Rahut, and M. L. Jat, "Climate change and agriculture in South Asia: Adaptation options in smallholder production systems," *Environ. Dev. Sustain.*, vol. 22, no. 6, 2020, doi: 10.1007/s10668-019-00414-4.

[3] K. Yulianto, "Agroekologi: Model pertanian berkelanjutan masa depan," *J. Tambora*, vol. 1, no. 3, 2016, doi: 10.36761/jt.v1i3.142.

[4] World Meteorological Organization, *Global Climate Report—August 2020: State of the Climate*. Geneva, Switzerland: WMO, 2020.

[5] S. A. Woznicki, A. P. Nejadhashemi, and M. Parsinejad, "Climate change and irrigation demand: Uncertainty and adaptation," *J. Hydrol. Reg. Stud.*, vol. 3, pp. 247–264, Mar. 2015, doi: 10.1016/j.ejrh.2014.12.003.

[6] G. Fischer, F. N. Tubiello, H. van Velthuizen, and D. A. Wiberg, "Climate change impacts on irrigation water requirements: Effects of mitigation, 1990–2080," *Technol. Forecast. Soc. Change*, vol. 74, no. 7, pp. 1083–1107, Sep. 2007, doi: 10.1016/j.techfore.2006.05.021.

[7] E. Rasmikayati, B. R. Saefudin, D. Rochdiani, and R. S. Natawidjaja, "Dinamika respon mitigasi petani padi di Jawa Barat dalam menghadapi dampak perubahan iklim serta kaitannya dengan pendapatan usaha tani," *J. Wil. Lingkung.*, vol. 8, no. 3, pp. 247–260, Dec. 2020, doi: 10.14710/jwl.8.3.247-260.

[8] V. Gitz, A. Meybeck, L. Lipper, C. Young, and S. Braatz, *Climate Change and Food Security: Risks and Responses*. Rome, Italy: Food and Agriculture Organization of the United Nations, 2016.

[9] A. B. Sekaranom, E. Nurjani, and F. Nucifera, "Agricultural climate change adaptation in Kebumen, Central Java, Indonesia," *Sustainability*, vol. 13, no. 13, Art. no. 7069, 2021, doi: 10.3390/su13137069.

[10] Y. K. Khotimah, S. Supardi, and E. Antriyandarti, "Pemanfaatan sumber daya pertanian lahan kering di Pegunungan Karst Gunungkidul," in *Proc. Semin. Nas. Sumber Daya Pertan. Berkelanjutan dalam Mendukung Ketahanan dan Keamanan Pangan Indones. pada Era Revolusi Ind. 4.0*, vol. 3, no. 1, 2019, pp. 50–57.

[11] Direktorat Jenderal Cipta Karya, *Rencana Terpadu & Program Investasi Infrastruktur Jangka Menengah Kabupaten Gunungkidul 2015–2019*. Yogyakarta, Indonesia, 2014.

[12] N. Daldjoeni, "Pranatamangsa, the Javanese agricultural calendar—Its bioclimatological and sociocultural function in developing rural life," *Environmentalist*, vol. 4, suppl. 7, pp. 15–18, 1984, doi: 10.1007/BF01907286.

[13] D. N. Azizah, E. Banowati, Juhadi, and R. Hayati, "Intercropping as a farmer adaptation strategy during drought: A case study of Karangwuni and Semugih Sub-districts, Gunungkidul," *JPG (J. Pendidik. Geogr.)*, vol. 13, no. 1, 2026, doi: 10.20527/jpg.v13i1.24481.

[14] R. D. Handayani, Z. K. Prasetyo, and I. Wilujeng, *Pranata Mangsa dalam Tinjauan Sains*. Indonesia: CV. Calina Media, 2018.

[15] A. A. Satriaji, "Pranata Mangsa," *SCLM17*, Mar. 2016. [Online]. Available: https://sclm17.blogspot.com/2016/03/pranata-mangsa.html. [Accessed: Feb. 12, 2026].

[16] A. Cahyadi *et al.*, "Rainfall variability in Gunung Sewu karst area, Java Island, Indonesia," *Indones. J. For. Res.*, vol. 8, no. 1, pp. 23–35, 2021, doi: 10.20886/IJFR.2021.8.1.23-35.

[17] Z. He, X. Gu, F. Qiu, M. Wang, M. Xu, and S. Chen, "Spatiotemporal variability of rainfall in central Guizhou: Multi-time scale analysis and implications for climate change adaptation," *J. Clim. Change*, vol. 11, no. 2, pp. 226–243, 2025.

[18] M. K. Zaki, K. Noda, K. Ito, K. Komariah, S. Sumani, and M. Senge, "Adaptation to extreme hydrological events by Javanese society through local knowledge," *Sustainability*, vol. 12, no. 24, Art. no. 10373, 2020, doi: 10.3390/su122410373.

[19] Sumani, Suntoro, Komariah, and Mujiyo, "Existences and perception of Javanese local knowledge for climate change adaptation," *IOP Conf. Ser.: Earth Environ. Sci.*, vol. 824, no. 1, Art. no. 012075, 2021, doi: 10.1088/1755-1315/824/1/012075.

[20] H. O. Salsabila, "The existence of Pranata Mangsa calendar in the midst of global climate change," in *Proc. Int. Conf. Sharia Law (ICOSLAW)*, vol. 1, no. 1, 2022, pp. 85–89.

INERSIA

JURNAL TEKNIK SIPIL DAN ARSITEKTUR

UNIVERSITAS NEGERI YOGYAKARTA

Departemen Pendidikan Teknik Sipil dan Perencanaan
Fakultas Teknik, Universitas Negeri Yogyakarta
Jl. Colombo No.1, Karangmalang, Yogyakarta 55281